Západočeská univerzita v Plzni
Fakulta aplikovaných věd

MOTORCYCLIST BIOMECHANICAL MODEL

Lic. Eng. Pedro Miguel de Almeida Talaia, MSc

Declaration

Herewith I, Pedro Miguel de Almeida Talaia, declare that I compose this work alone except when I clearly indicated otherwise. I have used only the literature listed in the bibliography section.

In Pilsen, 31.08.2013

Pedro Miguel de Almeida Talaia

Abstrakt

Úvodní kapitola popisuje projekt, motivaci práce a zabývá se také problematikou poranění lidského těla. V první řadě je představen projekt, v rámci něhož práce vznikla. Následuje stručný rozbor scénářů možných nehod vozidel typu motorové jednostopé vozidlo (PTW – Powered Two-wheeler). Dále práce shrnuje důvody, proč jsou uživatelé motorových jednostopých vozidel na pozemních komunikacích považováni za málo chráněné z hlediska aktivní i pasivní bezpečnosti. Po představení možných následků nehod práce předkládá názory zdravotníků na téma nehod účastníků provozu pohybujících se na motorových jednostopých vozidlech. V neposlední řadě je popsána anatomie částí lidského těla pro idealizaci crashové analýzy.

Druhá kapitola se zabývá modelováním lidského těla. S vývojem technologií je možné model lidského těla zpřesňovat a zahrnovat složitější principy a popisy. Zkoumán je model lidského těla vhodný pro crashovou simulaci.

Třetí kapitola se zabývá základními principy pro každý scénář nehody. Většina literatury se orientuje na nehody motorových vozidel z pohledu uživatelů automobilů – pasivní i aktivní bezpečnost. Tato práce se soustředí na bezpečnost a nehody uživatelů motorových jednostopých vozidel. Detailní rozbor jednotlivých částí lidského těla a jejich chování bude v následujících kapitolách.

Čtvrtá kapitola popisuje některé základní koncepty zahrnující lidskou anatomii, fyziologii, traumatologii, některé podrobnější analýzy jsou rozděleny z hlediska částí lidského těla. Z literatury je převzat základ pro simulace – ať už kvantitativní hodnoty jako zrychlení, deformace, energie, tak kvalitativní popsané v AIS. Tělo je rozděleno do 6ti oblastí zájmu – hlava, páteř, hrudník, břicho, horní a dolní končetiny. Pro každou oblast zájmu je naznačeno použití multibody modelu HUMOS2.

Pátá kapitola představuje 2D model jednostopého vozidla včetně motocyklisty. Je zahrnut popis stavby modelu.

Šestá kapitola rozvíjí kapitolu pátou. 2D model je rozšířen na 3D model. Tento model je plně parametrický. V kapitole je popsána implementace multibody HBM (Human body model – model lidského těla) pro potřeby naší simulace.

Sedmá kapitola se zabývá možnými scénáři nehod: střet s chodcem, různé scénáře čelních nehod s dalšími vozidly. Části těla, ve kterých dochází při střetu ke kontaktu, jsou modelovány detailněji. Z nelineárního modelu s velkými deformacemi jsou získány standardní kritéria jako "HIC", 3ms, max(g), ThAC a další. Dále mohou být vyhodnoceny zlomeniny žeber a další poškození těla. Části těla z "dummy" jsou nahrazeny ve výpočtovém FEM modelu jejich ekvivalentní konečno prvkovou (FEM) idealizací získanou z multi-body simulace. Může být zjištěna pravděpodobnost zranění jako zlomeniny kostí, velké deformace a tím pádem zranění vnitřních orgánů (aorta, játra, srdce, slezina atd.). Také je možné zjistit poměrné deformace a hladiny energií v mozku a obratlích, které jsou důležitými ukazateli pro poškození nervů – poškození míchy. Porovnání matematických kritérií a pozorování z modelu dávají možnost lépe pochopit a posoudit mechanismy vzniku traumatických úrazů. Napomáhají také k diagnostice příčin a možnosti hledání způsobů snížení následků.

Abstract

In the first chapter as introductory section of this work is presented the project, the motivation and the problems of human body injuries. Firstly, it will be given a big picture of the project where this work is integrated. Then, a brief analysis of the contextualization of the PTW (Powered Two-Wheeler) as a problem is presented as well as the numbers that rules the accidents involving such family of vehicles. There are summarized some reasons why the PTW is a vehicle that fits in the fragile group of road users. After the injuries evaluation is presented, some scores used by the medical staff and their meaning are mentioned. Then, it is explained why we should be aware of the body particularities and how to understand the need of bearing in mind the anatomy and physiology in the crash study.

In the second chapter, is shown aspects of the modelling parts of the body. In our days the concept of model has gained a new dimension with the advent of the computing technologies. Such technologies can mimic in projected 3D environment human actions and, mimic in real time our emotions and expressions. If we look around, from the 3D games, crossing the 3D animation, until reach the virtual crash dummies, all these human models shares the same principle as background, the computer science. This chapter explores how the human body is modelled for crash proposes, and what informatics tools are able to handle with such models.

The third chapter is intended to give a first approach of the global definition of each concept. Particular emphasis is applied in our final propose, PTW users, since the majority of the literature was done considering, or having in mind car occupants, with the correspondent active and/or passive constrains. Detailed information for each body segment will be presented in the following chapter. Some sub-concepts or aspects concerning some part of the human body will not be include in this copter view of the definitions, but will be enclosed in the respective body-segment sections.

The fourth chapter presents some basic concepts concerning the human anatomy, physiology and trauma, some more detailed analysis is presented divided in terms of body segments. Data from literature is compiled and presented as needed, being this chapter as base to detail analysis of the simulations, relating quantitative results (accelerations, deformations, energy, etc.) with qualitative variables like the described in AIS. The body is so segmented in 6 groups of segments: head, spine, thorax, abdomen, Pelvis and lower extremities, and upper extremities. Is also illustrated in each section of this chapter the parts of the used models: the implemented multibody model, and the finite element model used, the HUMOS2.

In the fifth chapter is presented a two-dimensional (2D) model of a PTW including a motorcyclist. The description how the data was build and implemented is presented too.

The sixth chapter comes as a major development of the chapter 5. In this chapter a three-dimensional version of the human body was implemented. This new model is fully parametric. So this chapter describes the implementation of a multibody HBM (Human Body Model) to our work.

The seventh chapter focus in the injury assessment in several cases: a pedestrian hit and several variations of a head-to-head collision between a PTW and other vehicle. The body segments involved in any particular load observed in the accident simulation can be

analysed in more detail. The standard criteria's as HIC, 3ms, max(g), ThAC and others can be obtained from a deformable not linear model. Furthermore, rib fractures and other injuries related to the deformable model can be evaluated. The body segment from the dummy and the impacted objected are replaced in FEM for their equivalent FEM models, with the conditions obtained from the MBM simulation. The mathematical parameters can be complemented with injury analysis from the result from the simulation, like broken bones, high deformed bodies, and energy or stress levels in organs. Critical aspects can be observed. The imposed deformations imposed to the aorta, heart, spleen and liver are possible to analyse. It's possible to evaluate the levels of energy found in the brain, or the relative displacement found between vertebras. The association between the mathematical criteria's and the observation of the "injured" model gives a better assess to the trauma mechanisms, helping diagnosing the trigger effects and possible remedies to reduce/avoid such consequences.

Résumé

Le premier chapitre de ce travail comme partie introductive présente le projet, la motivation et les problèmes de blessures du corps humain. Tout d'abord, l'on donnera une vue d'ensemble du projet où cette activité est intégrée. Ensuite, après une brève analyse de la contextualisation de la PTW (deux-roues propulsé, de l'Anglais «Powered Two-Wheeler») comme un problème sont présentés des chiffres correspondant aux accidents impliquant des véhicules de même classe (catégorie). Il y a un résumé qui montre les raisons pour lesquelles le PTW est un véhicule qui s'inscrit dans le groupe fragile des usagers de la route. Après l'évaluation des blessures, sont présentées certaines partitions utilisées par le personnel médical et leur signification sont mentionnées. Ensuite, il est expliqué pourquoi nous devrions être conscients des particularités du corps et comment comprendre la nécessité de tenir compte de l'anatomie et la physiologie dans l'étude de l'accident.

Le deuxième chapitre montre les aspects des modélisations des parties du corps. De nos jours, le concept du modèle a acquis une nouvelle dimension avec l'avènement des technologies de l'informatique. Ces technologies peuvent imiter nos émotions et expressions en temps réel dans un environnement virtuel (3D). Si nous regardons autour des jeux 3D en passant par le cinéma, jusqu'à atteindre les mannequins d'accidents de simulation, tous ces (actions de) modèles humains ont le même principe que le fond informatique. Ce chapitre explore comment le corps humain est modélisé sous les effets d'accident, et quels outils informatiques sont en mesure de traiter ces modèles.

Le troisième chapitre est destiné à donner une première approche de la définition globale de chaque concept. Un accent particulier est appliqué dans notre objectif final, qui concerne les usagers de PTW, puisque la majorité de la littérature a tenu en considération les occupants de voiture avec les contraintes actives et/ou passives correspondantes. L'information détaillée pour chaque segment du corps sera présentée dans le chapitre suivant. Certains sous-concepts ou les aspects relatifs à certaines parties du corps humain ne seront pas inclus dans cette vue kaléidoscopique des définitions, mais seront focalisés dans les sections respectives de segment de corps.

Le quatrième chapitre révèle quelques concepts de base concernant l'anatomie, la physiologie et le traumatisme. C'est une analyse plus détaillée et divisée en termes de segments du corps. Des données de la littérature sont compilées et présentées selon les besoins de ce chapitre comme base de l'analyse détaillée des simulations, concernant les résultats quantitatifs (accélérations, déformations, énergie, etc.) avec des variables qualitatives comme le décrit en AIS. Le corps est donc fractionné en 6 groupes de segments: tête, colonne vertébrale, thorax, abdomen, bassin et membres inférieurs et membres supérieurs. Les parties des modèles utilisés (le modèle multicorps mis en œuvre et le modèle éléments finis utilisés, l'HUMOS2) sont également illustrées dans chaque section de ce chapitre.

Dans le cinquième chapitre un modèle à deux dimensions (2D) d'une PTW dont un motocycliste est présenté. La description de comment les données ont été construites et mises en œuvre est aussi exposée.

Le sixième chapitre se présente comme une évolution majeure du chapitre 3. Dans ce chapitre, une version en trois dimensions du corps humain a été mise en place. Ce nouveau modèle est entièrement paramétrable. Ce chapitre décrit la mise en œuvre d'un HBM multicorps (modèle du corps humain).

Le septième chapitre se concentre sur l'évaluation du préjudice dans plusieurs cas: un succès pour piétons et plusieurs variantes de collision tête-à-tête entre un 2RM et autres véhicules. Les segments corporels impliqués dans n'importe quelle charge particulière observée dans la simulation d'accident peuvent être analysés plus en détail. Les critères standards HIC, 3ms, max(g), ThAC et autres peuvent être obtenus d'un modèle non linéaire déformable. Par ailleurs, les fractures de côtes et autres blessures liées au modèle déformable peuvent être évaluées. Le segment du corps de mannequin et les objets qui ont souffert le choque (l'impact) sont remplacés dans le MEF par leurs modèles équivalents de MEF, avec les conditions obtenues de la simulation de MBM. Les paramètres mathématiques peuvent être complétés par l'analyse du préjudice du résultat de la simulation, comme des os cassés, des corps très déformés et des niveaux d'énergie ou le tenseur dans les organes. Des aspects critiques peuvent être observés. Il est possible d'analyser les déformations imposées à l'aorte, au cœur, à la rate et au foie de même qu'évaluer les niveaux d'énergie dans le cerveau, ou le déplacement relatif entre les vertèbres. L'association entre les critères mathématiques et les dommages observés du modèle «blessé» nous donne une meilleure évaluation des mécanismes de lésion, nous aide à diagnostiquer les effets de la détente et les remèdes possibles pour réduire ou éviter de telles conséquences.

Keywords

Human modelling

Multibody

Injury assessment

Motorcyclist

Crash analysis

Mots-clés

Modélisation humaine

Systèmes Multicorps

Évaluation de la lésion

Motocycliste

Accident analyse

Acknowledgments

To come through this long path, from the very first step until this present, effort and dedication was given, sometimes alone, sometimes in the crowd. All this experience makes myself a new person in competences, knowledge, friendship and culture.

Being 3 years of my life in a new city, Plzeň, in a new university: Západočeská Univerzita v Plzni, with new colleagues and new professors that have been a great experience, which will be always in my heart. To all of my colleagues, professors and directors, my thankfully. A special thank you to Jana Kovářová and Miroslava Tringelová, my office mates for the help in all. To Michal Hajžman a special dedication for the tutoring, the time and the talks that gives courage to raise this enterprise, but always pointing my mistakes and giving a fix path, like a good friend does. Finally, Luděk Hynčík, my supervisor, my professor and a friend that gives me the opportunity to embrace this project, trusting and helping in all stages of this work, having an infinity portion of patient.

In the project MYMOSA, thanks to all you folks, a great family in all meetings, dinners and drinks after hours! A note to two persons: Ugo Galvanetto and Marco Pierini.

In France, thanks to all personal in ALTAIR France that supports me in my stage. Special thanks to Franck Njiliet to all discussions that we have in so short time, but with great output. To Milan Toma, a special place in my heart not for Paris, but all stages together and the friendship to my now Slovak-Portuguese-Japanese-world friend. To ALTAIR the acknowledgment for provision of HUMOS2 models.

In German, a special thanks to Thomas Mertens and DEKRA, for the training and the professionalism in the training in the Magdeburg facilities.

In Netherlands, thanks to Lex van Rooij and Filipe Fraga, since they received me as one of them in my TNO stage, in Eindhoven. Thanks to Filipe to all discussions out-of-the box, that always as given solutions (but with a lot of questions also…).

In Belgian, a thanks to LMS International N.V., CAD division for the software, software training, courses, support, and stage. A reference to Joris De Cuyper, Jian Kang, David Moreno, Marco Gubitosa, and Michal Manka for their time and support.

A final reference to Casserta, Ioannis, Mazdak, and Gkoumplia.

As final notes, my family. To my wife, Aliona, for all the adventures and travels together, to all weekends lost seeing myself in a relation with a laptop, and all my changes of mood too. To my soon, Miguel, all the patient to wait for the free laptop to see a movie, or to go to the park… To my parents, all their effort in my education and supporting me and my family in all this project.

To all that I make a reference, and to all others that have been close to me

A thank you from the deep of my heart

Pedro Miguel de Almeida Talaia

Table of contents

List of figures

List of tables

Nomenclature

AIS .... Abbreviated Injury Scale
ARL.............. Alderson Research Laboratory
AT .... Austria
ATD .... Anthropometric Test Devices
BE................. Belgium
CAD .... Computer Aided Design
CAE.............. Computer Aided Engineering
CPU.............. Central Processing Unit
CRABI .... Child Restrain Air-Bag Interaction
CTI .... Combined Thoracic Index
DE .... Deutschland, Germany
DK................. Denmark
ES .... Spain
EU .... European Union
FEM .... Finite Element Modeling
FERD .... Ford Engineering Research Department (it names a dummy family)
FFC................ Femur Force Criteria
FI................... Finland
FR.................. France
GAMBIT....... Generalized Acceleration Model for Brain Injury Threshold
GARD .... Grumman-Alderson Research Dummy
GDP.............. Gross Domestic Product
GM .... General Motors
GR .... Greece
HIC............... Head Injury Criterion
HPC.............. Head Protection Criterion
IE................... Ireland
ISS .... Injury Severity Score
IT................... Italy
LU .... Luxemburg
MB .... Multibody
MBD.............. Multibody Dynamics
MBM............. Multibody Model
MYMOSA..... MotorcYcle and MOtorcyclist Safety
NHTSA .... National Highway Traffic Safety Administration
NL .... Netherlands
PT.................. Portugal
PSPF.............. Pubic Symphysis Peak Force
PTW .... Powered Two-Wheeler
SID .... Side Impact Dummy
SV.................. Slovak
TI................... Tibia Index
TNO .... Netherlands Organization for Applied Technical Research
TTI................ Thoracic Trauma Index
UK................. United Kingdom
USA.............. United States of America
VC .... Viscous Criterion

WHO .... World Health Organization
WP................. Work Package
WSTC............ Wayne State Tolerance Curve

1

Introduction

In this chapter the introductory sections of the work are presented: the project, the motivation and the problems of human body injuries.

Firstly, it will be given a big picture of the project where this work is integrated.

Then, a brief analysis of the contextualization of the PTW (Powered Two-Wheeler) as a problem is presented as well as the numbers that rules the accidents involving such family of vehicles. There are summarized some reasons why the PTW is a vehicle that fits in the fragile group of road users.

Finally, after the injuries evaluation is presented, some scores used by the medical staff and their meaning are mentioned. Then, it is explained why we should be aware of the body particularities and how to understand the need of bearing in mind the anatomy and physiology in the crash study.

1.1 MYMOSA as project

This work is a part of a European network project, named MYMOSA [1], from **M**otorc**Y**cle and **MO**torcyclist **Sa**fety, focused on PTW safety and people training.

The project is arranged in four work packages (WP), analysing in each one a topic of the problem concerning the PTW safety: accident dynamics, integrated safety, protective equipment and biomechanics (Figure 1-1).
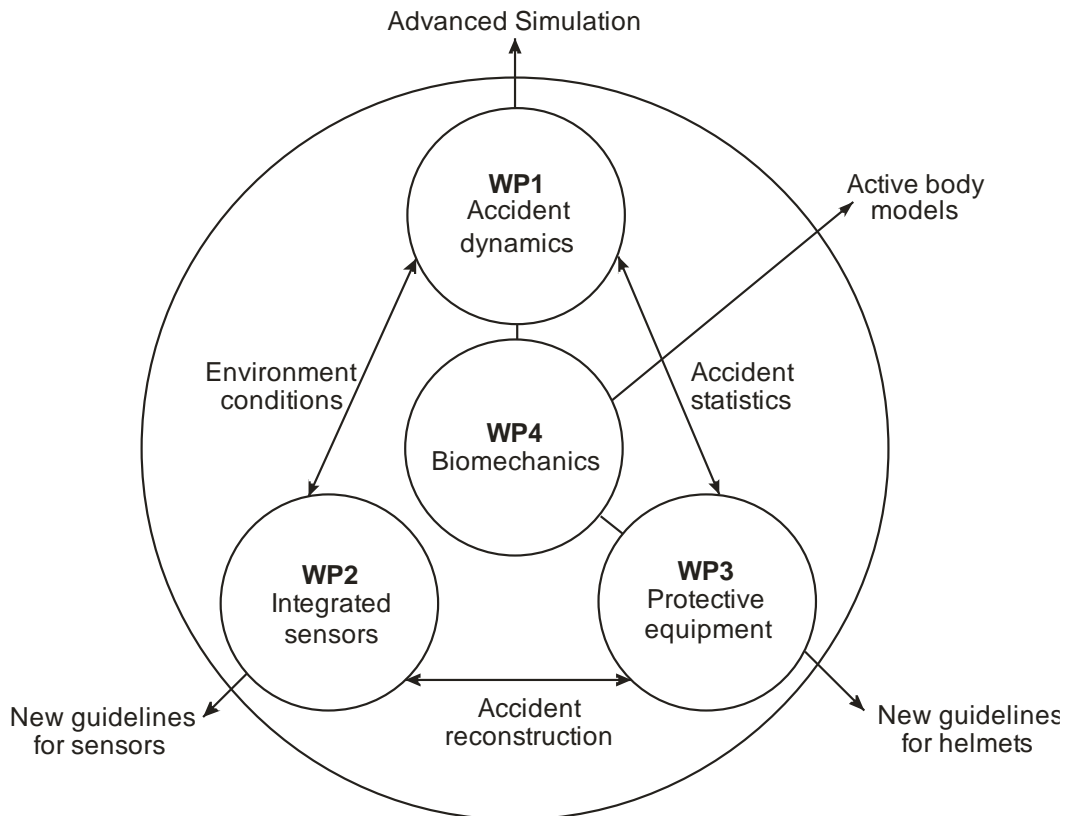
Figure 1-1 – MYMOSA project organization scheme

The flow of information and transfer of knowledgment presented in the Figure 1-1 shows how some work-have shared efforts in the PTW safety thematic. Such share of efforts has been in form of formation and secondments of several project researchers, as direct share and common work between researchers itself.

The work-packages in the project have been not permeable even with a not defined share WP, meaning that all the partners have an active role in the way that each researcher was guiding his researcher work. Such influence from the partners has been in form of training in different fields, from software training, numerical methods, trauma and injury, personal skills and others. Other forms of influence have been in form of researchers share, secondments, or on the presentation in the project scheduled meetings.

Some of the work presented in this thesis have been already discussed and presented in chapters of 4 of the project deliverables. Each deliverable, with a pre-defined topic: development of overall methodology for accident simulations [2]; detailing of the underlying critical aspects [3]; integration into a vehicle/rider model for full-scale simulations [4]; and investigation of accident scenarios and validation of the vehicle/rider

model , have been discussed in the WP where we are included, the WP1 – accident dynamics.

The main tasks in each WP can be summarized by:

- Accident dynamics
    - Realize a well-validated CAE (Computer Aided Engineering) methodology – and corresponding toolset – describing the interaction between vehicle-rider-environment during PTW driving, as well as in the pre-accident and accident phase;
- Integrated safety
    - The development of an integrated safety system capable to detect impending dangerous situations (e.g. instability) and accident scenarios, and inform the rider or influence the PTW behaviour with the purpose of reducing the injury risk;
- Personal protective equipment
    - To develop new protection concepts (such as devices to reduce head rotational accelerations) and examine new materials for further reduction of the injury risk of PTW riders with a special emphasis on motorcycle helmets with respect to three major occurring head injuries.
- Biomechanics
    - To develop new biomechanical knowledge specifically for motorcyclists based on the current knowledge of car occupants and pedestrians.

The work presented in this thesis is done inside of the work package envelop: accident dynamics. The main goal is the development of a human multibody model for crash simulations.

1.2 Accidents and Casualties

The accidents are a sad reality of the European Union (EU). The impact in the society and in the economy is great. According to the European Commission, it was registered 50,000 casualties in the year of 2001 in the EU roads [5]. The number of causalities has been decreased slowly with the efforts of several entities, but the absolute number of casualties involving PTW remains almost equal, meaning a not successful increase off safety in this particular group of rood users. The contribution of the PTW in terms of fatalities is around a total of 20% (Figure 1-2).

The figures from the year of 2006 points that the contribution of the road accidents in the EU GDP (Gross domestic product) is much as 2% from direct and indirect cost [6]. With the improvement of the primary cares, and improved of performance on the first-aid and emergency transportation mechanisms, the part of the accidents on GBP can increase in a short future base. We should notice that for the year 2010, which cost was much as 326 million Dollars', what represents the Finland GBP or 150% the Portuguese GBP for the same year.
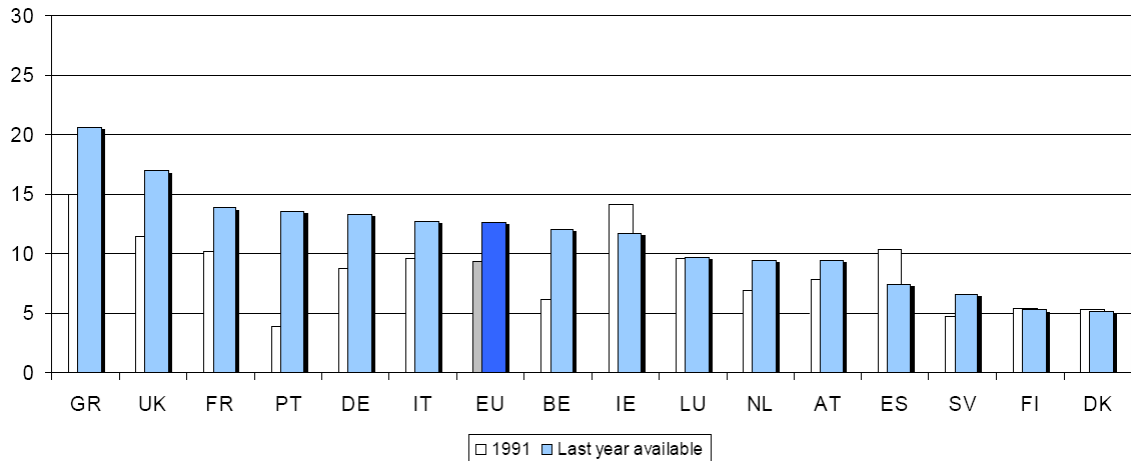
Figure 1-2 – Percentage of motorcycles fatalities versus total of fatalities by country [5]

Figures from one of the lasted "Global status report on road safety", from the WHO[1], point the 1 million and 270 thousand dead people in world roads in the year 2008, such numbers are only for the called fragile groups: PTW, bicycles and pedestrians.

A brief look to the graphs of the casualties shows us one dark scenario, e.g.: if we make an analysis in the distribution of the casualties according to gender and age, we see clearly that males between the age of 18 and 30 are overrepresented (Figure 1-3). A peak occurs either in the group of females in the interval 21 to 30. These age segments of the society are persons in the beginning of their productive work life, having a direct impact in them and in them family life. Such age envelope points to a great economic impact in the society, since they have a high formation cost, and will not return such investment to the society. But if we don't have a fatality, but a heavy injured person, such social and economic cost can be even bigger, since we have to add hospitalization, expensive orthopaedics intervention, long physiotherapy periods, and some cases, permanent disability to be reintegrated in the productivity society. Such scenario for a heavy injured must be added the emotional impact with their close ones.
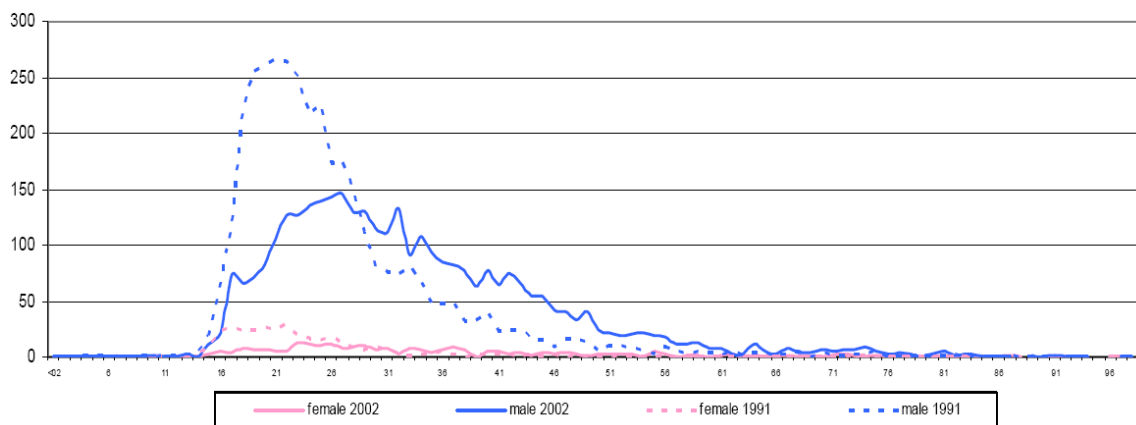
Figure 1-3 – Motorcycle fatalities by age and gender – Evolution: 1991-2002 [5]

---

[1] World Health Organization, http://www.who.int/en/

Someone that have grown up in a region where the PTW are common, can have a 1st person experience how much an accident can be deadly involving a PTW (Figure 1-4).

Figure 1-4 – Result of one accident between one PTW and one car in Sweden [7]

All the road users can give some type of explanation to prove why the PTW user is so "exposed" to high risk. The explanation given can be rational or not, even can come from some cultural cliché, but usually the statistics shows a clear "guilty" coming from the other vehicle than the PTW rider.

Their incoming contour can, maybe, explain how and why so much drivers involved in an accident said that they haven't be able to see the incoming PTW, or it appears more far-away, that it was in reality.

The fact is that the PTW rider is over-exposed comparing to the majority of the other users of the road, only comparable with bicycle drivers and pedestrians. One proof of this is e.g. the use of reflectors or the use of crossing lights during the whole day. These measures have helped to reduce the number of accidents or reduce their severity. The PTWs and their riders are the best observed (or perceived) by the other drivers [8]. In our days it's usual to see recommendations to advice PTW and bicycle users to use a reflector jacket and/or to choose a bright helmet[2, 3].

The fragility of this group is clearly presented in the traffic safety campaign "Think!" in the United Kingdom. It is possible to see the message transmitted to both groups in some of their publicity spots, the PTW drivers and other vehicles drivers, as illustrated in Figure 1-5, from the spot "take longer to look for bikes", from the year 2006.

A fast travel around the world can be interesting. Try to compare the use of the type of the PTW in several scenarios: rush hour in Bombay, rush hour in Barcelona, a weekend rider in USA, or a weekend traveller in Germany (Figure 1-6).

---

[2] A white dot in dark background looks bigger than a black dot in white background, even if they have the same size.

[3] A vivid point in a multi-colored background is better percept than a neutral color point.

Figure 1-5 – Key frames from the campaign from Think! , titled as "take longer to look for bikes", from the year 2006 [9]

a)

b)

c)

d)

Figure 1-6 – Stereotypes from the use of PTW in: a) India [10]; b) Cataluña, Spain [10], c) USA [11]; d) Germany [12]

Based on four scenarios only we can find the complete and total diversity of realities. The first thing that came into our minds might perhaps be the type of the PTW, safety equipment and interaction in traffic.

This means that the degree of exposure of the occupancies of the PTW depends on a great number of factors; and this can make all the different if the PTW rider will be involved in a traffic accident. The same crash in different places of the world will give a very distinguish in the consequences to the driver.

1.2.1   Motorcycle exposure

During a car accident, a big amount of the energy is dissipated by the car structure. The newest cars have several zones to perform this task. The driver and the other passengers are restrained and secured in an almost undeformed cell zone.

In a PTW accident, the driver is not so protected by an exterior barrier or cage, and he/she is not so fitted (safely positioned) or restrained.

This means that majority of the protections are too close to the rider, and he/she does not have the same space to dissipate the energy involved in the crash that one has in a car.

This is important because the most important parameter in an accident is the acceleration. When the human body is submitted to great differences of velocity in a short period of time, it means that the body was exposed to acceleration (positive or negative). And why is this parameter so important?

Big values of accelerations can mean injury. Big values correspond to big loads, and if these values go until the human body limits, they start to be destructive, even without any direct impact.

Other important aspect to understand the exposal of the passengers of PTW, if they just fall down, they have to dissipate the energy with their own body.

This can be minimised with e.g.: appropriate clothing, boots and helmets. But we cannot compare the capacity of a car to dissipate energy to this type of protections.

So, part of the solution can be done by the optimization that occurs after and before the accident (or if possible, to avoid it).

For the propose risk analysis in a crash, dummies are used since the 50's of XX century, but the majority of them have in mind an automobile or an aeroplane user, where the person is seated and usually with some type of restrain mechanism. This works will start with one brief analysis of the history and main characteristics of the actual dummies and human models for crash analysis, is proposed a new model. The model to develop in this work as main function should be able to handle the freedom seen in a crash where a motorcyclist is present, where no restrain mechanisms are presented, where the body will be free and subject of a several number of loads since a first impact until achieve a rest position. As result of this goal, the body model should have some degrees of freedom not found in the typical dummies in our days, should have also the ability to handle impacts in any arbitrary direction.

1.3   Injuries, anatomy and physiology

In this work, we focus on the human body interaction with his/her environment. In a crash scenario, the configuration of the incoming vehicle(s), speed, urban furniture, road design

and so on will play an important role in the way that the crash evolves from the approaching phase (pre-crash) until its end (usually rest position)

The way that the body decelerates, the way that some parts impact with others, or the way that some of the body segments interact with their adjacent segments, among others phenomena, will play a key role in the final level of injury.

To analyse the overall injury level, it is necessary to analyse the injury mechanisms of each body segment, and the respective anatomy and physiology.

To evaluate the severity of one or more injuries, a scale to quote the severity of the sum of the damages is needed [13].

These scales are used to evaluate the injury magnitude of a persons involved in an accident. One example is the scale AIS (Abbreviated Injury Scale) [13, 14], firstly developed in the year 1971 as a system to define the severity of injuries throughout the body. From this first version, the scale was reviewed several times and the version from 2004 was a score of seven marks that go from 0 until 6 where 0 means no injury and 6 means an untreatable injury.

It is important to say that AIS scale is not a linear scale, it means that one person with a score of 4 is only a bit more injured that other with 3. This means that it does not make any sense to make averages from this score.

Another scale is the ISS (Injury Severity Score). This scale better evaluates patients with multiple injuries. The principle of the ISS has begun in the division of the body in 6 parts or sections: head/neck, face, chest, abdomen, extremities including pelvis, external (i.e.: burns, lacerations, abrasions, contusions). The AIS scale is applied to each part and the ISS is the result of the sum of the squares of the three most severity injured regions.

The scale ISS goes from 0 to 75 (3 times the value 5, corresponding with critical life threat). If the value 6 is recoded[4] to any part, the ISS is automatically the maximum, 75. The psychological number in the ISS scale is 15, it is considered as a frontier to a major trauma.

These scales do not consider aspects like the long-term consequences, lost in the income, and so on. Other aspects are that the severity of the trauma or their score doesn´t reflects the physical load that made that.

It is proper to say that this type of scores is useful to give the result of the evaluation of the injury, but it does not give all the necessary information.

One solution to minimize this limitation is the use of other type of information, like the use of cadavers, animals and so on to compare and to try to adjust the relation action-reaction.

The use of a multibody human model to see what happens during the all crash as main goal, gives direct access to the typical injury indicators, as e.g. the known HIC (Head Injury Criteria). But more than getting indicators correlated to a probability of an injury, it's pretended to simulate the damage itself. For that, training and access to one full FEM human body is pretended. The FEM can be so used in sections to see what will occurs in the human body when impact occurs between something external and a respective body segment.

---

[4] The score 6 is given for a fatal, no reversible injury: cranium smash, decapitation, aorta rupture, heart perforation …

1.4   Injuries by human body section

The type of injuries is not the same, depending on the part of human body, gender, age, etc. The mechanical limits are not the same and the consequences from a load can be the damage.

In the terms of biomechanics, a body can be divided into several systems: locomotion (passive and active), digestive, respiratory, neurological, endocrine, skin..., and each major group has its particular mechanical properties.

Other questions that apply to the analysis of injury of humans concern the limits. The limits can be achieved by a big load, like supra-mentioned, but it can be reached by a large displacement, too, or quick movement of one joint or body section. This means that anthropomorphic data can give also several natural limits. This means that anatomical and anthropomorphic data must be considered together always when it is possible [15-18].

The way how one impact triggers damage in the body tissues should be a must to better understand the involved mechanisms, as a possible protective equipment like the helmet can influence in such mechanism. A mechanism to go from an accident analysis untl the injury study of a body part in a part of the crash should be find to get a full understand of all the phenomena's involved, using so an holistic approach.

1.5   Motivation and goals

To fulfil the aspiration of this work, the implementation of a Motorcyclist Biomechanical Model, taking the integration of the topic in the MYMOSA project and the thesis itself, we propose to achieve:

- Getting formation in the fields of multibody dynamics, anatomy and physiology, trauma, and accidentology applied to motorcyclists;
- Implement in a commercial software one multibody human dummy model for crash simulation,;
- Compute injury criteria's from the multibody human model;
- Analyse the effect of the impact in the human body in the physiology point of view by means of finite element analysis;
- Create a protocol to fast simulate a full crash scenario, with detail analysis in critical body parts.

The models and the protocols to implement should be also able to get and be integrated in others models in the project workgroup.

In perspective, it's proposed a new approach to study and analyse the crash involving motorcyclists. It's proposed also the addition of the local after analysis of impact using more detailed FEM to see not only the injury indicators computed, but also see what will happens in the tissue level. And is proposed also the full path with a low computing cost, so can be easily applicable in terrain with a laptop or desk computer and reduce waiting time.

2
Modelling the human body

Representations from the human body are one of the very first's forms of art. Such representations of the human body are being done as art portraits of the human quotidian or sacred deities.

Modelling parts of the body in a schematic with medicine proposes was found in ancient civilizations, as the Egyptian or the Babylonian civilization.

In our days the concept of model has gained a new dimension with the advent of the computing technologies. Such technologies can mimic in projected 3D environment human actions and, mimic in real time our emotions and expressions. If we look around, from the 3D games, crossing the 3D animation, until reach the virtual crash dummies, all these human models shares the same principle as background, the computer science.

The current section explores how the human body is modelled for crash proposes, and what informatics tools are able to handle with such models.

2.1   Introduction

Replying the human body as one model is a requirement in different disciplines. From the simple mannequins that are used for displaying clothes on vitrines, until the state of art computer models for animation and research, human models are used around the world in a countless number of applications, with different levels of realism and complexity (Figure 2-1).

a)   b)
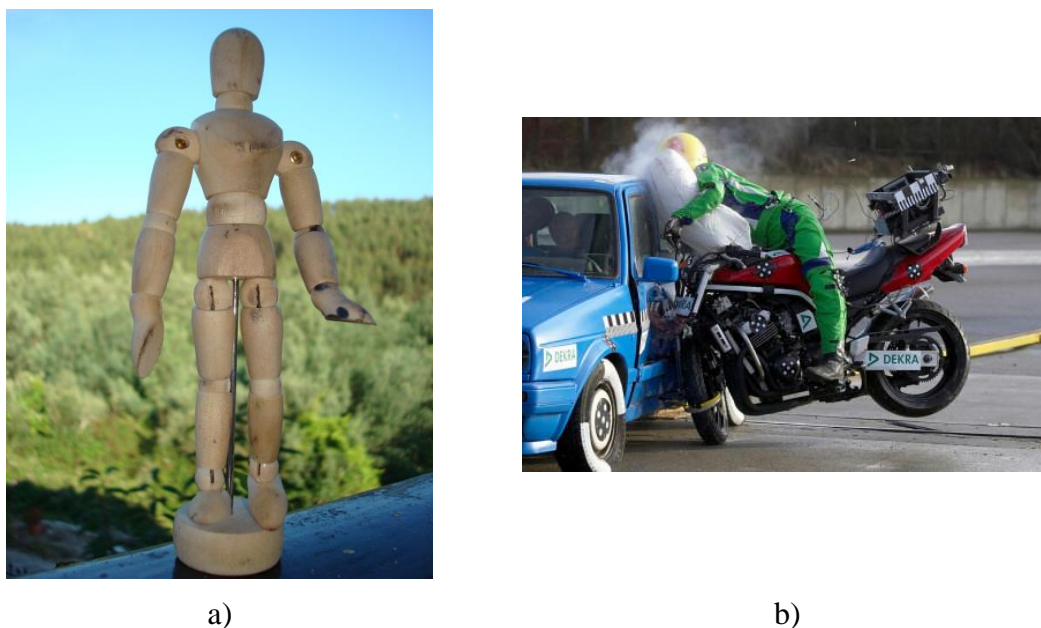
Figure 2-1 – Human model used: a) by painters, b) in automotive under a crash test [19]

In our work, we are manly focus in computer human models, which can describe primary the human body behaviour in crash conditions. On the real world, such human models are known as dummies. Such dummies can have a direct version in the digital world of computers. But since in the computer world we don't have some of the real-world constrains, we can have or develop more accurate dummies for certain applications.

The level of detail in such computer human models, and how they are correlated are software dependent too. Since our first approach will follow the multibody dynamics (MBD) formulation, that will constrain the number of suitable platforms to be used.

This chapter will show some dummies used, and their computer equivalents. Some only digital dummies will be presented too. Later on in this chapter computer software's are showed according to their suitable for such use, presenting a brief explanation of each software handle with virtual dummies models under crash situations.

2.2   Dummies

From this point and ahead, by default, the terminology "dummy" will be to address human models for crash proposes, being noticed the exceptions. Dummies or dummy refers to what is designated as Anthropometric Test Devices (ATD).

The dummies have been common used tool in our days by automakers, aviation, military and safety entities. But the dummies itself have not much as 60 years. When in the 30's

of last century the Wayne State University started to test how vehicles are safe using cadavers, how the body reacts against several types of loads, an all-new field of knowledge starts to emerge.

But the use of cadavers being an important source of data, surrogates several issues. One of the big constrainments is the lack of repeatability and how to compare different solutions against different test probes (the cadaver or pieces of it). Another issue was the lack of cadavers suitable for such experiments and tests, since the subject has to been from no crashed donators, and lesions free. Since the majority of such donators are persons that died from elderly age, the information taken can start to be biased from the change of properties by the advance of the age of the persons. If the majority of the used cadaver corresponds to an elderly population segment, that will not be a good representation of the average person. Taking all that constrains from the cadaver utilization, such tests remain until our days as one important source of data (Figure 2-2.a).

To culminate some of the previous issues, data have been taken from volunteers and from animals (alive or note, Figure 2-2. c). Such approach is until our days, used as complement to the cadavers use, being so a great set of tools to take data to characterise the human body. Being the combined use of cadavers, volunteers and animals the way to collect data, we still have the lack of a methodology to give repeatability results.

a)   b)   c)
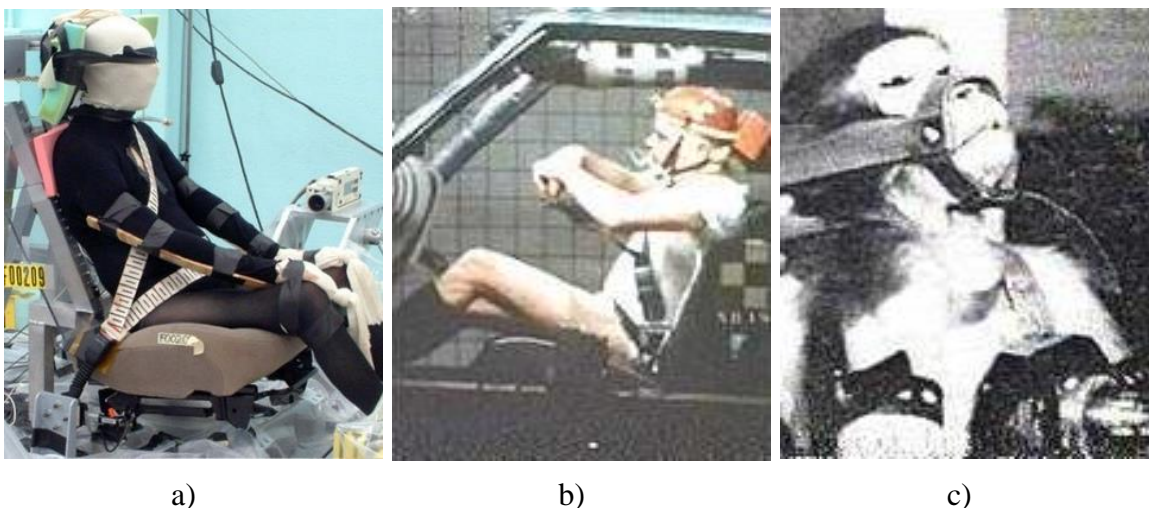
Figure 2-2 – Crash test using: a) an cadaver [20]; an volunteer [21]; c) an monkey [21]

But more that repeatability issues, ethical and religious concerns have been addressed. In such issue, the prohibition or restriction in some countries of tests in cadavers, child cadavers or animal experiments is found. Until our days, the debate remains being present in our societies, being claimed how beneficial is for us the experiments, manly, with cadavers, being such experiments a clear benefit for us in terms of safety and life's saved. The authors from a study claims that for each cadaver that was used, 60 life's have been saved, associated a countless number of injury reductions or injury preventions [22].

From the taken (and being take), was found primarily by the USA army, mainly for aeronautics that a mechanical humanoid that can mimics the human been can be a way to test safety issues, was in the year of 1949 that then the very first dummy was we know then have born, the Sierra Sam, representing a 95th percentile man (Figure 2-3).

Sierra Susie [24]

Sierra Sam [23]

FERD I and FERD II [25]

GARD [27]
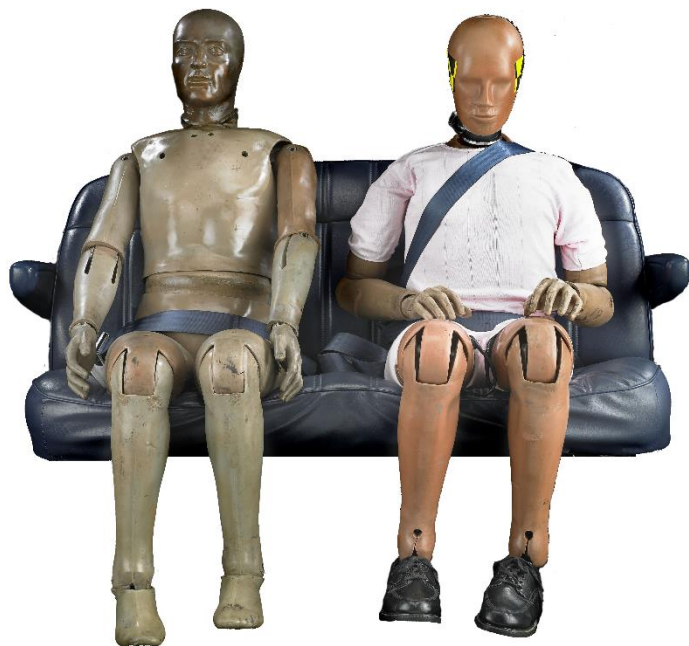
Hybrid II e Hybrid III [26]

Figure 2-3 – Examples of dummies have being used along the history.

2.2.1 Dummies and safety

Being the dummies or ATD mechanical humanoids that mimic the human response to the typical loads found in the environment for what they have been developed, they represent one valuable tool to asset how secure is certain vehicle in reference to pre-defined thresholds.

Being the dummy borne for air and space proposes, rapidly they are used in the automotive industry and their needs. Being the frontal the typical type of accident, followed by lateral and rear impact in terms of occupant injured and fatality, dose ware the line of development of such tools.

A summarize of the main dummies taking in account their historical importance and the USA market was presented by [28], and showed an adaptation in the

Table 2-1.

Developing speaking, the history of the dummies can be divided in decade bases.

2.2.1.1   Dummies in scope: the 50's

With the race for the moon and all the developments in air industry, particularly by the army needs, the use of tests to evaluate how safe are the vehicles used have been a must. Many tests have been done inside the army, being until our days a reference, as the tests done by the Colonel John Paul Stapp in himself, when in 1954 he was subjected to a maximum of $46.2g$ deceleration, not sustain any type of no-recover damage, revolutionizing the idea that a human can succumb to accelerations as $17g$.

In such environment, the first dummy was borne, the Sierra Sam (Figure 2-3), a 95th percentile man. Sierra Sam have appear in fact in the ends of 40's, in 1949, being used for ejection seats tests. In same period, other dummies have appeared for similar air-related tasks, as radiation space exposition, cloth tests, between other needs. The use of dummies started to be used in same period to asset the consequences from blasts and explosions in war and terrorist scenarios.

Is on the 50's that as appear two dummies that should be referred: OSCAR (Figure 2-4.a) and the very first Japanese dummy (Figure 2-4.b).

a)   b)

Figure 2-4 – Dummy: a) OSCAR [29], b) Japanese, the first developed there [29]

The interesting characteristic of the Japanese dummy is that he was developed taking in mind the PTW's safety The main characteristics of that dummy was: wood materials, stature and shape based in the developing researchers of the dummy, weight and centre of gravity based on anthropometric data from the USA. The dummy was developed by Tokyo Institute of Technology [29].

Table 2-1 – Notable dummies according to [28], in the XX century

Y	Dummy	Key features	Drawbacks	Usage
49	Sierra Sam 95th male (frontal)	Human-like exterior and body weight; articulated limb joints; durable	Stiffness not biofidelic; limited instrumentation; poor reproducibility	No
66	VIP Series 5th female, 50th and 95th male (frontal)	Human-like exterior and body weight; articulated limb joints; rubber neck; human shaped pelvis; instrumented to measure head and thoracic spine accelerations and femur loads	Stiffness not biofidelic; limited instrumentation; poor repeatability and reproducibility	No
67	Sierra Stan 50th male (frontal)	Human-like exterior and body weight; articulated limb joints; segmented neck; plastic shell for rib cage; instrumented to measure head and thoracic spine accelerations and femur loads	Stiffness not biofidelic; limited instrumentation; Poor neck bending response	No
68	Sophisticated Sam 50th male (frontal)	Fragile clavicles, humerus , radius, ulnas, femurs, tibias, fibulas, and patella's	Fracture levels of bones poorly controlled	No
70	Sierra Susie 5th female	Same features as Sierra Sam from with it was scaled	Same as Sierra Same	No
72	GM Hybrid II 50th male (frontal)	Uses parts from VIP-50 and Sierra Stan; human like shape, body weight, and ranges of motion of some articulated joints; repeatable, durable, and reproducible	Stiffness not biofidelic; limited instrumentation	No
76	GM Hybrid III 50th male (frontal)	Based on GM ATD-502 (NHTSA contract); human like shape and body weight; biofidelic response for head, neck, chest, knee; extensive instrumented; human-like automotive seated posture; excellent biofidelity, repeatability, reproducibility, and durability	Not appropriated for side impact studies	World
79	NHTSA/SID 50th male (side)	Modified Hybrid II with chest design for side impact	No shoulder or arm; not biofidelic in response; limited instrumentation; not recommended by ISO for side impact testing	No
82	GM 3-year-old air-bag dummy	Modified ARL VIP-3C dummy with foam-filled rib cage and segmented neck structure tuned to give human-like response; instrumented to measure loads associated with airbag deployment injuries	Not design to interface with child belt restrains	No
85	Hybrid-II-type 3- and 6-year-old dummies	Modified ARL-3 and 6 child dummies; specified for child restraint testing	Not biofidelic in impact response; limited instrumentation	USA
87	Hybrid III-type 5th female, 95th male, 6-years-old child (frontal and rear)	Scaled from Hybrid III midsize male with same level of biofidelity and measurements capacity	Not appropriate for side impact tests	World
89	EUROSID-1 50th male (side)	Hybrid III dummy modified for side impact testing, unique neck, chest, abdomen, and pelvis	Marginal biofidelity; shoulder design and back plate imped rib deflection; limited instrumentation	EU, Australia, Japan
90	CRABI, 6, 12 and 18 month	Designed to evaluate airbag interactions with rearward-facing infant restrains; biofidelic neck	Head impact response may not be biofidelic	World
92	Hybrid-III-type 3-year-old (frontal and rear)	Designed to evaluate airbags and child restrains; scaled from 6-year old; incorporates pertinent features of GM 3-year-old airbag dummy	Not instrumented nor durable enough for side impacts	World
97	TNO-Q3 3-year-old child (frontal and side)	Replacement for TNO-P3; improved biofidelity and instrumentation; designed for frontal and side impacts;	Not design for air-bag interaction testing	World

2.2.1.2   Dummies in scope: the 60's

It was on the 60's that the first automobile dummy has appeared the VIP series. In same period, Sierra Sam has seen the members added to his family, like Sierra Susie (Figure 2-3). Other dummies have appeared like FERD I and FERD 2 (Figure 2-3).

One notorious dummy from that decade is the GARD dummy (Figure 2-3), being used in air industry until our days.

It was in the 60's that an all use of the dummy was implemented, being used for several uses: medical dummies, rescue training dummies, space program, automotive crash dummies. Some of the solutions developed in that period are still use our days.

Other type of dummies starts to surge, the animal dummies.

2.2.1.3   Dummies in scope: the 70's

The need for more biofidelic dummies with more that anthropometric data, and impact performance start to emerge, so, in the 70's, have borne one of the most famous dummy families, Hybrid III (Figure 2-5), appearing only 4 years after is predecessor, the Hybrid II.
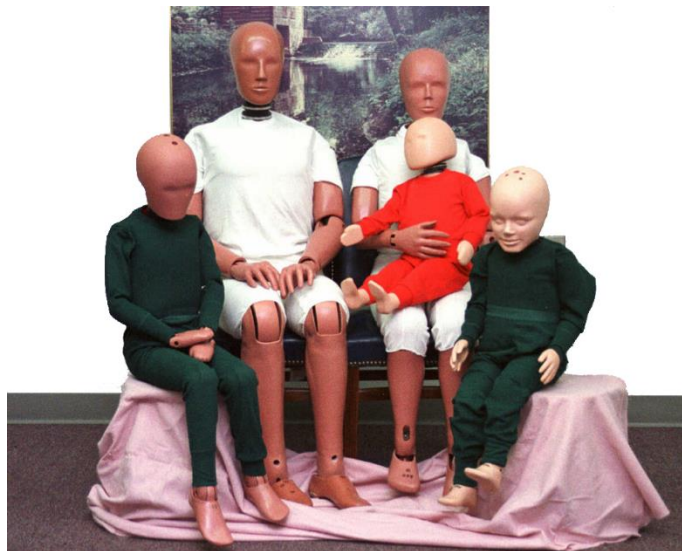
Figure 2-5 – Some members of the Hybrid III family [30]

The child dummies start to emerge with their one characteristics, correlated to the age segment that their represent.

Being more precise and more biofidelic, the dummies remains with use limitations, mainly being focused for frontal impacts.

2.2.1.4   Dummies in scope: the 80's

It was in the 80's that the hybrid III get his family. It was in the 80's that dummies use has "exploded". Such phenomena can be associated to the perception of the need of safer vehicles by the common user, from cars until aircrafts.

In the end of the 80's, the lateral impact start to be addressed, and the first lateral dummies appears: EUROSID-I and BIOSID (Figure 2-6); both dummies in 1989 in Europe and USA respectively. In fact the very first lateral dummy was SID, appearing 10 years

earlier, but being known his own limitations, that associated to the negative recommendation from ISO standard.

<div align="center">a)   b)   c)</div>
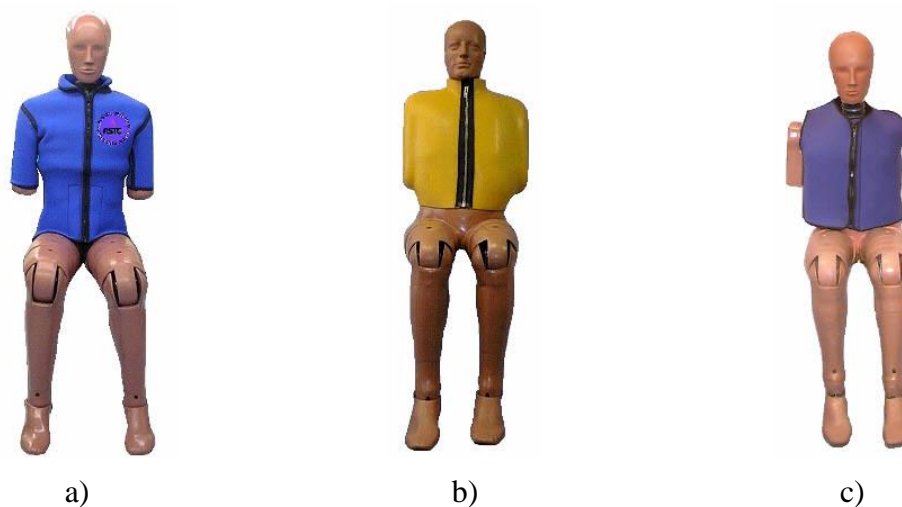
Figure 2-6 – Lateral impact dummies[29]: a) EUROSID; b) SID; c) BIOSID

2.2.1.5   *Dummies in scope: the 90's until our days*

Being the Hybrid III and the EUROSID-II the standard dummies used by EuroNCAP, from the 90's until our days some of the effort was for more advance dummies and their virtualization using computer tools.

The THOR dummy (Figure 2-7.a) was proposed for frontal impact, WorldSID dummy (Figure 2-7.b) for lateral impact and BioRID-II dummy (Figure 2-7.c) for rear impact.

Pedestrian dummies have been born, like the Polar (Figure 2-8.a) from Honda, HIII-50M (Figure 2-8.b), or the HIII-6C (Figure 2-8.c), allied to the pedestrian crash test by EuroNCAP using body forms to mimic head, upper and lower legs impacting the vehicle front.

Virtual dummies that mimic the human anatomy start to be developed, where the dummy is a more reliable representation of the human body. The virtualization itself represents a major field in terms of human modelling, being explained in the next section of the current chapter.

<div align="center">a)   b)   c)</div>
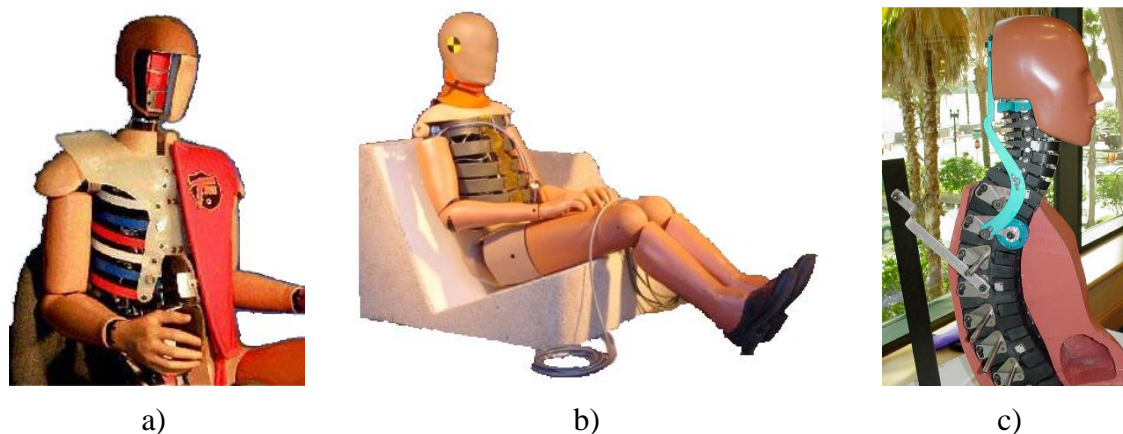
Figure 2-7 – Dummies a) THOR [31]; b) WorldSID [29]; c) BioRID-II [29]

<div align="center">a)   b)   c)</div>
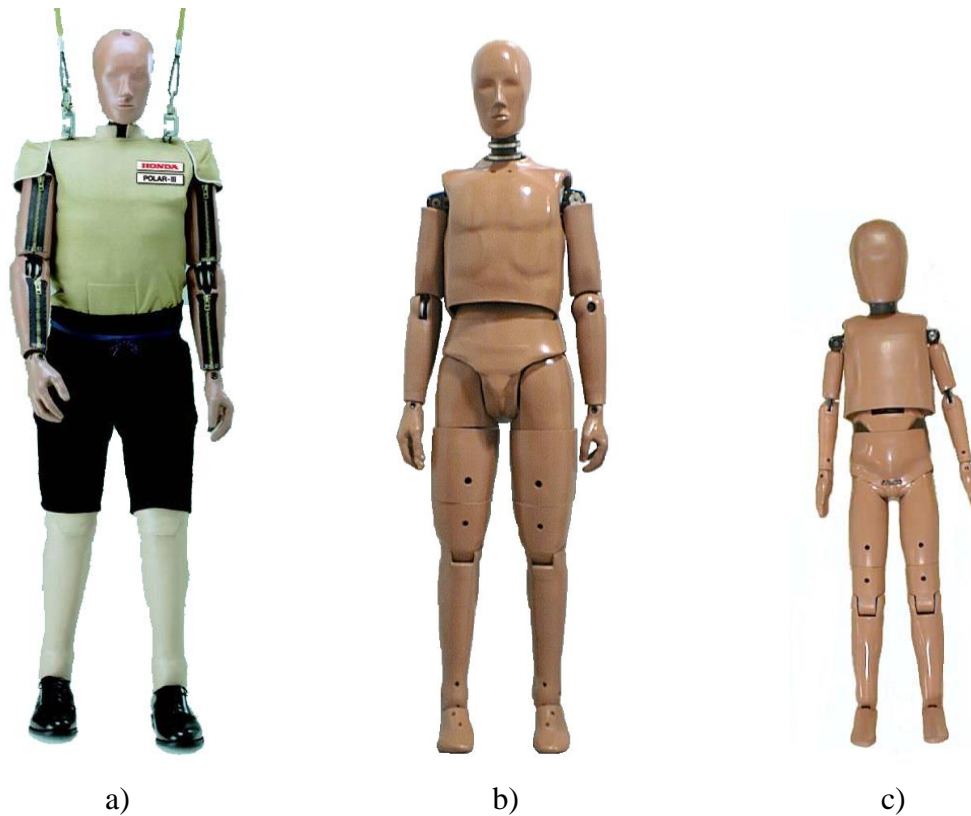
Figure 2-8 – pedestrian dummies: a) Polar III [32]; b) HIII-50M [29]; c) HIII-6C [29]

2.3   Software, emphasis in MBD

We will divide the virtual human modelling using two different approaches, the MBD and the FEM (Finite Element Modelling). Being the MBD the usual way to perform in CPU (Central Processing Unit) cost effective crash simulations, is the first methodology subject of analysis.

It's easy to find software's in the market for MBD simulation. A brief run in one major search engine using as keywords "multibody" and "software" will gives immediately thousands of results.

In terms of software, we can divide them in several big classes: academic projects, packages and add-ins, generic or focused MB software's, suits having a generic or focused MB software, and tailor-made software open or closed.

As examples of academic projects, we find e.g. Alaska [33] or Universal Mechanism [34]. Example of packages or add-ins are the COSMOS [35] for SolidWorks [36] or Dynamic Designer [37] for Solid Edge [38] and Inventor [38].

It's possible to use one suite[5] that includes several possibilities and solution to several problems or sub-applications. Following the suit philosophy, we have examples as:

---

[5] Software suit describes one collection of software for certain major use. Good examples of two suites for office usage are the Microsoft Office and the OpenOffice, both suites with a text editor, a spreadsheet editor, a presentation editor, etc.

Adams [39], several software's for different MB applications; LMS Virtual.Lab[6] [40], several software's for automotive simulation, including MB; madymo [41]; Pam-Crash [42]; or Hyperworks [43]. All these suites are real solutions for different simulation scenarios.

If the user wants to design or develop other functionalities or implement add-ins to the supra-mentioned software, he/she can use tools that give a tailor-made solution. Some of the platforms for such tailor-made libraries or software's are e.g. Matlab [44], Simulink [44], SimMechanics [44], DynaFlexPro [45], or Modelica [46], or software languages, like FORTRAN[7] or C and his variants.

The possibility to create or own specific software can be other solution, a pure tailor-made solution feat for the user needs.

2.3.1   Dedicated software

In the world of MBD software is possible to find applications made to study particular applications. We can have MBD software drawn for the human body, for cars dynamics or accident simulation, suspensions, tyres, etc.

To study the human body, software's' like SIMM [47] are offered in the market. This type of software's are indicated mainly to study the behaviour, kinematics, reactions and forces in the human movement (Figure 2-9).

A number of such software tuned for human analysis are integrated in major packages, giving to the researcher or engineering the power to study and simulate the interaction between persons and external equipment (interaction human-machine). An example of such capabilities in terms of human-machine interaction is the model to study ergonomics on CATIA V5 [48].

In commercial code we find solutions for articular scenarios like the simulation of accidents. Examples of software's for crash are madymo or Pam-Crash. This software's were validated models (Figure 2-10) and are part of the package or disposed as add-ins for model integration. Such Integration of several models and/or modules can be advantageous to similar scenarios study and analysis, for time reduction in translating models, and to avoid possible incompatibility in translating/importing models/results.

Some of these packages are suitable for modification or integration of new functionalities. Some of these new functionalities are open in the proper program, without need of external software. One example of these functionalities is presented in one package developed to Adams, the LifeMOD [49] (Figure 2-11).

---

[6] Virtual.Lab runs in the CATIA V5 engine, which means that all the applications appears to the user in an add-in appearance. We should retain that the CATIA by itself is a suit for CAD/CAM/CAE tools. More detailed information will be provided in next chapters.

[7] derived from "IBM Mathematical **For**mula **Tran**slating System".
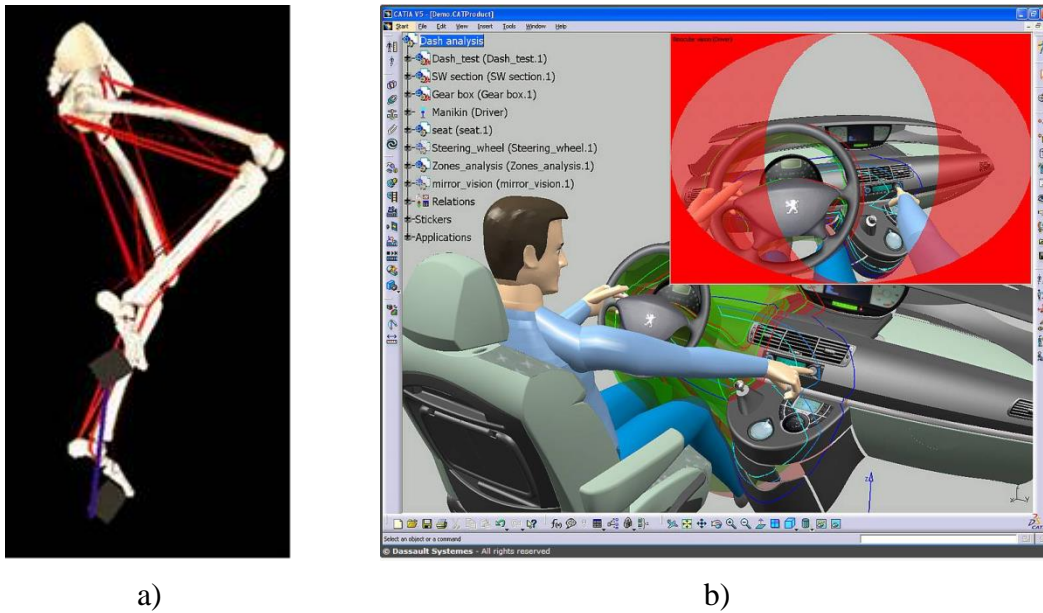
<p align="center">a)   b)</p>

Figure 2-9 – a) Pedalling model [47], b) ergonomics interaction study of human versus equipment [48]
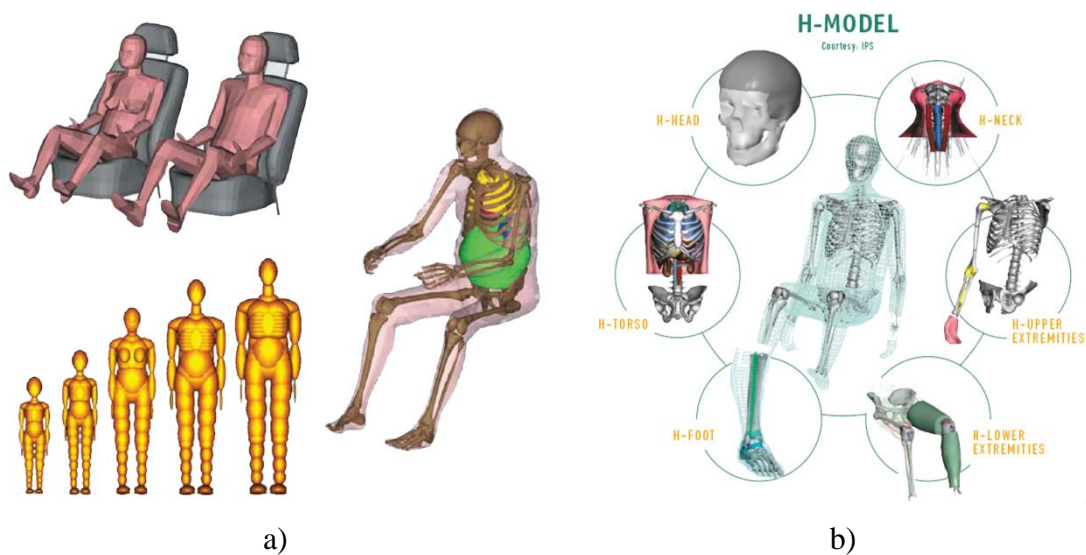
<p align="center">a)   b)</p>

Figure 2-10 – Human body models included respectively in: a) madymo [41]; b) Pam-crash [42]

The LifeMOD package is a plug-in (or add-in) made to Adams with a human body model made in several sizes and gender. It's possible e.g. to apply movements in the joins and forces in extremities and study the loads in skeleton and muscles. The software is suitable to introduce a new element in the body, like an internal prosthesis, and compare the new behaviour.

a)   b)
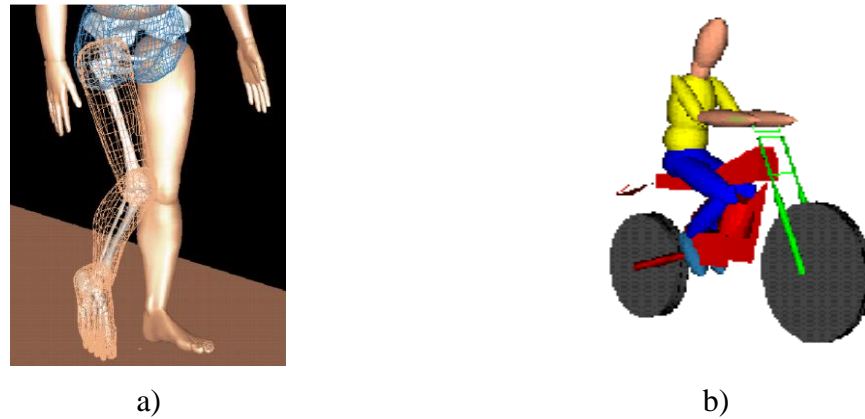
Figure 2-11 – Models using LifeMODE: a) lower extremity [49]; b) cyclist riding a moped [49]

2.3.2   Software suites

These are packages where is given to the user several tools to different tasks. The suit can have special modules or programs with tools for particular scenarios.

In the cited suits, there are several in this group, e.g. the Hyperworks suit has several modules or programs that illustrate this approach (as is in release 7):

- HyperMesh
- HyperView
- OptiStruct
- HyperStudy
- MotionView
- MotionSolve
- HyperGraph
- HyperForm
- HyperXtrude
- Process Manager
- HyperWeb
- HyperView Player

This are the modules presented in the Hyperworks version 7 (now with the version 12, the number is higher). Each model has its speciality and all together form a set of tools to help in CAE process. Note that the user can use external solvers and implement several tools to extend the possibilities of the package. This idea is illustrated in one scheme from the Altair web page, as is shown in Figure 2-12.

Figure 2-12 – A framework for finite-element and multi-body systems simulation [43]

The advantage of this type of approach is that the researcher has a number of tools ready to use in one package, what can be synonymous to faster development. Another feature in suits is the easier integration and sharing of results between parts of the package, since such integration is supported from the very beginning.

2.3.3   Tailor-made code development

To study MBD, other way is to make our individual code. Tailor-made code is a good approach to obtain solutions from some particular scenarios, some restrictions, some boundary conditions not so well implemented models or new functionalities.

Languages like C, FORTRAN, Modelica, and MatLab are powerful tolls to implement new mathematical models, or different applications.

In some cases, starting from the sketch can't be suitable. So, it's possible to implement new features, or tune standard functions from the commercial software's.

2.4   FEM dummies

Some of the previous models human models have some level of FEM modelling, like the MADYMO or the PAM-CRASH. Some have the support for such task, as the Hyperworks or the LMS Virtual.Lab Rev10 (only available after the end of the project).

Pure co-simulation when FEM and MBM run side-by-side is supported by MADYMO from long time ago with several FEM solvers.

In our case, we have been more focus in pure FEM models, since the goal is injury assessment and not crash simulations itself in the FEM simulation. That comes from several restrictions and considerations explained in next section of this chapter.

2.4.1   Dummies virtualized

With the advance in informatics and computer capabilities, the abilities of performing virtual simulations have being more and more feasible and complex. Taking in account that the 70's "Moore's law" have being roughly being applied, that shows that the capability to grow up is even more. Notice that the "Moore's law" tell us that the number of transistors in an integrated circuit doubles each 2 years. To give an idea of development, the most powerful computer cluster in the world in 1996, the "HITACHI

SR2201" has a benchmarked performance of 220GFLOPS, one actual processor, the Intel Xeon E7-4870 have a benchmarked performance of 351GFLOPS.

With such capacity, have been proved that for engineering, more and more the development phase is helped with virtual prototyping and virtual simulating. CAD, CAE and CAM tools have been pushing the development phase closer to the final product, with less physical experiments, and when those are needed, are in a final or close-to-final version. Such trend follows more and more a V-shape development philosophy.

Computer simulations have been pushed the automobile industry to a new level of safety standard, and in line with that, is natural to virtualise dummies, since the new vehicles to test are surging in the virtual world.

So, we have commercially the dummies delivered in physical and virtual choice. The dummies are found for commercial solutions, as LS-DYNA (Figure 2-13), PAM-CRASH or RADIOSS

a)   b)   c)
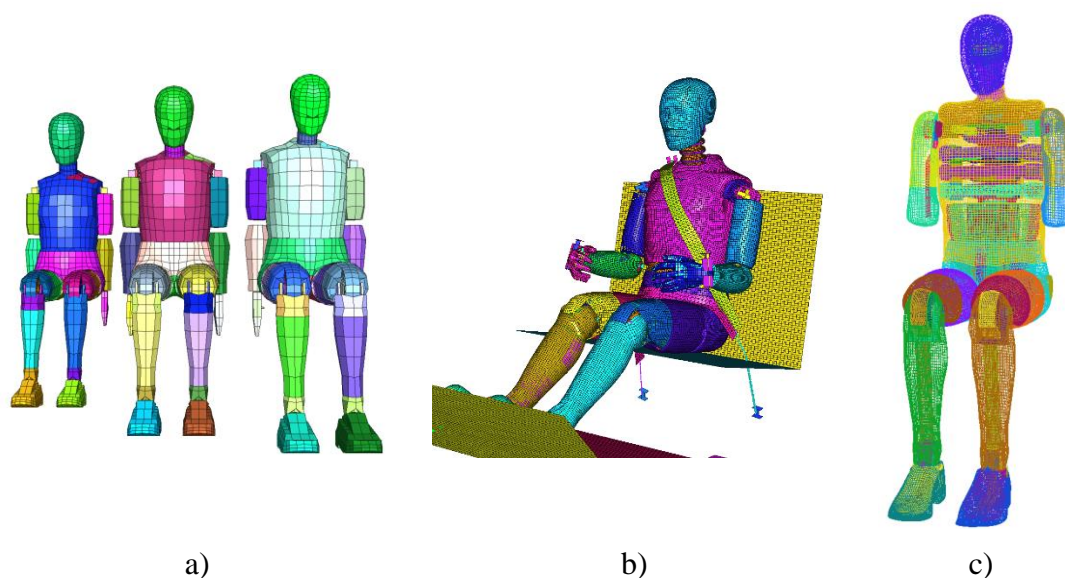
Figure 2-13 – LSTC dummies: a) Hybrid III rigid, version 1.0: 5th female, and 50th and 95th male respectively; b) Hybrid III refined 50th percentile man in sled position with sled and seat belt; c) EUROSID 2 (rendered on translucent mesh)

The virtual models are validated in similar way that the physical equivalents, but is possible to instrument them according to the user needs, not being limited in such point.

Another major tool of the virtual dummies is the laboratory crash planning, when the test can be simulated, and study best configuration, instrumentation and acquisition systems. Such approach results in a direct reduction of cost in the experimental phase of the project.

2.4.2   Human models as dummies

More than computer a replica is desirable that the computer models of dummies get am evolution closer to the real human anatomy and physiology. In this group we have two major groups of models: the articulated and the deformable models. We will focus in the deformable in FEM approach.

The FEM approach gives against the MBM the advantage of detail and precision in an organ level, relatively to the human been. Such advantage comes with a high price, the more need of computer resources, where the time scale of CPU used is different in several

orders of magnitude (a full human body model can be simulated for a crash scenario in a desk computer in less than $30min$ for a time frame of $5s$, a head model under impact will take in same computer as much as $2h$ for a time frame of $50ms$)

That high computer cost means that the use of the full body detailed FEM are too time consuming, not being now profitable for a fast analysis. In opposition, the use of body segments for "instantaneous" analysis is feasible without high computer resources.

Two major models rise: THUMS [50] (Figure 2-14) and HUMOS [51] (Figure 2-15).

a)   b)   c)
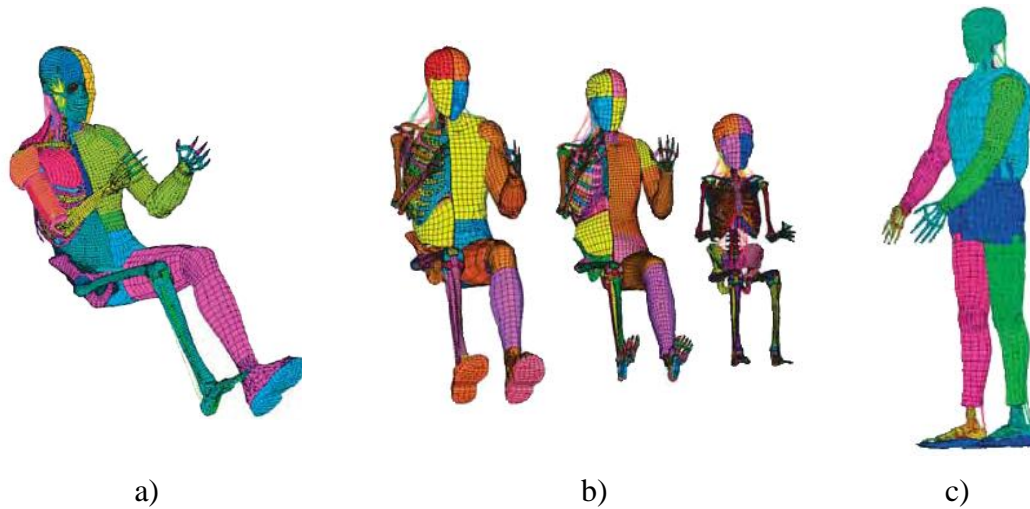
Figure 2-14 – THUMS model: a) 50th male [50]; b) family [52]: AM50, AF05 and 6-year-old child; c) AM50 pedestrian model [52]

a)   b)
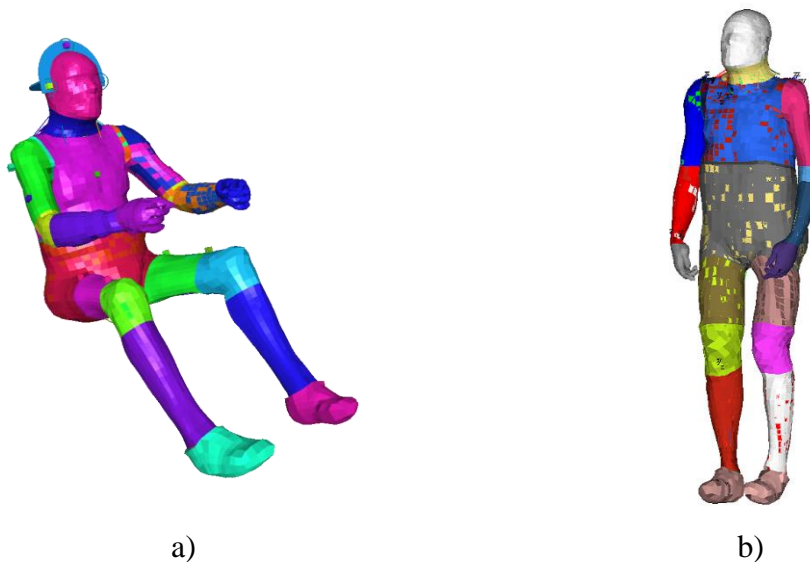
Figure 2-15 – HUMOS2 in RADIOSS: a) drive position; b) stand

In the HUMOS models, one cadaver was frozen in drive position, sliced and images acquired. Then it was reconstructed on 3D, including major human body organs: bones, flesh, skin, lungs, heart, etc. One stand version was done too. Both models are validated according with the standards and the data available.

But with so large level of details, these models sustain some limitations, like some poor material definitions, some no deformable bodies and lack of damage models for some soft

tissues [52]. The use of such models for loads that not the fontal, lateral or rear impact are suitable, but sometimes is found behaviours that can be not-biofidelic.

2.5 Dummies and MYMOSA: some considerations

Since the work to develop was inside of a European project, some decisions have been made having the consortium in mind and consortium advices.

It was decided from the beginning the need to develop our-one human MBM dummy, for PTW use. With that in mind, a translation of a dummy was a no-go path.

Being the gross work of the WP1 inside LMS, was decided that can be one advantage if all in the consortium have been using the some MB software, so was decided to use the LMS Virtual.Lab, being the versions to use always the last released (first version was R7B and the last used was R9). That choice has implied some initial advantages and constrains: a fast learning curve from the software bases (Catia V5), parametric, co-simulation with Matlab and Simulink for possible close-loop control. As disadvantages, the lack of any dummy model, the lack of a ellipsoid contact formulation, and the high memory cost of the CAD-contact, implying the move to a 64bit platform from the very beginning (that have been translated one advantage when was given multithread solver support for 32bit only platforms). But the major potential advantage is the easy flow of information and model's integration inside the WP between researchers (Figure 2-16).
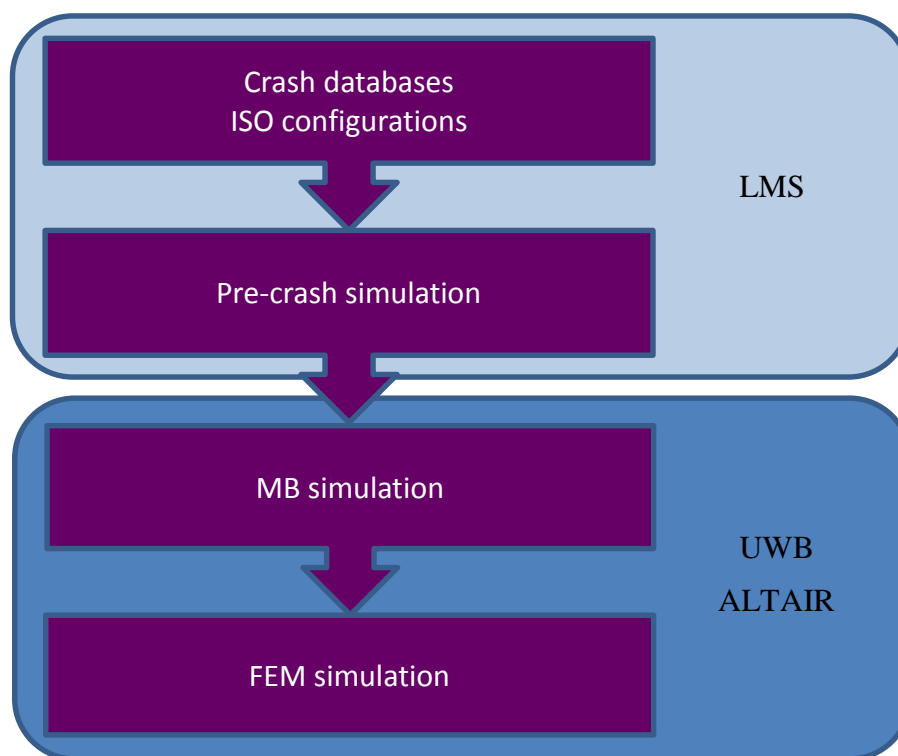
Figure 2-16 – Work diagram on MYMOSA WP1

For the FEM human model, the choice of the HUMOS against the THUMS was based in several facts: we have already a Hyperworks license, Altair was a consortium partner giving access to HUMOS model and several other dummies models, and a large secondment in the work plan was already planned for Altair France (on the former Mecalog facilities) allowing full support and formation on the model adopted and respective software.

3

Anatomy, physiology and trauma

We have seen in previous chapters several aspects concerning the human modelling, how such models are used in crash accidents. In the motivation section was mentioned the role of the particularities of the human body. Such particularities in our case can be summarized as anatomy, physiology and trauma.

This chapter is intended to give a first approach of the global definition of each concept.

Particular emphasis is applied in our final propose, PTW users, since the majority of the literature was done considering, or having in mind car occupants, with the correspondent active and/or passive constrains.

Detailed information for each body segment will be presented in the following chapter. Some sub-concepts or aspects concerning some part of the human body will not be include in this copter view of the definitions, but will be enclosed in the respective body-segment sections.

3.1   Introduction

In this chapter is exposed the basic notions concerning principles of anatomy, physiology and trauma related to PTW users and how they are linked between each other when an incident occurs. This section is just to give a copter view of some medical point-of-views approach of the accidentology involving PTW users.

After a brief explanation of several notions, is presented a detailed analysis of each body section, and respective joints.

All the data presented in this section are by default for an adult male 50th percentile, exceptions will be pointed.

3.2   Basic concepts

To a better understanding of the general concepts involving the human anatomy, physiology and trauma, several introductory notions are presented. Is presented either how to "read" some medical language by engineers.

Some concepts when related directly with certain body segment will be presented in the respective body chapter. Some more in deep definitions when necessary concerning some body part will be explained there in appropriate context.

3.2.1   Motorcycle exposures

Some key aspects of the over exposed have been pointed in the section 1.2.1. In fact, is notorious to anyone how different is a PTW from a car in several aspects, starting in the number of wheels, until the frame philosophy. Even a convertible have a roll-bar feature at least in the windscreen frame. In opposition, taking out the expectation of the retired BMW C1 (Figure 3-1.a), the most typical external protection in a PTW found in a PTW is the "Highway Bars", "Crash Bars" or "Engine Guard" (will not be addressed any favour or contra argument referring such safety accessory, Figure 3-1.b).

a)   b)

Figure 3-1 – a) photography of a BMW C1 [59]; b) PTW with Highway Bars", "Crash Bars" or "Engine Guard" [60]

Other issues that can increase the PTW exposure are in or around the road itself. Obstacles, signalization, road protection or the road itself can be present to the PTW as hazard, but totally inoculum for a car.

The PTW itself have dynamic proprieties that increase or triggers itself the accident. The called vibration modes of the frame (shared by the bicycle and the PTW, Figure 3-2) can initiate an uncontrolled scenario, when the driver without or even with experience, will lose totally control of the vehicle and the unexpected will be expected… the accident arises.
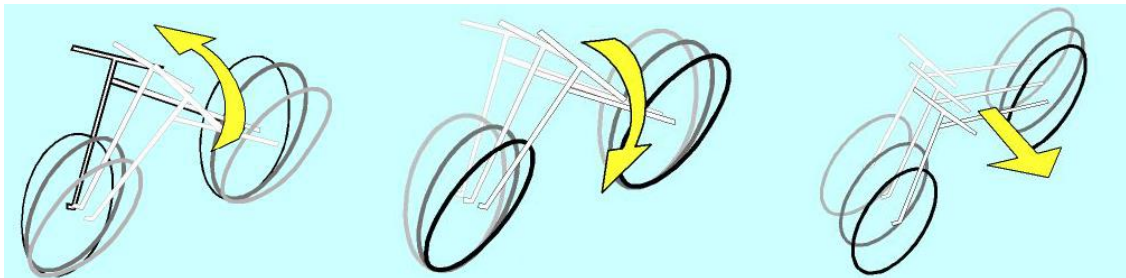
Figure 3-2 – Motorcycle vibration modes: stable capsize at low speed, unstable capsize at low speed and capsize at high velocity (adapted from [26])

PTW without ABS or traction control will be in particular hazardous in slippery conditions or aggravated in case of reckless behaviour. Some example is the heavy braking only with the rear tire. If the driver in such braking situation not falls down, he will not be able to stop anyway in a reasonable distance (very low deceleration, from low friction added from low mass from the mass transfer during braking). As opposite example, a hard brake only with the front wheel will trigger a quick mass transfer to the front wheel, the maximum deceleration is achieved, but the rear wheel will lose contact with the floor, flipping over and failing down. In both cases a ABS system with brake assistance will avoid wheel block and over brake mass transfer, not matter what wheel is braked by the driver (the system can have particularities or variations from brand to brand, or from segment to segment).

3.2.2   Injury evaluation

One of the issues in emergent situations is a simple way to define priority of patients and how to prepare medical services to receive a certain number of persons with different clinical problems.

In hospitals is usual to have a triage systems to access patient priority's to be attended by a doctor. The triage can be e.g. divided in emergent, very urgent, urgent, low urgent and not urgent, being observed respectively usually with no waiting time, less than 30 min, and so one. For emergent situations, the personnel have to score and set priorities depending with each person situation. That is important to optimize the medical cares from the very first moments.

In the limit, the optimum scenario is to bring the hospital to the accident scenario (Figure 3-3). More and more the first line of medical cares is taken place in the local of the accident. The key definition goes on the concept of the golden hour, the time frame that embraces the first minutes after the trauma to occur and the very first medical cares and respective interventions, being in the limit the difference of certain injury to be fatal or be totally recovered.
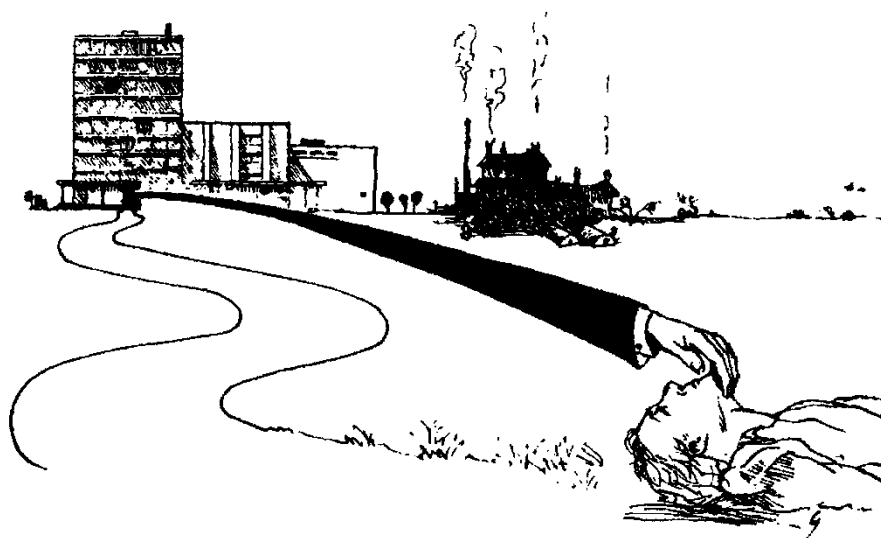
Figure 3-3 – Illustration concerning care after a big trauma [61]

For communications between paramedics' teams and hospitals, is needed to have a clear and explicit way to communicate patients' status in a fast and profitable way. Two examples of codes used are the Abbreviation Injury Scale, or AIS, and the Injury Severity Score, or ISS. Both scales are clear and explicit, being tabled in a standard way, giving easy communications between ground and central teams, no matter their background or origin.

It's clear that to evaluate the severity of one or more injuries, it's needed a scale to quote the severity of the sum of the damages [13]. These scales are used to evaluate the gravity of persons, when involved in an accident.

3.2.2.1   AIS

The standard AIS [13, 14], first developed in the year 1971 as a system to define the severity of injuries throughout the body. From his very first version, was subject of several reviews and the version from 2004 gives an score of seven (7) marks, going from zero (0) until the six (6), were the zero means non-injury and the 6 means an untreatable injury.

The rank is given by body sector, meaning that a person can have distinguished values in all body, depending of injury level in each area.

As important remark, the AIS scale isn't a linear scale. The non-linearity of AIS means that making averages from such score don't have any sense, being completely wrong doing such maths.

3.2.2.2   ISS

The ISS scale evaluates better patients with multiple injuries. The principle of the ISS began in the division of the body in 6 parts or sections: head/neck, face, chest, abdomen, extremities including pelvis, and external (i.e.: burns, lacerations, abrasions, contusions). After such division, is applied to each part the scale AIS. The ISS it's the result of the sum of the squares of the three most severity injured (most ranked) regions.

The scale ISS goes from zero (0) to 75 (3 times the value 5, corresponding with critical). If the value 6 is recoded to any part, the ISS is automatically the maximum, 75. The

psychological number in the ISS scale is the 15, being considered the frontier to a major trauma.

3.2.2.3 AIS and ISS remarks

This scales don't considerer aspects like the long-term consequences, lost in the income, and so on. Other aspects are that the severity of the trauma or their score don´t reflects the physical load that made that. We must retain in mind that this scores are manly to define priorities and to allocate medical care in emergent situations.

It's proper to said that this type of scores are useful to give the result of the evaluation of the injury, but don't give all the information needed.

One solution to minimise this limitation, are the use of other type of information, like the use of cadavers, animals and so on to compare and try to adjust the relation cause and effect.

3.2.3 Injuries by human body section

The type of injuries is not all the same, it depends' on the loaded part of the human body, gender, age, and many others factors. The own mechanical limits are not the same and the consequences of a load can be the damage by itself.

In terms of biomechanics, a body can be divided in several systems: locomotion (passive and active), digestive, respiratory, neurological, endocrine, skin, and so on.

Each major group have their mechanical proprieties, that proprieties have changes from organ to organ.

Other question that applies in the analysis of injury in humans, are known what is the limit. This limit can be achieved by a big load, like supra-mentioned, but can be reached too by a large displacement or quickly movement of one joint or body section. This will mean that anthropomorphic data can give several natural limits, meaning so that anatomical and anthropomorphic data must be considered together, always when it's possible [15-18].

3.2.3.1 Axis movements and orientations

In anatomy, the type of angular movements unlikely to the mechanical systems, have different names for the directions we use to look to the human body or one of his sections, the same is for angular movements.

The Figure 3-4 illustrates the several names used to identify how a section in certain direction is called. The most found directions are usually the lateral aspect (side view), anterior aspect (rear view), anterior view (front view), medial aspect (view from the middle plan between lateral aspects), superior view (view from above) and inferior view (view from button).
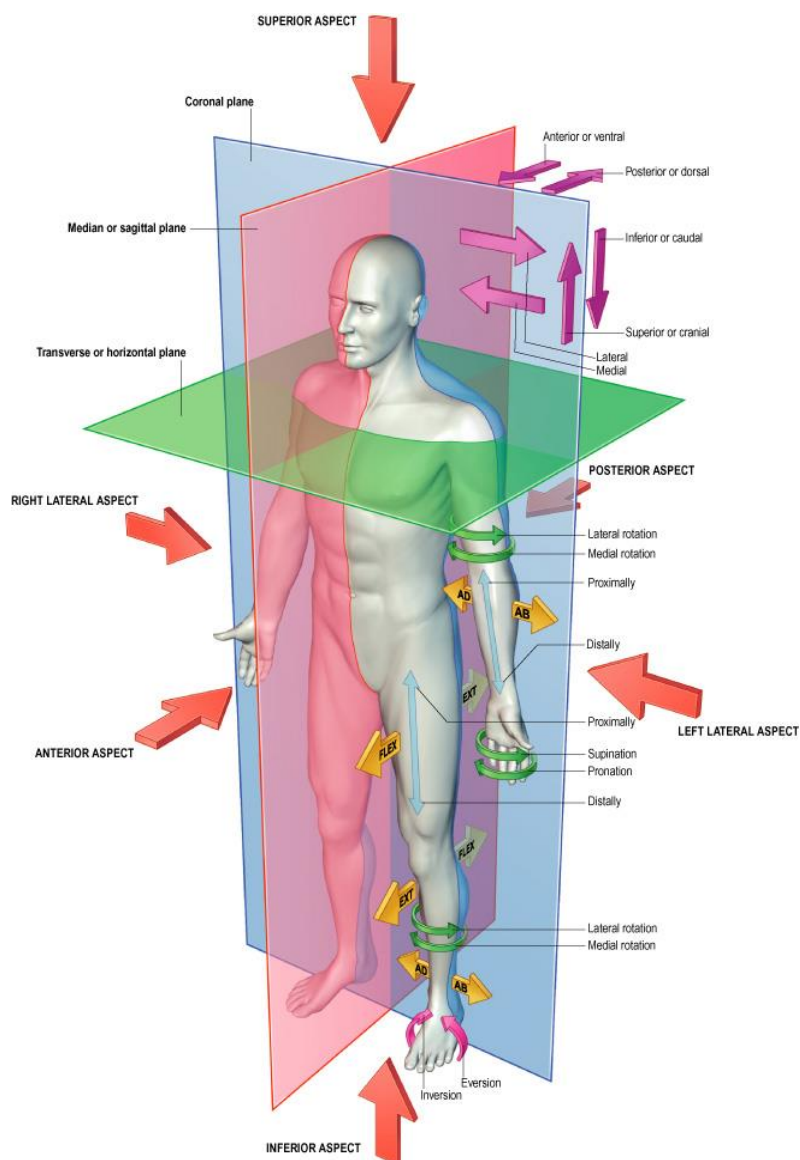
Figure 3-4 – Anatomical planes and orientations [62]

3.2.3.2 Skeleton

The main structure of the human body is the skeleton. The bones that compose this structure have several objectives, e.g.: sustain and protect.

The bone is composed mainly by trabecular and cancellous[8] (Figure 3-5). These two parts are the perfect joint to a structure light and straight. The main directions of the trabecular bone are optimized to the daily loads. Such optimization means that the strength of the bone depend by the type occupation, type of alimentation of the person and direction and type of solicitation [17].

---

[8] The cancellous is also mentioned as spongious bone.

<div align="center">a)   b)</div>
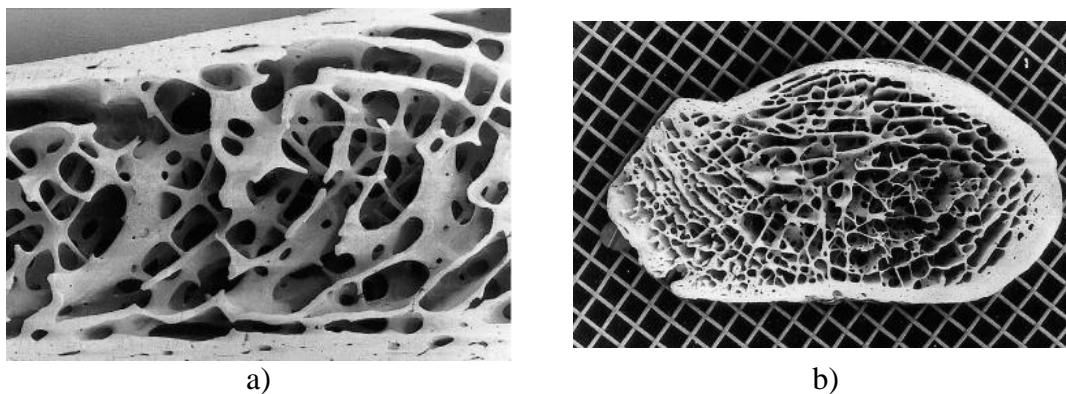
Figure 3-5 – a) Vertical section 2 cm below the anterosuperior border of the iliac crest (to the right of the field view as oriented; female, 42 years). The cancellous bone consists of intersecting curved plates and struts. Osteonal (Haversian) canals can just be seen in the two cortices at this magnification; b), Transverse section, femoral neck (male, 45 years) viewed from the distolateral aspect towards the femoral head, showing the predominant pattern of curved intersecting plates in the cancellous bone. [62]

The fact of the bone is a live structure, gives to the bone the ability to "learn" and be adaptable along the time to different realities or load conditions.

If someone start to ride horses in a regular bases, passed a few years the shape of the legs are changed, a reflection of the change of shape of the femur, by the new type of load (a person seated long hours riding horses).

The same phenomena it's observed in the differences presented in the bones of the right and left arm of a tennis player, or in the shortness of certain dancers.

Sometimes, these phenomena are seen in the presence of prosthesis, but in this scenario, the bone "can see" that are not so used, and can lower their density in the regions with a defect solicitation (compared with the anatomical load), phenomena known as bone reabsorption. These phenomena can result in catastrophic fault of the new system bone-prosthesis.

The capacity for the re-adaptation of the bone is a slowly process, not compatible with the changes occurred in a short time period. But if a lesions occur, such lesion can be corrected or fixed, the bone have the capacity to recover (it's possible to see the cicatrix or bone scare after more than a decade).

Other aspects from the bone stiffness, comes from the age, genre, life style, alimentation, previous lesions, etc.

Several bones (our groups of bones, Figure 3-6) are presented. Some of their mechanical proprieties, injury classification and model are presented too.
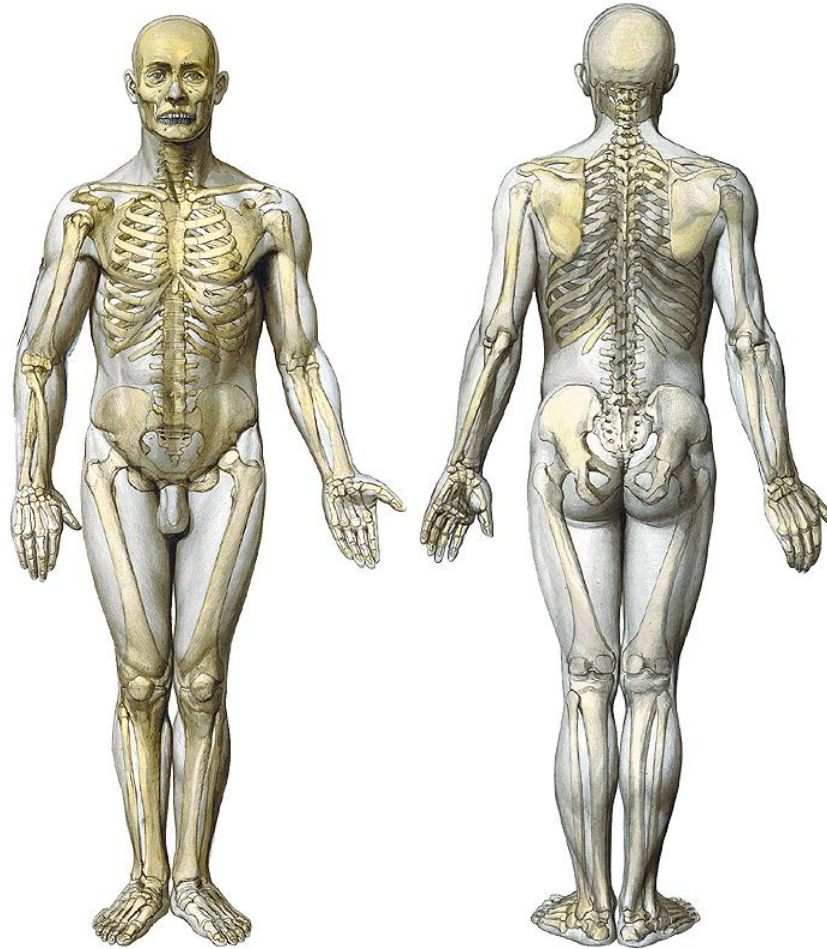
Figure 3-6 – Skeleton diagram (dorsal and ventral views) [63]

3.2.3.3   *Muscles, tendons and degrees of freedom*

The muscles and tendons work in the skeleton like actuators and cables in a machine. Are from their responsibility to make movements, or avoid them. Their together with the bones, can produced articulated and useful movements. To articulate each join, we must activate a certain quantity of muscles, but some movements are impossible: or the positions are not reachable, or the movement obliges other movement [17].

To each join, we have a correspondent certain number of degrees of freedom. Typically, the joints are simplified to perfect joints, meaning that only is presented the principals movements, being neglected the secondary movements or certain joint behaviour or interferences.

Extreme loads can cause injuries in one or several systems. Is common to see players e.g. from football, stopped by a few weeks until months, caused by lesions in the ligaments and muscle fatigue or rupture.

In extremes scenarios, the opposite can occurs; the excess muscle load causes the bone failure.

In all scenarios, if the anthropomorphic values are considerable crossed, this means that something will be by sure injured.

3.2.3.4 *Soft tissues*

The most protect and fragile parts of the body are mainly soft tissues. But their protection isn't suitable for some limit scenarios. In some cases, the soft tissues protection isn't enough and the consequence can be fatal. Some organs don't support great levels of accelerations or contusions.

The skin is the most exposed organ of the body, and the first natural layer of protection to our body. This organ must be protected from be injured in an accident. A great surface of skin burned by friction with asphalt can be one more problem easy so minimise with appropriate clothes. It's well known the advantages of leather clothes between PTW riders for their great performance against abrasion in asphalt surfaces.

Details concerning certain major organs are analysed in detail on the respective chapter where such organs are the brain, liver, heart, lungs, etc.

4

Body Segments

After the brief review in the chapter 3, where some basic concepts concerning the human anatomy, physiology and trauma, some more detailed analysis is presented divided in terms of body segments.

Data from literature is compiled and presented as needed, being this chapter as base to detail analysis of the simulations, relating quantitative results (accelerations, deformations, energy, etc.) with qualitative variables like the described in AIS (subchapter 3.2.2.1).

The body is so segmented in 6 groups of segments: head, spine, thorax, abdomen, Pelvis and lower extremities, and upper extremities.

Is also illustrated in each section of this chapter the parts of the used models: the implemented MBM (explanation and implementation in chapter 6), and the FEM used, HUMOS2 [51].

4.1   The Head

The head is the upper part in the body (Figure 4-1). In this part we can found the majority of the sensorial organs and is the enclosure of our brain too. That means that its position is very important, but very exposed to external risks too. The head is supported by the neck. The head as a totally can be viewed as head and face.
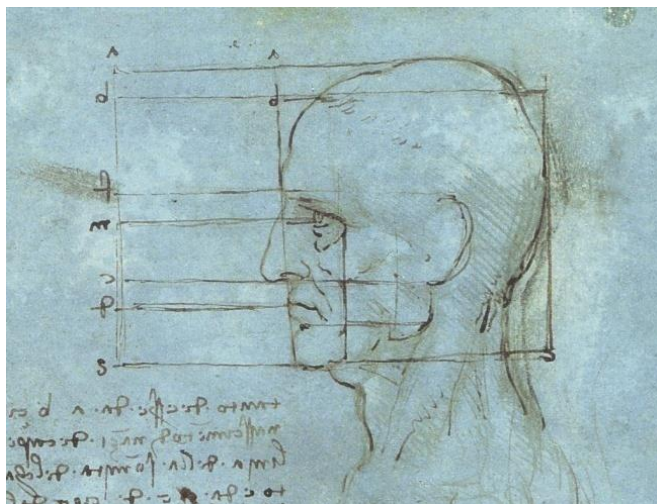
Figure 4-1 – Proportions of the head (from Leonardo da Vinci)

The head is one of more exposed member of a PTW driver, with the arms and legs. The head with the neck and thorax are the parts that have a fatal AIS 6 score. That gives immediately why his so important to understand what happens in this part of the body and to protect. To understand better why some governments apply the obligation to use homologated helmets, it's important to understand what are evolving in this part of the body.

Injuries on the head in traffic accidents involving PTW drivers represent an estimation of 44.5% of total facilities in these class of road user.

4.1.1   Anatomy

The human head can be looked like a multilayer's structure. The first interface with the exterior is the scalp (the hair isn't considered), and there, we have the skull and the meninges. In the interior it's the cerebrum [17]. Such view comes from the fact that the face can be analysed as a sub-part of the head.

The scalp is a layer with 5 to 7*mm* of thickness. Consist in the hair-bearing skin, a subcutaneous connective tissue layer, and a muscle and fascial layer.

The skull of an adult is a complex structure, composed by several bones fused together (Figure 4-2). The shape, resistance and thickness can vary from person to person. In the birth, the skull bones are not fused yet, giving to the cranium a certain level of flexibility

In one adult, the only bone in the skull that has freedom of movement is the mandible.
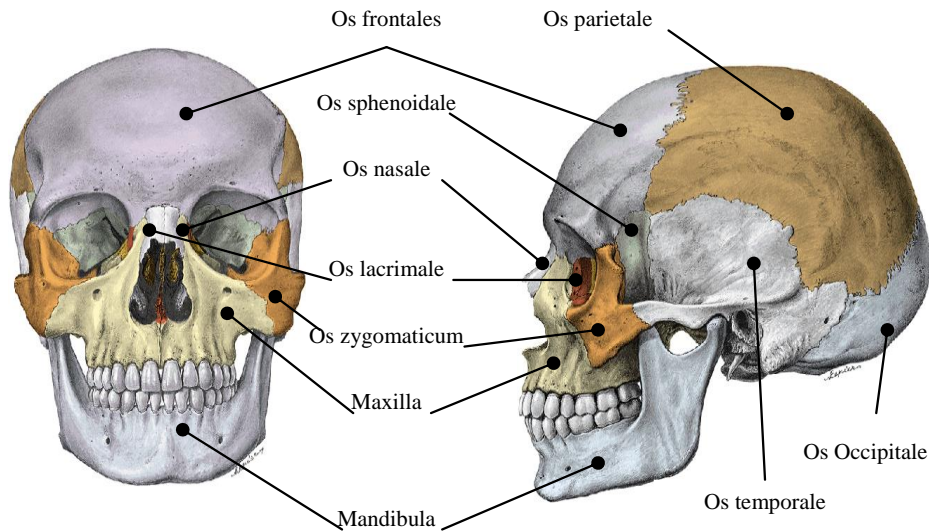
Figure 4-2 – Frontal and lateral vision of the cranium [63]

The inner surface of the cranial vault is concave with an irregular plate of bone forming the base. This base plate contains several small holes for arteries, veins and nerves as well as a large opening (foramen magnum) thought witch the brainstem passes into the spinal cord.

Three membranes called the meninges protect and support the spinal cord and the brain and separate them from the surrounding bones (Figure 4-3). From the outside to inside, we find the dura mater (Figure 4-4), the arachnoidea mater, and the pia mater.
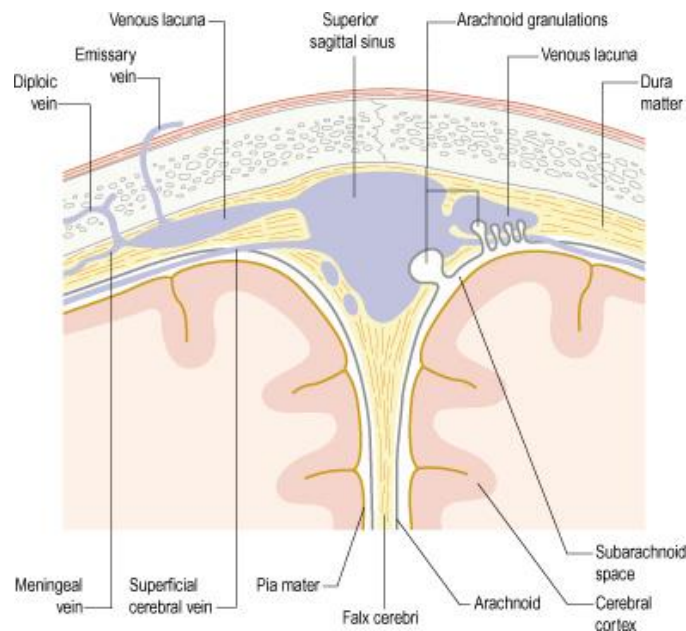
Figure 4-3 – Coronal section through the vertex of the skull showing the relationships between the superior sagittal sinus, meninges and arachnoid granulations [62]
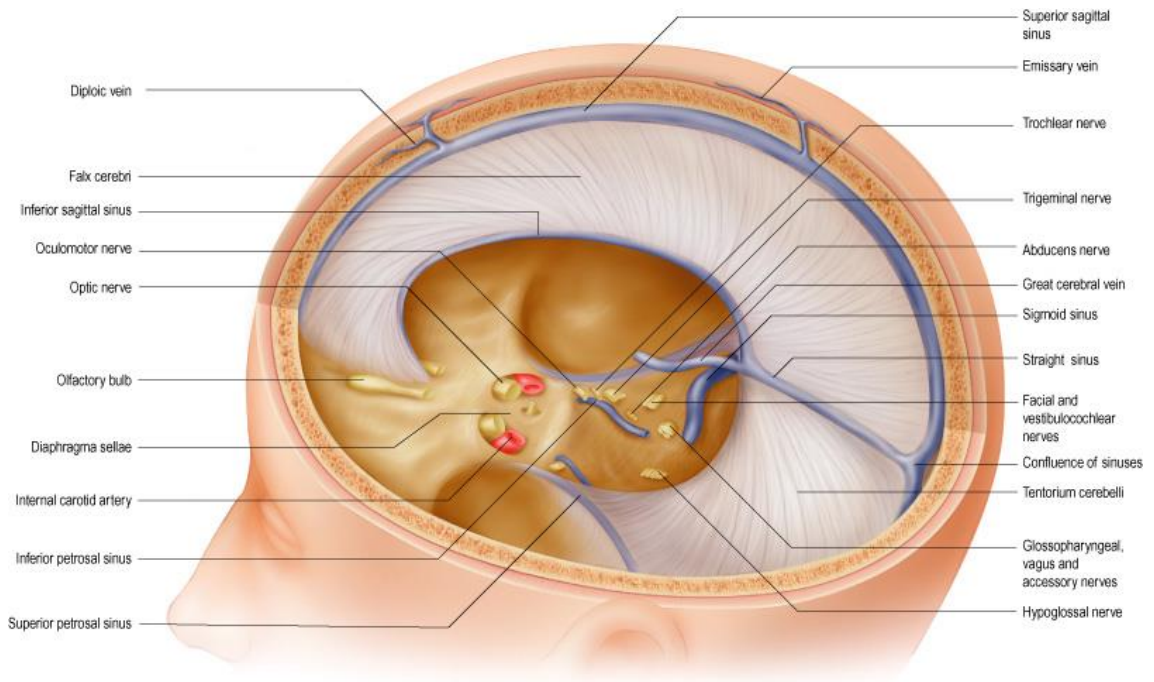
Figure 4-4 – The cerebral dura mater [62]

The dura mater is a tough, fibrous membrane, while the arachnoid mater resembles a spider-web. Both membranes are separated by a narrow space, the subdural space. The subarachnoidal space separates the arachonoidea mater and the pia mater. Cerebrospinal fluid fills the subarachnoidal space and the ventricles of the brain and thus cushions the brain from mechanical shock.

The way that the head protects the brain and how the brain can moves inside the skull is relevant to understand how the brain is exposed to overloads in scenarios of big accelerations (negative or positive, translational or rotational)

4.1.2   Head dimensions

The general characteristics of the head are listed in the Table 4-1 and Table 4-2.

Table 4-1 – Head volume and mass [54]

Volume	$10^{-3}\,m^3$	4.337
Mass	kg	4.137

Table 4-2 – Coordinates for head centre of mass, inertial and respective orientation according with
         anatomical axes, and joints coordinates [54]

		X	**Y**	**Z**
CoM	$10^{-3}\,m$	8.4	0	31
I	$10^{-4}\,kg\,m^2$	200.271	221.546	144.552
I axis rotation	X	36	90	54
	Y	90	0	90
	Z	126	90	36
head-neck	$10^{-3}\,m$	-13	0	-25

4.1.3   Head movements

The movement of the head is based on the neck articulations. The interaction between the head and the neck will be simplified in our study to a spherical joint, and the neck considered as a rigid beam. The movements done by the neck are simplified in two points, upper part of the neck (after explained) and lower part (by definition, the joint between the C7 and T1).

The natural resistance to the head movements is described in the curves in the Figure 4-5 and Figure 4-6 for the flexion-extension and lateral extension respectively. The head rotation stiffness was arbitrated as explained in future chapters, taking in consideration the natural limits.
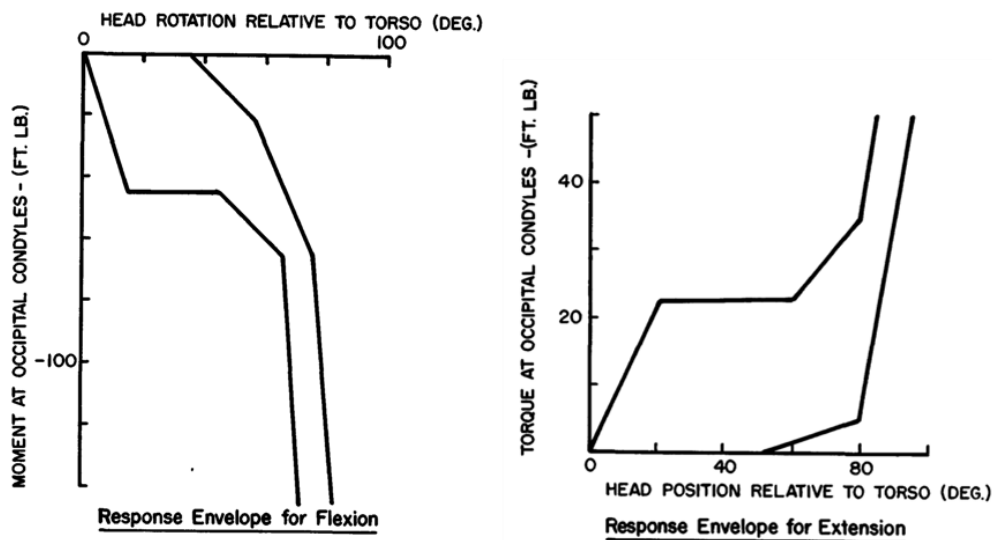
Figure 4-5 – Head resistance to flexion and extension envelops [54]
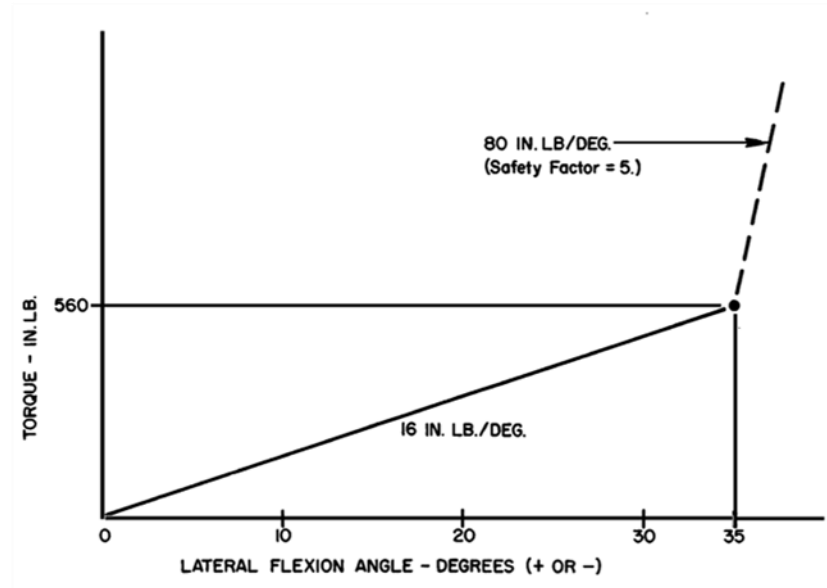
Figure 4-6 – Head resistance to lateral flexion [54]

The natural range limits of the head motion are listed in the Table 4-3.

Table 4-3 – Range motion of the head [64]

Type of motion	Representation	Rotation [deg]
Flexion		60
Hyperextension		60
Lateral flexion		40
Rotation		78

4.1.4   Head models in our work

In our work, 4 head models have been used: 1 on the MBM and 3 in FEM.

4.1.4.1   MBM Head

The head in our MBM is a rigid body (Figure 4-7), with the centre of mass defined according to the head referential axis, as the definition of the body inertia. The geometry was taken from a 50th percentile mannequin, and tessellated for contact proposes.

a)   b)
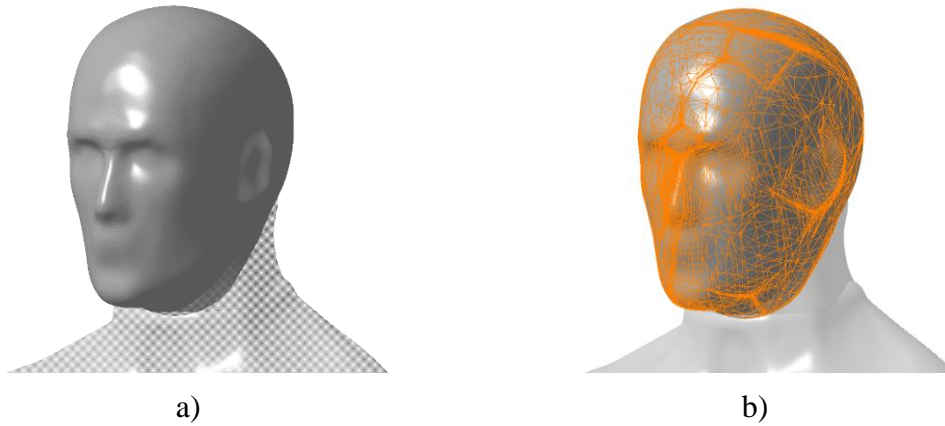
Figure 4-7 – MBM head a) geometry, b) geometry with tessellated surface for contact proposes

4.1.4.2   FEM Head

For the injury assessment, the HUMOS2 head's model was used (Figure 4-8). The model includes the scalp and face, cranium with mandible (with jaw articulation), nose cartilage, and brain (Table 4-5).

a)   b)
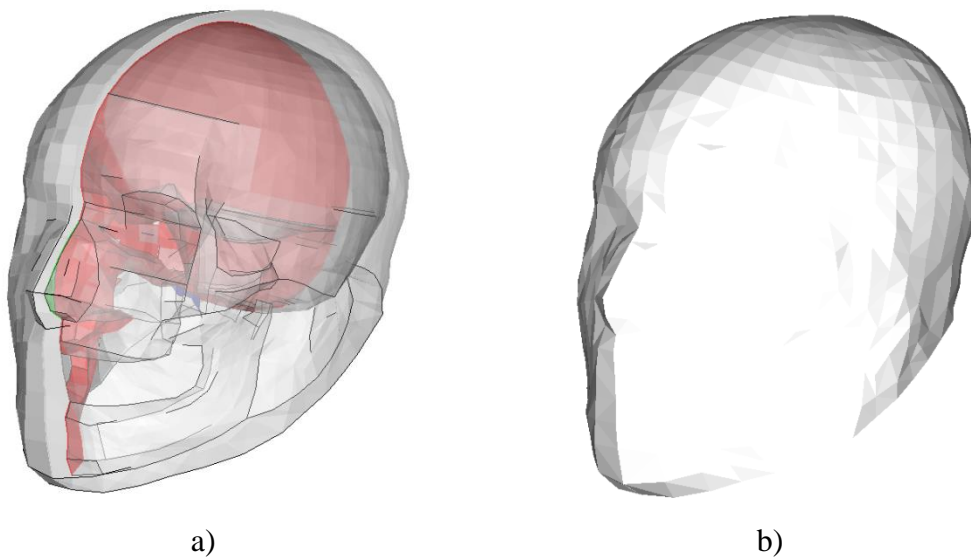
Figure 4-8 – HUMOS2 head a) section view, b) outside view

The brain is coupled to the skull by spring elements, mimicking the meninges. The head have also in his CoM one tri-axial accelerometer.

The head model in a first analysis, have a few visible limitations seen a priori. We have the lack of teeth and also the lack of mouth overture. The lack of teeth can point to some bizarre jaw movements. The lack of mouth overture points also to constrain on jaw opening, since the mouth will be always closed. Such limitations in the head comes from

the development, since probably they have in mind typical automobile crashes, since usually the occupant is retrained by a seat belt and/or an air bag, not being subjected to direct impacts where the mandible is loaded in such way that will over-closed or open.

Table 4-4 – List of head parts in FEM, their type of mesh and respective model formulation.

Head part	mesh type	Formulation
Skull / mandible	Shell	Johnson-Cook plasticity
scalp / face	Hexahedra	Generalized Maxwell-Kelvin-Voigt (Visco-Elastic Foam)
brain	Hexahedra	Boltzmann (Visco-Elastic)
nose cartilage	Shell	Elastic Material
skull occipital condyle	Shell	Elastic Material

Two other head models have been used for comparison proposes: HYBRID III (Figure 4-9) and the pedestrian crash test head (according to the Euro NCAP pedestrian test protocol [65], Figure 4-10). The role of such models will be explained in chapter XXXX (page ###).

a)   b)
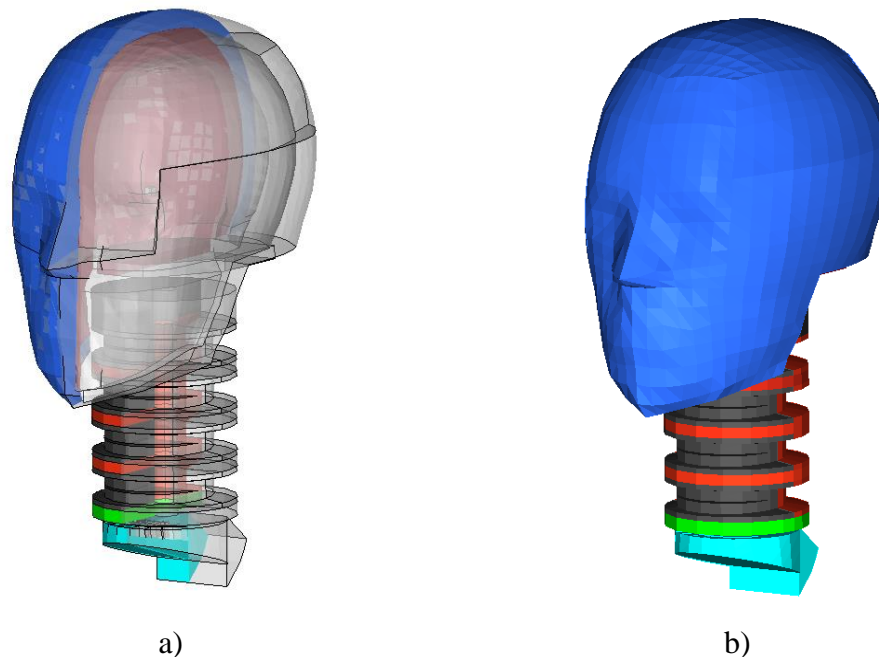
Figure 4-9 – HYBRID III head and neck a) section view, b) outside view

The HYBRID III head is also with the neck, since that in the study where the head is needed, the neck effect was also included. The neck of the HUMOS2 is presented in the section about the spine (4.2.1, p.60)

<div align="center">a)   b)</div>
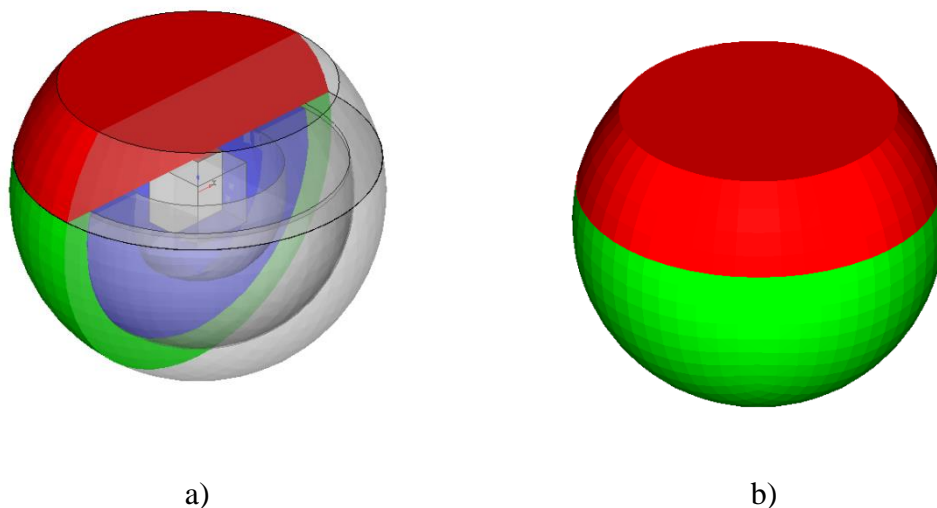
Figure 4-10 – pedestrian crash test head (Euro NCAP) a) section view, b) outside view

4.1.5   Injuries and associated mechanisms

The type of the injuries can be presented by the follow list [17]:

- Skull injury
  - o Fracture
    - ▪ Facial skull
      - Nasal bone fracture
      - Maxilla fracture
    - ▪ Skull
      - Vault fractures
      - Basilar fractures
  - o Soft tissue injury
    - Laceration
    - Contusion
- Brain injury
  - o Focal
    - ▪ Hematoma
      - Epidural hematoma
      - Subdural hematoma
      - Intracerebral hematoma
    - ▪ Contusion
      - Coup/contre-coup
  - o Diffuse
    - Concussions
    - Swelling
    - Diffuse axonal injury

Other score needed is the classification LeFort (Figure 4-11). This scale evaluates the type maxilla fracture.
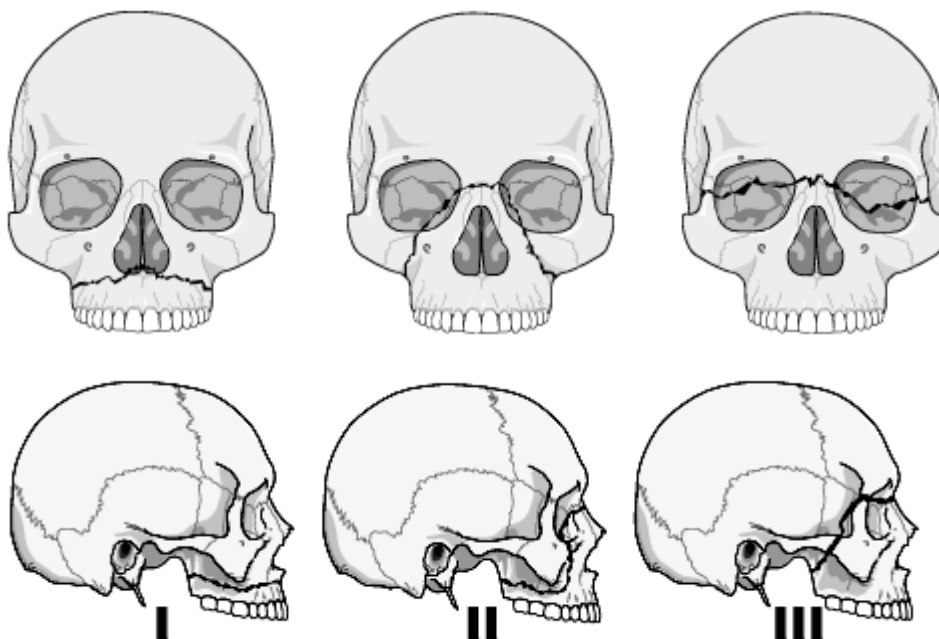
Figure 4-11 – Three types of facial fractures as classified by LeFort [63]

The classification of head injury according with the AIS is presented in the Table 4-5.

Table 4-5 – AIS classified head injury [17]

AIS code	Description
1	Skin/scalp: abrasion, superficial laceration Face: nose fracture
2	Skin: major avulsion Vault fracture: simple, andisplaced Mandible fracture: LeFort I and II
3	Basilar fracture Maxilla fracture: LeFort III Total scalp loss Single contusion cerebellum
4	Vault fracture: complex, open with torn, exposed or loss of brain tissue Small epidural or subdural hematoma
5	Major penetrating ($> 2cm$) Brain stem compression Large epidural or subdural hematoma Diffuse axonal injury
6	Massive destruction of both cranium and brain (crush injury)

But what are the loads needed to produce this type of injuries? Studies made in cadavers gave some information's. The generality of the tests, the impact response were described in terms of head acceleration and impact force. The dependency of the mass and inertial moments is presented.

The typical test is a drop test to a flat surface. The peek force is saved for fracture. Typical values are presented in Table 4-6.

Table 4-6 – Peak force for fracture at different regions of skull [17]

Impact area	Force [kN]	Reference
Frontal	4.2	Nahum *et al*. (1968)
	5.5	Hodgson *et al*. (1971
	4.0	Schneider and Nahum (1972)
	6.2	Advani *et al*. (1975)
	4.7	Allsop *et al*. (1988)
Lateral	3.6	Nahum *et al*. (1968)
	2.0	Schneider and Nahum (1972)
	5.2	Allsop *et al*. (1988)
Occipital	12.5	Advani *et al*. (1975)

In terms of acceleration acquire, remains as problems: the impossibility to introduce accelerometers in the head centre of the mass, the other problem is the fact that the head is not a rigid body, meaning that the centre of mass in reality changes along the time. To overtake these problems, several solutions have been presented to measure the acceleration. In addition, was recommended to analyse too the rotational acceleration as parameter.

The majority of the methods are focus to a frontal car accident; this means that the main direction is the anterior-posterior direction.

One of the rules have been presented by the Wayne State University Cerebral Concussion Tolerance Curve, are the abbreviation, WSTC (Wayne State Tolerance Curve). The relation between the average translational acceleration and the duration of the acceleration pulse that accounts for similar head injury severity in head contact impact is presented in the Figure 4-12.

This curve indicates the frontier to the irreversible damage zone. Conjugations of acceleration and time lower that the curve means that if the damage occurs, is reversible. The first version of this curve only goes to times of $6 ms$. The extended information was added using data from tests in animals and volunteers (Table 4-7).
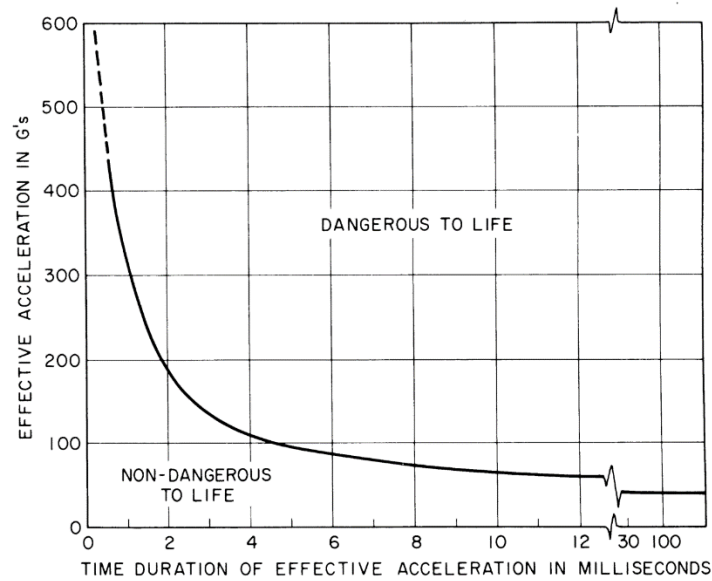
Figure 4-12 – The Wayne State Tolerance Curve [17]

Table 4-7 – Test conditions of the experiments the WSTC is based upon [17]

Pulse duration	Test objects	Test set-up	Response measured	Injury criterion
$2-6ms$	Cadavers	Drop test	Acceleration at the back of the head	Skull fracture
$6-20ms$	Cadavers and animals	Impact test	Acceleration of skull, brain pressure	Pathological changes
$>20ms$	volunteers	Sled tests	Whole body acceleration without head impact	Concussion, state of consciousness

Further tests and studies were performed to evaluate the rotational influence in the injury. The mass of the brain was found as threshold to cause injury in angular acceleration. The main tests made in primates are scaled to humans (Figure 4-13).
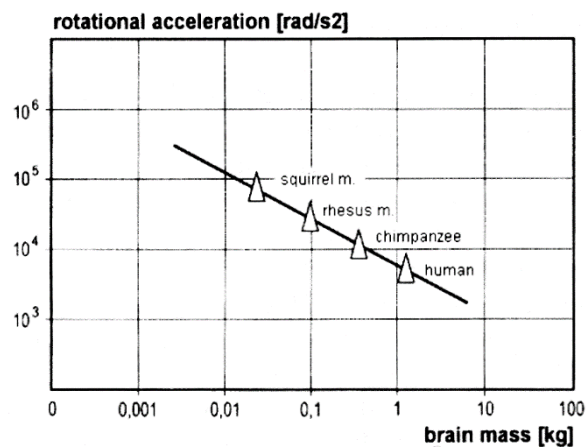
Figure 4-13 – Results from experiments and scaling addressing tolerance towards rotational acceleration [17]

The Table 4-8 shows the tolerances to rotational movements. Some authors' shows that are possible achieve value of $25000\,rad\,s^{-2}$ for very short durations.

Table 4-8 – Tolerance threshold for rotational acceleration and velocity of the brain [17]

Tolerance threshold	Type of brain injury	Reference
50% probability: $\ddot{\alpha} = 1800\,rad\,s^{-2} \quad for \quad t < 20ms$ $\dot{\alpha} = 30\,rad\,s^{-1} \quad for \quad t \ge 20ms$	Cerebral concussion	Ommaya et al. (1967)
$\ddot{\alpha} < 4500\,rad\,s^{-2} \quad and/or \quad \dot{\alpha} < 70\,rad\,s^{-1}$	Rupture of bridging vein	Loüwenhielm (1975)
$2000 < \ddot{\alpha} < 4500 \left[rad\,s^{-2} \right]$	Brain surface shearing	Advani et al. (1982)
$\dot{\alpha} \le 30\ rad\ s^{-1}$ $\begin{cases} safe: & \ddot{\alpha} \le 4500\ rad\ s^{-2} \\ AIS\ 5: \ddot{\alpha} > 4500\ rad\ s^{-2} \end{cases}$ $\dot{\alpha} > 30\ rad\ s^{-1}$ $\begin{cases} AIS\ 2: \ddot{\alpha} = 1700\ rad\ s^{-2} \\ AIS\ 3: \ddot{\alpha} = 3000\ rad\ s^{-2} \\ AIS\ 4: \ddot{\alpha} = 3900\ rad\ s^{-2} \\ AIS\ 5: \ddot{\alpha} = 4500\ rad\ s^{-2} \end{cases}$	(general)	Ommaya et al. (1967)

4.1.6   Injury criteria

We have seen previously that in some way it's possible to correlate what it's possible to measure and what was the consequence in the subject. It's possible to define thresholds that define safe areas, and areas where some type of injury can be expected with more or less gravity.

In such way, as the emergency staff have the need of an indicator to define the patient severity as AIS, can be found equivalent indicators derivate from variables that can be measured as acceleration.

4.1.7   HIC (Head Injury Criteria)

The main criterion to access the head injury used in our days is the HIC, meaning Head Injury Criteria.

The usual mathematical formulation for the HIC is given by:

$$\text{HIC} = \max_{t^1,t^2}\left\{\left[\frac{1}{\left(t^2-t^1\right)}\int_{t^1}^{t^2}a(t)\cdot dt\right]^{2.5}\right\}, \tag{4.1}$$

where the t^1 and t^2 are respectively any arbitrary time during the acceleration pulse, measured in $[s]$, and where $a(t)$ is the acceleration recorded, given in $[g]$.

4.1.7.1   HIC – the genesis

Until we get in our days the definition of HIC formulated as we find in equation (4.1), a long path was been done.

The very beginning of the parameter HIC have been summarized in the year of 1971 (one year before the HIC definition *per se*), by John Versace.

In those days, he was able to assume how difficult it is to establish a valid threshold for predicting head injuries, comparing this problem with other fields that handle with life sciences.

In his words: "*when a toxicologist wants to find out how much chemical stress an insect species can tolerate, he does a very direct experiment. He puts 100 insects in each of 7 jars and then he sprays them with the insecticide, incrementing the dosage from jar to jar. He determines the tolerance limit or threshold dosage for some designated degree of response to occur, and the scaling by x% increase in dosage...*"

It's obvious that such approach isn't suitable to be used to access the head injury threshold in humans. The go-around was (and still is[9]) to use animal's heads, cadaveric human heads and volunteers[10].

The first criteria to use such data is known as WSUTL (Wayne State University Tolerance Limit) or WSTC (Wayne State Tolerance Curve) (Figure 4-12)

Proposals to the WSTC have been made, being the most notable done by Gadd. Gadd's have suggested a log-log correlation line approximating the WSTC curve, given by the equation

$$1000 = T\cdot\left(A\right)^{2.5}, \tag{4.2}$$

where T is the load time in $[s]$ and A the load acceleration in $[g]$.

The Gadd's curve can be seen in the Figure 4-14 and superposed to the WSTC curve in Figure 4-15.

---

[9] In our days, it's possible to use too FEM models to simulate head impacts.

[10] The tests in volunteers are done usually without meaning damage (or sometimes in a reversible damage region).
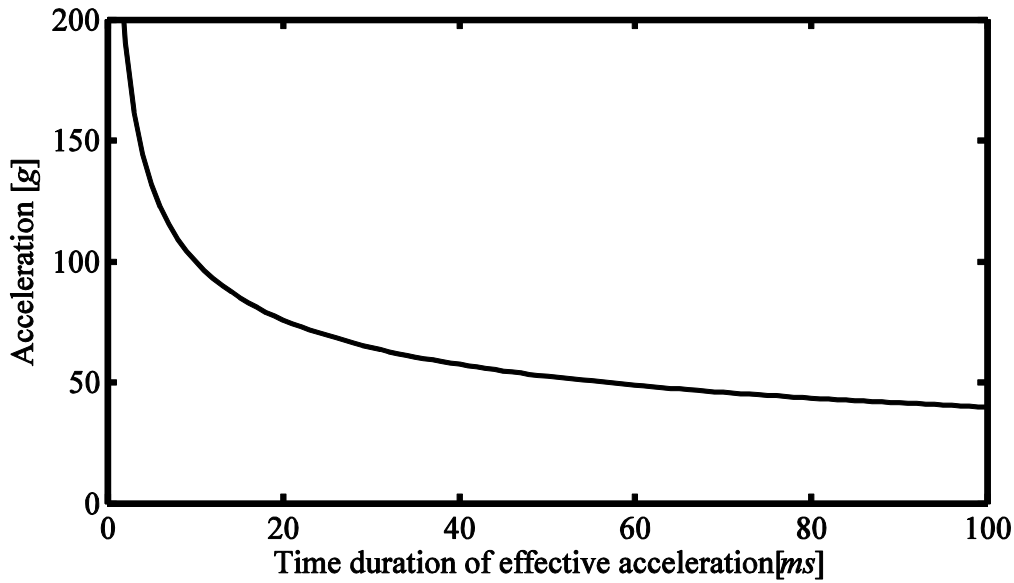
Figure 4-14 – Impact tolerance for the human brain according with Gadd's correlation
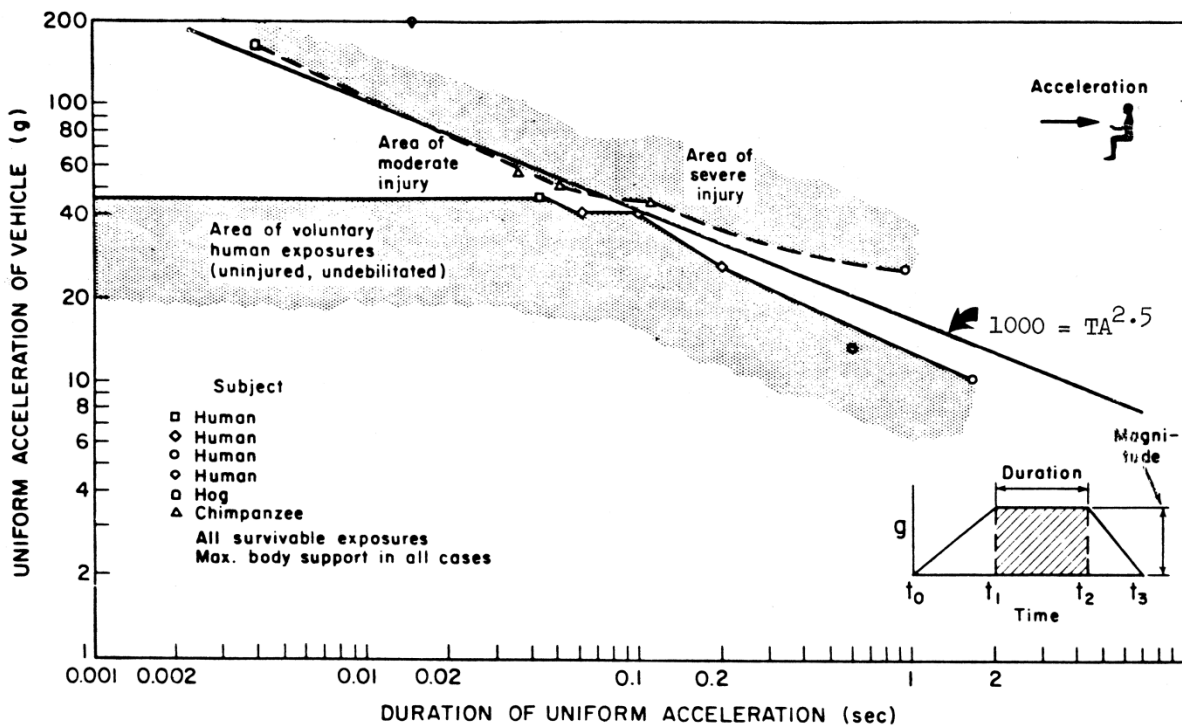
Figure 4-15 – Frontal deceleration in the human head

Some problems have been addressed in those days. Some have been describing that the data came from the different experimental methodologies, being not comparable, and what was/is the real meaning of the parameter acceleration in such correlation. One of the interesting's incompatibilities, was that in academic labs, usually acceleration was recorded directly in the head, getting an acceleration curve similar with a triangle shape; and in the army, the acceleration was recorded (and impose) in the vehicle that was fixing the head or person, giving a typical rectangular shape impulse curve.

It was suggested too that the limit of $42g$ for long-time accelerations was to conservative, being a reasonable value a value of $60-80g$.

It is important to make reference that in such times, WSTC or Gadd's curves have been made as curves of type: "go/no-go".

It's interesting to note that the threshold for long time accelerations given by Gadd's is similar with the recorded by Col. (Dr.) John Paul Stapp (Figure 4-16)
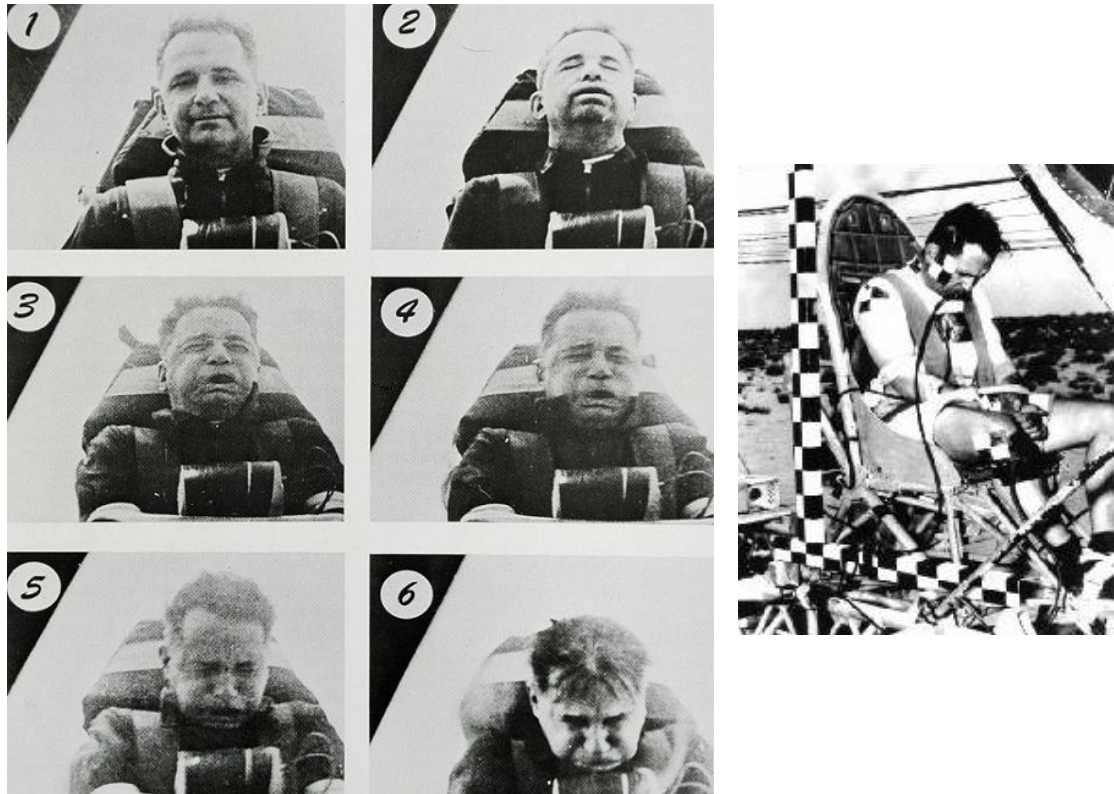
Figure 4-16 – Col. (Dr.) John Paul Stapp during heavy deceleration ($\sim 45g$) [66], and final position [67]

4.1.7.2   The Severity Index

The Severity Index, or SI, was a relation, where have been used from Gadd's curve the parameters "1000" and "2.5", and then gotten the follow formula:

$$1000 = \int (a)^{2.5} \cdot dt \,. \tag{4.3}$$

According with Versace, "*Constants have been taken from the formula of the Tolerance Limit line for severity scaling purposes, a use which cannot be justified conceptually or mathematically*".
It's interesting that such parameters have been superposed with more 3 by Versace, being resumed in the Table 4-9 and plotted in the Figure 4-17.

Table 4-9 – Constants for Several Tolerance Curves

Constant	Power	Comment
1000	2.5	Above the WSTC beyond $2ms$.
		Goes through a reference point about $23g$ at $400ms$.
3780	2.9	Only slightly above WSTC beyond $4ms$.
		Also goes through same reference point.
9580	3.2	Extremely tight fit to WSTC from about $7ms$ on.
		Ditto on reference point.
30.8	1.9	Extremely tight fit to WSTC for less than $12ms$.
		Diverges elsewhere.
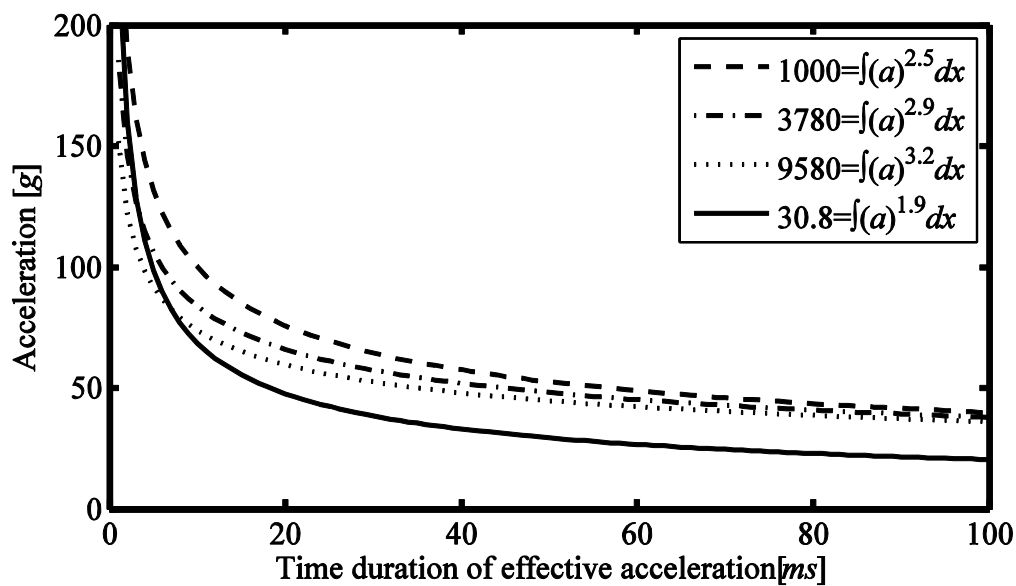
Figure 4-17 – Superposition of the several injury criteria's given by several parameters pars

4.1.7.3 HIC - computing

Being the area of a half-sine given by

$$a(t) = A \cdot \sin \frac{\pi \cdot t}{T} \tag{4.4}$$

and the analytical expression for HIC

$$HIC = \max_{t^1, t^2} \left\{ \frac{1}{\left(t^2 - t^1\right)^{3/2}} \cdot \left[\int_{t^1}^{t^2} a(t) \cdot dt \right]^{5/2} \right\} \tag{4.5}$$

making

$$\Delta t = t^2 - t^1 \tag{4.6}$$

and

$$a(t) = A \cdot k(t) = A \cdot \sin\frac{\pi \cdot t}{T} \tag{4.7}$$

and knowing that the maximum value of HIC for a half-sine impulse is for the interval $\left[\frac{1}{4} \cdot T \quad \frac{3}{4} \cdot T\right]$. Rewriting

$$\text{HIC} = (\Delta t)^{-3/2} \cdot (A)^{5/2} \cdot \left(\int_{t^1}^{t^2} k(t) \cdot dt\right)^{5/2} \tag{4.8}$$

and since

$$A = a^{\max} \tag{4.9}$$

we get

$$a^{\max} = \left[\text{HIC} \cdot (\Delta t)^{3/2} \cdot \left(\int_{t^1}^{t^2} k(t) \cdot dt\right)^{-5/2}\right]^{2/5} \tag{4.10}$$

since we are working with limited ranges of indexes for HIC,

$$t^i = \begin{cases} \dfrac{1}{4} \cdot T & \dfrac{T}{2} < index^{\text{HIC}} \\ \dfrac{T}{2} - index^{\text{HIC}} & \dfrac{T}{2} \geq index^{\text{HIC}} \end{cases} \tag{4.11}$$

$$t^f = \begin{cases} \dfrac{3}{4} \cdot T & \dfrac{T}{2} < index^{\text{HIC}} \\ \dfrac{T}{2} + index^{\text{HIC}} & \dfrac{T}{2} \geq index^{\text{HIC}} \end{cases} \tag{4.12}$$

and being

$$K = \int_{t^1}^{t^2} k(t) \cdot dt \tag{4.13}$$

so

$$K = \frac{T}{\pi} \cdot \left[\cos\left(\frac{\pi \cdot t^i}{T}\right) - \cos\left(\frac{\pi \cdot t^f}{T}\right)\right] \tag{4.14}$$

we get

$$a^{\max} = \left[\text{HIC} \cdot (\Delta t)^{3/2} \cdot (K)^{-5/2} \right]^{2/5} \tag{4.15}$$

With this relation, we can evaluate the meaning of the different HIC parameters in for diverse types of impulses.

So, since the HIC is one factor that correlates the average acceleration and the WSTC. The actual mathematical expression is:

$$HIC = \max \left[\frac{1}{t_2 - t_1} \int_{t_1}^{t_2} a(t) dt \right]^{2.5} (t_2 - t_1) \tag{4-16}$$

where t_2 and t_1 are any arbitrary times during the acceleration pulse. Acceleration is measured in multiples of acceleration of gravity, $[g]$ and time is measured in seconds. The important HIC are to times $36ms$ and $15ms$, represented by HIC_{36} and HIC_{15} respectively. For a HIC_{36} for a 50th percentile male can't pass the 1000.

To determine the relationship between the HIC and injuries of the skull and brain, it's presented the formula to a $AIS \geq 2$

$$p(fracture) = N \left(\frac{\ln(HIC - \mu)}{\sigma} \right) \tag{4-17}$$

where $N(\ )$ is the cumulative normal distribution, $\mu = 6.96352$ and $\sigma = 0.84664$.

The data used to establish the risk is usually shorter than $12ms$, so, the HIC curve is applicable to both HIC_{15} and HIC_{36} in such cases. The threshold value is 700 for the HIC_{15}, to a middle-sized male with a probability of 31%, and a threshold is the value of 1000 for the HIC_{36} with a probability of 48%.
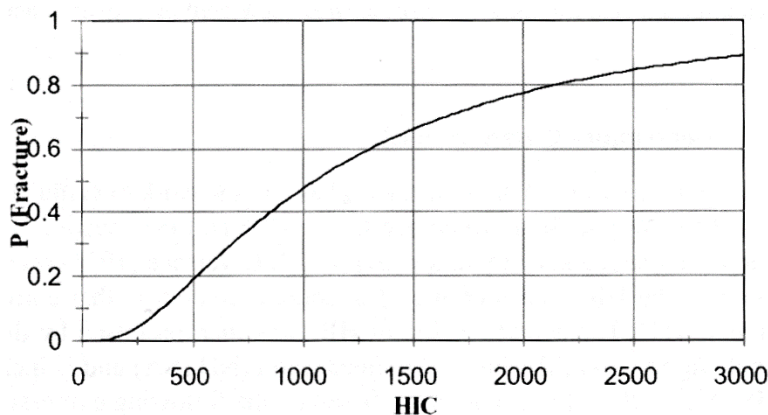
Figure 4-18 – Probability of skull fracture (AIS >= 2) in relation to the HIC as determined by Hertz [17]

4.1.8   Other Injury Criteria's

The main criteria in wide use our days is the HIC (Head Injury Criterion), as already reviewed and explained. With HIC we have in use the European version HPC (Head

Protection Criterion), the "$3ms$ criteria" and the GAMBIT (Acceleration Model for Brain Injury Threshold). Note the fact of all these criteria's with exception of GAMBIT are based only in the translational acceleration, and GAMBIT only adds the rotational acceleration parameter [17].

4.1.8.1   HPC

The rules applied to the HPC are similar to the HIC.

Another criteria is known by the "$3ms$ criteria". This parameter give a threshold of $80\,g$ in a time of $3ms$. This value cannot be passed. To helmet tests, is used an adaptation of this rule, with a threshold of $150\,g$ in a time of $5ms$.

4.1.8.2   GAMBIT

Until now, all the criteria's use only the translational acceleration. The GAMBIT criteria were proposed to combine translational and rotational accelerations. The relationship proposed is:

$$GAMBIT = \left[\left(\frac{a(t)}{a_c} \right)^n + \left(\frac{\ddot{\phi}(t)}{\ddot{\phi}_c} \right)^m \right]^{\frac{1}{k}} \tag{4-18}$$

here $a(t)$ and $\ddot{\phi}(t)$ denote translational and rotational acceleration, respectively. a_c and $\ddot{\phi}_c$ represent critical tolerance levels for those accelerations and n, m and k are constants. Feting these constants to experimental data, it's found the solution to GAMBIT criteria:

$$GAMBIT = \left[\left(\frac{a(t)}{250} \right)^{2.5} + \left(\frac{\ddot{\phi}(t)}{25} \right)^{2.5} \right]^{\frac{1}{2.5}} \tag{4-19}$$

with $a(t)$ and $\ddot{\phi}(t)$ given in $[g]$ and $\left[krad\ s^{-2} \right]$ respectively. The curve for a GAMBIT of 1.0 was determinate to represent a probability of 50% for irreversible head injury. The Figure 4-19 shows' some curves for values of GAMBIT.

transl. acceleration [g]
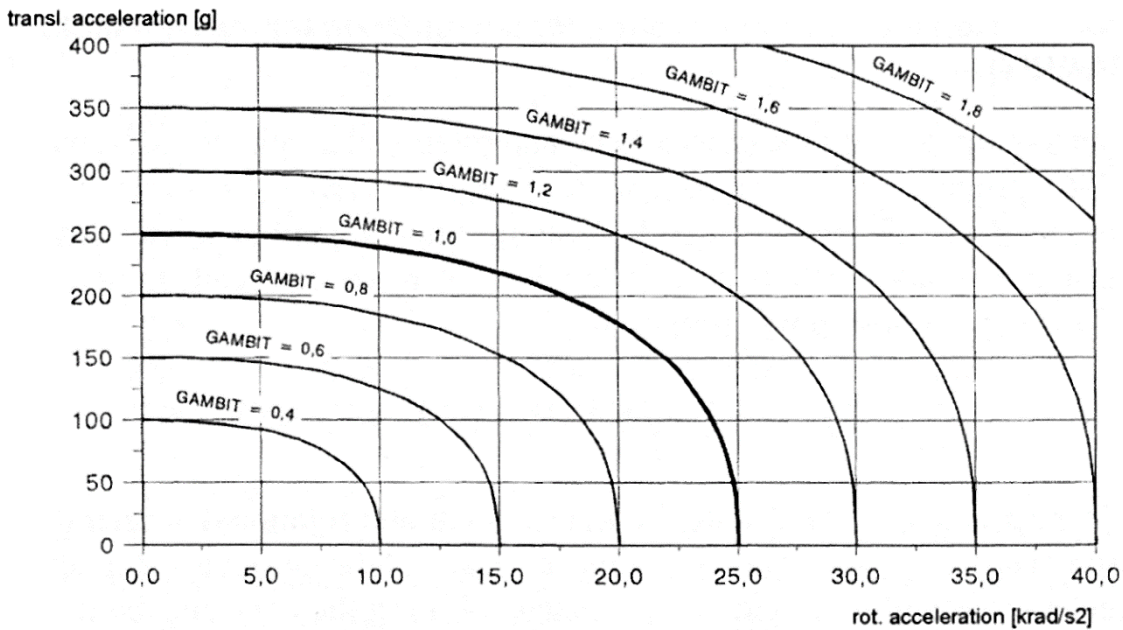
Figure 4-19 – GAMBIT curves for constant GAMBIT values [17]

4.2 The Spin

The spin is one system that when injured, can have collateral long-term consequences, like paraplegia and quadriplegia, or in the limit the head if heavy injured in the neck region (e.g. decapitation). One aspect is the relationship between solicitations in the head and in the spine, generally, the first implies the second.

The impact in the society of spin injuries is huge. In some cases, the injured person needs for the rest of their life healthcare assistance, and/or personal care.

It's important recall how importance is the neck section in the spin.

4.2.1 Neck

Neck (Figure 4-20) is the element that allows the head to move in such great range in relation with the body. Part of the moments are described like head movements. The fact that the neck is composed by the cervical vertebras, gives to this part of the body a great flexibility. The usual approximations are the division of the neck in one (only one joint in middle of the neck) or two parts (the adopted simplification in this work, which consists in two joints, in C1 with the cranium and C7 with T1).
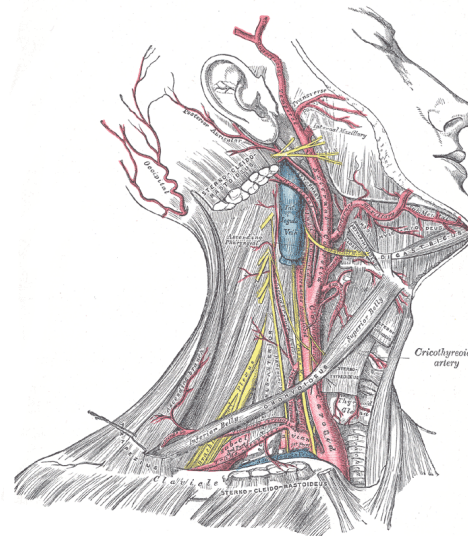
Figure 4-20 – Neck details (from Gray's Anatomy, 1918)

4.2.1.1 Neck dimensions

The general characteristics of the neck are listed in the Table 4-10 and Table 4-11.

Table 4-10 – Neck volume and mass [54]

Volume	$10^{-3}m^3$	1.012
Mass	kg	0.965

Table 4-11 – Coordinates for neck centre of mass, inertial and joints (local coordinates) [54]

		X	**Y**	**Z**
CoM	$10^{-3}m$	57.2	0	49.8
I	$10^{-4}kg\,m^2$	14.798	18.463	22.910
I axis rotation	X	11	90	79
	Y	90	0	90
	Z	101	90	11
head-neck	$10^{-3}m$	30	0	117
C7-T1	$10^{-3}m$	75	0	7

4.2.1.2 Neck movements

The characterization of the head movements is dependent of the head neck. The data presented to the described joint (C1 with cranium) can be considered the whole neck, not in one point only. We must adapt the values for a natural neck movement (neck with head and neck with the thorax.

4.2.2 Anatomy

The spine is composed mainly by 24 vertebras more one set of vertebras funded in one assemble: the sacrum and coccyx. In their interior, passes the spinal medulla, a vital part of the neurological system [17].

So, the spine is divided by: cervical (7 vertebras, neck section), thoracic (12 vertebras), lumbar (5 vertebras), sacrum, and coccyx (Figure 4-21)
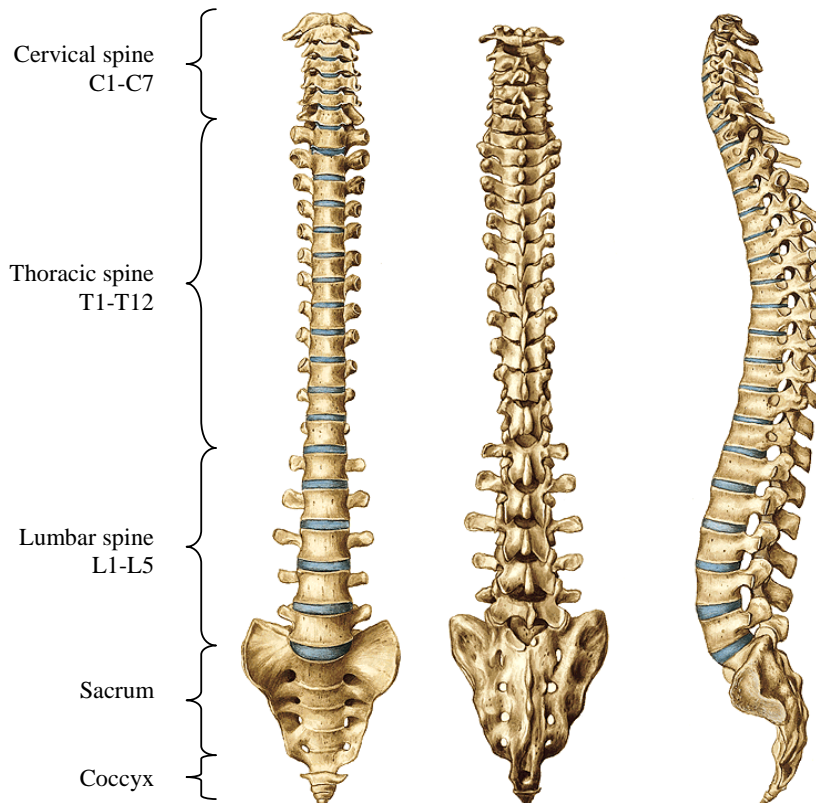
Figure 4-21 – Human spine [63]

The won physiognomy of the vertebras varies along the spine (Figure 4-22). Its intercession sees that the transverse section of the vertebra increases from the aspect cranial to the aspect caudal.
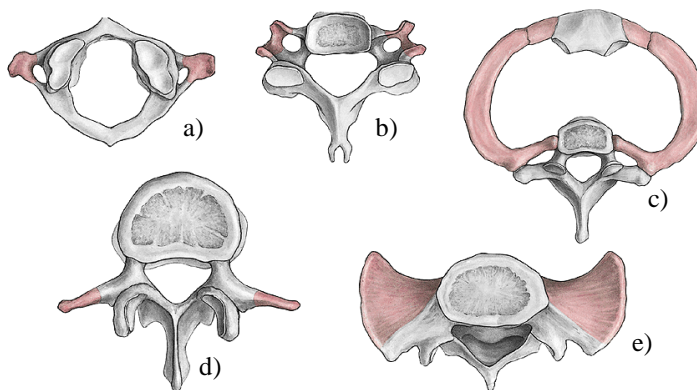
Figure 4-22 – Characteristics of several vertebras; a) 1st cervical vertebra, atlas or C1; b) 4th cervical vertebra, C4, c) 1st thoracic vertebra, T1, with ribs and sternum; d) 3rd lumbar vertebra, L3 [63]

The spinal module is protected by the cerebrospinal fluid. Between each vertebra, are found the intervertebral disc (the exception is found between the C1 and the C2). Concerning off the basic neck motions, these are represented in the Figure 4-23.

| Neutral | Flexion | extension | lateral extension | Rotation |
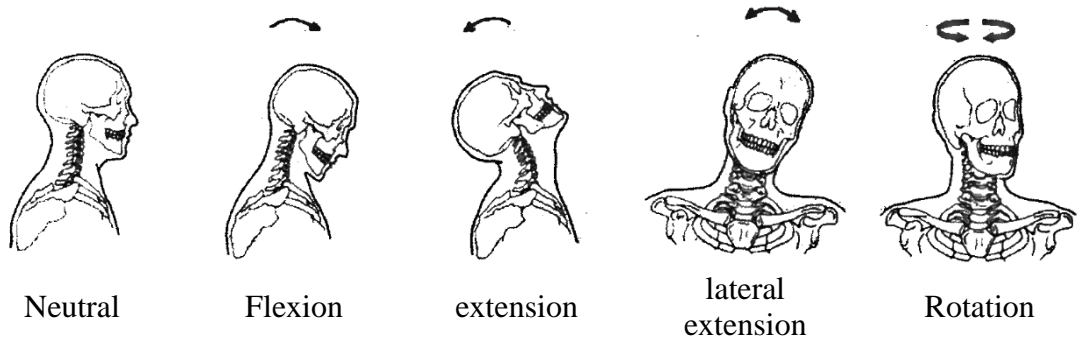
Figure 4-23 – The four basic movements of the head and neck [17]

4.2.3 Neck models in our work

In our work, one model of each type have been used: 1 MBM neck and 1 FEM neck.

4.2.3.1 MBM neck

The Neck in our MBM is a rigid body (Figure 4-24), with the centre of mass defined according to the head referential axis, as the definition of the body inertia. The geometry was taken from a 50th percentile mannequin. The neck surface was tessellated for contact proposes.

a)   b)
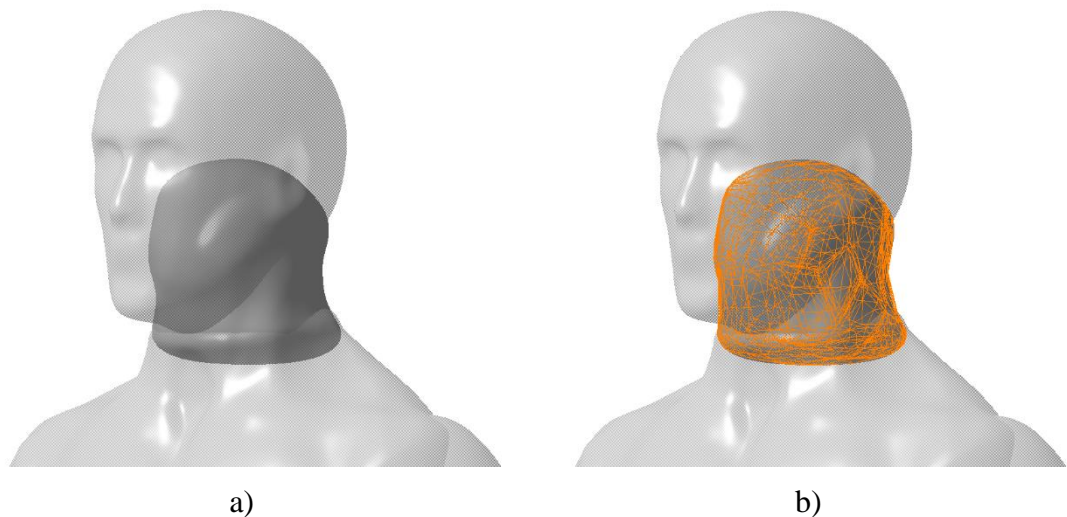
Figure 4-24 – MBM neck a) geometry, b) geometry with tessellated surface for contact proposes

4.2.3.2 FEM neck

For the injury assessment, the HUMOS2 neck's model was used (Figure 4-25). The model includes the cervical vertebras and respective discs, flesh and skin (Table 4-12).

a)   b)
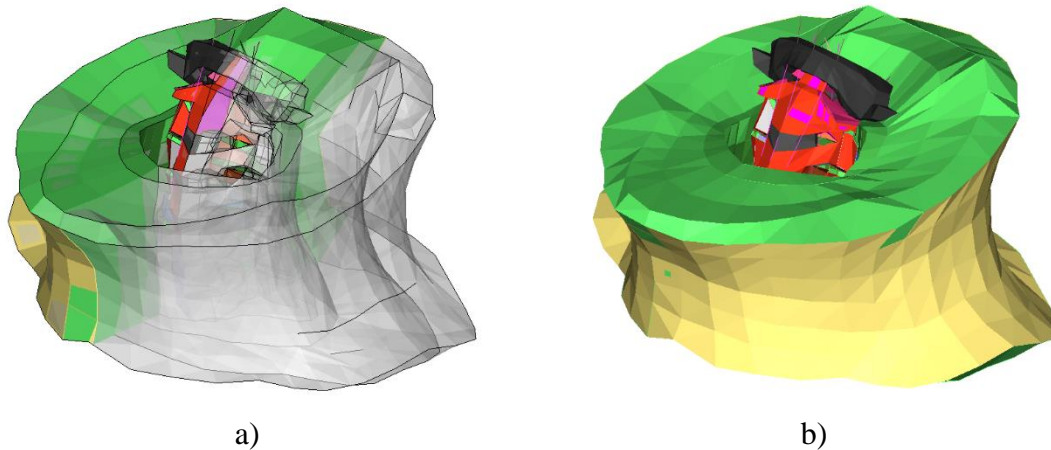
Figure 4-25 – HUMOS2 neck a) section view, b) outside view

The neck have also the defined joints, ligaments and defined muscles as linear actuators.

The neck model in a first analysis, have a few visible limitations seen a priori. We have the vertebras defined as rigid bodies. If this limitation helps in the joint definition between vertebras, will avoid the injury assessment in case that vertebras loads can imply fracture.

Table 4-12 – List of neck parts in FEM, their type of mesh and respective model formulation.

Head part	mesh type	Formulation
Vertebras cortical	Shell / Hexahedra	Elastic Material
Vertebras spongous	Hexahedra	Elastic Material
Discs	Hexahedra	Elastic Material
Flesh	Hexahedra	Generalized Maxwell-Kelvin-Voigt (Visco-Elastic Foam)
skin	Shell	Johnson-Cook plasticity

4.2.4   Injuries and associated mechanisms

Exists too one injury scale to spin according with the AIS (Table 4-13). In general, the injuries in the upper cervical are considered being more serious and life threatening than those at lower level. The injuries in the cervical can be described according with the type of movement (Figure 4-23) and loading (Figure 4-26) [17].

Bending   Compression   tension   Torque   Shear
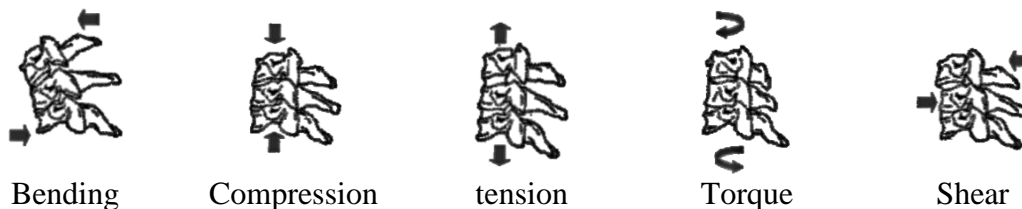
Figure 4-26 – Possible loadings of the neck [17]

The mode how the injury can appear in several types of solicitations can be generally compression-flexion (Figure 4-27), tension-extension (Figure 4-28), Compression-extension and lateral bending and compression (Figure 4-29).

The injuries of the soft tissues of the neck are observed too in several accidents.

Table 4-13 – Examples of spinal injuries according to AIS scale [17]

AIS code	Description
1	Skin, muscle abrasion, contusion (hematoma), minor laceration
2	Vertebral artery: minor laceration Cervical/thoracic spine: dislocation without fracture Thoracic/lumbar spine: disc herniation
3	Vertebral artery: major laceration Cervical/thoracic spine: multiple nerve root laceration
4	Cervical/thoracic spine: spinal cord contusion incomplete
5	Cervical/thoracic spine: spinal cord laceration without fracture
6	Decapitation Cervical/thoracic spine: spinal cord laceration at C3 or higher with fracture
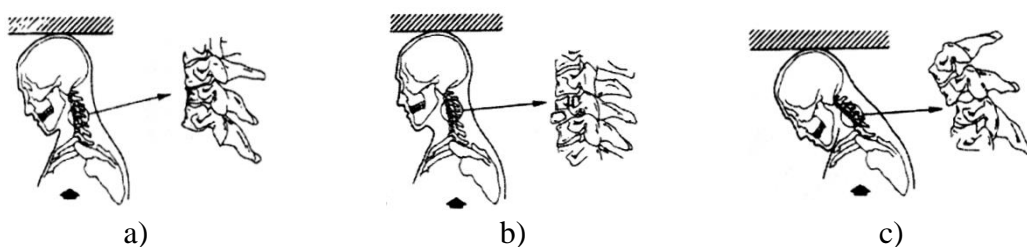
Figure 4-27 – Compression-flexion injury mechanism: a) wedge fracture; b) burst fracture; c) bilateral facet dislocation [17]
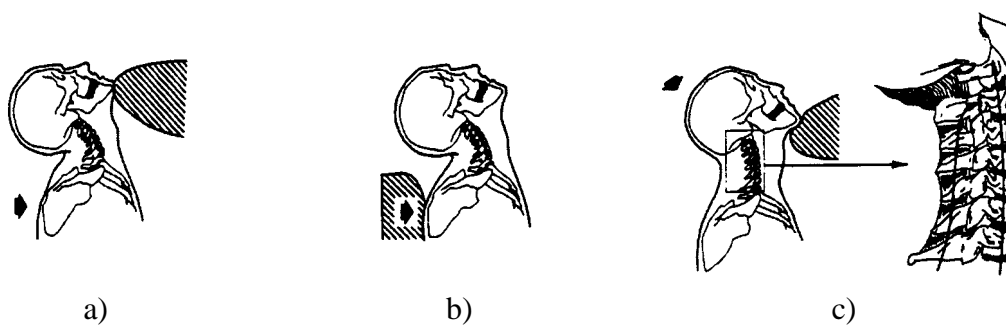
Figure 4-28 – Tension-extension occurred by: a) fixation of the head with continued forward acceleration of the body; b) inertial loading of the neck following an abrupt forward acceleration of the torso; c) forceful loading below the chin directed posterosuperiorly [17]
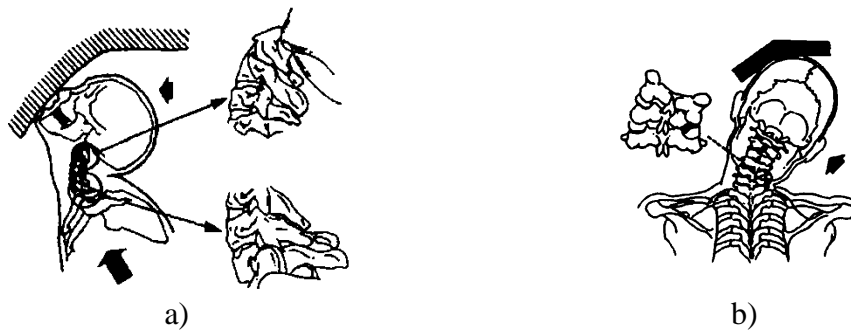
Figure 4-29 – Injury caused by: a) compression-extension mechanism; b) lateral bending and compression [17]

To evaluate the mechanical proprieties of the spine was performed several studies in: volunteers, cadavers, animals and dummies. Dynamic and static loads, various set-ups, and several scenarios are carry out to get the most proximally data. One problem is the limitations of this type of experiments, by the fact that in cadavers, e.g. the muscles are out of tonus, the functional units (generally one set of two or three vertebras without external tissues like muscles) are too simplified, and so on. The experiments in volunteers are limited to lower loads (to not provoke injury).

Some data about the cervical spine are presented in the Table 4-14.

4.2.5   Injury criteria

The criteria's developed to spine are few, the majors part of them for the neck region and optimised to car crashes scenarios. It's possible list the Neck Injury Criterion, the N_{ij}, the N_{km}, the Intervertebral Neck Injury Criterion, the Neck Displacement Criterion, and the Lower Neck Load Index. All these criteria's are optimized to frontal and/or rear impacts to a seated car passenger, usually restrained with a seat belt, a scenario to far way of the reality of a PTW driver or passenger, which are completely free and usually not seat like in a car posture. Other question is the impossibility to perform data acquire in dummies in all types of solicitations, by the fact that they do not have all of these degrees of freedom [17].

By these facts, is difficult in the present days to give a suitable criterion to correlate the simulated results and the respective injuries, by the exception of the limits presented in the Table 4-14.

4.3   The thorax

The major part of the injuries in the thorax is caused by a direct impact. In several PTW accidents, the exposure of the thorax to impacts is considerable, and by this fact, an important body section to considerer too. These problems are intensified by the mechanical characteristics of the rib cage against the mechanical characteristics of usual protective equipment used and respective capabilities problems.

Table 4-14 – Tolerance of the cervical spine to injury [17]

Response measured	*Test objects*	*Threshold criterion*	*Threshold value*	*R*
Extension $[Nm]$	Volunteers	No-injury (static)	23.7	A
		Pain	47.3	B
		No-injury	47.5	A
	Cadavers	AIS2, ligamentous injury	56.7	A
Flexion $[Nm]$	Volunteers	Pain	59.4	B
			59.7	A
		Maximum voluntary loading	87.8	B
			88.1	A
	Cadavers	AIS2 (no fractures)	189	B
			190	A
Compression $[kN]$	Cadavers	Bilateral facet dislocation	1.72	C
		Compression injuries (range)	4.8 5.9	D
Tension $[kN]$	Volunteers	No-injury (static)	1.1	B
	Cadavers	Failure	3.1	E
Shear (a-p) $[kN]$	Volunteers	No-injury	0.845	B
	Cadavers	Irreversible damage	2	A
	Functional unit	(odontoid) fractures	1.5	E
	Functional unit	Ligament rupture	0.824	F

Notes: R – reference
A – Goldsmith & Ommaya (1984); B – Mertz & Patrick (1971); C – Myesrs et al. (1991); D – Maiman et al. (1993); E – Shea et al. (1991); E – Doherty et al. (1993); F – Fielding at al. (1974)

Major parts found in this section are the rib cage (thorax vertebras, ribs and sternum), lungs, heart, and aorta (Figure 4-30).
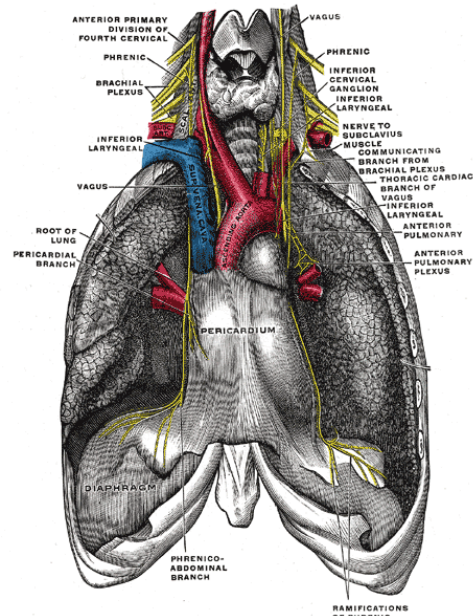
Figure 4-30 – Detail of internal organs of the thorax and part of the neck (from Gray's Anatomy, 1918)

The thorax as one part of the body can be simplified as a rigid body in relation with the movements of the whole body.

4.3.1   Thorax dimensions

The general characteristics of the thorax are listed in the Table 4-15 and Table 4-16.

Table 4-15 – Thorax volume and mass [54]

Volume	$10^{-3} m^3$	24.909
Mass	kg	23.763

Table 4-16 – Coordinates for thorax centre of mass, inertial and joints (local coordinates) [54]

		X	**Y**	**Z**
CoM	$10^{-3} m$	58	0	190
I	$10^{-4} kg\, m^2$	4,566.400	3,222.558	3,015.877
I axis rotation	X	14.5	90	75.5
	Y	90	0	90
	Z	104.5	90	14.5
C7-T1	$10^{-3} m$	70	0	392
L2-L3	$10^{-3} m$	85	0	38
Glenohumeral	$10^{-3} m$	60	±173	314

4.3.2   Thorax movements

For the thorax, the movement is between this body and 4 others: upper arms (2), neck and abdomen. The movement of each member relative to the thorax is described like a

spherical joint: right and left elbow (described in upper limbs section), C7-T1 (described in head section) and L2-L3 (described in pelvis section).

4.3.3 Anatomy

The thorax consist mainly in a rib cage and internal organs, and goes from the base of the neck to the diaphragm. Twelve pairs of ribs, come from the thorax vertebras forms the base structure. The upper seven ribs connect directly to the sternum in the anterior aspect. The others are connected indirectly to the sternum with the exception of the last two, which are so called floating ribs (Figure 4-31). They are all interconnected by muscles, given flexibility to allow ventilation, but enough rigid to protect their interior (Figure 4-32) [17].
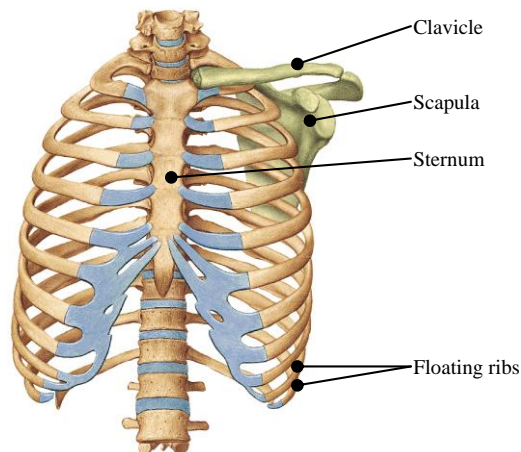
Figure 4-31 – Anterior aspect of thorax with left clavicle and scapula [63]
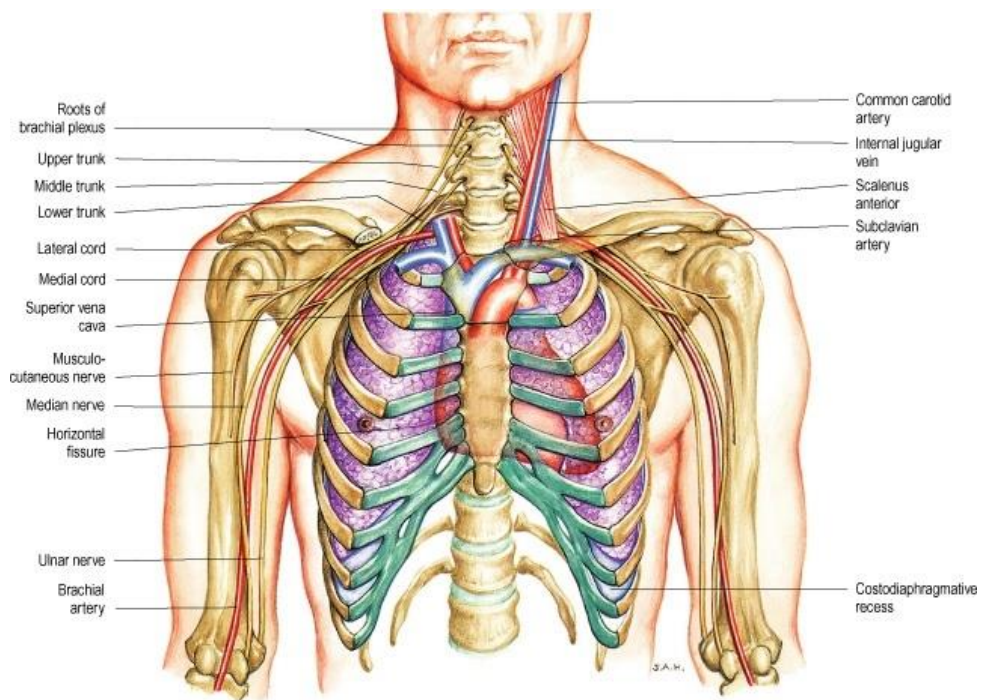
Figure 4-32 – Anterior view of thorax, root of neck and axilla, showing heart, great vessels and bronchial plexus [62]

The sternum is a part in the front that increases their rigidity along the years, by the fact that proceeds by an ossification process. This lowers the flexibility of the assembly and increases the probability of rib fracture.

The main organs inside the rib cage are the lungs (three lobes in right and two lobes in left), the heart, trachea, and large vessels.

The ventilation is helped by the combined movement of the ribs and diaphragm.

The centre section (mediastinum) is a zone with restricted space. By this characteristic, a compression of the anterior rib cage may easily cause injuries to internal structures.

4.3.4 Thorax models in our work

In our work, one model of each type have been used: 1 MBM thorax and 1 FEM thorax.

4.3.4.1 MBM thorax

The thorax in our MBM is a rigid body (Figure 4-33), with the centre of mass defined according to the head referential axis, as the definition of the body inertia. The geometry was taken from a 50th percentile mannequin. The thorax surface was tessellated for contact proposes.

a) b)

Figure 4-33 – MBM thorax a) geometry, b) geometry with tessellated surface for contact proposes

4.3.4.2 FEM thorax

For the injury assessment, the HUMOS2 thorax model was used (Figure 4-34). The model includes the rib cage (thoracic vertebras, ribs and sternum), scapula, clavicle, lungs, heart, aorta, diaphragm, flesh, skin and main muscles (Table 4-17).

a)   b)
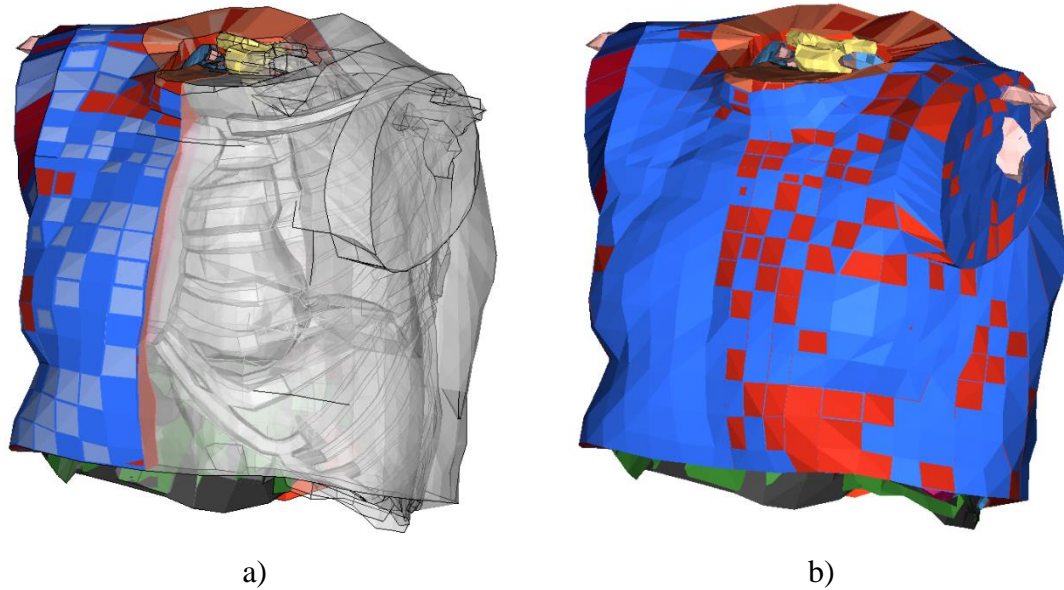
Figure 4-34 – HUMOS2 thorax a) section view, b) outside view

The thorax model in a first analysis, have a few visible limitations seen a priori. The vertebras are defined as rigid bodies. The defined muscles as elements 1D are not defined in the same way with the neck, not being so biofidelity with the human anatomy. The scapula's defined as rigid body to.

Table 4-17 – List of some thorax parts in FEM, their type of mesh and respective model formulation.

Thorax part	mesh type	Formulation
In rib cage organs	Hexahedra	Boltzmann (Visco-Elastic)
Ribs'	Shell / Hexahedra	Johnson-Cook plasticity / Elastic Material
Clavicula	Shell / Hexahedra	Johnson-Cook plasticity
Scapula	Shell	Elastic Material

4.3.5   Injury and associated mechanisms

The mainly types of solicitation are contact and sharply impacts. In car scenarios, the most commons are the firsts, by the contact with the seat belt, steering wheel, etc. In PTW accidents, the second is most frequently, by the fact of the body can be projected or intersect one obstacle [17].

The injury processes can be from three mechanisms: compression, viscous loading and inertial loading. The injury process can be presented by one or conjugations these types of mechanisms.

The result can be skeletal, soft tissue or both. In the Table 4-18 and Table 4-19, is presented the AIS scale to skeletal and soft tissues injuries of thorax.

Table 4-18 – Examples of skeletal injuries according to AIS scale [17]

AIS code	Description
1	One rib fracture
2	2-4 ribs fractures Sternum fracture
3	4 or more ribs fractured on one side 2-3 rib fractures with hemathorax or pneumothorax
4	Flail chest 4 or more rib fractures on each of two sides 4 or more rib fractures with hemathorax or pneumothorax
5	Bilateral flail chest
6	Not applied

Table 4-19 – Examples of soft tissue injuries according to AIS scale [17]

AIS code	Description
1	Contusion of bronchus
2	Partial thickness brochures tear
3	Lung contusion Minor heart contusion
4	Bilateral lung laceration Minor aortic laceration Major heart contusion
5	Major aortic laceration Lung laceration with tension pneumothorax
6	Aortic laceration with haemorrhage not confined to mediastinum

The generally lesions in soft tissue thoracic injuries are [17]:

- Respiratory system
    - Lung contusion
    - Lung laceration
    - Pneumothorax
    - Hemathorax
    - Trachea rupture
- Heart
    - Contusion
    - Laceration
    - Perforation
    - Pericardial tamponed
    - Cardiac arrest
- Aorta
    - Rupture
    - Laceration
- Others
    - Oesophagus rupture
    - Diaphragm laceration

Usually, the ribs fractures or in the point of maximum curvature or in the local of the solicitation, depending of the geometry and acceleration caused (Figure 4-35).

Figure 4-35 – Site of rib fracture depending on impact body [17]

The multiple rib fracture occurs usually in lateral impacts. In this scenario, the patient starts to have problems in chest stability, having by this difficulty and pain in the ventilation process. A big level of destruction can difficult in extremis the ventilation and cause hypoxemia.

If one part of the ribs goes out of their space, they can perforate external or internal tissues. If their moves out, we have an exposed or open fracture. In opposite, if their goes to the interior, we can have perforation of vital organs or causing ventilation problems.

In first aid care, the rib fracture can difficult the stabilization, or in certain cases, increase the AIS score of the victim.

In the lung, the injury can be caused by exceed acceleration, perforation, contusion, laceration and so on (Figure 4-36.a).
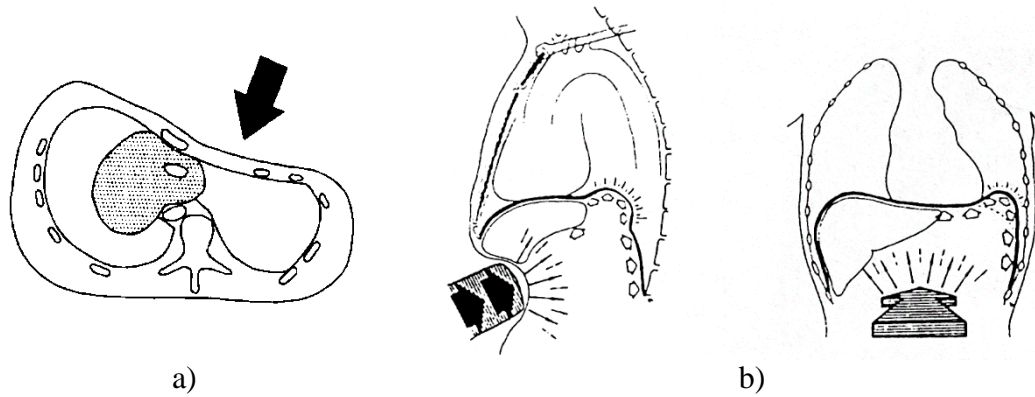
Figure 4-36 – Injury by: a) compression of the heart; b) laceration of the diagram due to blunt impact on the abdomen [17]

The heart can be subject of injuries to, like contusion and laceration. In high speeds impacts, the heart may undergo to arrhythmia, fibrillation or arrest. High speed blunt impacts ($15-20ms$) appear to interrupt the electromechanical transduction of the heart wall.

Major thoracic blood vessels can be injured too (Figure 4-37). Aortic rupture is trough to occur either from traction or shear forces generated between relatively mobile portions of vessels and points of fixation or, secondly, due to direct compression over the vertebral column or, thirdly, caused by an excessive sudden increase of intraluminal pressure. Aortic rupture and fluent blood vessels can be also rupture with the association of large extension associated with chest compression (Figure 4-38)
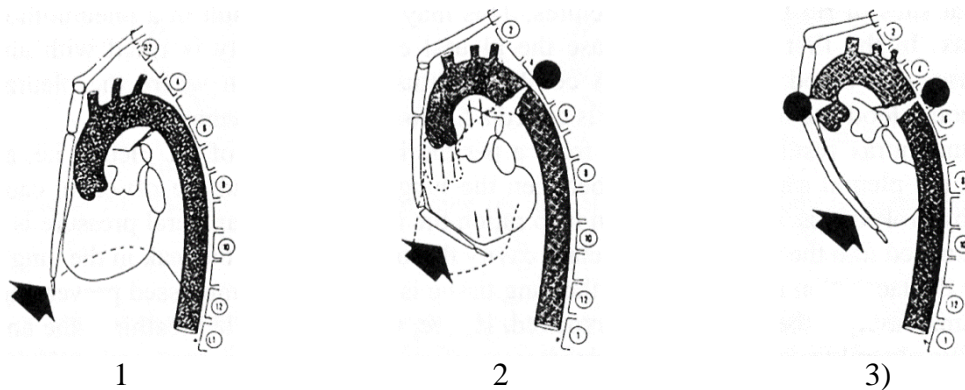
Figure 4-37 – Compression of the heart and possible sites of aortic rupture [17]

Figure 4-38 – Thorax compression in combination with hyperextension of the neck can cause the laceration of the aorta [17]

The rupture of the oesophagus and laceration of the diaphragm are other injuries observed. Other possibility is the hernia.

4.3.6 Injury Criteria

Was already said, the main factor to cause injury are the compression, viscous and inertial loading or combinations of them. Using different methods and subjects, it was obtained data likely that is presented in the Table 4-20 and Table 4-21 for frontal and lateral impacts respectively. The main propose of this data was to use in car crashes, this give us no information about posterior aspect [17].

Table 4-20 – Frontal impact tolerances of the thorax [17]

Tolerance type	*Tolerance level*	*Injury level*	*reference*
Force	$3.3kN$ to sternum	Minor injury	Pattrick et al. (1969)
	$8.8kN$ to chest and shoulders	Minor injury	Pattrick et al. (1969)
acceleration	$60g$	$3ms$ value for Hybrid III	FMVSS 208
deflection	$58mm$	No rib fracture	Stalnaker and Mohan (1974)
	$76mm$	Limit for Hybrid III	FMVSS 208
compression	20%	Onset of rib fracture	Kroell et al. (1971, 1974)
	40%	Flail chest	Kroell et al. (1971, 1974)
VC_{max}	$1.0ms^{-1}$	25% probability of $AIS \geq 4$	Viano and Lau (1985)
	$1.3ms^{-1}$	50% probability of $AIS \geq 4$	Viano and Lau (1985)
CTI	$\dfrac{A_{max}}{60g} + \dfrac{D_{max}}{76mm}$	50% probability of $AIS \geq 3$ in cadavers	Kleinberger et al. (1998)

Table 4-21 – Lateral impact tolerances of the thorax [17]

Tolerance type	Tolerance level	Injury level	reference
	7.4kN	AIS0	Tarriere at al. (1979)
Force	10.2kN	AIS3	Tarriere at al. (1979)
	5.5kN	25% probability of AIS $\geq$ 4	Viano (1989)
	T8-Y 45.2g	25% probability of AIS $\geq$ 4	Viano (1989)
acceleration	T12-Y 31.6g	25% probability of AIS $\geq$ 4	Viano (1989)
	60g	25% probability of AIS $\geq$ 4	Cavanaugh at al. (1993)
	TTI (d) 85g	Max. in SID dummy for 4-doors cars	FMVSS 214
	TTI (d) 90g	Max. in SID dummy for 2-doors cars	FMVSS 214
TTI (d)	TTI 145g	25% probability of AIS $\geq$ 4	Cavanaugh at al. (1993)
	TTI 151g	25% probability of AIS $\geq$ 4	Pintar et al. (1997)
Compression of half thorax	35%	AIS3	Stalnaker et al. (1993) Tarriere at al. (1979)
	33%	25% probability of AIS $\geq$ 4	Cavanaugh at al. (1993)
Compression of whole thorax	38.4%	25% probability of AIS $\geq$ 4	Viano (1989)
VC_{max} to half thorax	0.85ms^{-1}	25% probability of AIS $\geq$ 4	Cavanaugh at al. (1993)
VC_{max} to whole thorax	1.00ms^{-1}	50% probability of AIS $\geq$ 3	Viano (1989)
	1.47ms^{-1}	25% probability of AIS $\geq$ 4	Viano (1989)

The most simplified injury criterion gives a limit of 60g in a maximum of 3ms in a frontal impact. From this, considering a mass of 30kg to the thorax gets a force limit of 3.3kN. Comparing this value with the reported in several analyses, we found values of 3.3kN until minor skeletal injuries to a direct impact to the sternum.

More complex criteria's are proposed, like the TTI (Thoracic Trauma Index). The TTI is presented for side impacts. The criteria are given by:

$$TTI = 1.4AGE + 0.5\left(RIB_y + T12_y\right)\frac{M}{M_{std}} \tag{4-20}$$

where the units are $[g]$, AGE is age of the person in years, RIB_y the maximum of the absolute value of acceleration in 4th and 8th rib, $T12_y$ the maximum of absolute value in the 12th thorax vertebra, M the mass of the person and M_{std} the standard mass, $75kg$. A variation of the TTI is the TTI(d), using for this Hybrid III dummies, not considering the age and using a mass correlation of 1. The TTI parameter are a statistical parameter, not make a direct relationship between mechanisms involved and corresponding injury.

One criterion to blunt impact test is the compression criteria (C). It correlates the chest deformation directly with the AIS score using:

$$AIS = -3.78 + 19.56C \tag{4-21}$$

Other criteria are the VC, or the viscous criterion. These criteria take into account that soft tissue injury is compression-dependent and rate-dependent. It's applied to lateral and frontal solicitations using the rib or chest deflection. The value is obtained using:

$$VC = V\left(t\right)C\left(t\right) = \frac{d\left[D\left(t\right)\right]}{dt}\frac{D\left(t\right)}{b} \tag{4-22}$$

where VC comes in $\left[ms^{-1}\right]$, $V(t)$ is the derivate of the deformation, $D(t)$, in time and $C(t)$ the quotient between the deformation and the initial torso thickness, b. The critical velocity to lateral and frontal impact are the $1ms^{-1}$ value.

The Combined Thoracic Index (CTI) represents a criterion to the chest in frontal impact. The calculation is obtained by:

$$CTI = \frac{A_{max}}{A_{int}} + \frac{D_{max}}{D_{int}} \tag{4-23}$$

where A_{max} is the $3ms$ value of the resultant acceleration of the spine, A_{int} the critical $3ms$ intercept value, D_{max} the deflection of the chest, and D_{int} the intercept value for deflection. The acceleration and the deflection are presented in $[g]$ and $[mm]$ respectively.

4.4   The Abdomen

The abdominal cavity is a body section that is vulnerable to blunt or perforation injuries. Usually this type of trauma is not seen in the first evaluation. By the particular aspects and characteristics of this part of the body, its particular difficult in establishing injury mechanisms.
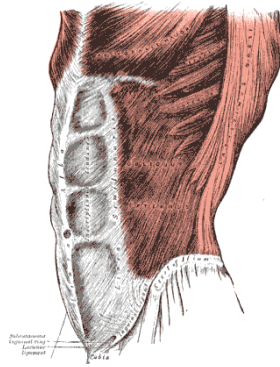
Figure 4-39 – Muscles of the abdominal wall (from Gray's Anatomy, 1918)

Like the thorax, the abdomen is considered in this work as rigid beam in the model, moving in relation of thorax and pelvis using revolute joint's (Figure 4-39).

4.4.1 Abdomen dimensions

The general characteristics of the abdomen are listed in the Table 4-22 and Table 4-23.

Table 4-22– Abdomen volume and mass [54]

Volume	$10^{-3}\,m^3$	2.479
Mass	kg	2.365

Table 4-23 – Coordinates for abdomen centre of mass, inertial and joints (local coordinates) [54]

		X	**Y**	**Z**
CoM		-4	0	-24.2
I	$10^{-4}\,kg\,m^2$	167.611	106.560	254.838
I axis rotation	X	2.6	90	92.2
	Y	90	0	90
	Z	87.8	90	2.6
L2-L3	$10^{-3}\,m$	-39	0	6
L5-S1	$10^{-3}\,m$	-40	0	-87

4.4.2 Abdomen movements

Considering the abdomen as a rigid beam, his joints relatively with the adjacent bodies are: L2-L3 with the thorax and L5-S1 with the hip. These joints are described and explained in the pelvis section.

4.4.3 Anatomy

The abdomen goes from diaphragm until the pelvic bones (Figure 4-40). The lower abdomen is protected mainly by musculature (lateral and anterior aspects). The floating ribs wave an important aspect in posterior impacts [17].
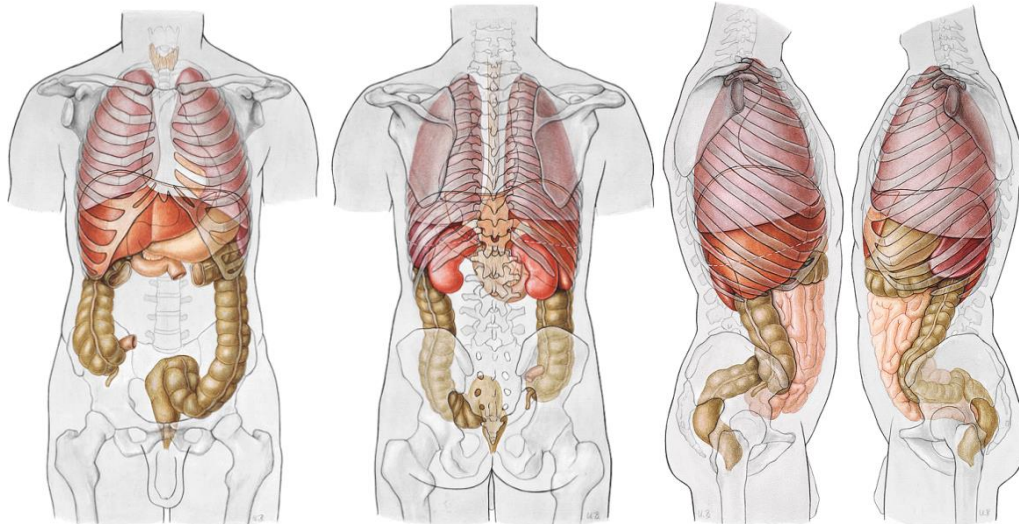
Figure 4-40 – The abdominal organs as a projection on the body surface [63]

In terms of anterior impact, usually the most exposed are the superficial organs.

The abdominal cavity hosts several organs that are generally divided into solid and hollow organs. The main difference is their density.

Solid organs like liver, spleen, pancreas, kidneys, ovaries and adrenal glands have a higher density than hollow organs such as the stomach, large and small intestines, bladder and uterus (usually by the internal cavity of this organs).

In terms of biomechanical response, its important said that the organs inside the abdominal cavity inner a relativity high degree of mobility. Partly are involved partially by fat or tethered by folds of the peritoneum, one membrane that covers the inner abdominal walls and surrounds each organ. This membrane works too to easily the movements between organs. By these facts, the organs can adjust to diverse positions or solicitations, like seat or stand. This flexibility has a great influence in terms of injury mechanisms.

4.4.4   Abdomen models in our work

In our work, one model of each type have been used: 1 MBM abdomen and 1 FEM abdomen plus pelvis.

4.4.4.1   MBM abdomen

The abdomen in our MBM is a rigid body (Figure 4-41), with the centre of mass defined according to the head referential axis, as the definition of the body inertia. The geometry was taken from a 50th percentile mannequin. The abdomen surface was tessellated for contact proposes.

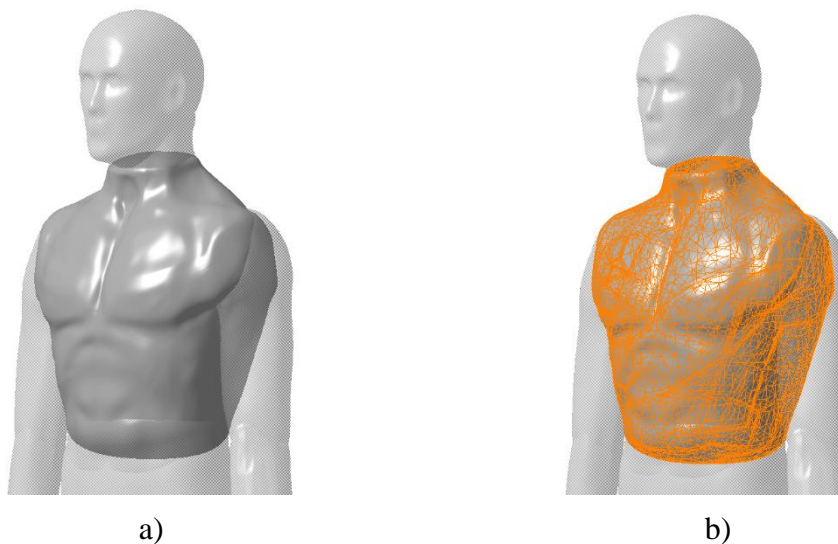<center>a)   b)</center>
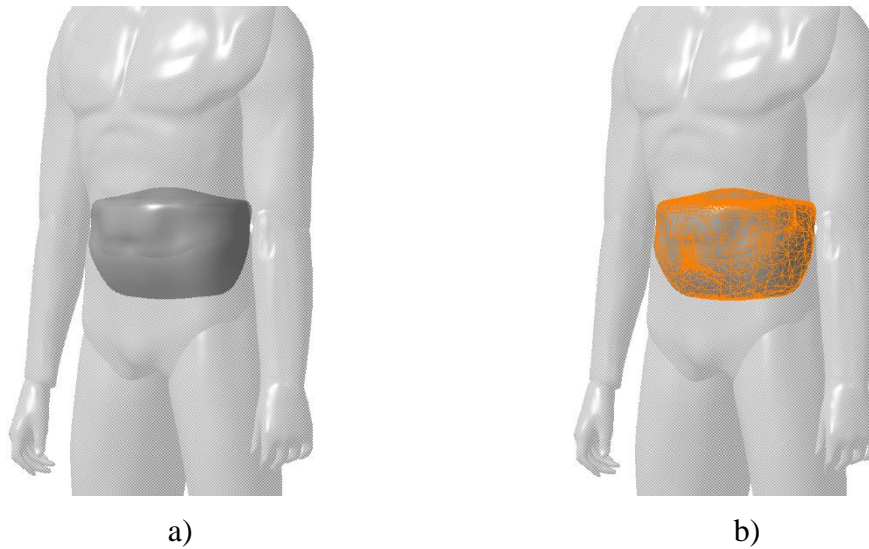
Figure 4-41 – MBM abdomen a) geometry, b) geometry with tessellated surface for contact proposes

4.4.4.2   FEM abdomen and pelvis

For the injury assessment, the HUMOS2 abdomen and pelvis was used (Figure 4-42). Both abdomen and pelvis are in same section since some organs are divided between both sub-segments. The model includes the lumbar vertebras and respective discs, pelvic bone, intestines, liver, spline, kidneys, stomach, flesh and skin.

<center>a)   b)</center>
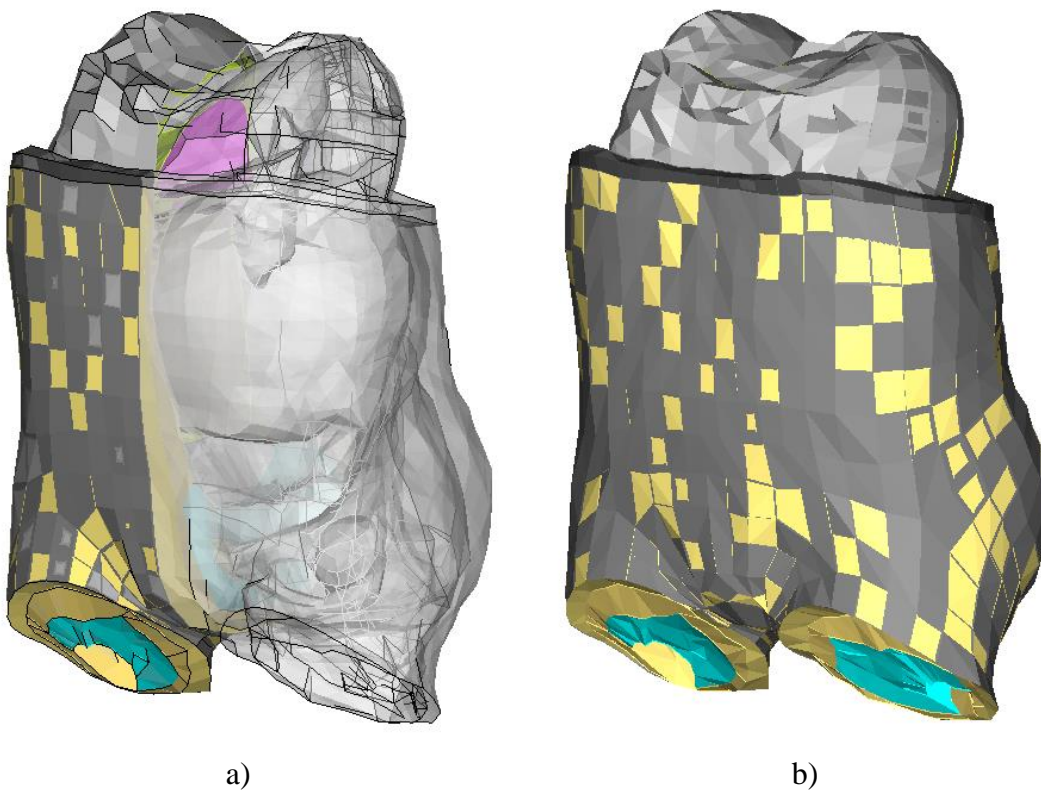
Figure 4-42 – HUMOS2 abdomen and pelvis a) section view, b) outside view

As major limitations found in the model are the fact that the lumbar vertebras and the pelvic bones are modelled as rigid bodies.

4.4.5 Injuries and associated mechanisms

The numbers of factors to this structure are huge. The type of injury depends too much of the orientation of the load and the dispositions of the interior in that position. An example is the organs that are located in frontal of spine are exposed to compression in frontal impacts, by the compression of the all set. The asymmetry influences too the grade of trauma according with the direction of the solicitation [17].

Usually, the called solid organs are more proposed to trauma. Other aspects are the health of the person, previous surgeries or lesions, and the age by itself. In the kids, the injury of this part has a more probability by the more relative volume of the abdomen comparing with an adult.

Table 4-24 – Examples of abdominal injuries according to AIS scale [17]

AIS code	Description
1	Skin, muscles: contusions (hematoma)
2	Spleen or liver contusion (<50% surface area)
3	Major kidney contusion Spleen: rupture
4	Abdominal aorta: minor laceration Kidney/liver: rupture
5	Kidney: total destruction of organs and its vascular system
6	Hepatic avulsion (total separation of all vascular attachments)

The possible injuries in blunt impact to the abdomen are [17]:

- liver
    - Laceration, haemorrhage
        - Compression against the spin
        - Viscous injury: high rate loading increases the fluid pressure and thus causes strains
        - Rapid deceleration causing motion relative to the body
- Spleen
    - Lacerations, disrupter
        - Direct impact on left side
        - Indirect loading causing rapid deceleration and large displacement relative to the body
- kidneys
    - Contusion, laceration
        - Lateral impact

Likely that what happens in thorax, appears that the best correlation between the mechanical load and the injury is obtained using the acceleration and the displacement (compression).

4.4.6   Injury criteria

The mainly threshold found to injury criteria are given by the European regulations, and it's for lateral impacts. It's marked a maximum internal force of $2.5kN$ (equivalent to an external force of $4.5kN$) [17].

4.5   The pelvis and lower extremities

In PTW accidents, the exposure of these parts of the body is considerable. The fall of a heavy parked PTW can be enough to injury a lower extremity. This section of the body is associated with several injuries, but usually not life threating in very-short time, but with a high impact in socio-economical cost.

4.5.1   Pelvis

The pelvis is the base of the trunk (Figure 4-43). In the trunk, this is the unique sector that is a true rigid body when compare with the other two segments: the abdomen and the thorax.
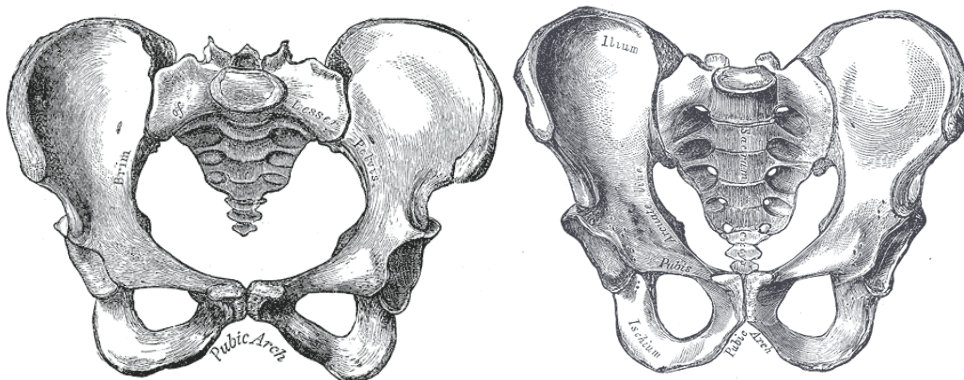
Figure 4-43 – Female and male pelvis (from Gray's Anatomy, 1918)

4.5.1.1   Pelvis dimensions

The general characteristics of the pelvis are listed in the Table 4-25 and Table 4-26.

Table 4-25 – Pelvis volume and mass [54]

Volume	$10^{-3} m^3$	11.964
Mass	kg	11.414
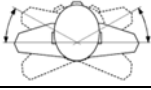
Table 4-26 – Coordinates for pelvis centre of mass, inertial and joints (local coordinates) [54]

		X	**Y**	**Z**
CoM		-81.8	0	10.7
I	$10^{-4} kg\, m^2$	1,015.738	942.376	1,184.697
I axis rotation	X	8.4	90	81.6
	Y	90	0	90
	Z	98.4	90	8.4
L5-S1	$10^{-3} m$	-67	0	29
Hip	$10^{-3} m$	-61	±82	-62

4.5.1.2 Pelvis movements

The pelvis movement will interact with upper bodies. The main range of the trunk can be defined by the joint L5-S1. This approximation gives us the movement characterization detailed in the Table 4-27. The L5-S1 joint and the hip joints are considered like spherical joints.

Table 4-27 – Range motion of the thorax and abdomen [64]

Type of motion	Representation	Rotation [deg]
Flexion		70
Hyperextension		30
Lateral Flexion		35
Rotation		35

The movement resistance is given by the correlation illustrated as can be seen in the Figure 4-44.
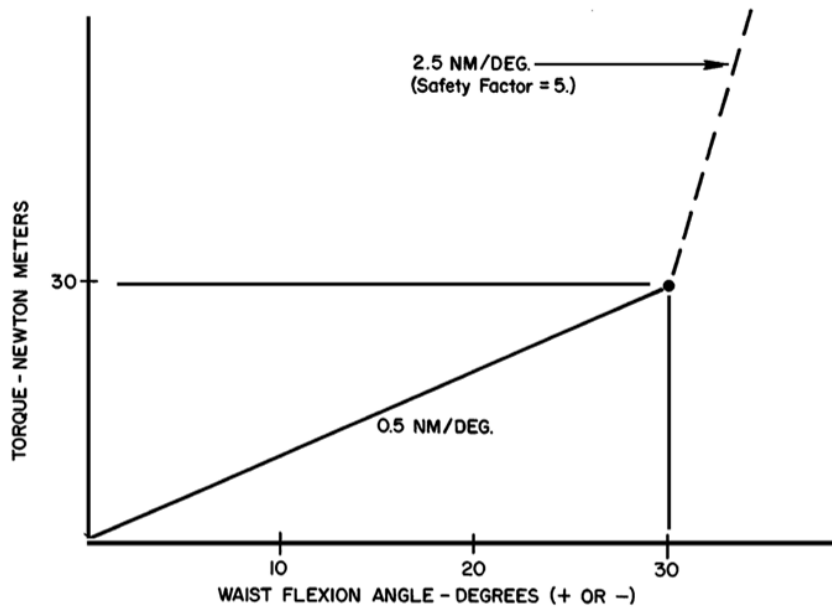
Figure 4-44 – Hip resistance to flexion and extension [54]

4.5.1.3   Pelvis models in our work

In our work, one model of each type have been used: 1 MBM pelvis and 1 FEM pelvis plus abdomen (presented in section 4.4.4.2, p.80).

4.5.1.3.1   MBM pelvis

The pelvis in our MBM is a rigid body (Figure 4-45), with the centre of mass defined according to the head referential axis, as the definition of the body inertia. The geometry was taken from a 50th percentile mannequin. The pelvis surface was tessellated for contact proposes.

a)   b)
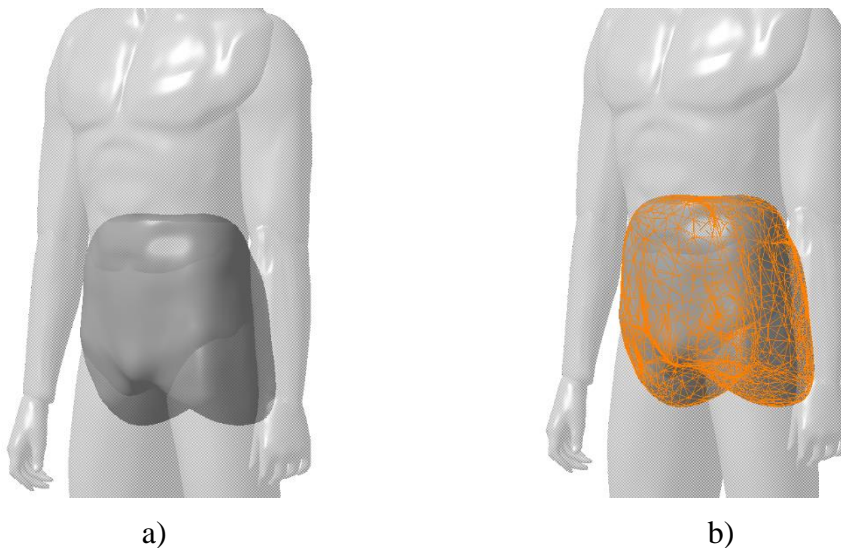
Figure 4-45 – MBM pelvis a) geometry, b) geometry with tessellated surface for contact proposes

4.5.2   Upper legs

The upper leg is connected to the hip by the hip joint and to the lower leg by the knee.

4.5.2.1   *Upper legs dimensions*

The general characteristics of the upper legs are listed in the Table 4-28 and Table 4-29.

Table 4-28 – Upper legs volume and mass [54]

Volume	$10^{-3}m^3$	9.029
Mass	kg	8.614

Table 4-29 – Coordinates for upper legs centre of mass, inertial and joints (local coordinates) [54]

		X	**Y**	**Z**
CoM	$10^{-3}m$	6	±66	-200
I	$10^{-4}kg\,m^2$	1,230.899	1,301.540	367.118
I axis rotation	X	9.8	90 ∓ 9.8	89.8
	Y	90±9.8	9.8	90.9
	Z	90.1	89.1	1.1
Hip	$10^{-3}m$	13	±123	7
Knee	$10^{-3}m$	0	±51	-418

4.5.2.2   *Upper legs movements*

The upper leg movements are set by the hip joint. The main characteristics of this spherical joint are presented in the Table 4-27 and Figure 4-46
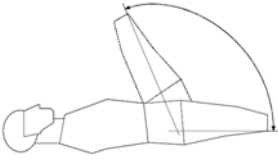
4.5.2.3   *Upper legs models in our work*

In our work, one pair of models of each type have been used: 1 MBM pair of upper legs and 1 FEM pair of upper legs.

4.5.2.3.1   MBM upper legs
The upper legs in our MBM are rigid bodies (Figure 4-47), with the centre of mass defined according to the head referential axis, as the definition of the body inertia. The geometry was taken from a 50th percentile mannequin. The upper legs surface was tessellated for contact proposes for both left and right body.

Table 4-30 – Range motion of the upper leg [64]

Type of motion	Representation	Rotation [deg]
Flexion		102
Hyperextension		45
Abduction / Abduction		53 / 31
Medial Rotation / Lateral Rotation		39 / 34
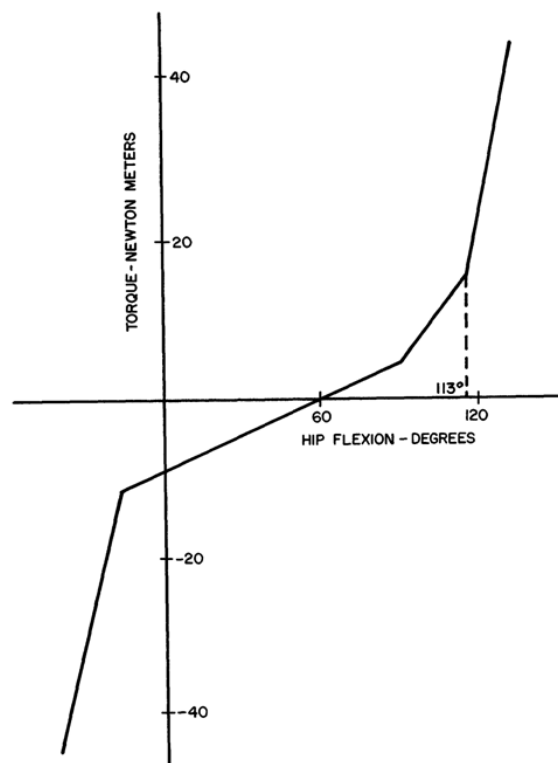
Figure 4-46 – resistance to hip flexion and extension [54]

<center>a)</center> <center>b)</center>
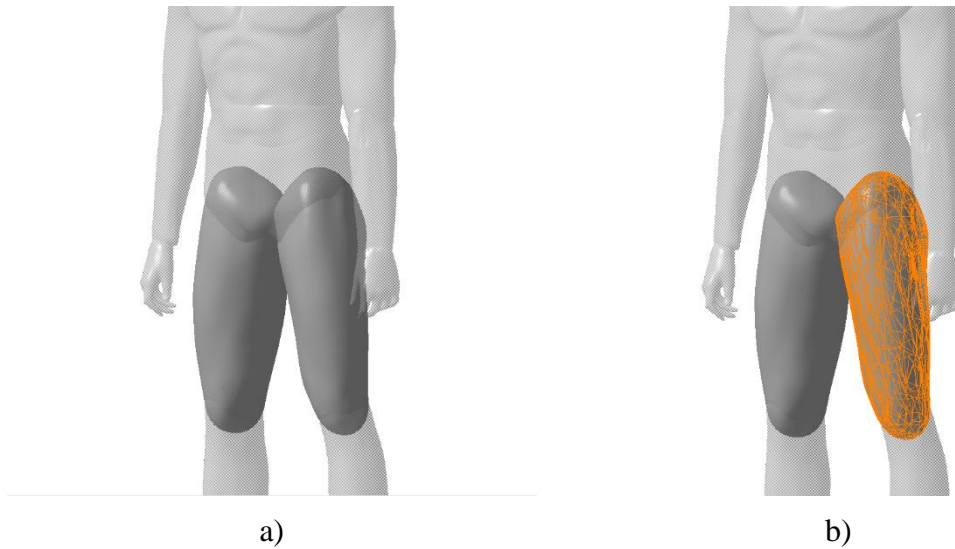
Figure 4-47 – MBM pelvis a) geometry, b) geometry with tessellated surface for contact proposes (left side)

4.5.2.3.2 FEM lower limbs – upper and lower legs with feet

For the injury assessment, the HUMOS2 lower limbs have been used (Figure 4-48). The right and left lower limbs models includes bones, cartilage, flesh and skin of the upper and lower legs and the feet.

<center>a)</center> <center>b)</center>
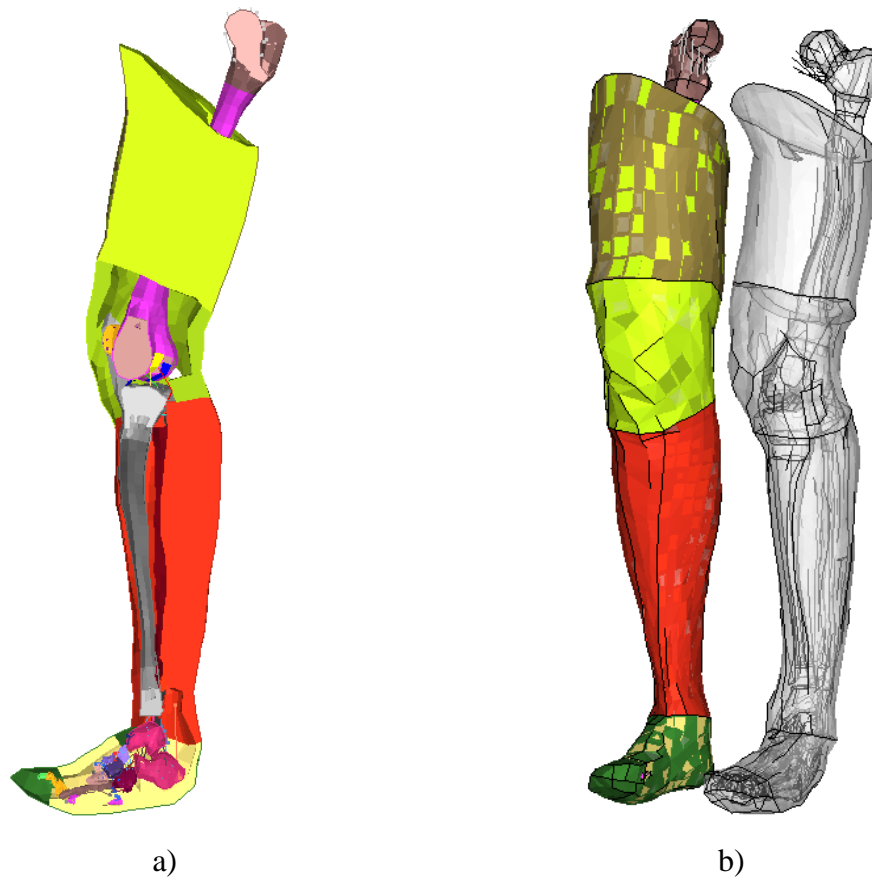
Figure 4-48 – HUMOS2 abdomen and pelvis a) section view, b) outside view

4.5.3   Lower legs

Lower leg goes from the knee to the ankle is shown in the Figure 4-49.

Figure 4-49 – Lower legs details, with the foot (from Gray's Anatomy, 1918)

4.5.3.1   Lower legs dimensions

The general characteristics of the lower legs are listed in the Table 4-31 and Table 4-32.

Table 4-31 – Lower legs volume and mass [54]

Volume	$10^{-3} m^3$	3.760
Mass	kg	3.587
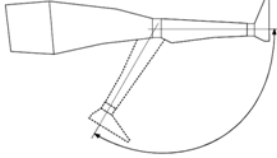
Table 4-32 – Coordinates for lower legs centre of mass, inertial and joints (local coordinates) [54]

		X	**Y**	**Z**
CoM	$10^{-3} m$	-11.9	±57	-149
I	$10^{-4} kg\, m^2$	520.397	528.342	60.688
I axis rotation	X	24	90±9.8	90
	Y	90∓24	90∓2	90±2
	Z	90		1
Knee	$10^{-3} m$	12	±48	22
Ankle	$10^{-3} m$	0	±37	-393

4.5.3.2   Lower legs movements

The movement of the lower leg is set by the knee. This revolute joint is described in the Table 4-33 and the Figure 4-50.

Table 4-33 – Range motion of the lower leg [64]

Type of motion	Representation	Rotation [deg]
Flexion		25
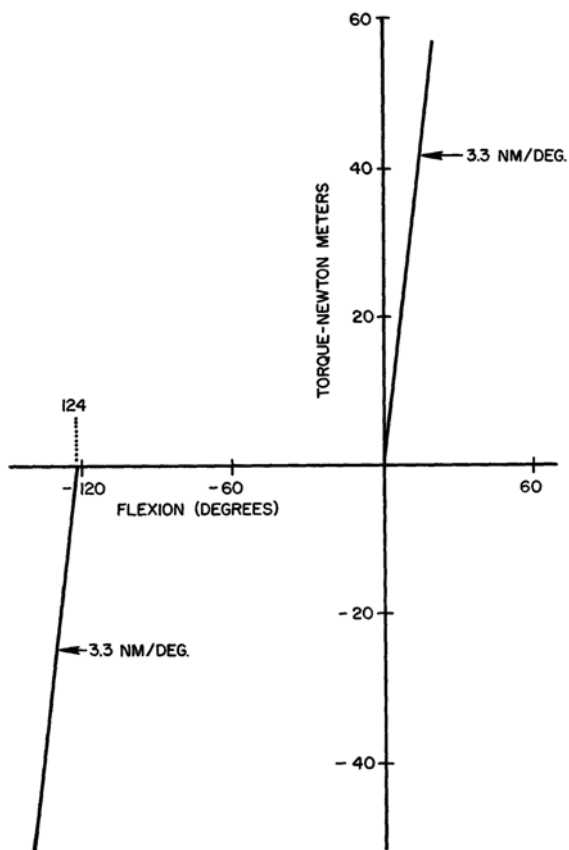
Figure 4-50 – resistance of flexion at knees [54]

4.5.3.3 Lower legs models in our work

In our work, one pair of models of each type have been used: 1 MBM pair of lower legs and the respective FEM pair (presented in section 4.5.2.3.2, p.87).

4.5.3.3.1 MBM lower leg

The lower legs pair in our MBM are two rigid bodies (Figure 4-51), with the centre of mass defined according to the head referential axis, as the definition of the body inertia. The geometry was taken from a 50th percentile mannequin. The lower legs surfaces were tessellated for contact proposes.

a)   b)
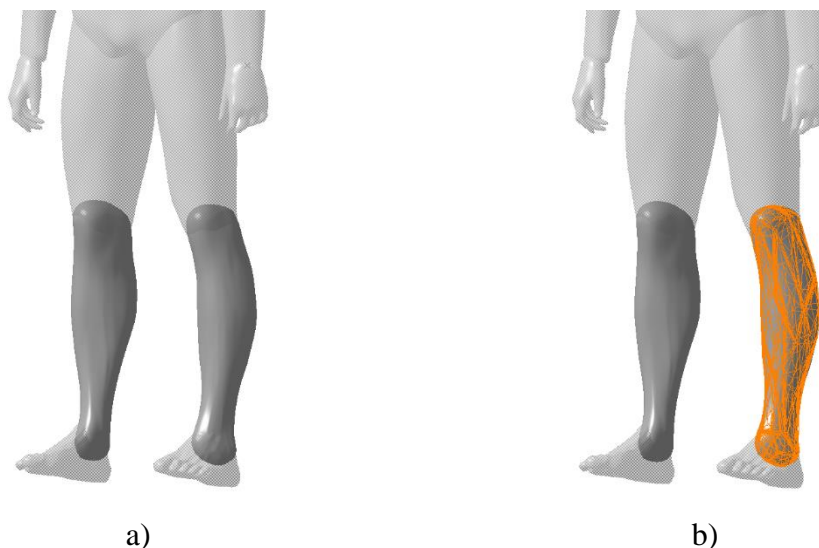
Figure 4-51 – MBM pelvis a) geometry, b) geometry with tessellated surface for contact proposes (left side)

4.5.4 Foot

The lower extremity of the body is the foot (Figure 4-52).

Figure 4-52 – The bones of the human foot (William Cheselden, 1733)

4.5.4.1 Feet dimensions

The general characteristics of the foot are listed in the Table 4-34 and Table 4-35.

Table 4-34 – Feet volume and mass [54]

Volume	$10^{-3} m^3$	1.028
Mass	kg	0.981
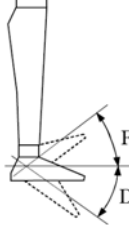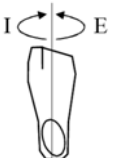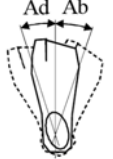
4.5.4.2 Feet movements

The feet are joined to the lower legs by the respective ankles, simplified to a spherical joint. The details about this joint are presented in the Table 4-36.

Table 4-35 – Coordinates for feet centre of mass, inertial and joints (local coordinates) [54]

		X	**Y**	**Z**
CoM	$10^{-3}m$	-76.9	±0.6	-6.2
I	$10^{-4}kg\,m^2$	8.728	42.966	44.132
I axis rotation	X	10	90±4	81
	Y	90∓4	7	90±5
	Z	99	90∓5	10
Ankle	$10^{-3}m$	-124	±14	58

Table 4-36 – Range motion of the foot [64]

Type of motion	**Representation**	**Rotation [deg]**
Flexion / Dorsiflexion		20 / 35
Inversion / Eversion		35 / 25
Abduction / Abduction		5 / 5

4.5.4.3 *Pelvis models in our work*

In our work, 1 feet model of each type have been used: 1 MBM feet pair and the respective FEM pair (presented in section 4.5.2.3.2, p.87).

4.5.4.3.1 MBM feet
The feet in our MBM are two a rigid bodies (Figure 4-53), with the centre of mass defined according to the head referential axis, as the definition of the body inertia. The geometry was taken from a 50th percentile mannequin. The feet surface was simplified and tessellated for contact proposes.

a)   b)
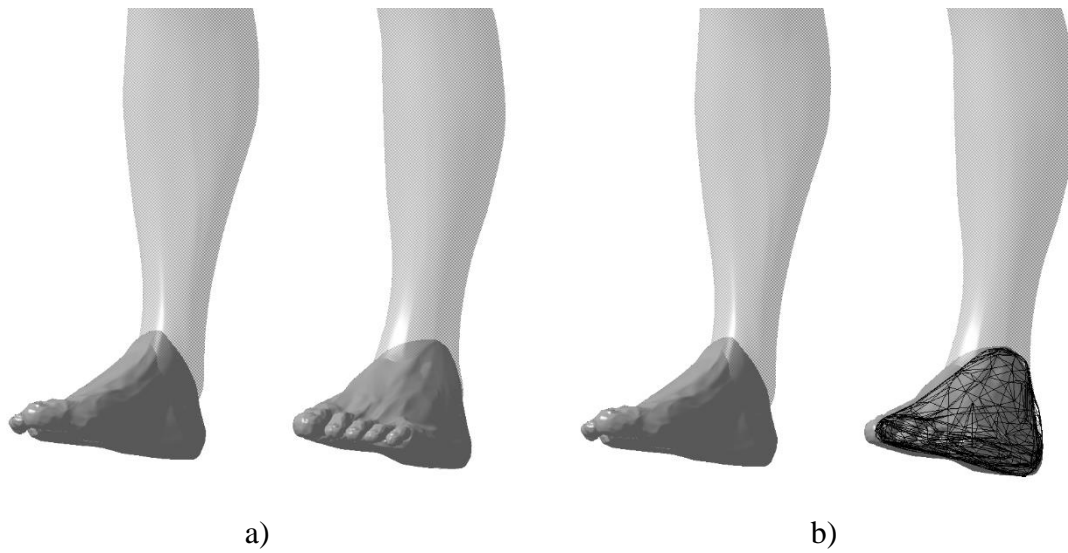
Figure 4-53 – MBM pelvis a) geometry, b) geometry with tessellated surface for contact proposes (left side)

4.5.5   Anatomy

Generally, we have the pelvis, thigh, knee, lower leg, ankle and foot (Figure 4-54).
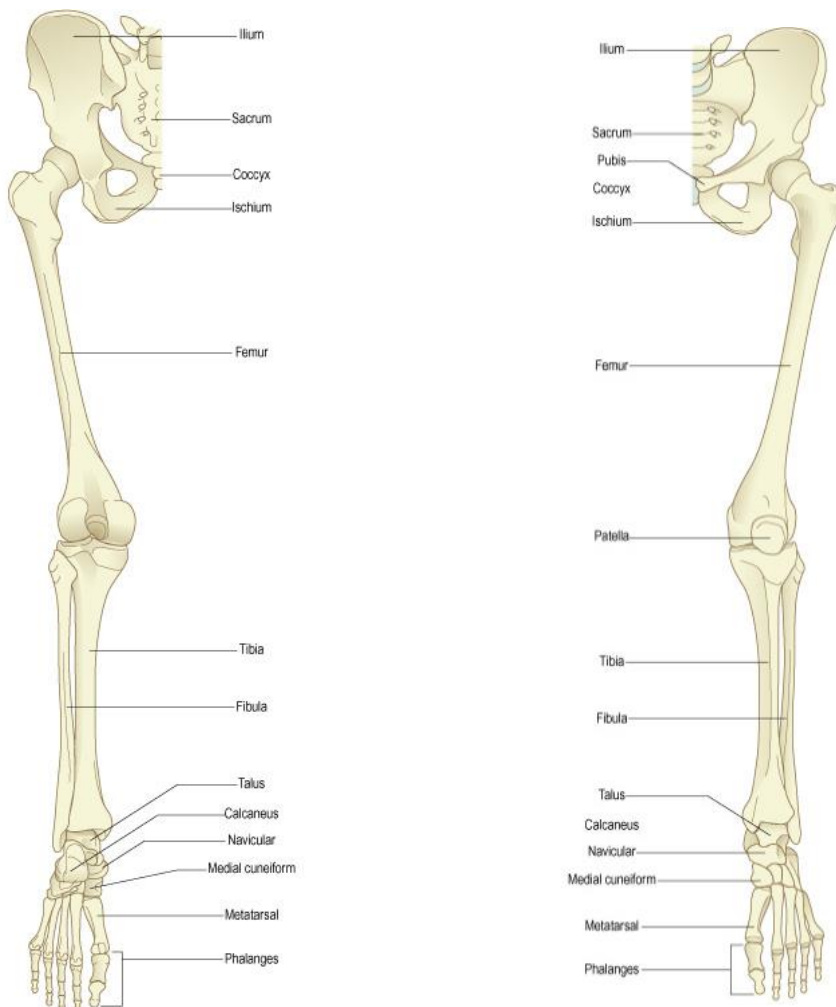
Figure 4-54 – Overview of bones of the lower limb: posterior and anterior view respectively [62]

The pelvis which links the lower extremities to the spine is a ring of bones basically composed of four bones: the hipbones, sacrum and coccyx (Figure 4-55).
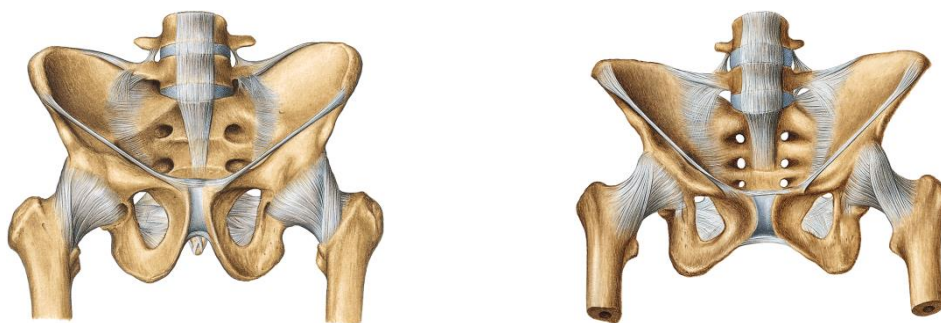
Figure 4-55 – Anterior and inferior overview of pelvis: male and female respectively [63]

The hipbone is composed by three fused bones, the ilium, ischium and pubis. In this set, resides the acetabulum that with the femur head forms the hip joint. The femur is the longest bone in the human body.

The knee joint is a region anatomically dense involving several muscles, tendons and the patella.

For last, the foot, a complex set of bones: calcaneus, talus, metatarsal bones and phalanx bones.

The details about the pelvic and lower extremities injuries are presented in the Table 4-37.

Table 4-37 – Examples of pelvis and lower extremities injuries according to AIS scale [17]

AIS code	Description
1	Ankle, hip: sprain, contusion
2	Patella, tibia, calcaneus, metatarsal: fracture Pelvis: fracture (closed, andisplaced) Toe: amputation, crush Hip, knee dislocation Muscles, tendons: laceration (rupture, tear, avulsion)
3	Femur: fracture Pelvis: fracture (open, displaced) Traumatic amputation below knee
4	Pelvis: "open book" fracture Traumatic amputation above knee
5	Pelvis: substantial deformation with associated vascular disruption and blood loss >20% by volume
6	Not applied

4.5.6   Injuries and associated mechanisms

One typical injury is in the hip joint, evolving on or more bones of this area, like the proximal femur or the hipbones.

The mainly types of injury are: bone fractures, or ligament ruptures. Several thresholds are presented to the bones in the lower extremities in the Table 4-38.

Table 4-38 – Mechanical strength of the bones of the lower limbs [17]

		femur		*tibia*		*fibula*	
		male	*female*	*male*	*female*	*male*	*female*
Torque	$[Nm]$	175	136	89	56	9	10
Bending	$[kN]$	3.92	2.58	3.36	2.24	0.44	0.30
Maximum moments	$[Nm]$	310	180	207	124	27	17
Long axis compression	$[kN]$	7.72	7.11	10.36	7.49	0.60	0.48

4.5.7   Injury criteria

Several criteria's are defined to injury in the lower extremities.

The compression force gives the maximum value of $10kN$ to an axial load in the hip-thigh-knee complex. Gives too the maximum value of $8kN$ to each tibia.

The FFC (Femur Force Criteria) gives the maximum compression force acting in certain duration. For times greats than $10ms$, its marked a force of $7.58kN$. To lower times, the is the linear variation between $9.07kN (t = 0ms)$ and $7.58kN (t = 10ms)$.

The TI (Tibia Index) involves the bending moments as well as the axial force in the tibia. The mainly idea is to prevent tibia shaft fractures. It's given by the expression:

$$TI = \frac{M}{M_{crit}} + \frac{F}{F_{crit}}$$ (4-24)

with M being the bending moment and F the compressive force. M_{crit} and F_{crit} represent critical intercept values and read $225 Nm$ and $35.9kN$, respectively, for a 50th percentile male.

For side impact, the PSPF (Pubic Symphysis Peak Force) give a maximum value of $6kN$ to the pelvic strain.

A maximum tibial displacement of $15mm$ to protect the knee ligaments is presented too.

4.6   The Upper Extremities

This part of the human body is probably the less presented in injury involving traffic accidents.

4.6.1 Upper arms

The upper arms are connected to the thorax in the Glenohumeral joint (Figure 4-56).
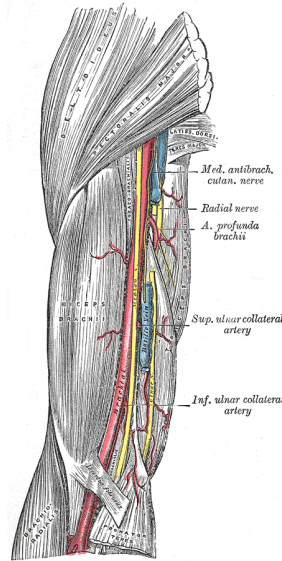
Figure 4-56 – Detail view of upper arm (from Gray's Anatomy, 1918)

4.6.1.1 Upper arm dimensions

The general characteristics of the upper arm are listed in the Table 4-39 and Table 4-40.

Table 4-39 – Upper arms volume and mass [54]

Volume	$10^{-3}\,m^3$	1.854
Mass	kg	1.769
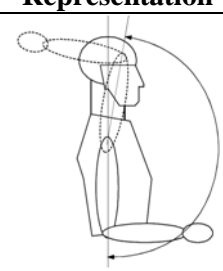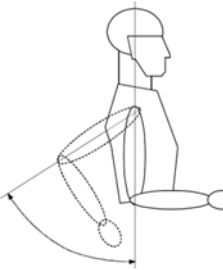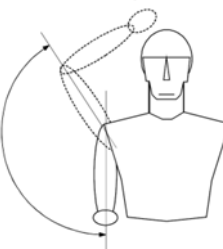
Table 4-40 – Coordinates for upper arms centre of mass, inertial and joints (local coordinates) [54]

		X	**Y**	**Z**
CoM	$10^{-3}\,m$	16.5	±30	-172
I	$10^{-4}\,kg\,m^2$	112.467	122.526	23.115
I axis rotation	X	33.69	90 ∓ 33.4	91.1
	Y	90±33.4	34.3	90 ∓ 7
	Z	90	90±7	7
Glenohumeral	$10^{-3}\,m$	12	±33	-42
Elbow	$10^{-3}\,m$	-6	±39	-337

4.6.1.2 Upper arms movements

The movements of the upper arms are detailed presented in the Table 4-41. The upper arm has two joints, one spherical in the Glenohumeral, and other revolute, in the elbow. The respective resistance to the movement is illustrated in the Figure 4-57 and Figure 4-58.

Table 4-41 – Range motion of the upper arm [64]

Type of motion	Representation	Rotation [deg]
Flexion		180
Hyperextension		58
Abduction		130
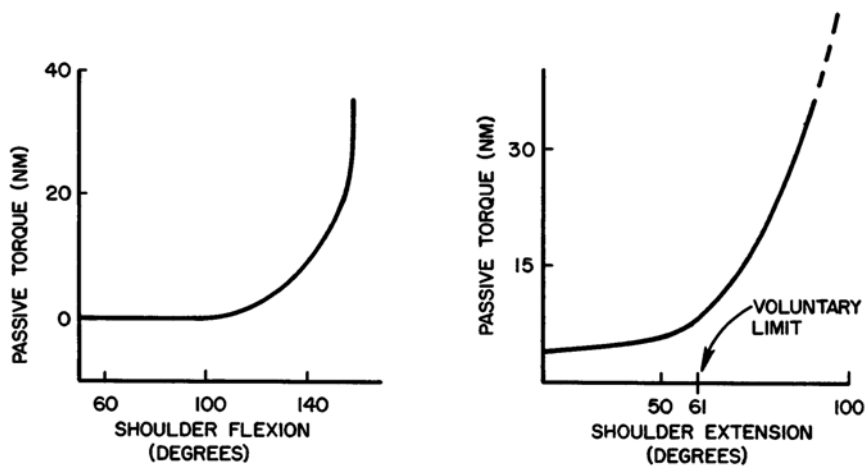
Figure 4-57 – Shoulder resistance to flexion and extension [54]
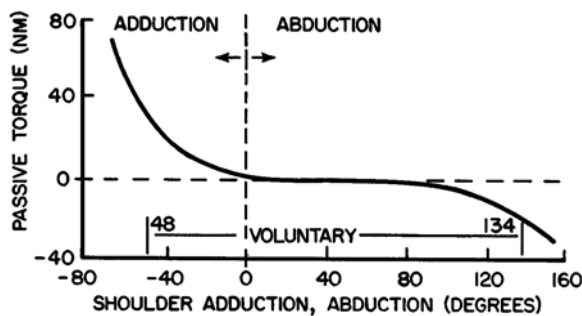
Figure 4-58 – Shoulder resistance to adduction and abduction [54]

4.6.1.3   Upper arm models in our work

In our work, 1 pair of upper member's models of each type have been used: 1 MBM and 1 FEM.

4.6.1.3.1   MBM upper arm
The upper arm pair in our MBM are two rigid bodies (Figure 4-59), with the centre of mass defined according to the respective upper arm referential axis, as the definition of the body inertia. The geometry was taken from a 50th percentile mannequin. The upper arms surfaces have been tessellated for contact proposes.

a)   b)
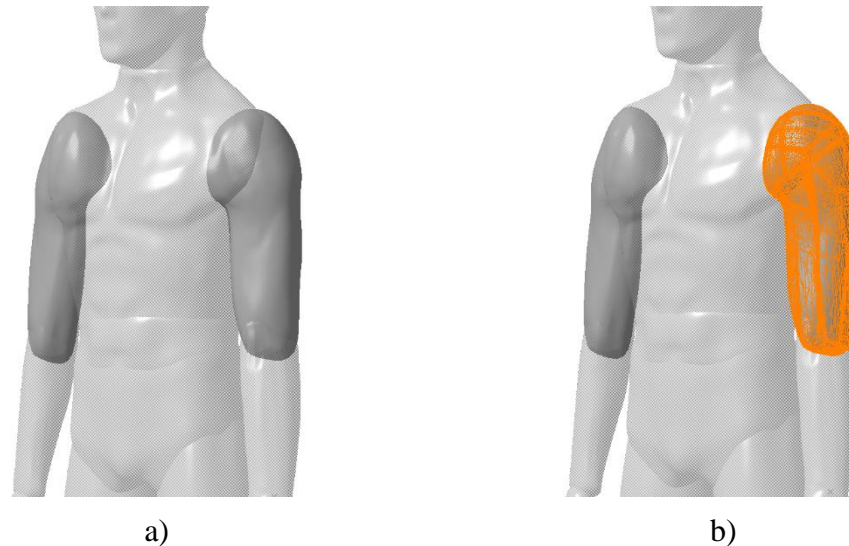
Figure 4-59 – MBM pelvis a) geometry, b) geometry with tessellated surface for contact proposes

4.6.1.3.2   FEM upper limbs – upper and lower arms with hands
For the injury assessment, the HUMOS2 pair of upper limbs have been used (Figure 4-60). The right and left upper limbs models includes bones, cartilage, flesh and skin of the upper and lower arm and the hands.

a)   b)
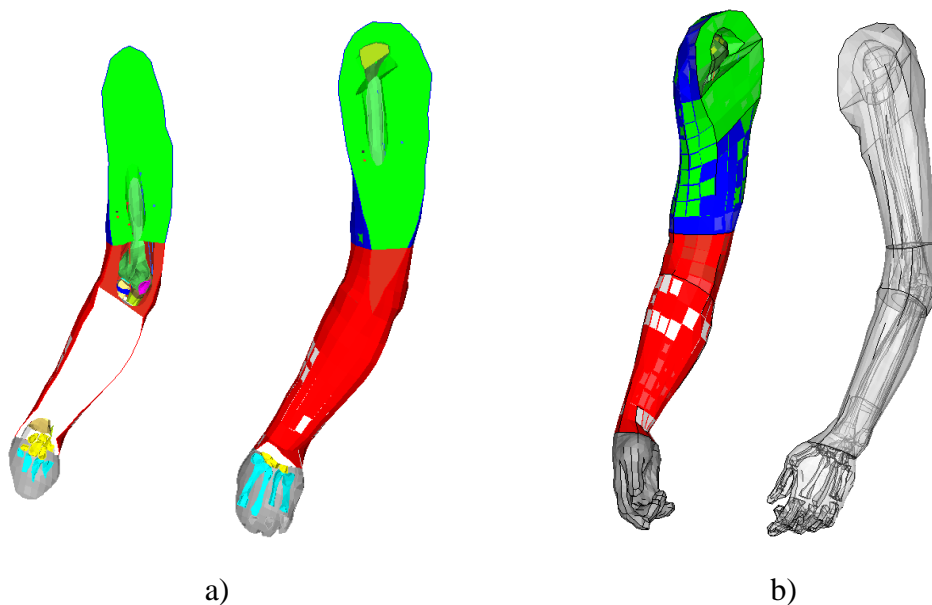
Figure 4-60 – HUMOS2 arms a) section views', b) outside view (left arm transparent)

4.6.2   Lower arms and hands

The lower arm goes from the elbow until the wrist (Figure 4-61). Is considered too a rigid body, and the only movements will be described in the elbow and the wrist.
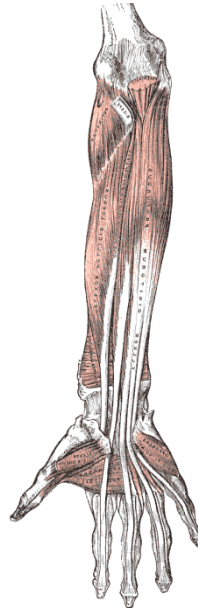
Figure 4-61 - Deep muscles of the lower arm (from Gray's Anatomy, 1918)

The general characteristics of the lower arms are listed in the Table 4-42 and Table 4-43.

Table 4-42 – Lower arms volume and mass [54]

Volume	$10^{-3} m^3$	2.120
Mass	kg	2.022

Table 4-43 – Coordinates for lower arms centre of mass, inertial and joints (local coordinates) [54]

		X	**Y**	**Z**
CoM	$10^{-3} m$	-10	±35	166
I	$10^{-4} kg\, m^2$	310.769	309.252	20.148
I axis rotation	X	19.5	90 ∓ 19.5	90
	Y	90±19.5	19.5	90
	Z	90	90	1
Elbow	$10^{-3} m$	-11	±35	5
Wrist	$10^{-3} m$	-7	±30	-271

4.6.2.1   Lower arms movements

The movement of the lower arm is function of the elbow, and is summarized in the Figure 4-62 and the Table 4-44. The pronation and supination is set in the wrist, to simplify the implementation of the model.

The joints in the lower arm are the elbow (revolute) and wrist (spherical).
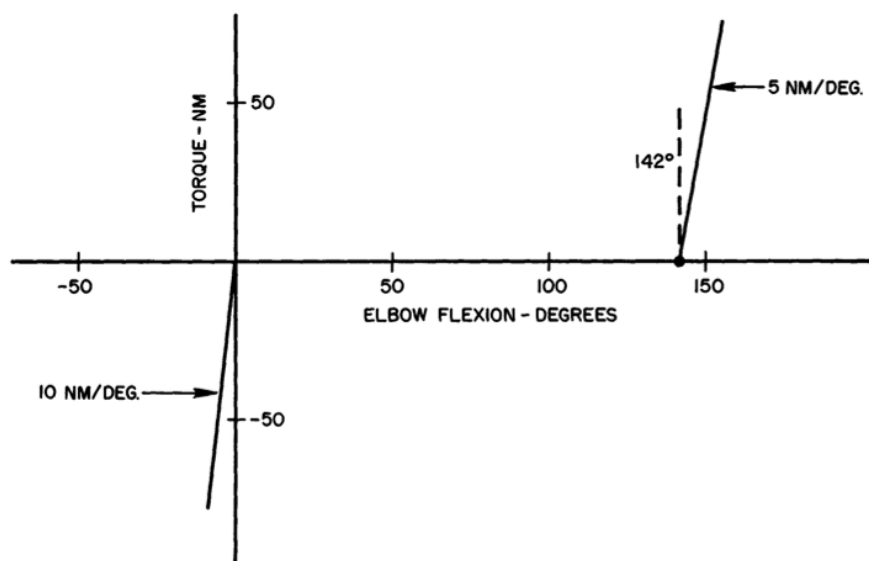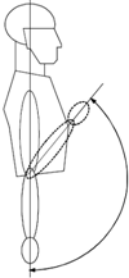
Figure 4-62 – Elbow resistance to flexion [54]

Table 4-44 – Range motion of the lower arm [64]

Type of motion	Representation	Rotation [deg]
Flexion		141

The hand is included too in this body. The wrist range movements are presented in the Table 4-45.
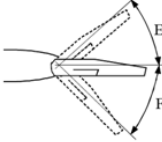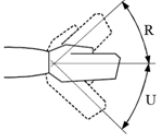
4.6.2.2   *Lower arm and hand models in our work*

In our work, 1pair of lower arms and hands models have been used, in total: 4 MBM bodies and 2 FEM groups (presented in section 4.6.1.3.2, p.97).

4.6.2.2.1   MBM lower arm and hand
The lower arm and hand in our MBM are rigid bodies (Figure 4-63 and Figure 4-64), with the centre of mass defined according to the respective referential axis, as the definition of the body inertia. The geometries have been taken from a 50th percentile mannequin. The lower arm surface and a hand simplified surface were tessellated for contact proposes.

Table 4-45 – Range motion of the hand [64]

Type of motion	Representation	Rotation [deg]
Pronation / Supination (lower arm)		90 / 90
Flexion / Extension		70 / 65
Deviation Radial / Deviation Ulnar		15 / 30
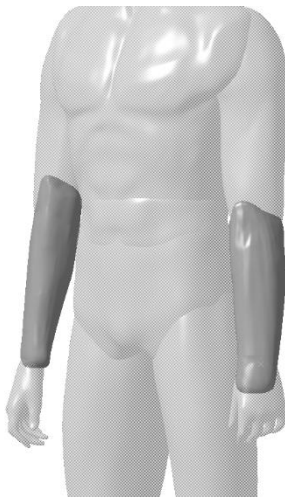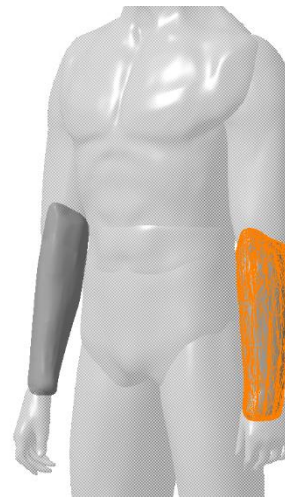
a)   b)

Figure 4-63 – MBM pelvis a) geometry, b) geometry with tessellated surface for contact proposes

4.6.3 Anatomy

The upper extremities can be separate manly in four parts: shoulder, arm, forearm and hand (Figure 4-65). The shoulder comprises scapula, clavicle and joint articulation that attach the upper extremities to the torso. The arm is formed by the humerus and is linked to the shoulder by the shoulder joint

The elbow joint connects the arm to the forearm which consists of the ulna and radius. The wrist joint, finally, connects the forearm to the hand.

a)   b)
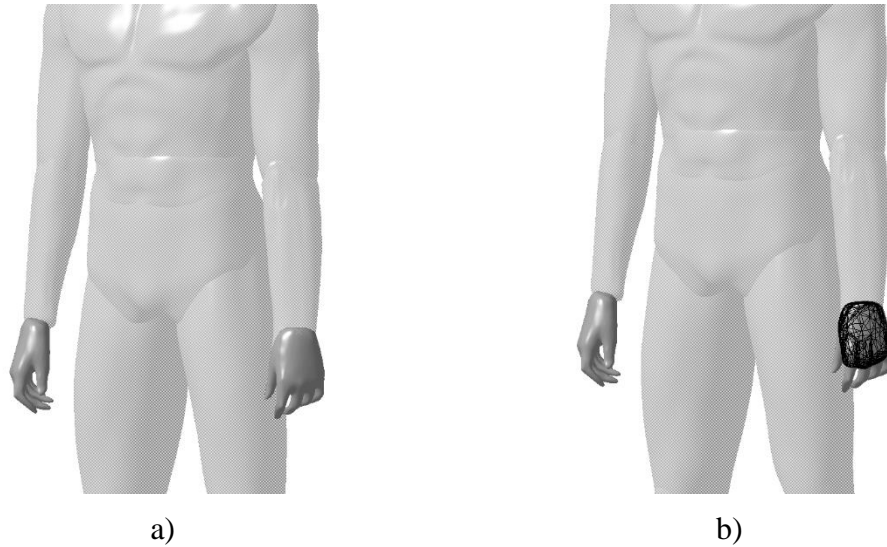
Figure 4-64 – MBM pelvis a) geometry, b) geometry with tessellated surface for contact proposes
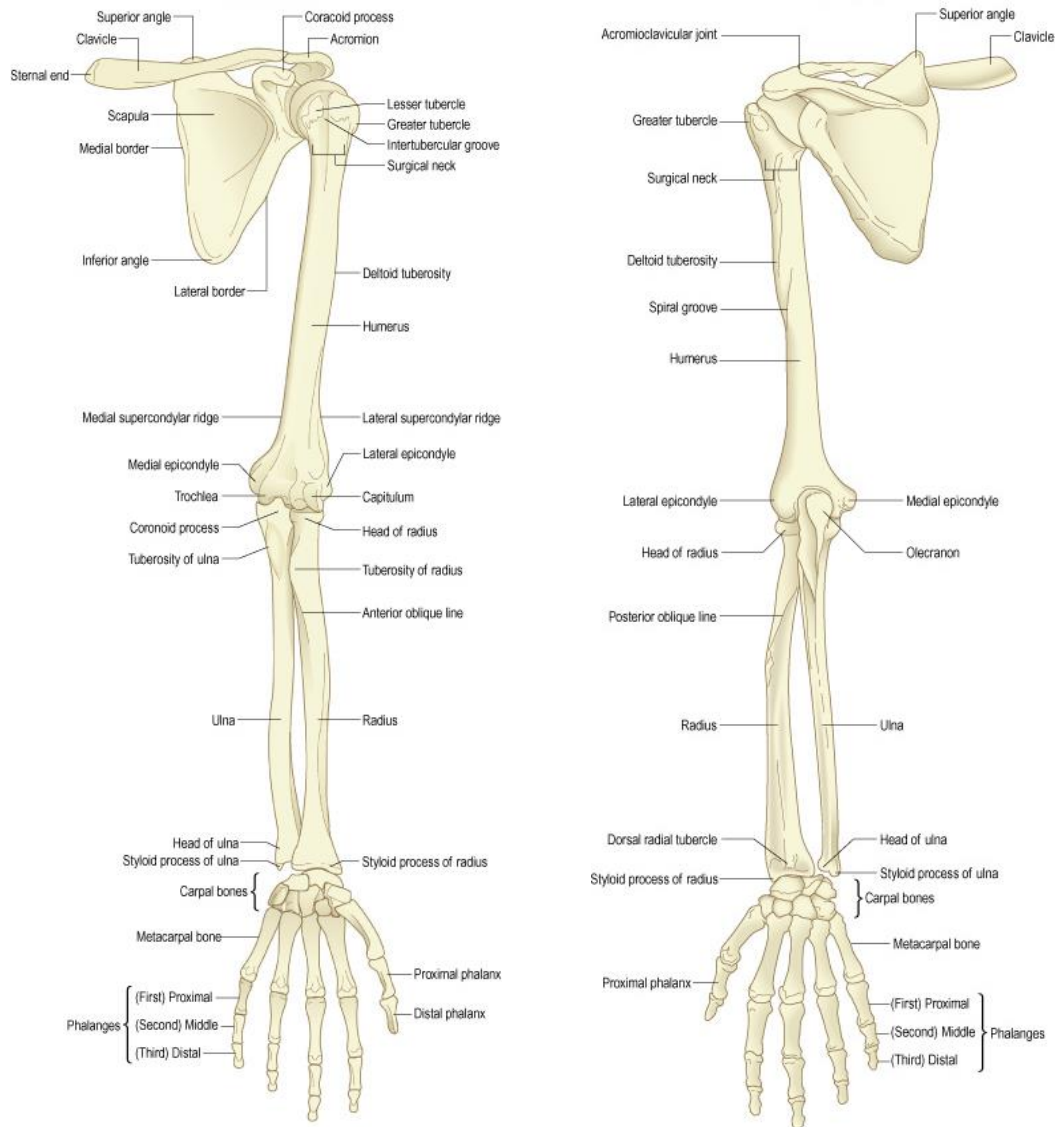
Figure 4-65 – Overview of the bones of the left pectoral girdle and upper limb: anterior and posterior
view respectively [62]

4.6.4   Injuries and associated mechanisms

Like in lower extremities, the injuries focus manly in long bones fracture and ligaments ruptures.

4.6.5   Injury criteria

The manly data are presented to the humerus (Table 4-46).

Concerning with injury criteria, the main criteria's are set to car environments, not suitable directly to PTW accidents.

Table 4-46 – Mechanical strength of humerus [17]

Bending moment		Shear force		
Male $[Nm]$	*female* $[Nm]$	*male* $[kN]$	*female* $[kN]$	*reference*
115	73			Weber (1859)
151	85			Messerer (1880)
157	84	1.96		Kirkish et al (1996)
230	130	2.5	1.7	Kirkish et al (1996)*
138				Kallieris at al.(1997)
	154			Duma et al. (1998a)
217	128			Duma et al. (1998b)*

 *scaled to 50 percentile male and 5 percentile female

5

Multibody model formulation

In this section, a two-dimensional (2D) model of a PTW including a rider is presented.
The description how the data was build and implemented is presented too.

5.1   Introduction

In the PTW driving, the influence of the driver is important in the own behaviour of the system [53]. Usually, the MBS (Multi-Body Simulation) of PTW uses a simplified model of the rider using one or two bodies to represent all the upper part of a human body (head, neck, thorax, abdomen, pelvis, and upper and lower arms with hands).

Several approaches can be used to perform the computer simulations, namely the MBS (Multi-Body Simulation), FEA (Finite Element Analysis), or hybrid approaches. Usually, the use of MBS is suitable for long time simulations with a low CPU cost, but without the possibility to closely evaluate the injuries from the contact areas due to the simplifications typical for the MB model. The use of FEA is more accurate for assessing the injuries, since it involves more detailed description of the body, but is CPU costly for long simulations.

In this section, we have chosen the MBS, since the model propose was not to handle with impacts, but just simulating the driver typical manoeuvres.

To implement the MBS, MATLAB (version 2007a from Mathworks) was used. The implementation of a 2D model of the rider and the PTW was set according to the literature data for the two main parts.

5.1.1   Model basics

The human model was implemented using anthropometric data [54], considering the lower segments of the body (legs) as a part of the PTW frame and the hands as a part of the handlebar. A five body model was used for the human body. It consists of a head, a neck, a body (thorax, abdomen and pelvis), an upper arm and a lower arm (Figure 5-1). The left and right arms have been implemented as one, with the assumption that the shoulder position is coincident in the projected plane.

The PTW model was implemented using the data from Suzuki GSX-R1000K1 [55]. The PTW was considered as the system of five bodies – a rear wheel, a front wheel, a swing arm, a main body (a frame, a handlebar, an upper fork, a hands, upper and lower legs, and feet), and a lower fork (Figure 5-2). The PTW was connected to the ground in the rear and front wheel, allowing its translations in the vertical axis (assuming a vertical movement). In total, the assembly of the human body and the PTW is characterized by ten joints (nine revolute and one prismatic). The joints are actuated by passive force elements (spring-damper elements).

The Lagrange dynamics [56] was used to describe the developed Multi-Body System (MBS). To describe each body, the absolute coordinates were used since the planar motion of a free body can be described by three independent coordinates. Two coordinates define the translation of the body and the third one describes the rotation.
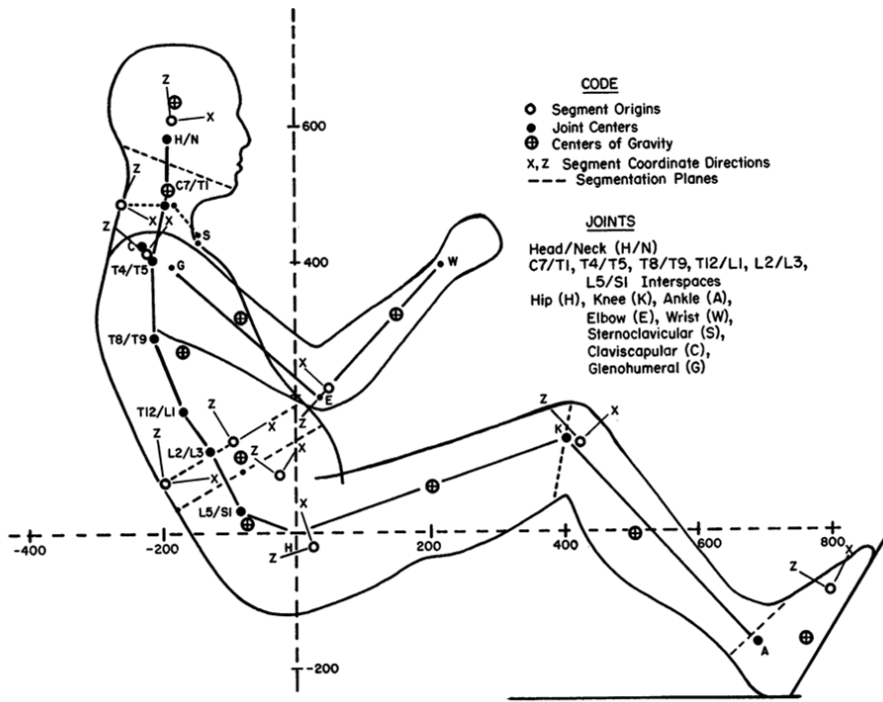
Figure 5-1 – Anthropometric specifications for mid-sized male dummy [54]
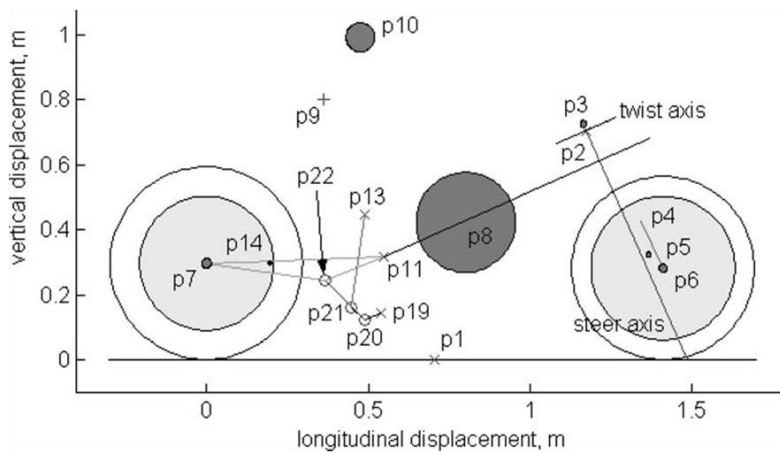
Figure 5-2 – Scaled diagrammatic motorcycle in side view [55]

The proposed model has similar aspect as the illustrated one in the Figure 5-3. The bodies are summarized in Table A1-4.
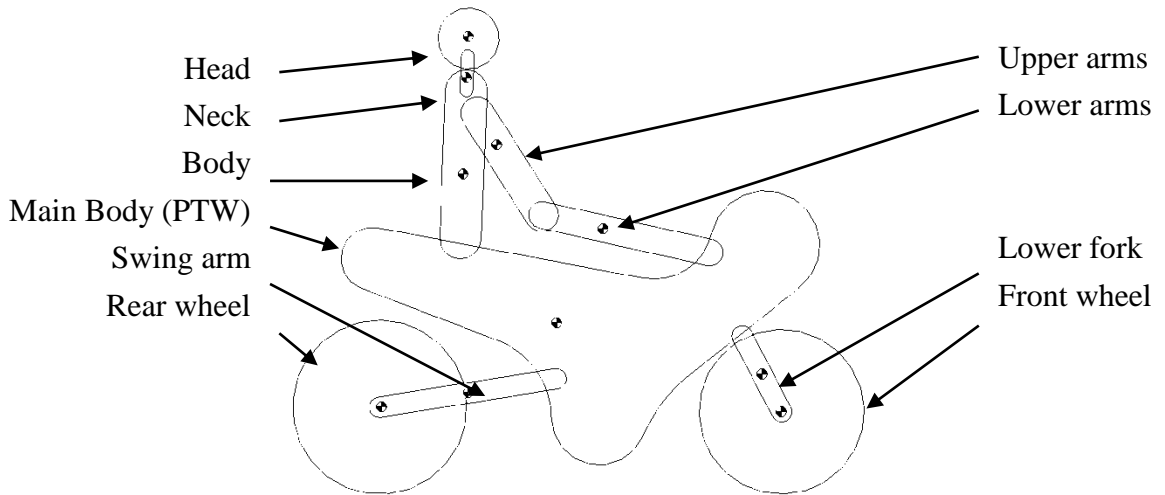
Figure 5-3 – Schematic representation of the human body and PTW model (not to scale)

5.2   Mathematical formulation

5.2.1   Position, velocity and acceleration

To describe motion of a rigid body in a MBS, one has to assign a coordinate system to each body. The origin of the particular coordinate system is attached to a point on the body. That means that the system coordinates share with the body all its movements.

Let $X^i Y^i$ be the body coordinates system and let XY be the global coordinate system, as illustrated in the Figure 5-4. Let P^i be an arbitrary point on the body. The coordinates of the point P^i can be described by vector

$$\overline{\mathbf{u}}_P^i = \begin{bmatrix} \overline{x}_x^i & \overline{y}_y^i \end{bmatrix}^{\mathrm{T}} \tag{5-1}$$

or written in terms of unit vectors along axes of coordinates $X^i Y^i$ as

$$\overline{\mathbf{u}}_P^i = \overline{x}_P^i \cdot \mathbf{i}^i + \overline{y}_P^i \cdot \mathbf{j}^i \tag{5-2}$$

where $\mathbf{i}^i$ and $\mathbf{j}^i$ are, respectively, unit vectors along X^i and Y^i axes of the body system. From equations (5-1) and (5-2), $\overline{\mathbf{u}}_P^i$ can be described in global coordinates as

$$\mathbf{u}_P^i = \overline{x}_P^i \cdot \left(\cos \theta^i \cdot \mathbf{i} + \sin \theta^i \cdot \mathbf{j} \right) + \overline{y}_P^i \cdot \left(-\sin \theta^i \cdot \mathbf{i} + \cos \theta^i \cdot \mathbf{j} \right) \tag{5-3}$$

where $\mathbf{u}_P^i$ is the global representation of the vector $\overline{\mathbf{u}}_P^i$. Equation (5-3) can be rearranged as

$$\mathbf{u}_P^i = \begin{bmatrix} \overline{x}_P^i \cdot \cos \theta^i + \overline{y}_P^i \cdot \sin \theta^i \\ -\overline{x}_P^i \cdot \sin \theta^i + \overline{y}_P^i \cdot \cos \theta^i \end{bmatrix} \tag{5-4}$$

or written in the matrix form as

$$\mathbf{u}_P^i = \begin{bmatrix} \cos\theta^i & -\sin\theta^i \\ \sin\theta^i & \cos\theta^i \end{bmatrix} \cdot \begin{bmatrix} \bar{x}_P^i \\ \bar{y}_P^i \cdot \end{bmatrix}. \tag{5-5}$$
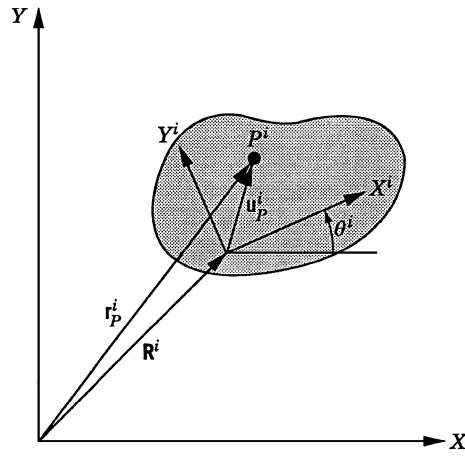
Figure 5-4 – Rigid body motion [56]

Using equation (5-2), the equation (5-5) can be written as

$$\mathbf{u}_P^i = \mathbf{A}^i \cdot \bar{\mathbf{u}}_P^i \tag{5-6}$$

where $\mathbf{A}^i$ is the planar transformation matrix defined as

$$\mathbf{A}^i = \begin{bmatrix} \cos\theta^i & -\sin\theta^i \\ \sin\theta^i & \cos\theta^i \end{bmatrix}. \tag{5-7}$$

The matrix $\mathbf{A}^i$ is an orthogonal matrix because

$$\mathbf{A}^i \cdot \left(\mathbf{A}^i\right)^{\mathrm{T}} = \left(\mathbf{A}^i\right)^{\mathrm{T}} \cdot \mathbf{A}^i = \mathbf{I} \tag{5-8}$$

where $\mathbf{I}$ is an square identity matrix of order 2.

The global position vector of the point P^i is defined by the sum of two vectors: $\mathbf{R}^i$ with $\mathbf{u}_P^i$. The vector $\mathbf{R}^i$ is the global position of the origin O^i of the body coordinate system $X^i Y^i$. We can get the equation

$$\mathbf{r}_P^i = \mathbf{R}^i + \mathbf{u}_P^i. \tag{5-9}$$

From equations (5-6) and (5-9), we get

$$\mathbf{r}_P^i = \mathbf{R}^i + \mathbf{A}^i \cdot \bar{\mathbf{u}}_P^i \tag{5-10}$$

From equation (5-10), we can describe the position for a generic point (point belonging to the moving body) after body rotation and translation.

5.2.1.1 Velocity

After the position analysis, the next step is the velocity analysis. The absolute velocity of a point on a rigid body that goes in a planar motion can be described by the differentiation of equation (5-10) as

$$\dot{\mathbf{r}}_P^i = \dot{\mathbf{R}}^i + \dot{\mathbf{A}}^i \cdot \overline{\mathbf{u}}_P^i \tag{5-11}$$

since from equation (5-7) we get the derivation

$$\dot{\mathbf{A}}^i = \dot{\theta}^i \cdot \mathbf{A}_\theta^i \tag{5-12}$$

where $\mathbf{A}_\theta^i$ is the partial derivative of the rotation matrix with respect to the rotation θ^i given by

$$\mathbf{A}_\theta^i = \begin{bmatrix} -\sin\theta^i & -\cos\theta^i \\ \cos\theta^i & -\sin\theta^i \end{bmatrix} \tag{5-13}$$

From equations (5-11) and (5-12) we get

$$\dot{\mathbf{r}}_P^i = \dot{\mathbf{R}}^i + \dot{\theta}^i \cdot \mathbf{A}_\theta^i \cdot \overline{\mathbf{u}}_P^i. \tag{5-14}$$

5.2.1.2 Acceleration

To get the acceleration, the partial derivative of velocity by the time should be made. So, the derivative of equation (5-14) is

$$\ddot{\mathbf{r}}_P^i = \ddot{\mathbf{R}}^i + \dot{\theta}^i \cdot \dot{\mathbf{A}}_\theta^i \cdot \overline{\mathbf{u}}_P^i + \ddot{\theta}^i \cdot \mathbf{A}_\theta^i \cdot \overline{\mathbf{u}}_P^i. \tag{5-15}$$

In case of a planar motion, the following identity can be verified

$$\dot{\mathbf{A}}_\theta^i = -\mathbf{A}^i \cdot \dot{\theta}^i. \tag{5-16}$$

By applying equation (5-16) to equation (5-15), we get

$$\ddot{\mathbf{r}}_P^i = \ddot{\mathbf{R}}^i - \left(\dot{\theta}^i\right)^2 \cdot \mathbf{A}^i \cdot \overline{\mathbf{u}}_P^i + \ddot{\theta}^i \cdot \mathbf{A}_\theta^i \cdot \overline{\mathbf{u}}_P^i. \tag{5-17}$$

5.2.1.3 Absolute coordinates

A point in a generic body can be described by independent coordinates. Two coordinates define the body origin translation; one coordinate defines the body rotation. This coordinates are represented by $\mathbf{R}^i$ and θ^i, respectively.

The generalized coordinates of the body i is given by

$$\mathbf{q}_i = \left[\left(\mathbf{R}^i\right)^{\mathrm{T}} \quad \theta^i\right]^{\mathrm{T}} \tag{5-18}$$

or

$$\mathbf{q}_i = \left[R_x^i \quad R_y^i \quad \theta^i\right]^{\mathrm{T}}. \tag{5-19}$$

A multi-body system composed by n_b bodies will have the vector of generalized coordinates as

$$\mathbf{q} = \left[\left(\mathbf{q}^1 \right)^\mathrm{T} \quad \left(\mathbf{q}^2 \right)^\mathrm{T} \quad \cdots \quad \left(\mathbf{q}^i \right)^\mathrm{T} \quad \cdots \quad \left(\mathbf{q}^{n_b} \right)^\mathrm{T} \right]^\mathrm{T}.$$ (5-20)

5.2.2 Virtual work

The principle of virtual work represents a powerful tool for deriving the equations of motion of multi-body systems. One of the advantages consists in the fact that constraint forces are not to be considered, scalar work quantities to define static and dynamics are only needed. This principle gives another advantage that a minimum set of equations of motion of the multi-body system by eliminating constraint forces is needed.

5.2.2.1 *Virtual displacements*

By definition, *virtual displacement* is an infinitesimal displacement that is consistent with the kinematic constraints imposed on the motion of the system. Virtual displacements are unreal in the sense that they are assumed to occur while time is held fixed. Let us analyse the unconstraint body illustrated in the Figure 5-5. The position vector of an arbitrary point P^i on the rigid body from equation (5-10) is given by

$$\mathbf{r}_P^i = \mathbf{R}^i + \mathbf{A}^i \cdot \overline{\mathbf{u}}_P^i.$$ (5-21)
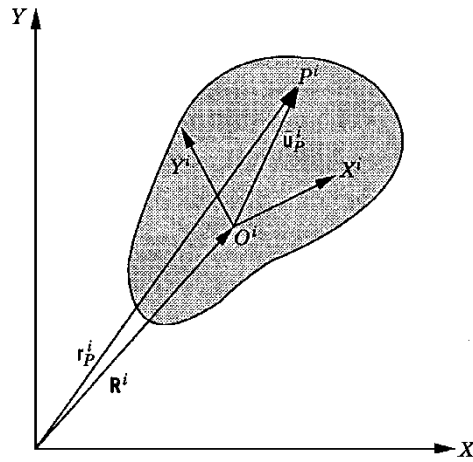
Figure 5-5 – Position vector [56]

A virtual change in the position vector of point P^i of equation (5-21) is denoted as $\delta \mathbf{r}_P^i$ and is given by

$$\delta \mathbf{r}_P^i = \delta \mathbf{R}^i + \delta \cdot \left(\mathbf{A}^i \cdot \overline{\mathbf{u}}_P^i \right).$$ (5-22)

Since the vector $\mathbf{A}^i \cdot \overline{\mathbf{u}}_P^i$ depends only on one variable, the angular rotation θ^i, equation (5-22) can rewritten as

$$\delta \mathbf{r}_P^i = \delta \mathbf{R}^i + \mathbf{A}_\theta^i \cdot \overline{\mathbf{u}}_P^i \cdot \delta \theta^i$$ (5-23)

where $\mathbf{A}_\theta^i$ is

$$\mathbf{A}_\theta^i = \frac{\partial \mathbf{A}^i}{\partial \theta_i} = \begin{bmatrix} -\sin\theta_i & -\cos\theta_i \\ \cos\theta_i & -\sin\theta_i \end{bmatrix}. \tag{5-24}$$

In equation (5-23), the virtual change in position vector is expressed in terms of the virtual changes in the body coordinates. In case of body degrees of freedom, the equation can be written like

$$\delta \mathbf{r}_P^i = \mathbf{r}_{q^i}^i \cdot \delta \mathbf{q}^i \tag{5-25}$$

where

$$\mathbf{r}_{q^i}^i = \left[\left(\mathbf{R}^i \right)^{\mathrm{T}} \quad \theta^i \right]^{\mathrm{T}}$$
$$\delta \mathbf{q}^i = \frac{\partial \mathbf{r}^i}{\partial \mathbf{q}^i} = \left[\mathbf{I} \quad \mathbf{A}_\theta^i \cdot \bar{\mathbf{u}}_P^i \right] \tag{5-26}$$

Since the virtual displacements can be seen as partial differentials with time assumed to be fixed, the differential of time is taken to be zero. To exemplify the difference between the actual displacement and the virtual displacement, we consider the case of a position vector that is an explicit function of the generalized coordinates $\mathbf{q}$ and time t. This vector can be written as

$$\mathbf{r} = \mathbf{r}(\mathbf{q}, t) \tag{5-27}$$

Differentiating the equation (5-27) in order to time, we have

$$\frac{\partial \mathbf{r}}{dt} = \frac{\partial \mathbf{r}}{\partial \mathbf{q}} \dot{\mathbf{q}} + \frac{\partial \mathbf{r}}{\partial t} \tag{5-28}$$

or multiplied by dt,

$$\partial \mathbf{r} = \frac{\partial \mathbf{r}}{\partial \mathbf{q}} d\mathbf{q} + \frac{\partial \mathbf{r}}{\partial t} dt. \tag{5-29}$$

5.2.2.2   *Virtual work in dynamics*

For a rigid body i, the generic equations of planar motion is

$$\mathbf{F}^i - m^i \cdot \mathbf{a}^i = \mathbf{0}$$
$$M^i - J^i \cdot \ddot{\theta}^i = 0 \tag{5-30}$$

where $\mathbf{F}^i$ is the vector of resultant forces acting on the body, m^i is the mass of the body, $\mathbf{a}^i$ is the acceleration vector of the centre of mass, M^i is the sum of all moments applied to the body, J^i is the inertial moment of the body and $\ddot{\theta}^i$ is the angular acceleration of the centre of mass.

If forces $\mathbf{F}^i$ are described to act in the centre of mass, we can multiply in both equations (5-30) by $\delta \mathbf{R}^i$ and $\delta\theta^i$ respectively. We get

$$\left(\mathbf{F}^i - m^i \cdot \mathbf{a}^i\right)^{\mathrm{T}} \cdot \delta\mathbf{R}^i = \mathbf{0}$$
$$\left(M^i - J^i \cdot \ddot{\theta}^i\right) \cdot \delta\theta^i = 0$$

(5-31)

obtaining equation

$$\left(\mathbf{F}^i - m^i \cdot \mathbf{a}^i\right)^{\mathrm{T}} \cdot \delta\mathbf{R}^i + \left(M^i - J^i \cdot \ddot{\theta}^i\right) \cdot \delta\theta^i = 0$$

(5-32)

or

$$\left(\mathbf{F}^i\right)^{\mathrm{T}} \cdot \delta\mathbf{R}^i + M^i \cdot \delta\theta^i - m^i \cdot \left(\mathbf{a}^i\right)^{\mathrm{T}} \cdot \delta\mathbf{R}^i - J^i \cdot \ddot{\theta}^i \cdot \delta\theta^i = 0.$$

(5-33)

The equation (5-33) can be written as

$$\delta W^i - \delta W_i^i = 0$$

(5-34)

where δW^i is the virtual work of the external and reaction forces and moments that act on the body and δW_i^i, is the virtual work of inertial forces and moments of the body, that is

$$\delta W^i = \left(\mathbf{F}^i\right)^{\mathrm{T}} \cdot \delta\mathbf{R}^i + M^i \cdot \delta\theta^i$$
$$\delta W_i^i = m^i \cdot \left(\mathbf{a}^i\right)^{\mathrm{T}} \cdot \delta\mathbf{R}^i + J^i \cdot \ddot{\theta}^i \cdot \delta\theta^i$$

(5-35)

The component δW^i can be decomposed in

$$\delta W^i = \delta W_c^i + \delta W_e^i$$

(5-36)

where δW_c^i is the virtual work of constraint forces and moments and δW_e^i is the virtual work of the external forces and moments. The equation (5-34) can be rewritten as

$$\delta W_c^i + \delta W_e^i - \delta W_i^i = 0.$$

(5-37)

5.2.2.3 Connectivity conditions

When the mechanical system consists of n_b interconnected rigid bodies, the use of equation (5-37) will be

$$\sum_{i=1}^{n_b}\left(\delta W_c^i + \delta W_e^i - \delta W_i^i\right) = 0.$$

(5-38)

Since the joint constraint forces from two adjacent bodies are equal in magnitude and opposite direction, so

$$\sum_{i=1}^{n_b} \delta W_c^i = 0.$$

(5-39)

Applying the equation (5-39) in equation (5-38), we get

$$\sum_{i=1}^{n_b} \delta W_e^i - \sum_{i=1}^{n_b} \delta W_i^i = 0.$$ (5-40)

This means that the virtual work of external forces and moments acting on the system is equal to the virtual work of inertia forces and moments of the system. We can rewrite the equation (5-40) like

$$\delta W_e - \delta W_i = 0$$ (5-41)

where

$$\delta W_e = \sum_{i=1}^{n_b} \delta W_e^i$$

$$\delta W_i = \sum_{i=1}^{n_b} \delta W_i^i$$ (5-42)

5.2.2.4 *Lagrange's equation*

The principle of virtual work allows the formulation of dynamic equations using any set of independent generalized coordinates.

The virtual work of the inertia forces of a rigid body i is defined as

$$\delta W_i^i = \int_{V^i} \rho^i \cdot \left(\ddot{\mathbf{r}}^i\right)^{\mathrm{T}} \cdot \delta \mathbf{r}^i \cdot dV^i$$ (5-43)

where ρ^i is the density of the body i, V^i is the respective volume and $\mathbf{r}^i$ is the global position vector (equation (5-27)). This vector can be written as

$$\mathbf{r}^i = \mathbf{r}^i\left(\mathbf{q},t\right).$$ (5-44)

It follows that

$$\delta \mathbf{r}^i = \frac{\partial \mathbf{r}^i}{\partial \mathbf{q}} \delta \mathbf{q}.$$ (5-45)

From equations (5-43) and (5-45) we get

$$\delta W_i^i = \int_{V^i} \rho^i \cdot \left(\ddot{\mathbf{r}}^i\right)^{\mathrm{T}} \cdot \frac{\partial \mathbf{r}^i}{\partial \mathbf{q}} \cdot \delta \mathbf{q} \cdot dV^i$$ (5-46)

or

$$\delta W_i^i = \left(\mathbf{Q}_i^i\right)^{\mathrm{T}} \cdot \delta \mathbf{q}$$ (5-47)

where

$$\mathbf{Q}_i^i = \int_{V^i} \rho^i \cdot \ddot{\mathbf{r}}^i \cdot \left(\frac{\partial \mathbf{r}^i}{\partial \mathbf{q}}\right)^{\mathrm{T}} \cdot dV^i$$ (5-48)

is the vector of generalized inertia forces of body i associated with the system generalized coordinates $\mathfrak{q}$.

For the absolute velocity vector, it will be

$$
\begin{aligned}
\dot{\mathbf{r}}^i &= \frac{\partial \mathbf{r}^i}{\partial q^1} \cdot \dot{q}^1 + \frac{\partial \mathbf{r}^i}{\partial q^2} \cdot \dot{q}^2 + \cdots + \frac{\partial \mathbf{r}^i}{\partial q^n} \cdot \dot{q}^n + \frac{\partial \mathbf{r}^i}{\partial t} \\
&= \sum_{j=1}^{n} \frac{\partial \mathbf{r}^i}{\partial q^j} \cdot \dot{q}^j + \frac{\partial \mathbf{r}^i}{\partial t} \\
&= \frac{\partial \mathbf{r}^i}{\partial \mathbf{q}} \cdot \dot{\mathbf{q}} + \frac{\partial \mathbf{r}^i}{\partial t}
\end{aligned}
\tag{5-49}
$$

from that one can deduce identity

$$
\frac{\partial \dot{\mathbf{r}}^i}{\partial \dot{\mathbf{q}}} = \frac{\partial \mathbf{r}^i}{\partial \mathbf{q}} .
\tag{5-50}
$$

Using the same procedure for the acceleration, we get

$$
\frac{\partial \ddot{\mathbf{r}}^i}{\partial \ddot{\mathbf{q}}} = \frac{\partial \dot{\mathbf{r}}^i}{\partial \dot{\mathbf{q}}} = \frac{\partial \mathbf{r}^i}{\partial \mathbf{q}} .
\tag{5-51}
$$

So we can rewrite the equation (5-48) to

$$
\mathbf{Q}_i^i = \int_{V^i} \rho^i \cdot \ddot{\mathbf{r}}^i \cdot \left(\frac{\partial \ddot{\mathbf{r}}^i}{\partial \ddot{\mathbf{q}}} \right)^{\mathrm{T}} \cdot dV^i .
\tag{5-52}
$$

Taking in account that

$$
\frac{d}{dt}\left[\left(\frac{\partial \dot{\mathbf{r}}^i}{\partial \dot{\mathbf{q}}} \right)^{\mathrm{T}} \cdot \dot{\mathbf{r}}^i \right] = \left[\frac{d}{dt}\left(\frac{\partial \dot{\mathbf{r}}^i}{\partial \dot{\mathbf{q}}} \right)^{\mathrm{T}} \right] \cdot \dot{\mathbf{r}}^i + \left(\frac{\partial \dot{\mathbf{r}}^i}{\partial \dot{\mathbf{q}}} \right)^{\mathrm{T}} \cdot \ddot{\mathbf{r}}^i
\tag{5-53}
$$

,

applying the equation (5-50)

$$
\begin{aligned}
\left(\frac{\partial \dot{\mathbf{r}}^i}{\partial \dot{\mathbf{q}}} \right)^{\mathrm{T}} \cdot \ddot{\mathbf{r}}^i &= \frac{d}{dt}\left[\left(\frac{\partial \dot{\mathbf{r}}^i}{\partial \dot{\mathbf{q}}} \right)^{\mathrm{T}} \cdot \dot{\mathbf{r}}^i \right] - \frac{d}{dt}\left[\frac{\partial \mathbf{r}^i}{\partial \mathbf{q}} \right] \cdot \dot{\mathbf{r}}^i \\
&= \frac{d}{dt}\left[\frac{\partial}{\partial \dot{\mathbf{q}}}\left\{ \frac{1}{2}\left(\dot{\mathbf{r}}^i \right)^{\mathrm{T}} \cdot \dot{\mathbf{r}}^i \right\} \right] - \frac{\partial}{\partial \mathbf{q}}\left\{ \frac{1}{2}\left(\dot{\mathbf{r}}^i \right)^{\mathrm{T}} \cdot \dot{\mathbf{r}}^i \right\}
\end{aligned}
\tag{5-54}
$$

and substituting the equation (5-54) in the equation (5-53), and using the definition of kinetic energy, we get

$$
T^i = \frac{1}{2} \int_{V^i} \rho^i \cdot \left(\dot{\mathbf{r}}^i \right)^{\mathrm{T}} \cdot \dot{\mathbf{r}}^i \cdot dV^i
\tag{5-55}
$$

and now the generalized inertial forces can be expressed in terms of body kinetic energy

$$\mathbf{Q}_i^i = \frac{d}{dt}\left(\frac{\delta T^i}{\delta \dot{\mathbf{q}}}\right)^{\mathrm{T}} - \left(\frac{\delta T^i}{\delta \mathbf{q}}\right)^{\mathrm{T}}. \qquad (5\text{-}56)$$

For a system with n_b bodies, the system of inertial forces can be written as

$$\begin{aligned} \mathbf{Q}_i &= \sum_{i=1}^{n_b} \mathbf{Q}_i^i \\ &= \sum_{i=1}^{n_b} \left[\frac{d}{dt}\left(\frac{\delta T^i}{\delta \dot{\mathbf{q}}}\right)^{\mathrm{T}} - \left(\frac{\delta T^i}{\delta \mathbf{q}}\right)^{\mathrm{T}} \right] \\ &= \frac{d}{dt}\left(\frac{\delta T}{\delta \dot{\mathbf{q}}}\right)^{\mathrm{T}} - \left(\frac{\delta T}{\delta \mathbf{q}}\right)^{\mathrm{T}} \end{aligned} \qquad (5\text{-}57)$$

where

$$T = \sum_{i=1}^{n_b} T^i . \qquad (5\text{-}58)$$

Using the virtual work principle in dynamics, one conclusion is when the generalized coordinates are independent, the system of motion equations can be

$$\frac{d}{dt}\left(\frac{\delta T}{\delta \dot{q}_j}\right) - \frac{\delta T}{\delta q_j} = Q_j \quad j = 1, 2, \ldots, n \qquad (5\text{-}59)$$

where q_j, $j = 1, 2, \ldots, n$ are independent coordinates or system degrees of freedom and Q_j is generalized applied force associated with independent coordinates q_j.

Equation (5-59) is called Lagrange's equation of motion.

5.2.3   Dynamics

Dynamics is related to the motion of the bodies with its causes, namely the forces acting on the bodies and the properties of the bodies.

5.2.3.1   *Inertia, mass and centrifugal forces*

When the centre of mass is coincident with the body coordinate systems, the inertia force consists of two components

$$\mathbf{F}_i^i = m^i \cdot \begin{bmatrix} \ddot{R}_x^i & \ddot{R}_y^i \end{bmatrix}^{\mathrm{T}} \qquad (5\text{-}60)$$

and the inertia moment is

$$M_i^i = J^i \cdot \ddot{\theta}^i \qquad (5\text{-}61)$$

where m^i is the mass of the body and J^i is the mass moment of inertia. The mass moment of inertia is defined as

$$J^i = \int_{V^i} \rho^i \cdot \left(\overline{\mathbf{u}}^i\right)^{\mathrm{T}} \cdot \overline{\mathbf{u}}^i \cdot dV^i \ . \tag{5-62}$$

The virtual work of the inertia force and the inertia moment is

$$\delta W_i^i = \left(\mathbf{F}_i^i\right)^{\mathrm{T}} \cdot \delta \mathbf{R}^i + M_i^i \cdot \delta \theta^i \ . \tag{5-63}$$

Substituting the equation (5-23) into equation (5-63), we get

$$\delta W_i^i = \left(\mathbf{F}_i^i\right)^{\mathrm{T}} \cdot \delta \mathbf{r}_P^i + \left[M_i^i - \left(\mathbf{F}_i^i\right)^{\mathrm{T}} \cdot \mathbf{A}_\theta^i \cdot \overline{\mathbf{u}}_P^i\right] \cdot \delta \theta^i \ . \tag{5-64}$$

Since the global position vector is given by

$$\mathbf{r}^i = \mathbf{R}^i + \mathbf{A}^i \cdot \overline{\mathbf{u}}^i \ , \tag{5-65}$$

the differentiation is

$$\dot{\mathbf{r}}^i = \dot{\mathbf{R}}^i + \mathbf{A}_\theta^i \cdot \overline{\mathbf{u}}^i \cdot \dot{\theta}^i \tag{5-66}$$

or

$$\dot{\mathbf{r}}^i = \begin{bmatrix} \mathbf{I} & \mathbf{A}_\theta^i \cdot \overline{\mathbf{u}}^i \end{bmatrix} \cdot \begin{bmatrix} \left(\dot{\mathbf{R}}^i\right)^{\mathrm{T}} & \dot{\theta}^i \end{bmatrix}^{\mathrm{T}} . \tag{5-67}$$

For the mass matrix, we will start with the equations (5-55) and (5-67) to get

$$T^i = \frac{1}{2} \cdot \int_{V^i} \left(\rho^i \cdot \begin{bmatrix} \left(\dot{\mathbf{R}}^i\right)^{\mathrm{T}} & \dot{\theta}^i \end{bmatrix} \cdot \begin{bmatrix} \mathbf{I} & \mathbf{A}_\theta^i \cdot \overline{\mathbf{u}}^i \end{bmatrix}^{\mathrm{T}} \cdot \begin{bmatrix} \mathbf{I} & \mathbf{A}_\theta^i \cdot \overline{\mathbf{u}}^i \end{bmatrix} \cdot \begin{bmatrix} \left(\dot{\mathbf{R}}^i\right)^{\mathrm{T}} & \dot{\theta}^i \end{bmatrix}^{\mathrm{T}} \right) \cdot dV^i \ . \tag{5-68}$$

Since $\left(\mathbf{A}_\theta^i\right)^{\mathrm{T}} \cdot \mathbf{A}_\theta^i = \mathbf{I}$, equation (5-68) can be rewritten to

$$T^i = \frac{1}{2} \cdot \begin{bmatrix} \left(\dot{\mathbf{R}}^i\right)^{\mathrm{T}} & \dot{\theta}^i \end{bmatrix} \cdot \left\{ \int_{V^i} \left(\rho^i \cdot \begin{bmatrix} \mathbf{I} & \mathbf{A}_\theta^i \cdot \overline{\mathbf{u}}^i \\ \left(\overline{\mathbf{u}}^i\right)^{\mathrm{T}} \cdot \left(\mathbf{A}_\theta^i\right)^{\mathrm{T}} & \left(\overline{\mathbf{u}}^i\right)^{\mathrm{T}} \cdot \overline{\mathbf{u}}^i \end{bmatrix} \right) \cdot dV^i \right\} \cdot \begin{bmatrix} \dot{\mathbf{R}}^i \\ \dot{\theta}^i \end{bmatrix} \tag{5-69}$$

or

$$T^i = \frac{1}{2} \cdot \left(\dot{\mathbf{q}}^i\right)^{\mathrm{T}} \cdot \mathbf{M}^i \cdot \dot{\mathbf{q}}^i \tag{5-70}$$

where $\mathbf{M}^i$ is the mass matrix of the rigid body given by

$$\mathbf{M}^i = \begin{bmatrix} \mathbf{m}_{RR}^i & \mathbf{m}_{R\theta}^i \\ \mathbf{m}_{\theta R}^i & m_{\theta\theta}^i \end{bmatrix} \tag{5-71}$$

in which

$$\mathbf{m}_{RR}^{i} = \int_{V^{i}} \rho^{i} \cdot \mathbf{I} \cdot dV^{i} = m^{i} \cdot \mathbf{I}$$

$$\mathbf{m}_{R\theta}^{i} = \left(\mathbf{m}_{\theta R}^{i}\right)^{\mathrm{T}} = \mathbf{A}_{\theta}^{i} \cdot \int_{V^{i}} \rho^{i} \cdot \bar{\mathbf{u}}^{i} \cdot dV^{i} \,. \qquad (5\text{-}72)$$

$$m_{\theta\theta}^{i} = J_{\theta\theta}^{i} = \int_{V^{i}} \rho^{i} \cdot \left(\bar{\mathbf{u}}^{i}\right)^{\mathrm{T}} \cdot \bar{\mathbf{u}}^{i} \cdot dV^{i}$$

When we select the centre of mass as a reference point, we find a special case when

$$\int_{V^{i}} \rho^{i} \cdot \bar{\mathbf{u}}^{i} \cdot dV^{i} = \mathbf{0} \qquad (5\text{-}73)$$

meaning that the parameters $\mathbf{m}_{R\theta}^{i}$ and $\mathbf{m}_{\theta R}^{i}$ are null, giving a more simple form of the mass matrix described in the equation (5-71), so we get

$$\mathbf{M}^{i} = \begin{bmatrix} \mathbf{m}_{RR}^{i} & \mathbf{0} \\ \mathbf{0} & m_{\theta\theta}^{i} \end{bmatrix} \qquad (5\text{-}74)$$

and the kinetic energy of the body as

$$T^{i} = \frac{1}{2} \cdot m^{i} \cdot \left(\dot{\mathbf{R}}^{i}\right)^{\mathrm{T}} \cdot \dot{\mathbf{R}}^{i} + \frac{1}{2} \cdot m_{\theta\theta}^{i} \cdot \left(\dot{\theta}^{i}\right)^{2}. \qquad (5\text{-}75)$$

5.2.3.2   *Equations of motion*

The equations of motion are described by means of absolute Cartesian coordinates, representing the translation of the body reference point and body orientation. Applying the principle of virtual work described in equation (5-36), written as

$$\delta W_{i}^{i} = \delta W_{c}^{i} + \delta W_{e}^{i} \qquad (5\text{-}76)$$

and expressing the virtual work for the external forces acting in the rigid body i as

$$\delta W_{e}^{i} = \left(\mathbf{Q}_{e}^{i}\right)^{\mathrm{T}} \cdot \delta \mathbf{q}_{i} \qquad (5\text{-}77)$$

and the virtual work of constraint forces as

$$\delta W_{c}^{i} = \left(\mathbf{Q}_{c}^{i}\right)^{\mathrm{T}} \cdot \delta \mathbf{q}_{i}, \qquad (5\text{-}78)$$

the virtual work can be so expressed as

$$\delta W_{i}^{i} = \left[\left(\ddot{\mathbf{q}}^{i}\right)^{\mathrm{T}} \cdot \mathbf{M}^{i}\right] \cdot \delta \mathbf{q}_{i}. \qquad (5\text{-}79)$$

Substituting equations (5-77), (5-78) and (5-79) in equation (5-76), we obtain

$$\left[\left(\ddot{\mathbf{q}}^{i}\right)^{\mathrm{T}} \cdot \mathbf{M}^{i}\right] \cdot \delta \mathbf{q}_{i} = \left(\mathbf{Q}_{e}^{i}\right)^{\mathrm{T}} \cdot \delta \mathbf{q}_{i} + \left(\mathbf{Q}_{c}^{i}\right)^{\mathrm{T}} \cdot \delta \mathbf{q}_{i}. \qquad (5\text{-}80)$$

Since the mass matrix is symmetric, we can rewrite the equation as

$$\left[\mathbf{M}^i \cdot \ddot{\mathbf{q}}^i - \mathbf{Q}_e^i - \mathbf{Q}_c^i \right]^{\mathrm{T}} \cdot \delta \mathbf{q}_i = 0 \tag{5-81}$$

or

$$\mathbf{M}^i \cdot \ddot{\mathbf{q}}^i = \mathbf{Q}_e^i + \mathbf{Q}_c^i \tag{5-82}$$

or in a more explicit way as

$$\begin{bmatrix} m^i \cdot \mathbf{I} & \mathbf{0} \\ \mathbf{0} & J^i \end{bmatrix} \cdot \begin{bmatrix} \ddot{\mathbf{R}}^i \\ \ddot{\theta}^i \end{bmatrix} = \begin{bmatrix} \left(\mathbf{Q}_e^i \right)_R \\ \left(\mathbf{Q}_e^i \right)_\theta \end{bmatrix} + \begin{bmatrix} \left(\mathbf{Q}_c^i \right)_R \\ \left(\mathbf{Q}_c^i \right)_\theta \end{bmatrix} . \tag{5-83}$$

5.2.3.3   *System of rigid bodies*

Using the equation (5-82), the equation of motion of a multi-body system consisting of n_b interconnected bodies are given by

$$\mathbf{M}^i \cdot \ddot{\mathbf{q}}^i = \mathbf{Q}_e^i + \mathbf{Q}_c^i \quad i = 1, 2, \ldots, n_b . \tag{5-84}$$

This means that from the equation (5-84) we get a system of $3 \times n_b$ scalar equations represented by

$$\begin{bmatrix} \mathbf{M}^1 & & & & & \\ & \mathbf{M}^2 & & & 0 & \\ & & \ddots & & & \\ & & & \mathbf{M}^i & & \\ & 0 & & & \ddots & \\ & & & & & \mathbf{M}^{n_b} \end{bmatrix} \cdot \begin{bmatrix} \ddot{\mathbf{q}}^1 \\ \ddot{\mathbf{q}}^2 \\ \vdots \\ \ddot{\mathbf{q}}^n \\ \vdots \\ \ddot{\mathbf{q}}^{n_b} \end{bmatrix} = \begin{bmatrix} \mathbf{Q}_e^1 \\ \mathbf{Q}_e^2 \\ \vdots \\ \mathbf{Q}_e^n \\ \vdots \\ \mathbf{Q}_e^{n_b} \end{bmatrix} + \begin{bmatrix} \mathbf{Q}_c^1 \\ \mathbf{Q}_c^2 \\ \vdots \\ \mathbf{Q}_c^n \\ \vdots \\ \mathbf{Q}_c^{n_b} \end{bmatrix} \tag{5-85}$$

or

$$\mathbf{M} \cdot \ddot{\mathbf{q}} = \mathbf{Q}_e + \mathbf{Q}_c \tag{5-86}$$

where the matrix $\mathbf{M}$ and the vectors $\mathbf{q}$, $\mathbf{Q}_e$ and $\mathbf{Q}_c$ are

$$\mathbf{M} = \begin{bmatrix} \mathbf{M}^1 & & & & & \\ & \mathbf{M}^2 & & & 0 & \\ & & \ddots & & & \\ & & & \mathbf{M}^i & & \\ & 0 & & & \ddots & \\ & & & & & \mathbf{M}^{n_b} \end{bmatrix} , \tag{5-87}$$

$$\mathbf{q} = \left[\left(\mathbf{q}_1 \right)^{\mathrm{T}} \quad \left(\mathbf{q}_2 \right)^{\mathrm{T}} \quad \left(\mathbf{q}_3 \right)^{\mathrm{T}} \quad \cdots \quad \left(\mathbf{q}_n \right)^{\mathrm{T}} \right]^{\mathrm{T}} , \tag{5-88}$$

$$\mathbf{Q}_e = \left[\left(\mathbf{Q}_e^1 \right)^{\mathrm{T}} \quad \left(\mathbf{Q}_e^2 \right)^{\mathrm{T}} \quad \left(\mathbf{Q}_e^3 \right)^{\mathrm{T}} \quad \cdots \quad \left(\mathbf{Q}_e^n \right)^{\mathrm{T}} \right]^{\mathrm{T}},$$

(5-89)

$$\mathbf{Q}_c = \left[\left(\mathbf{Q}_c^1 \right)^{\mathrm{T}} \quad \left(\mathbf{Q}_c^2 \right)^{\mathrm{T}} \quad \left(\mathbf{Q}_c^3 \right)^{\mathrm{T}} \quad \cdots \quad \left(\mathbf{Q}_c^n \right)^{\mathrm{T}} \right]^{\mathrm{T}}.$$

(5-90)

The equations (5-86) contain the generalized constraint forces, since these equations are not expressed in terms of the system degrees of freedom.

5.2.3.4   *Elimination of constraint forces*

We can rewrite the equation (5-40) as

$$\sum_{i=1}^{n_b} \left(\delta W_e^i - \delta W_i^i \right) = 0 .$$

(5-91)

Applying equations (5-77) and (5-79) to this equation, we get

$$\sum_{i=1}^{n_b} \left[\mathbf{M}^i \cdot \ddot{\mathbf{q}}^i - \mathbf{Q}_e^i \right]^{\mathrm{T}} \cdot \delta \mathbf{q}_i = 0$$

(5-92)

or in a matrix form as

$$\begin{bmatrix} \mathbf{M}^1 \cdot \ddot{\mathbf{q}}^1 - \mathbf{Q}_e^1 \\ \mathbf{M}^2 \cdot \ddot{\mathbf{q}}^2 - \mathbf{Q}_e^2 \\ \vdots \\ \mathbf{M}^i \cdot \ddot{\mathbf{q}}^i - \mathbf{Q}_e^i \\ \vdots \\ \mathbf{M}^{n_b} \cdot \ddot{\mathbf{q}}^{n_b} - \mathbf{Q}_e^{n_b} \end{bmatrix}^{\mathrm{T}} \begin{bmatrix} \delta \mathbf{q}^1 \\ \delta \mathbf{q}^2 \\ \vdots \\ \delta \mathbf{q}^n \\ \vdots \\ \delta \mathbf{q}^{n_b} \end{bmatrix} = 0$$

(5-93)

or

$$\begin{bmatrix} \delta \mathbf{q}^1 \\ \delta \mathbf{q}^2 \\ \vdots \\ \delta \mathbf{q}^n \\ \vdots \\ \delta \mathbf{q}^{n_b} \end{bmatrix}^{\mathrm{T}} \cdot \left\{ \begin{bmatrix} \mathbf{M}^1 & & & & & \\ & \mathbf{M}^2 & & & 0 & \\ & & \ddots & & & \\ & & & \mathbf{M}^i & & \\ & 0 & & & \ddots & \\ & & & & & \mathbf{M}^{n_b} \end{bmatrix} \cdot \begin{bmatrix} \ddot{\mathbf{q}}^1 \\ \ddot{\mathbf{q}}^2 \\ \vdots \\ \ddot{\mathbf{q}}^n \\ \vdots \\ \ddot{\mathbf{q}}^{n_b} \end{bmatrix} - \begin{bmatrix} \mathbf{Q}_e^1 \\ \mathbf{Q}_e^2 \\ \vdots \\ \mathbf{Q}_e^n \\ \vdots \\ \mathbf{Q}_e^{n_b} \end{bmatrix} \right\} = 0$$

(5-94)

or

$$\left(\delta \mathbf{q} \right)^{\mathrm{T}} \cdot \left[\mathbf{M} \cdot \ddot{\mathbf{q}} - \mathbf{Q}_e \right] = 0 .$$

(5-95)

The equation (5-95) is a scalar equation that does not contain constraint forces. The coefficient vector $\left[\mathbf{M} \cdot \ddot{\mathbf{q}} - \mathbf{Q}_e \right]$ of vector $\delta \mathbf{q}$ cannot be set equal to zero, since the components of the vector of coordinates $\mathbf{q}$ are not totally independent because of the

kinematic constraints that represent specified motion trajectories and mechanical joints in the system.

These constraints can be expressed by

$$\mathbf{C}(\mathbf{q},t)=0 \tag{5-96}$$

where $\mathbf{C}(\mathbf{q},t)=\begin{bmatrix} \mathbf{C}_1(\mathbf{q},t)^T & \mathbf{C}_2(\mathbf{q},t)^T & \cdots & \mathbf{C}_{n_c}(\mathbf{q},t)^T \end{bmatrix}^T$ is the vector of linearly independent constraint equations of n_c constraint functions.

For a virtual change in the system coordinates, equation (5-96) becomes

$$\mathbf{C_q} \cdot \delta\mathbf{q} = 0 \tag{5-97}$$

where $\mathbf{C_q}$ is the Jacobean matrix defined by

$$\mathbf{C}_q = \begin{bmatrix} \dfrac{\partial \mathbf{C}_1}{\partial q_1} & \dfrac{\partial \mathbf{C}_1}{\partial q_2} & \dfrac{\partial \mathbf{C}_1}{\partial q_3} & \cdots & \dfrac{\partial \mathbf{C}_1}{\partial q_n} \\ \dfrac{\partial \mathbf{C}_2}{\partial q_1} & \dfrac{\partial \mathbf{C}_2}{\partial q_2} & \dfrac{\partial \mathbf{C}_2}{\partial q_3} & \cdots & \dfrac{\partial \mathbf{C}_2}{\partial q_n} \\ \vdots & \vdots & \vdots & \ddots & \vdots \\ \dfrac{\partial \mathbf{C}_{n_c}}{\partial q_1} & \dfrac{\partial \mathbf{C}_{n_c}}{\partial q_2} & \dfrac{\partial \mathbf{C}_{n_c}}{\partial q_3} & \cdots & \dfrac{\partial \mathbf{C}_{n_c}}{\partial q_n} \end{bmatrix} \tag{5-98}$$

In which $\mathbf{q} = \begin{bmatrix} q_1 & q_2 & \cdots & q_n \end{bmatrix}^T$ is a vector of size n of system coordinates.

5.2.3.5 *Lagrange multipliers*

Starting from two rigid bodies i and j coupled in the point P without any degree of freedom, we get the restrain equations

$$\mathbf{R}^i + \mathbf{A}^i \cdot \bar{\mathbf{u}}_P^i - \mathbf{R}^j - \mathbf{A}^j \cdot \bar{\mathbf{u}}_P^j = 0$$
$$\theta^i - \theta^j = 0 \tag{5-99}$$

or the vector of constraint equation

$$\mathbf{C}(\mathbf{q}^i, \mathbf{q}^j) = 0. \tag{5-100}$$

The Jacobean matrix will be

$$\mathbf{C_q} = \begin{bmatrix} \mathbf{C}_{\mathbf{q}^i} & \mathbf{C}_{\mathbf{q}^j} \end{bmatrix} \tag{5-101}$$

where

$$\mathbf{C}_{\mathbf{q}^i} = \begin{bmatrix} \mathbf{I} & \mathbf{A}_{\theta}^i \cdot \bar{\mathbf{u}}_P^i \\ \mathbf{0} & 1 \end{bmatrix}$$

$$\mathbf{C}_{\mathbf{q}^j} = -\begin{bmatrix} \mathbf{I} & \mathbf{A}_{\theta}^j \cdot \bar{\mathbf{u}}_P^j \\ \mathbf{0} & 1 \end{bmatrix}.$$

(5-102)

For the reactions forces acting in the bodies i and j resulting from the connection, they can be expressed by means of the vector λ, where

$$\lambda = -\begin{bmatrix} \mathbf{F}^{\mathrm{T}} & M \end{bmatrix}^{\mathrm{T}}$$

(5-103)

and

$$\mathbf{F}^i = -\mathbf{F}^j = -\lambda.$$

(5-104)

We can describe the constraint forces by

$$\mathbf{Q}_c^i = \begin{bmatrix} \mathbf{F} \\ M + \left(\bar{\mathbf{u}}_P^i\right)^{\mathrm{T}} \cdot \left(\mathbf{A}_{\theta}^i\right)^{\mathrm{T}} \cdot \mathbf{F} \end{bmatrix}$$

$$\mathbf{Q}_c^j = -\begin{bmatrix} \mathbf{F} \\ M + \left(\bar{\mathbf{u}}_P^j\right)^{\mathrm{T}} \cdot \left(\mathbf{A}_{\theta}^j\right)^{\mathrm{T}} \cdot \mathbf{F} \end{bmatrix}$$

(5-105)

or in matrix notation

$$\mathbf{Q}_c^i = \begin{bmatrix} \mathbf{I} & 0 \\ \left(\bar{\mathbf{u}}_P^i\right)^{\mathrm{T}} \cdot \left(\mathbf{A}_{\theta}^i\right)^{\mathrm{T}} & 1 \end{bmatrix} \cdot \begin{bmatrix} \mathbf{F} \\ M \end{bmatrix}$$

$$\mathbf{Q}_c^j = -\begin{bmatrix} \mathbf{I} & 0 \\ \left(\bar{\mathbf{u}}_P^j\right)^{\mathrm{T}} \cdot \left(\mathbf{A}_{\theta}^j\right)^{\mathrm{T}} & 1 \end{bmatrix} \cdot \begin{bmatrix} \mathbf{F} \\ M \end{bmatrix}.$$

(5-106)

From equations (5-102) and (5-106) we get

$$\mathbf{Q}_c^i = -\left(\mathbf{C}_{\mathbf{q}^i}\right)^{\mathrm{T}} \cdot \lambda$$

$$\mathbf{Q}_c^j = -\left(\mathbf{C}_{\mathbf{q}^j}\right)^{\mathrm{T}} \cdot \lambda.$$

(5-107)

The equation (5-107) contains three force components: two associated with translation and one with the rotational component. The vector λ whose dimension is equal to the number of constraint equation is called the vector of the Lagrange multipliers.

For a system with n_i joints, the constraint equation is expressed by

$$\mathbf{C}_1(\mathbf{q}, t) = \mathbf{0}$$
$$\mathbf{C}_2(\mathbf{q}, t) = \mathbf{0}$$
$$\vdots$$
$$\mathbf{C}_{n_i}(\mathbf{q}, t) = \mathbf{0}$$

(5-108)

and the system of constraint forces is

$$\mathbf{Q}_1^i = -\left\{ \left(\mathbf{C}_1 \right)_{\mathbf{q}^i} \right\}^{\mathrm{T}} \cdot \boldsymbol{\lambda}_1$$

$$\mathbf{Q}_2^i = -\left\{ \left(\mathbf{C}_2 \right)_{\mathbf{q}^i} \right\}^{\mathrm{T}} \cdot \boldsymbol{\lambda}_2$$

$$\vdots$$

$$\mathbf{Q}_{n_i}^i = -\left\{ \left(\mathbf{C}_{n_i} \right)_{\mathbf{q}^i} \right\}^{\mathrm{T}} \cdot \boldsymbol{\lambda}_{n_i}$$

(5-109)

The generalized reaction forces due to all the constraint can be expressed by

$$\mathbf{Q}_c^i = \mathbf{Q}_1^i + \mathbf{Q}_2^i + \cdots + \mathbf{Q}_{n_i}^i$$

$$= \sum_{k=1}^{n_i} \mathbf{Q}_k^i$$

(5-110)

or

$$\mathbf{Q}_c^i = -\left\{ \left(\mathbf{C}_1 \right)_{\mathbf{q}^i} \right\}^{\mathrm{T}} \cdot \boldsymbol{\lambda}_1 - \left\{ \left(\mathbf{C}_2 \right)_{\mathbf{q}^i} \right\}^{\mathrm{T}} \cdot \boldsymbol{\lambda}_2 - \cdots - \left\{ \left(\mathbf{C}_{n_i} \right)_{\mathbf{q}^i} \right\}^{\mathrm{T}} \cdot \boldsymbol{\lambda}_{n_i}$$

$$= -\sum_{k=1}^{n_i} \left\{ \left(\mathbf{C}_k \right)_{\mathbf{q}^i} \right\}^{\mathrm{T}} \cdot \boldsymbol{\lambda}_k$$

(5-111)

or in a matrix format

$$\mathbf{Q}_c^i = -\left[\left\{ \left(\mathbf{C}_1 \right)_{\mathbf{q}^i} \right\}^{\mathrm{T}} \quad \left\{ \left(\mathbf{C}_2 \right)_{\mathbf{q}^i} \right\}^{\mathrm{T}} \quad \cdots \quad \left\{ \left(\mathbf{C}_{n_i} \right)_{\mathbf{q}^i} \right\}^{\mathrm{T}} \right] \cdot \left[\boldsymbol{\lambda}_1 \quad \boldsymbol{\lambda}_2 \quad \cdots \quad \boldsymbol{\lambda}_{n_i} \right]^{\mathrm{T}}$$ (5-112)

meaning that the global system of constraint forces is

$$\mathbf{Q}_c = -\left(\mathbf{C}_{\mathbf{q}} \right)^{\mathrm{T}} \cdot \boldsymbol{\lambda} .$$

(5-113)

5.2.3.6   Constrained dynamic equations

From equations (5-86) and (5-113),

$$\mathbf{M} \cdot \ddot{\mathbf{q}} = \mathbf{Q}_e - \left(\mathbf{C}_{\mathbf{q}} \right)^{\mathrm{T}} \cdot \boldsymbol{\lambda}$$

(5-114)

or

$$\mathbf{Q}_e = \mathbf{M} \cdot \ddot{\mathbf{q}} + \left(\mathbf{C}_{\mathbf{q}} \right)^{\mathrm{T}} \cdot \boldsymbol{\lambda} .$$

(5-115)

These are n second-order differential equations of motion, where n is the total number of system coordinates.

When differentiating equation (5-96) twice by time, we get the vector $\mathbf{Q}_d$ expressed by

$$\mathbf{Q}_d = \mathbf{C_q} \cdot \ddot{\mathbf{q}}$$
$$= -\left(\mathbf{C}_q \cdot \dot{\mathbf{q}} \right)_q \cdot \dot{\mathbf{q}}^{\cdot} \tag{5-116}$$

Expressing the equations (5-115) and (5-116) in a matrix format, we get

$$\begin{bmatrix} \mathbf{M} & \left(\mathbf{C_q}\right)^{\mathrm{T}} \\ \mathbf{C_q} & \mathbf{0} \end{bmatrix} \cdot \begin{bmatrix} \ddot{\mathbf{q}} \\ \lambda \end{bmatrix} = \begin{bmatrix} \mathbf{Q}_e \\ \mathbf{Q}_d \end{bmatrix}. \tag{5-117}$$

The vector of accelerations and Lagrange multipliers can be obtained by solving the equation (5-117) as

$$\begin{bmatrix} \ddot{\mathbf{q}} \\ \lambda \end{bmatrix} = \begin{bmatrix} \mathbf{M} & \left(\mathbf{C_q}\right)^{\mathrm{T}} \\ \mathbf{C_q} & \mathbf{0} \end{bmatrix}^{-1} \cdot \begin{bmatrix} \mathbf{Q}_e \\ \mathbf{Q}_d \end{bmatrix}, \tag{5-118}$$

By matrix multiplication, we can have

$$\begin{bmatrix} \mathbf{M} & \left(\mathbf{C_q}\right)^{\mathrm{T}} \\ \mathbf{C_q} & \mathbf{0} \end{bmatrix}^{-1} = \begin{bmatrix} \mathbf{H}_{qq} & \mathbf{H}_{q\lambda} \\ \mathbf{H}_{\lambda q} & \mathbf{H}_{\lambda\lambda} \end{bmatrix} \tag{5-119}$$

where

$$\begin{cases} \mathbf{H}_{\lambda\lambda} = \left[\mathbf{C_q} \cdot \mathbf{M}^{-1} \cdot \left(\mathbf{C_q}\right)^{\mathrm{T}} \right]^{-1} \\ \mathbf{H}_{qq} = \mathbf{M}^{-1} + \mathbf{M}^{-1} \cdot \left(\mathbf{C_q}\right)^{\mathrm{T}} \cdot \mathbf{H}_{\lambda\lambda} \cdot \mathbf{C_q} \cdot \mathbf{M}^{-1} \\ \mathbf{H}_{q\lambda} = \left(\mathbf{H}_{\lambda q}\right)^{\mathrm{T}} = -\mathbf{M}^{-1} \cdot \left(\mathbf{C_q}\right)^{\mathrm{T}} \cdot \mathbf{H}_{\lambda\lambda} \end{cases} \tag{5-120}$$

getting

$$\lambda = \mathbf{H}_{\lambda q} \cdot \mathbf{Q}_e + \mathbf{H}_{\lambda\lambda} \cdot \mathbf{Q}_d$$
$$\ddot{\mathbf{q}} = \mathbf{M}^{-1} \cdot \mathbf{Q}_e + \left(\mathbf{C_q}\right)^{\mathrm{T}} \cdot \lambda^{\cdot} \tag{5-121}$$

5.2.4   Joint definition

To describe the rider and PTW multi-body model, we have a total of 9 revolute joints and 1 prismatic joint. The joint passive actuators (springs and dampers) with the linear parameters obtained from the literature were introduced in order to represent suspension elements of the motorcycle and simplified physiological behaviour of human joints.

5.2.4.1   Revolute joint

When two bodies are connected by a revolute joint, only relative rotation is allowed between both bodies. The Figure 5-6 depicts two rigid bodies i and j that are connected by a revolute joint in the point P. It is clear from the figure that constraint points can be

defined by absolute coordinates with respect to the global inertia coordinate system and thus the kinematic constraint conditions of the revolute joint can be stated by equation

$$\mathbf{R}^i + \mathbf{r}^i - \mathbf{R}^j - \mathbf{r}^j = \mathbf{0} .$$
(5-122)

A special case arises when one of the bodies is the ground. In this case we get the relation expressed by

$$\mathbf{R}^i + \mathbf{r}^i - \mathbf{c} = \mathbf{0}$$
(5-123)

where **c** is the constant vector representing the position of the constraint point on the ground.
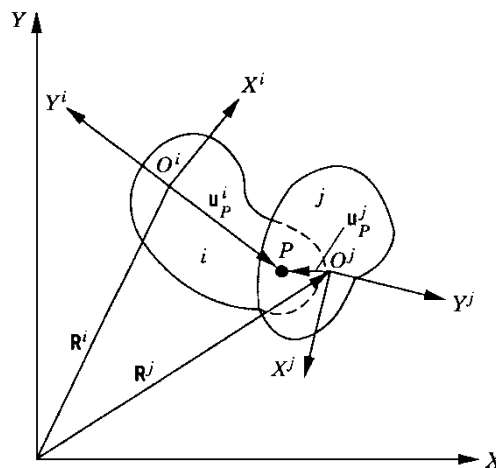
Figure 5-6 – Revolute joint [56]

5.2.4.2   *Prismatic joint*

A prismatic (translational) joint allows only relative translation between two bodies along the joint axis. Two degrees of freedom are constrained by this joint, defined by the respective equations. The definition of the constraint can be set by several ways. The adopted methodology is illustrated in Figure 5-7.
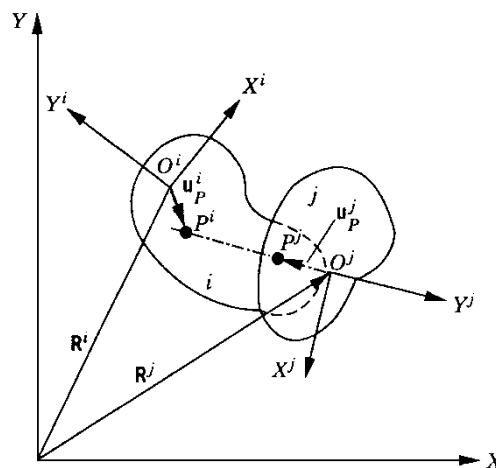
Figure 5-7 – Prismatic joint [56]

The adopted solution was the definition of the parallelism (no relative rotation) between two bodies

$$\theta^i - \theta^j - c = 0 \tag{5-124}$$

and the coincidence of the point P^i with the joint axis defined by the points P^j and O^j

$$
\begin{aligned}
\mathbf{p}^1 &= \mathbf{R}^i + \mathbf{A}^i \cdot \bar{\mathbf{u}}_p^i - \mathbf{R}^j - \mathbf{A}^i \cdot \bar{\mathbf{u}}_p^j \\
\mathbf{p}^2 &= \mathbf{R}^i + \mathbf{A}^i \cdot \bar{\mathbf{u}}_p^i - \mathbf{R}^j \\
p_x^1 \cdot p_y^2 &- p_y^1 \cdot p_x^2 = 0
\end{aligned}
\tag{5-125}
$$

since the translational axis crosses the origin of the body reference frame in our case.

5.2.5   Baumgarte's stabilization method

It is the fact that the constraint violation results from accumulated numerical integration errors and becomes more apparent with stiff systems (i.e. when natural frequencies of the system are widely spread). Even with the initial conditions not violating the constraint equations, during the course of numerical integration the numerical errors cause the violation of the constraint equations. The constant distance between two points can cease and the points move away from their initial position [57, 58].

When we are solving the equation (5-116), we are only satisfying the second derivative of the constraint equations. The solution can be improved by the replacement of the definition of the vector $\mathbf{Q}_d$ using expression

$$\mathbf{Q}_d = -\left(\mathbf{C}_q \cdot \dot{\mathbf{q}}\right)_q \cdot \dot{\mathbf{q}} - 2 \cdot \alpha \cdot \mathbf{C}_q \cdot \dot{\mathbf{q}} - \beta \cdot \mathbf{C}(\mathbf{q}, t) \tag{5-126}$$

The parameters α and β are arbitrary positive constants. The most optimal way how to choose these parameters is not well described in the literature. It depends on the nature of the solved problem and the suggestion of the parameters can be done by experimental tests.

5.2.6   Passive actuators

In each revolute joint, torsion spring and damper to react to external forces were implemented. Each of these spring-damper elements has zero deformation and velocity in the initial state.

For a generic revolute joint with a spring of stiffness K and damping B, the following expression for the moment applies in the one of the bodies

$$M = K \cdot \left(\theta_0^j - \theta_0^i - \theta^j + \theta^i\right) + B \cdot \left(\dot{\theta}^j - \dot{\theta}^i\right). \tag{5-127}$$

6

The multibody human body model

After the implementation of the 2D model (Chapter 5), a three-dimensional version of the human body was implemented. This new model is fully parametric. The used software was VL (Virtual.Lab Motion, from LMS), a software that runs using CATIA V5 engine. That means that to build the model, we use CATIA tools and tools provided by VL.

This chapter describes the implementation of a multibody HBM (Human Body Model) to our work.

The need of a human body model able to handle with the loads and kinematics found in accidents involving a PTW is completely different from the one found in usual constrained passenger car. Some of the loads and movements observed in the real world are in some cases incompatible with the prescriptions from dummies as Hybrid III in some way.

For the effect, a human model consisting in a multi-body model of fifth percentile male, described by 15 rigid bodies, coupled between them by 18 joints (14 spherical and 4 revolute), giving 22 DOF (Degrees Of Freedom) to control, was implemented (Figure 6-1). The model was created according to the geometries and data that have been already described in the chapter 4.
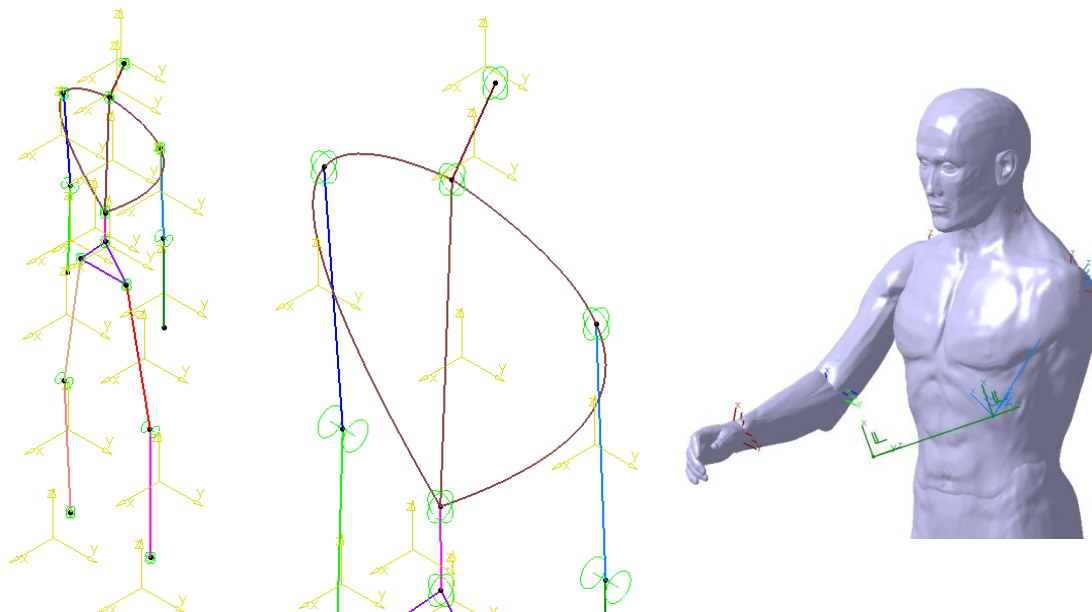
Figure 6-1 – Human body model, detail, and aspect of model with partial skin

In each "revolute joint", it was defined a passive spring-damper system, with non-linear parameters according to the physiologic resistance of the movement. In each revolute joint were defined one angle output and a torque input. This IO (Inputs and Outputs) allows the possibility to add an external controller implemented in Simulink (from Mathworks).

The IO function is presented in the appendix A2.

The implemented skin is used for contact purposes, being defined self-intersection contacts and allowing definition of contacts between the particular bodies of the human model and the external bodies (vehicles, other persons, floor, etc.)

In our model, some elements have been not found in the literature: contact stiffness between bodies, the respective damping, and the damping characteristic of the human joints.

As first attempt to get such values, a reverse analysis was used having as reference one pedestrian crash with data recorded.

6.1   Pedestrian crash

To get the unknown parameter in the model, a scenario of a van crashing in a pedestrian was selected. The van was braking, and the pedestrian, stopped and not aware of the incoming vehicle. To evaluate the simulation, the data was correlated with a crash test (Figure 6-2).

Figure 6-2 – Impact between one van and a dummy pedestrian [68]

The used dummy was equipped with axial accelerometers, 3 accelerometers in the head aligned to the head main axis, and the 4th one in the chest in the frontal posterior direction. The main acceleration is computed, filtered with CFC1000 for the head and CFC600 for the chest, and then the criteria are computed. The lack of 2 accelerometers in the chest concerns the assumption that such parameters are of minor importance.

The implemented HBM was configured in the same position against the vehicle as in the accident experiment; accelerations have been then taken from the centre of mass of the head and the thorax (chest sensor) and injury criteria are computed after filtration.

As first approaches to out model we assume that the contact parameters and the joint damping is the same in all bodies and between the bodies and the Van (exception to pairs with the thorax and abdomen). Also the van was modelled as single body, with perfect breaking systems and ignoring any type of tires of suspension model.

6.2   Parameter optimization

When a pedestrian is hit by a car, usually the crash is quite complex. In the crash phase, we can divide the general crash in several types of sub-crashes, as the first impact between pedestrian and vehicle, flying, possibly second impact with the vehicle followed by flying period, the first floor crash and skidding, possible impacts with other obstacles, and so on until full-stop.

As we can observe, a pedestrian being hit by a vehicle creates a sequence of simple type of impacts, which can also be observed as sequence of events. Each event can so be more analysed in detail.

The used model needs so data to the internal joints damping (element that e.g. absorbs energy along flying periods), as the contact parameters: stiffness and damping.

To get such parameters, a flowchart was created, as illustrated in the Figure 6-3.

To get the parameters estimation, the main focus was on the very first impact (pedestrian – van). So we need to estimate the passive joint damping, as well the contact damping and stiffness for the pedestrian-van contact.

The references values were the HIC values for the head [69], measured in the crash test. For this data, a grid of values for all combinations of joint damping and contact damping's was generated.

For the thorax, we used a variation of the ThAC [69] (Thorax Acceleration Criteria), computed only using the frontal axis (by the lack of data from the experiment for the other two directions).

As the first approximation, we have considered the same damping for the joints and the same damping for the flesh-van contact. The damping value for the head contact will be considered in the future simulations for all the other members, with exception of the thorax and the abdomen that will use the optimized value for the thorax.

6.2.1   Methodology

In the optimization process, we have used for the head two marks to approach: HIC15 and HIC36. In order to tune the model, each pair of damping values is used in the impact simulation, and then the HIC values for this respective simulation are computed. For the Thorax a similar approach was used, evaluating the ThAC.

The several computed HIC values for the simulations are shown in Table 6-1 and Table 6-2 for HIC15 and HIC36 respectively.

Table 6-1 – HIC15 values

Joint damping $\left[m^2 \cdot kg \cdot s^{-1} \cdot rad^{-1} \right]$	Contact damping $\left[kg \cdot s^{-1} \right]$						
	30	**50**	**80**	**100**	**120**	**150**	**200**
0	22741	18329	11152	8368	7348	9479	9220
0.01	22790	17400	11305	8453	7702	9341	8827
0.02	22536	17168	11205	8438	7386	9176	8592
0.05	22277	16508	11022	8506	7006	8561	8182
0.1	21138	16046	10697	8309	6886	7534	7662
0.2	18263	15017	10383	8447	6815	6325	6583
0.5	14672	11309	8976	7408	6336	4994	4879
1	12947	10329	7547	6382	5579	4907	4021
2	8054	7228	6146	5519	4996	4087	2933
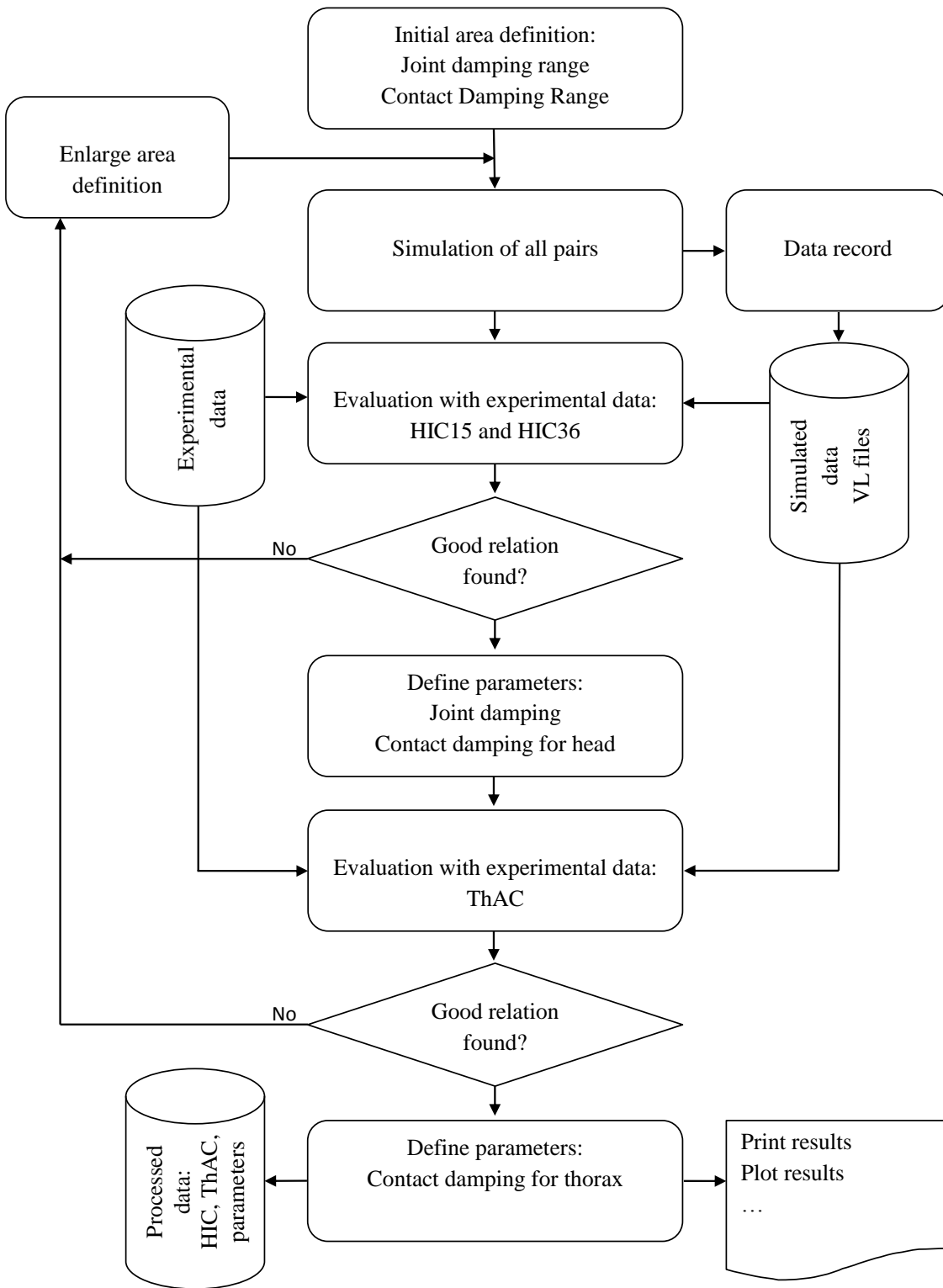
Figure 6-3 – Flow chart of the optimization

Table 6-2 – HIC36 values

Joint damping $\left[m^2 \cdot kg \cdot s^{-1} \cdot rad^{-1} \right]$	Contact damping $\left[kg \cdot s^{-1} \right]$						
	30	**50**	**80**	**100**	**120**	**150**	**200**
0	14038	10536	8669	5201	4524	5559	5873
0.01	13914	9714	6402	4853	4258	5401	5289
0.02	13715	9543	6262	4781	4068	5196	5112
0.05	13302	9022	5937	4645	3774	4635	4751
0.1	12366	8515	5460	4306	3558	3878	4217
0.2	10057	7718	4853	3950	3250	3072	3274
0.5	7427	5107	3845	3005	2529	2086	1957
1	6084	4523	2970	2361	1976	1744	1510
2	2918	2640	2261	2024	1841	1530	1126

The respective three-dimensional representation of the results is presented in the Figure 6-4 and Figure 6-6, as the respective two-dimensional projection with iso-lines in Figure 6-5 and Figure 6-7.
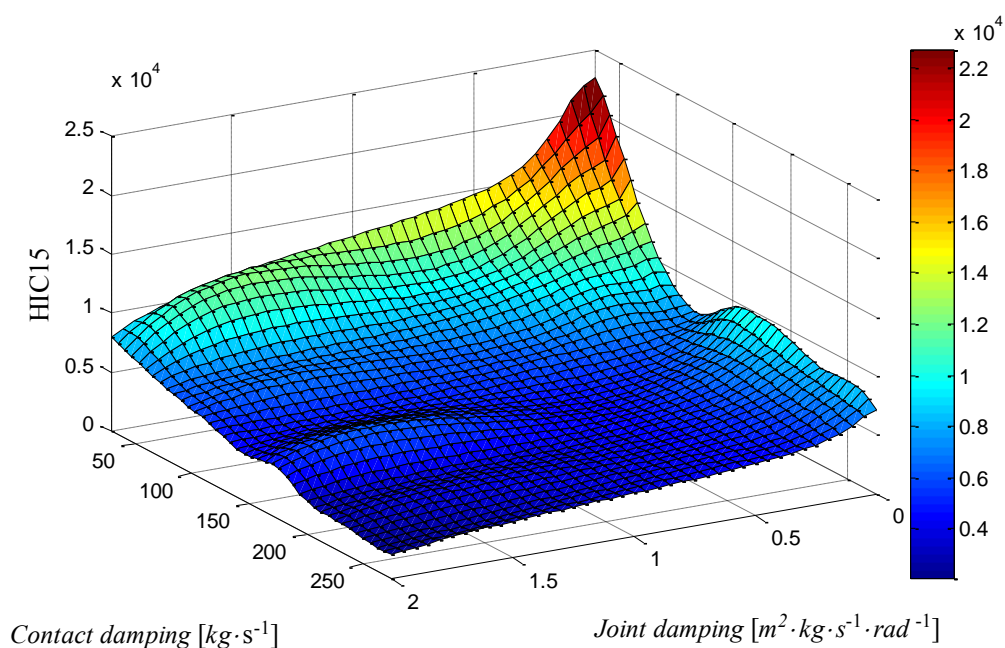
Figure 6-4 – HIC15 depending of contact and joint damping
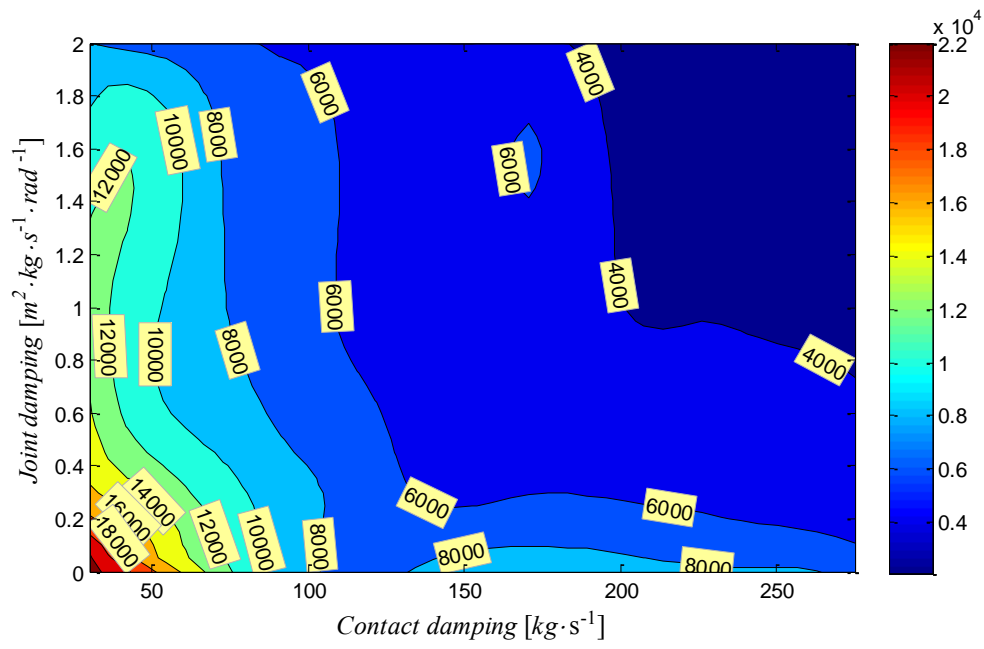
Figure 6-5 – HIC15 iso-lines
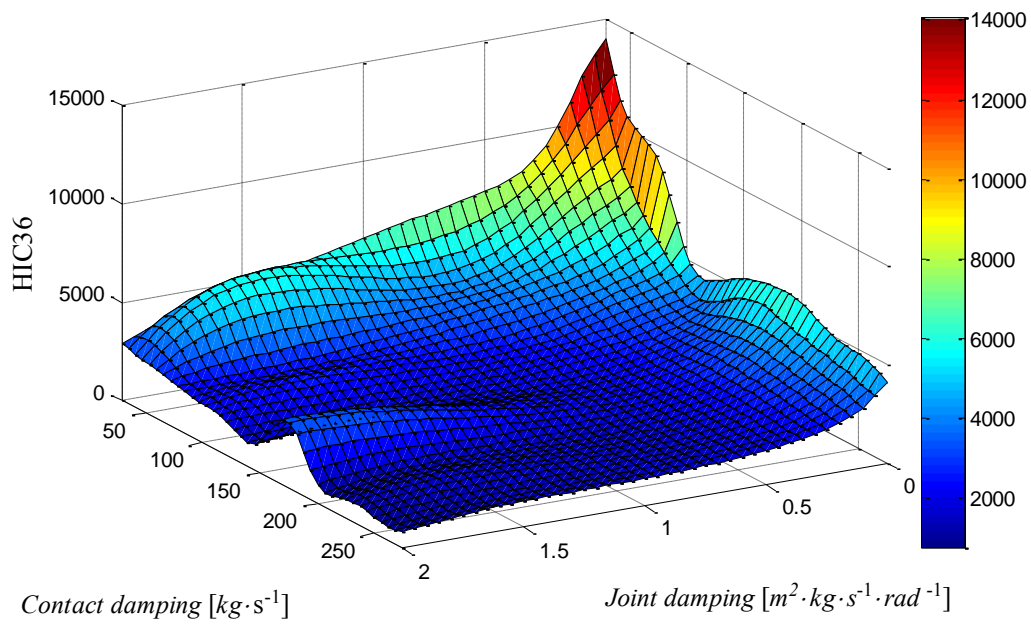
Figure 6-6 – HIC36 depending of contact and joint damping
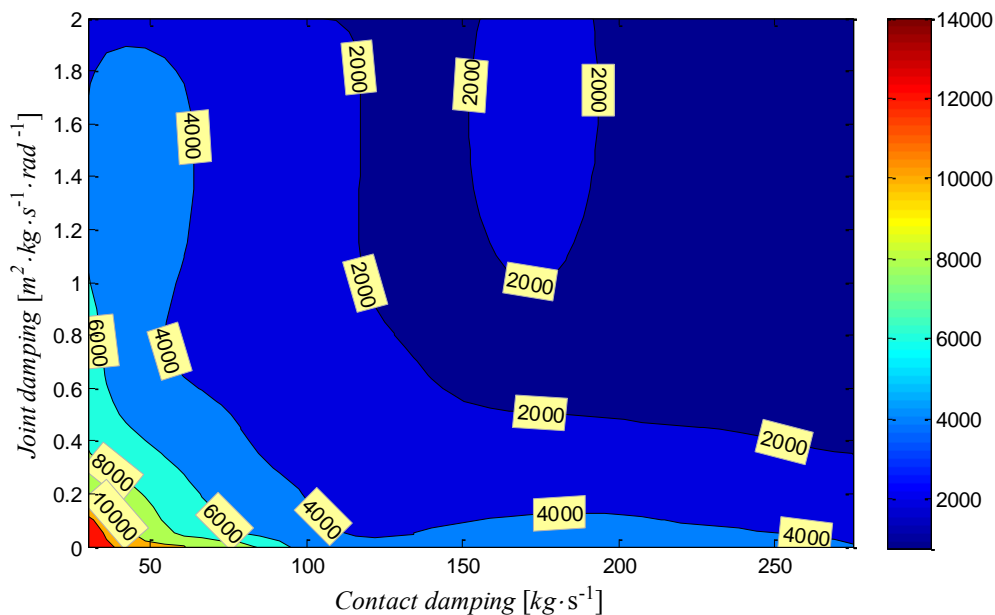
Figure 6-7 – HIC36 iso-lines

The several computed ThAC values for the simulations are shown in Table 6-3. The respective three-dimensional representation is presented in the Figure 6-8, and the respective two-dimensional projection with iso-lines in Figure 6-9.

Table 6-3 – ThAC values

Joint damping $\left[m^2 \cdot kg \cdot s^{-1} \cdot rad^{-1} \right]$	Contact damping $\left[kg \cdot s^{-1} \right]$						
	30	**50**	**80**	**100**	**120**	**150**	**200**
0	4981	5402	5931	6015	5210	3604	1949
0.01	4922	5358	5902	6004	5281	3581	2189
0.02	4879	5319	5852	5972	5341	3654	2235
0.05	4757	5209	5728	5883	5492	3876	2360
0.1	4615	5050	5535	5712	5653	4153	2545
0.2	4333	4783	5206	5414	5586	4361	2872
0.5	4068	4231	4653	4097	5111	5150	3690
1	3451	4170	4328	4393	4557	4766	4516
2	895	1750	1750	3013	3743	4401	4481
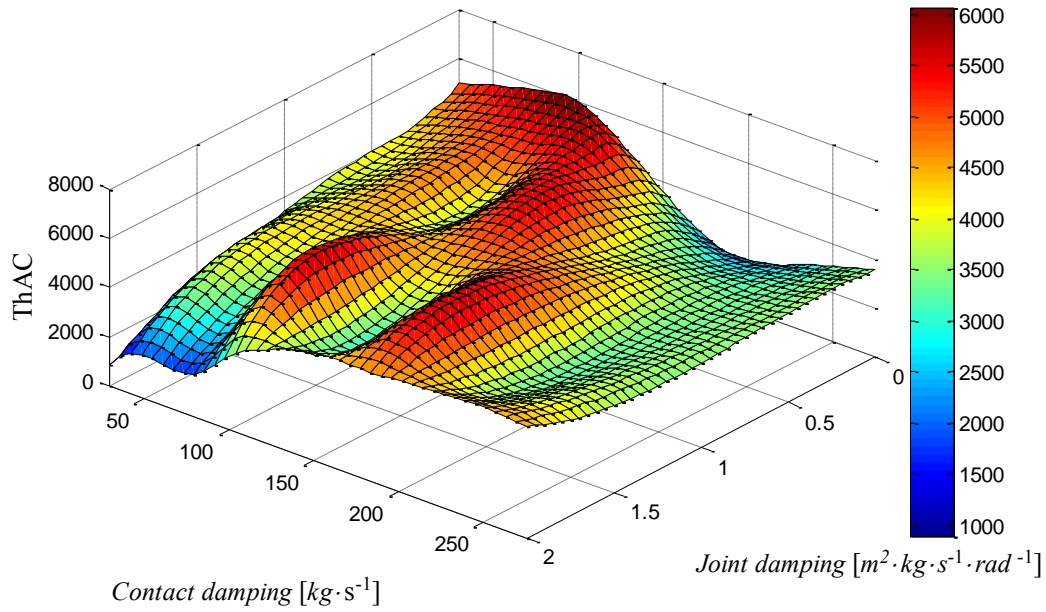
Figure 6-8 – ThAC depending of contact and joint damping
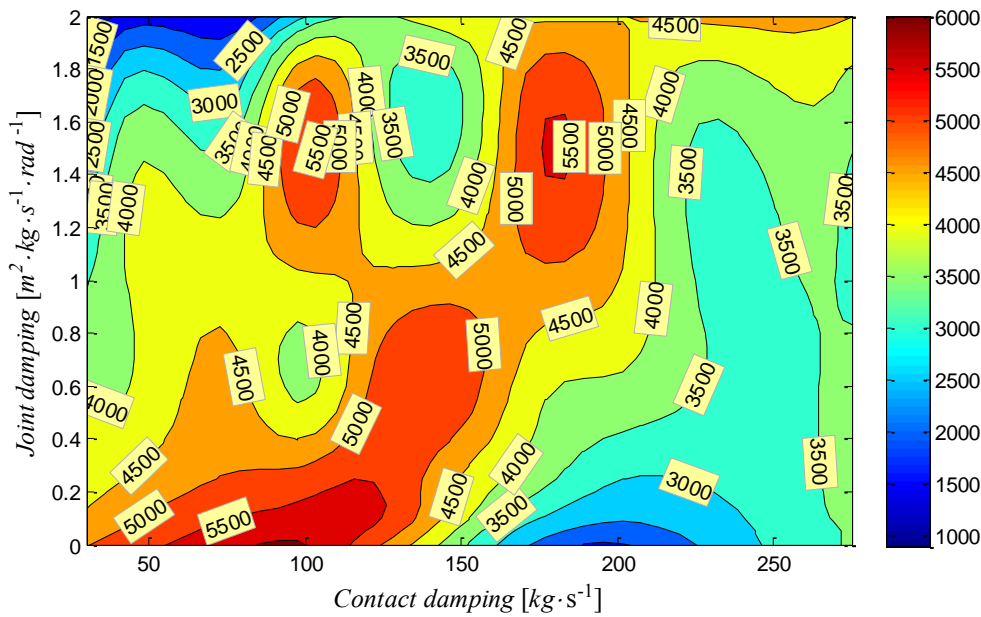
Figure 6-9 – ThAC iso-lines

The HIC15 and HIC36 values for the several simulations are then divided respectively with the correspondent experimental HIC value. The best fit will be where the lines of value 1 (same HIC value for simulation and experimental) for HIC15 and HIC36 are crossing each other or go closer. To help that, a plot of iso-lines is done for each HIC, and then, they have been overlapped as illustrated in Figure 6-10.
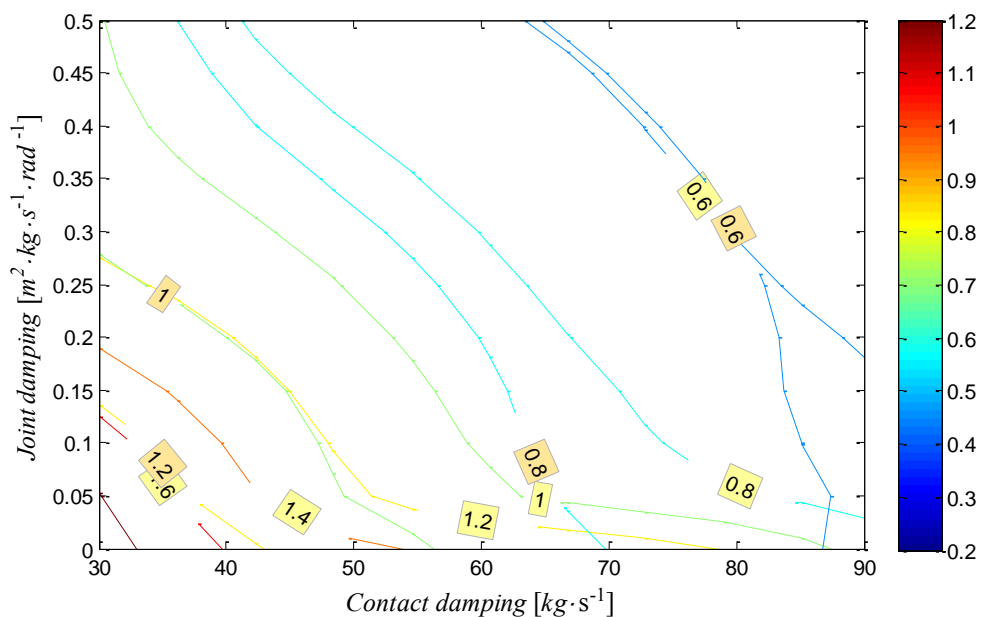
Figure 6-10 – Relative iso-lines overlapping for HIC15 and HIC36 respectively

From the Figure 6-10, the selected values were the pair (0.2, 50) for the damping value for the joints and contacts respectively, since the iso-line of value one for HIC15 and HIC36 don't intersect, we must select the pair that gives the minor deviation for both reference parameters. The HIC values can be seen in the Table 6-4.

Table 6-4 – HIC values for the experimental and simulation of optimized parameters

	experimental	simulated	Deviation [%]
HIC15	16698	15017	-10.1
HIC36	7366	7718	4.8

For the ThAC, after we have the value of joint damping, we get the respective pair for the contact damping that gives a good ThAC approximation. From the Figure 6-11 the stiffness damping for the thorax that is closer with the experimental value is 200 (in the line of joint damping 0.2).
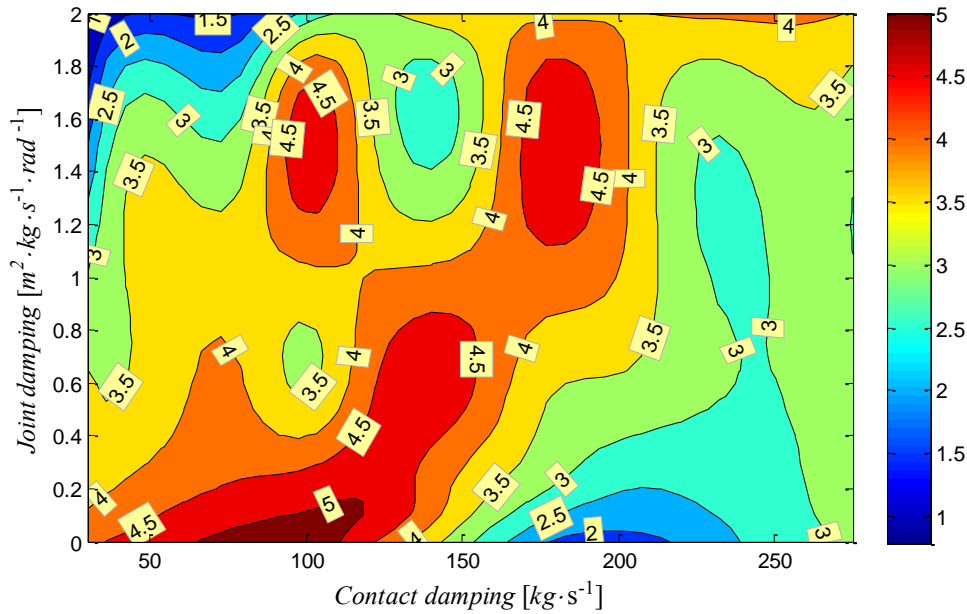
Figure 6-11 – ThAC relative iso-lines

The chosen values as optimal are shown in the Table 6-5

Table 6-5 – ThAC values for the experimental and simulation of optimized parameters

	experimental	**simulated**	**Deviation [%]**
ThAC	1135	2872	153

The final values for future computations are summarized in the Table 6-6

Table 6-6 – Optimized values

	Value	**Units**
Joint damping	0.2	$\left[m^2 \cdot kg \cdot s^{-1} \cdot rad^{-1} \right]$
Contact damping (head)	50	$\left[kg \cdot s^{-1} \right]$
Contact damping (thorax)	200	$\left[kg \cdot s^{-1} \right]$

6.3 Impact Simulation (best fit)

The impact simulation was performed from the very first impact instantly until the pedestrian achieves full rest position, less than a $5s$ time window. The critical periods for the head are presented in the Figure 6-12 and Figure 6-13, when the head impacts the vehicle windscreen and the floor respectively.

The parameters got from the optimization have been used and the damping in the contacts between flesh-flesh and flesh-floor has been arbitrarily increasing and lowering the value in reference to the damping value for the contact flesh-vehicle. In the presented simulation, the optimum parameter have been used. The presented values are for the first impact, the impact between the head and the windscreen.
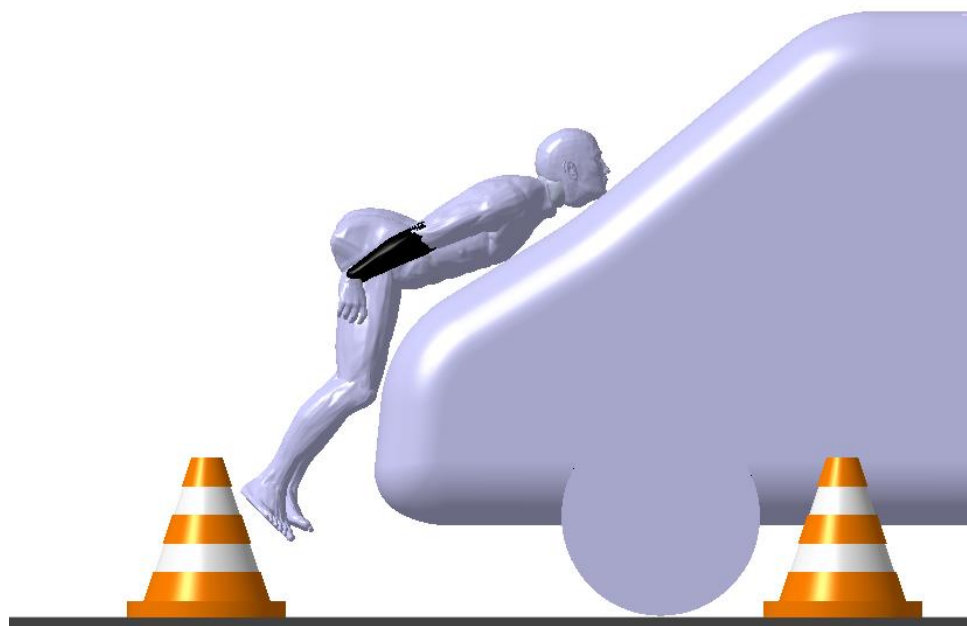
Figure 6-12 – The first impact (head-windscreen, $t = 0.08s$)

Figure 6-13 – The first impact with the floor (head-floor, $t = 1.01s$)

The acceleration magnitude of the head is shown in the Figure 6-14 for the simulation and experimental data, in the first impact (head-windscreen).
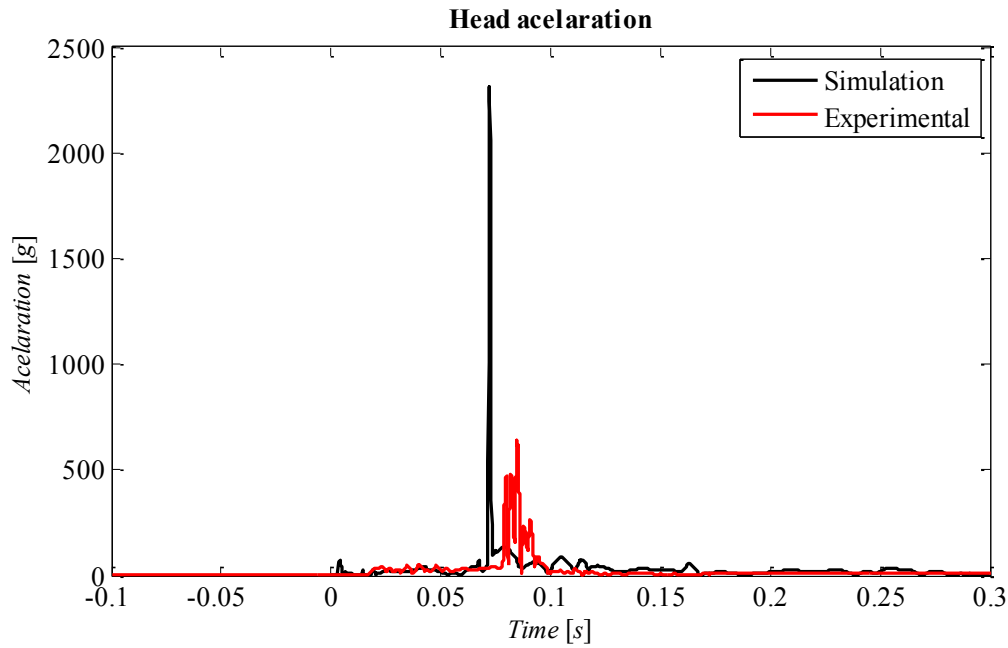
Figure 6-14 – Acceleration magnitude in the head for the simulation and experimental test

The full simulation can give the full trajectory of each body segment until its final position. Such information can be compared with typical marks found in a real accident scenario, as skid mark, blood or other trace of contact between some body part and the floor. The Figure 6-15 presents the head displacement along the time.
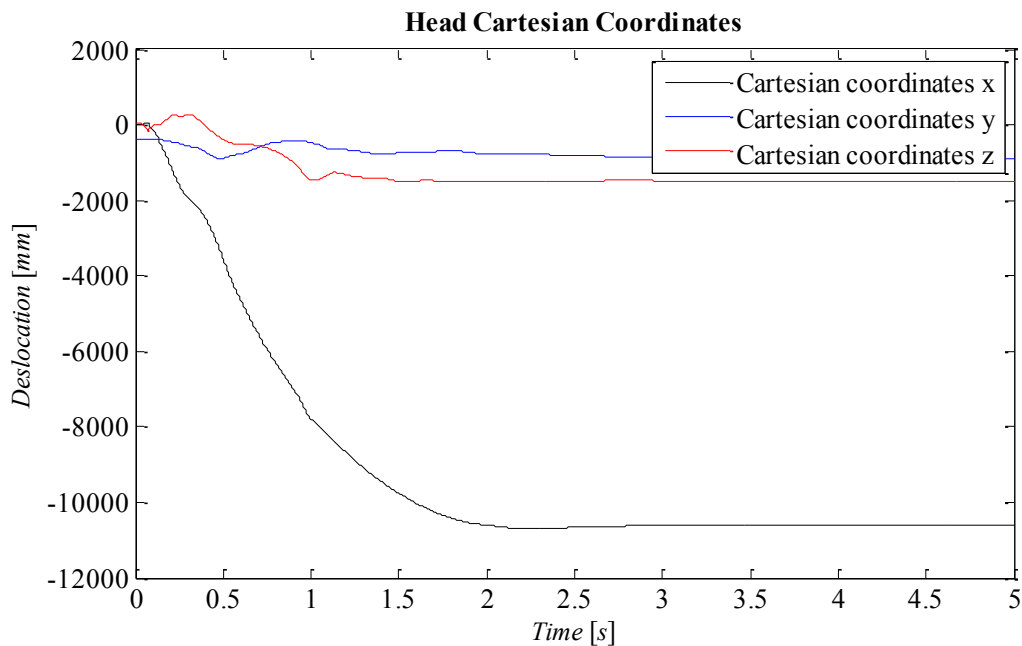
Figure 6-15 – Variation of the Cartesian coordinates of the head

The Figure 6-16 shows the head full path as seen from one observer above the accident (aerial view) or sideways to the accident (lateral view). In the plot, we can see that the head impacts the floor on a distance of approximately 8m from the initial position, having a skid until the distance of approximately 10m. The skid goes then to the pedestrian left side when it closes to the final distance, as seen from the upper view (left end of the upper subplot in the figure).
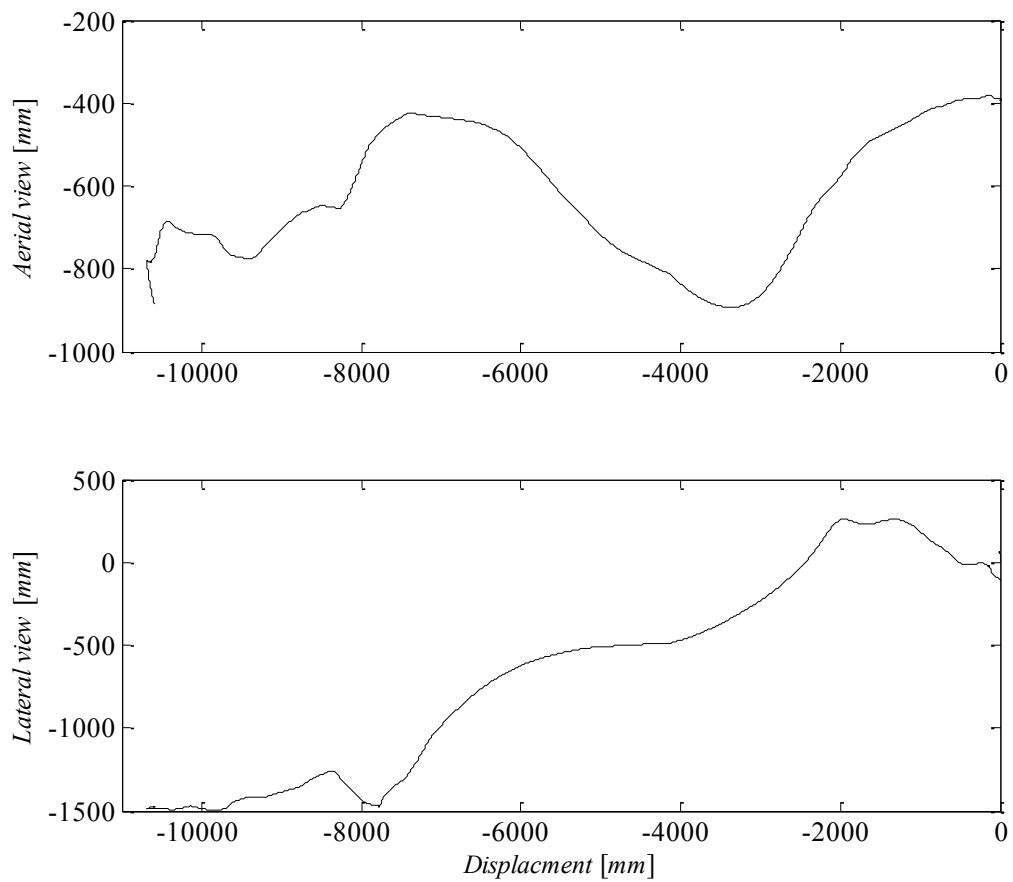
Figure 6-16 – Aerial and lateral view of the displacement of the head

The Cartesian velocities and accelerations, and the rotational velocities and accelerations are presented in the Figure 6-17 until Figure 6-21 respectively.
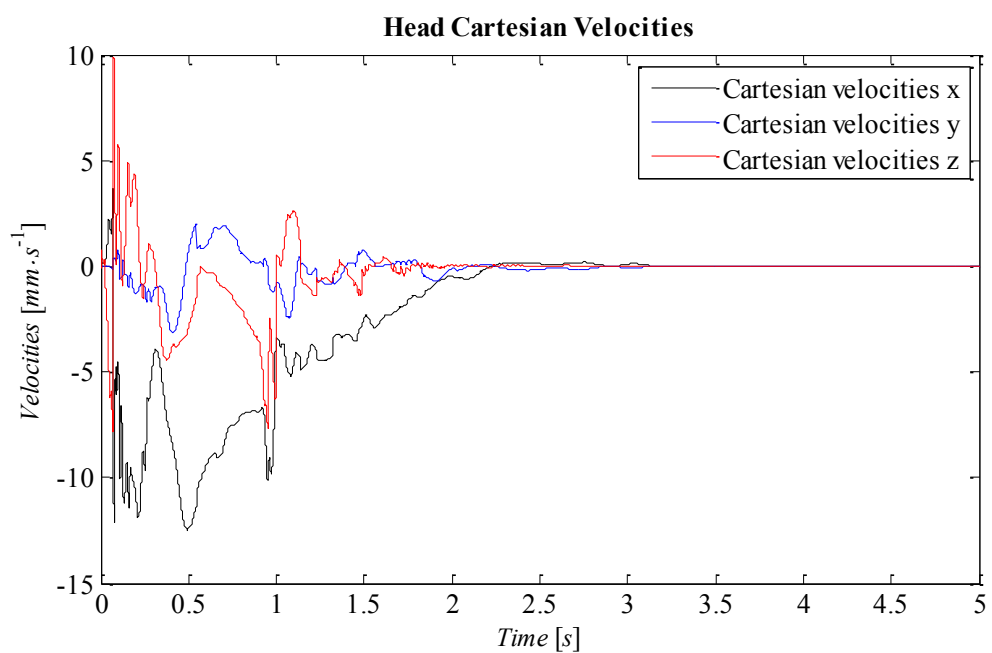
Figure 6-17 – Cartesian velocities of the Head

Head Cartesian Accelerations
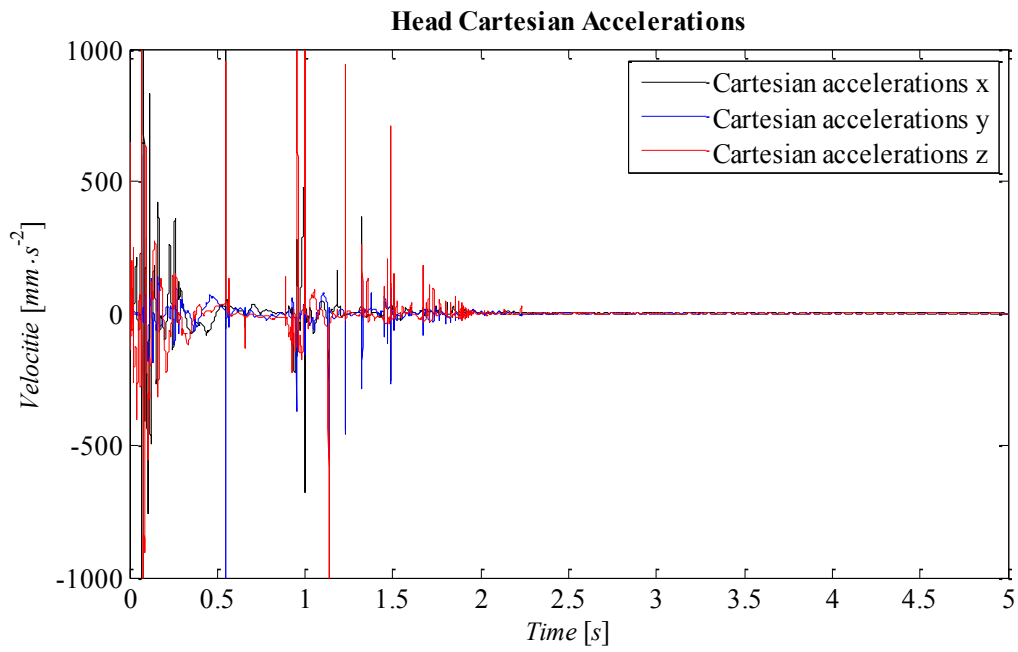
Figure 6-18 – Cartesian accelerations of the Head

Head Local Linear Accelerations
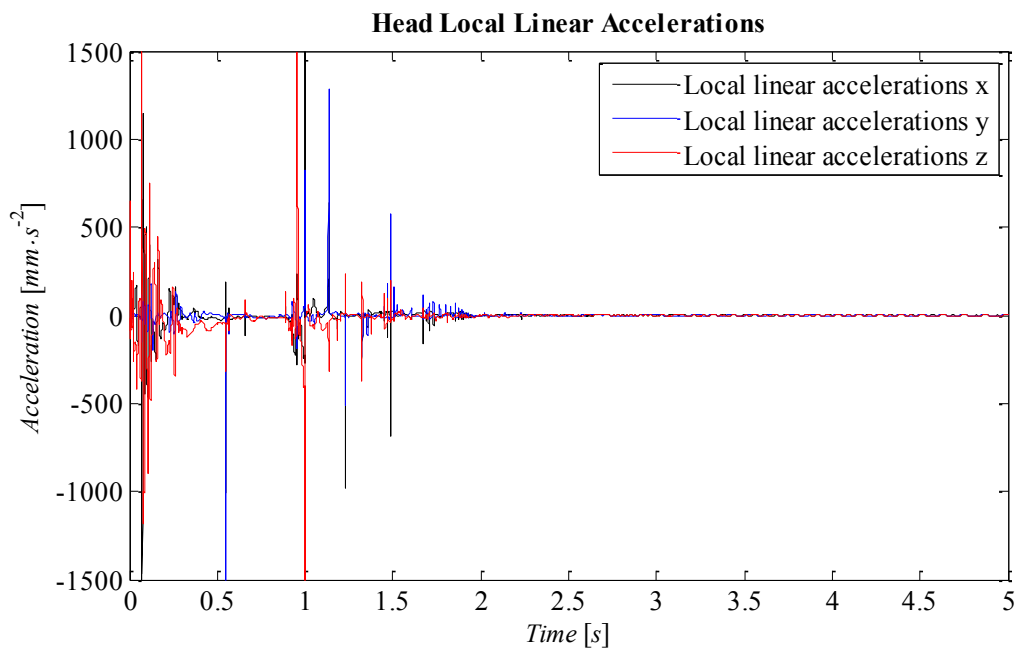
Figure 6-19 – Local linear accelerations of the Head
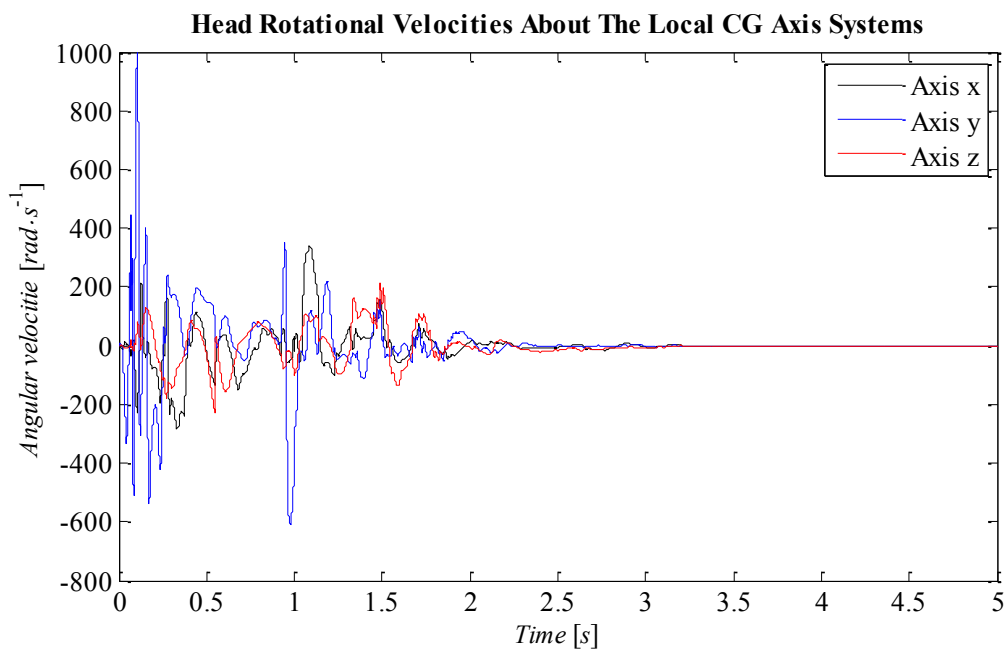
Figure 6-20 – Rotational Velocities of the Head in reference of the local Centre of Gravity Axis system
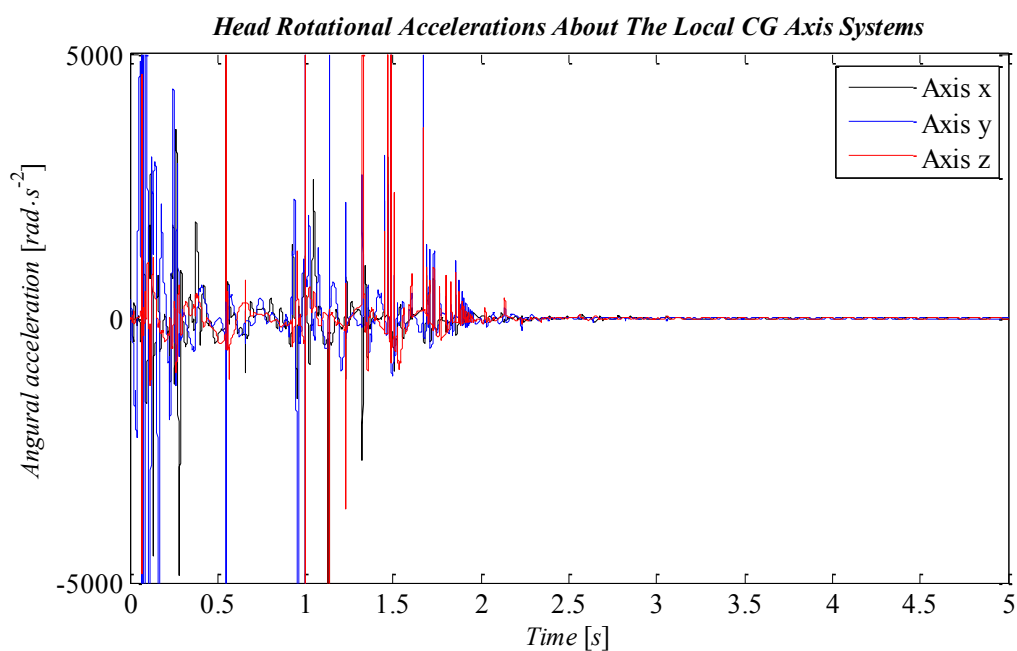
Figure 6-21 – Rotational acceleration of the Head in reference of the local Centre of Gravity Axis system

6.4   Contact tuning

The previous methodology have given a first approach for the contact parameters.

Since the developed MB human model is based on the anatomical and physiological data, some of the data is taken by means of virtual experiments. In this section, the methodology used to detect the contact parameters between the particular model segments is described.

As a reference, a rigid plane is used and body parts from HUMOS2 are dropped with diverse directions (medial, lateral, posterior and anterior) and velocities (referring

different drops from different heights). The drops are described in the way that rotations in any axis have been constrained, so the body was rebounded in the perpendicular direction to the plan and it does not start to rotate. Such virtual drop tests have been used to tune the contact parameters of the equivalent bodies in the MBM.

For such dropt tests, the contact can be described in the same way as described in standard MBS software's, or even by a simple one-dimensional Simulink model (Figure 6-22), were *const* is the position of the rigid plan, *g* is the gravity acceleration, *M* is the mass of the body segment, *B* and *K* are the damping and stiffness parameters of the contact, and results is the output dependent on time, position, velocity and acceleration.
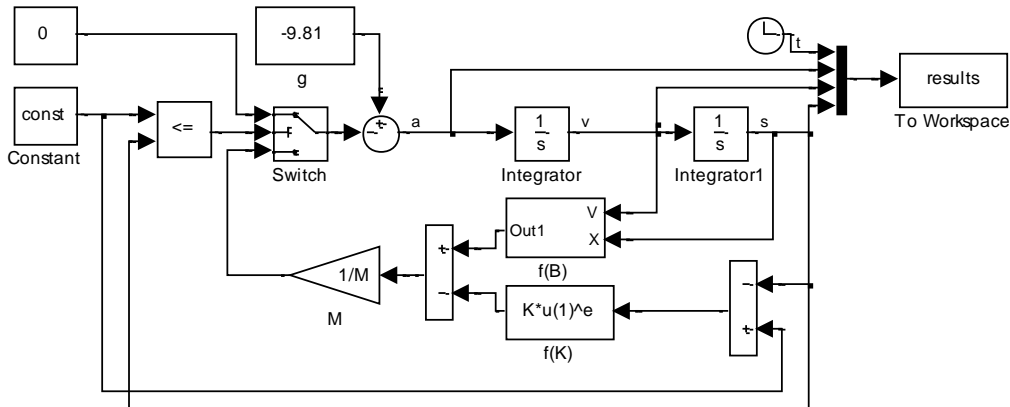
Figure 6-22 – Simulink model for 1D contact

The damping is given by (6-1), where *x* is the pseudo-penetration between the two bodies in contact, *d* is the maximum pseudo-penetration when the damping turns his maximum value, and the cubic equation describes how the damping evolves from null until his maximum value, following the shape illustrated in Figure 6-23 from null damping until maximum damping for one defined pseudo-penetration

$$B^* = \begin{cases} 0, if\ x \le 0 \\ \left(\dfrac{x}{d}\right)^2 \cdot \left(3 - 2 \cdot \dfrac{x}{d}\right), if\ 0 < x < d \\ 1, if\ x \ge d \end{cases} \tag{6-1}$$
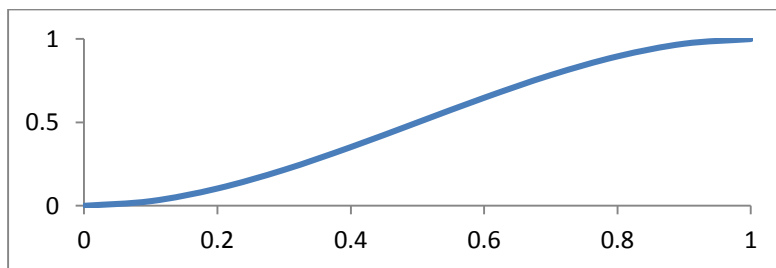
Figure 6-23 – Damping grow-shape from null (0) until defined (1) pseudo-penetration

For each numerical experiment, the contact parameters have been obtained by means of optimization, using Noesis Optimus Rev.8 (Figure 6-24). The first optimization has been obtained using Self-adaptive Evolution. The algorithm parameters used are: 5 parents,

sexuality 5, and population of 100, with a maximum of 75 interactions. The same seed for the optimization was used in all cases. A refinement for optimum was done using NLPQL with much thinner tolerance. The cost function comes from the sum of the product of the errors in position, velocity and acceleration by a correction factor, given by

$$out = k_s \cdot \sum \Delta s_i + k_{\dot{s}} \cdot \sum \Delta \dot{s}_i + k_{\ddot{s}} \cdot \sum \Delta \ddot{s}_i \qquad (6\text{-}2)$$
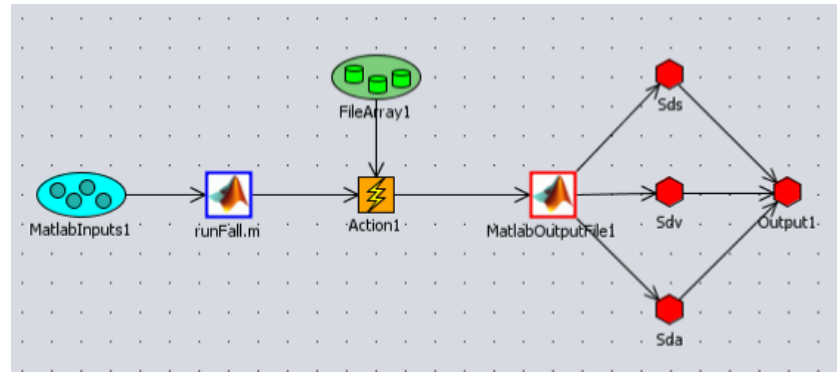
Figure 6-24 – Noesis Optimus program for contact optimization

The reference experiments have taken into account body segments from HUMOS2 model, taken in RADIOSS from ALTAIR, pre-processed using HyperCrash and post-processed using HyperView.

For each body segment, all the experiments have been taken, processed to obtain parameters for the contact. Then such data has been statistically processed to get an average reference value for each parameter with associated error.

The body-body pair contacts have been then obtained by computing the equivalent contact parameters.

It has been noted that the approach used have been changed for the head. It has been observed that for the head contact simplified to a single body, acceleration and position is incompatible in the optimization process. A good fitting for position comes with a divergence in acceleration and vice-versa.

A simple brain model has been coupled to the model, by a simple mass-spring-damper, with linear and not linear parameters, but good convergence has not been achieved. The used parameters are tuned for position (good approach for trajectory analysis), not giving suitable parameters for direct injury assessment.

6.4.1 Extremities contact tuning

For the extremities impact, a first set of configurations have been implemented on the FEM models from HUMOS2. The segments have been the upper and lower arm and the upper and lower leg. It was imposed an initial velocity to the body segments, and defined a contact with a wall (rigid or with material proprieties), in the absent of gravity.

The set of simulations with the HUMOS2 body parts was in the 4 directions: anterior, medial, posterior and lateral direction, with an initial velocity between 2.5 and 10 m/s, against a rigid wall. Two accelerometer have been coupled in the respective extremities of the longest bone in the respective body part. In the Figure 6-25 is shown one of the four tested positions to the bodies, the impact in the anterior aspect.
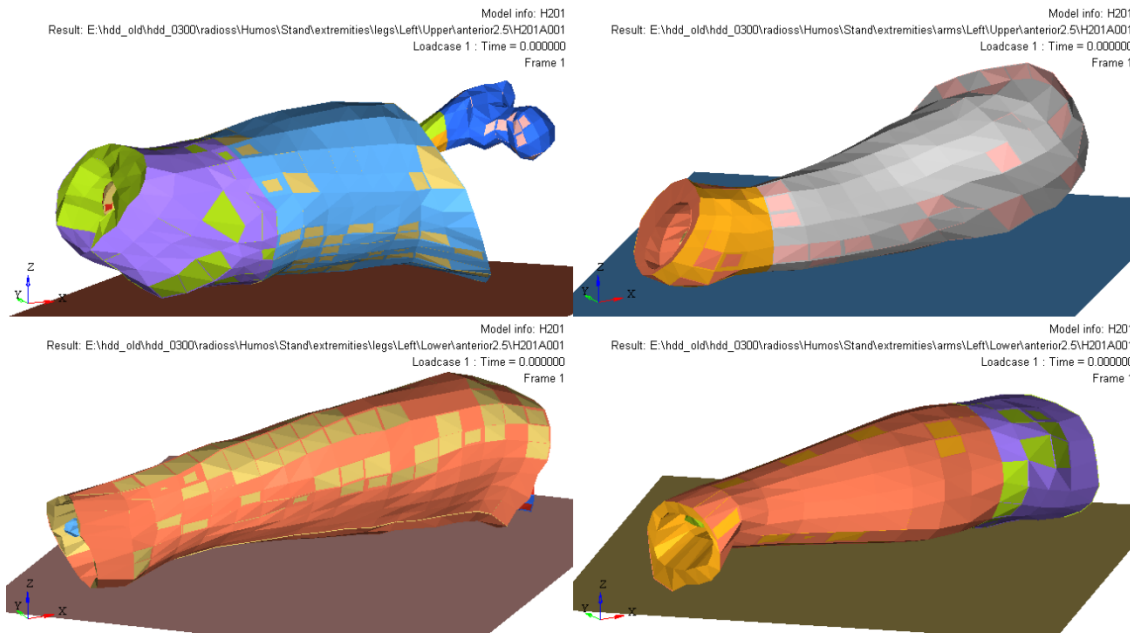
Figure 6-25 – Initial configuration of the four body parts (in clock wise: upper leg, upper arm, lower arm and lower leg) in an anterior impact configuration.

The simulations have been submitted to the solver and the data was extracted. An example of output, we as illustrated in Figure 6-26 have a plot of the acceleration in the accelerometer to the configuration presented in Figure 6-25, for an initial speed of 2.5m/s, on the ZZ axis (plots as seen in HyperView).
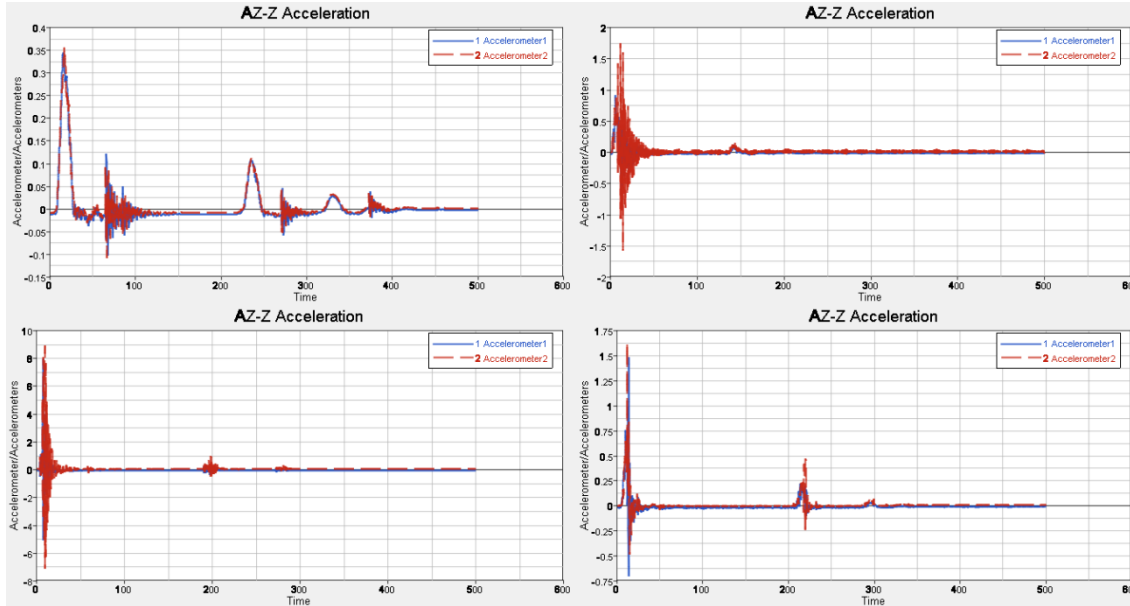
Figure 6-26 – Acceleration on ZZ axis measured in the accelerometers of the four body parts (in clock wise: upper leg, upper arm, lower arm and lower leg) in an anterior impact configuration, for an initial velocity of 2.5m/s.

After taking all the data of all cases: 4 aspects by 4 bodies by 4 speeds, the optimization was performed to each case. The output optimized parameters are summarized in the Figure 6-27 until the Figure 6-30.
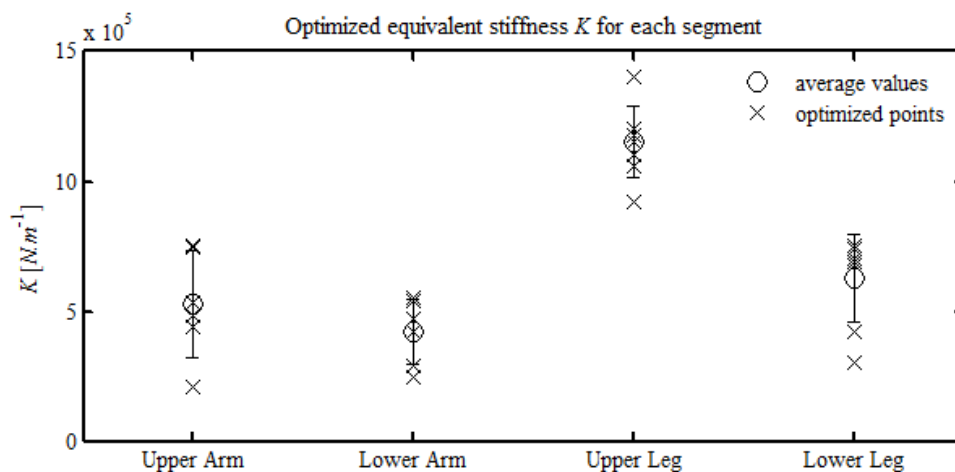
Figure 6-27 – Optimized values and respective average with error for the extremities K parameter.
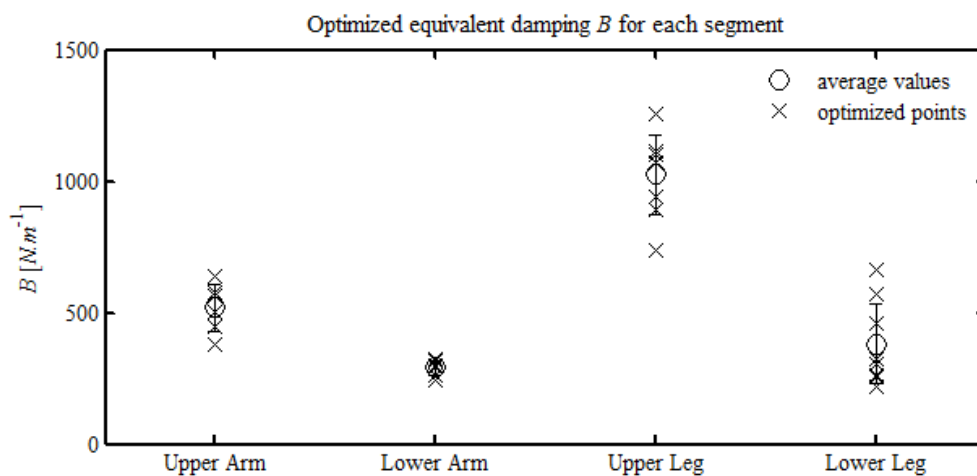
Figure 6-28 – Optimized values and respective average with error for the extremities B parameter.
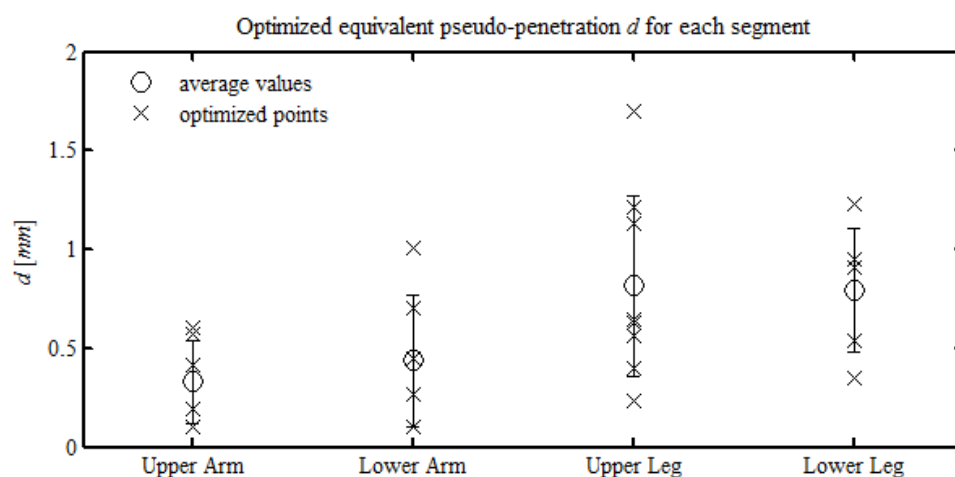
Figure 6-29 – Optimized values and respective average with error for the extremities d parameter.

Optimized equivalent exponent *e* for each segment
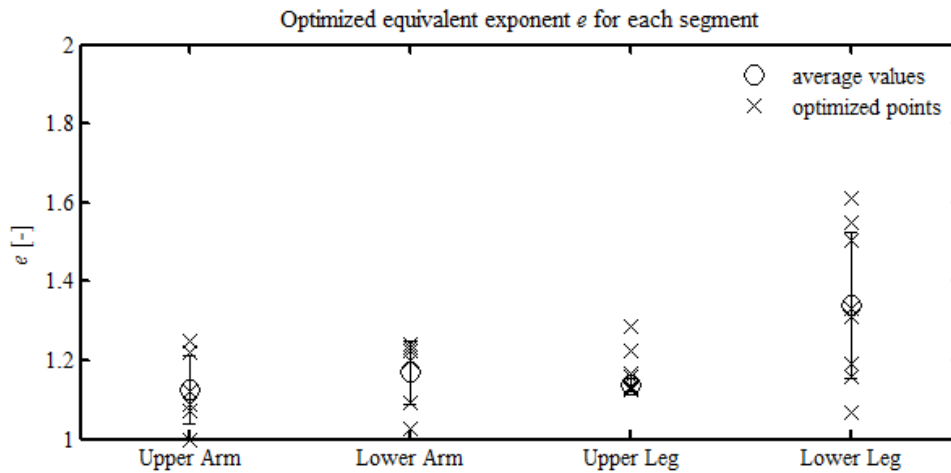
Figure 6-30 – Optimized values and respective average with error for the extremities *e* parameter.

6.4.2 Head contact tuning

For the head impact, a first set of configurations have been implemented with both models (FEM and our MBM). It was imposed an initial velocity to the head and the neck, and defined a contact with a wall (rigid or with material proprieties), in the absent of gravity.

The first simulation with the HUMOS2 head and neck was in the anterior direction (wall parallel with the mandible and maxilla), with an initial velocity between 2.5 and 20 m/s (~1/4 to ~2 times the standard velocity for tests for pedestrian impacts concerning head impact [70, 71]), against a rigid wall.

From the simulated velocities was found that the velocities greater than 10 m/s against a rigid wall, the simulation stops before the prescribed final time of simulation, related with the big levels of deformation in the skin/flesh of the face (negative volume error mainly). It's easy to see in the acceleration plot (Figure 6-31), one second peek. This second peek gives indications of a possible second impact inside of the head.
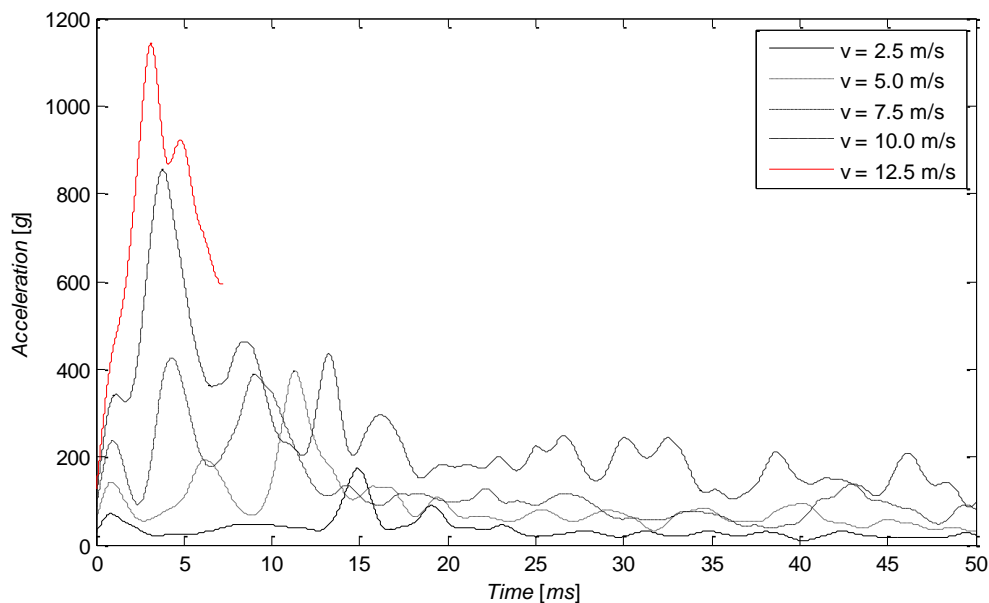
Figure 6-31 – Head CoM accelerations, for an anterior impact with an initial velocity from 2.5m/s until 12.5m/s with a rigid wall.

To understand why such peek appears, the head and neck of the HUMOS2 have been simulated in a range of directions. In some configurations, such second peek doesn't appear, or appear in a different way.

6.4.2.1   Head – HUMOS2 and Hybrid III

To get a better understanding of the phenomena, the same configurations have been described in the head and neck of the dummy model Hybrid III.

From the evaluation of the curves from both models, appears obvious the discordance of both models. This discordance is more notorious in some configurations than in others (Figure 6-32 and Figure 6-33).
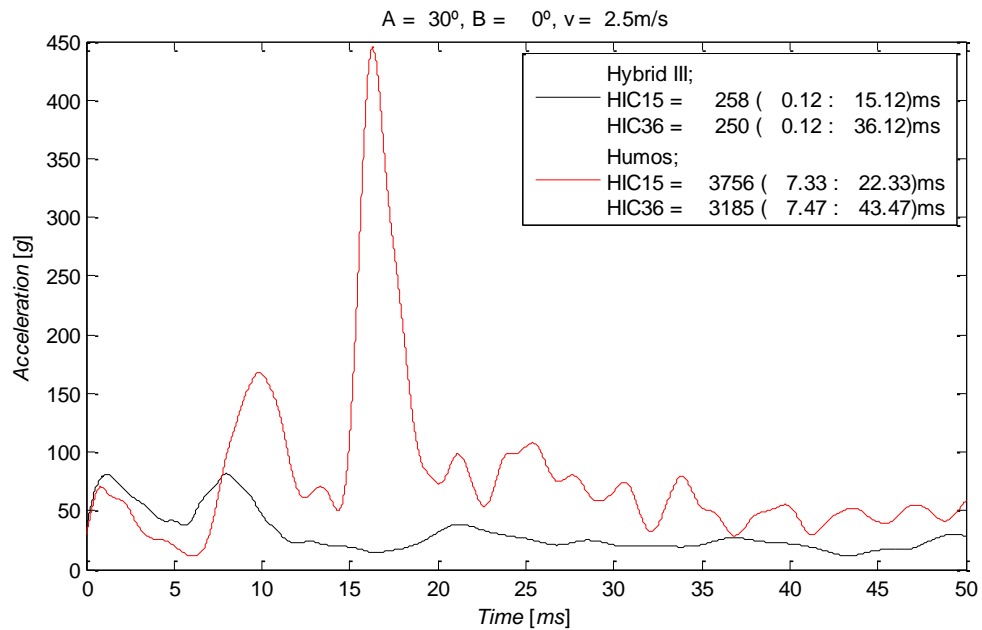
Figure 6-32 − Accelerations of the CoM in the head of the Hybrid III and HUMOS2 for rotation 30-0.
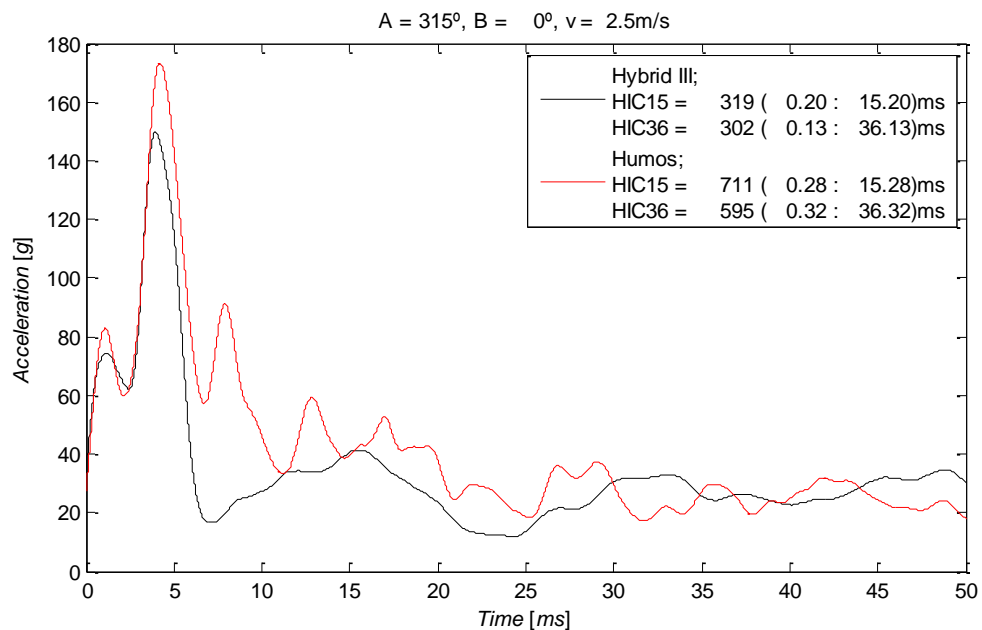
Figure 6-33 − Accelerations of the CoM in the head of the Hybrid III and HUMOS2 for rotation 315-0.

6.4.2.2   Head – HUMOS2 CoM

To understand such difference, we start to see how is defined the CoM in the HUMOS2 head, and how the head model was validated. The CoM point is described as a node in a rigid body, that shares 4 nodes with an element of the skull (rigid element), localized in the left condyle joint (Figure 6-34). The assumption is that the skull is closed to a rigid body, and the CoM will follow the rigid element. This assumption is valid for low levels of deformation of the skull.
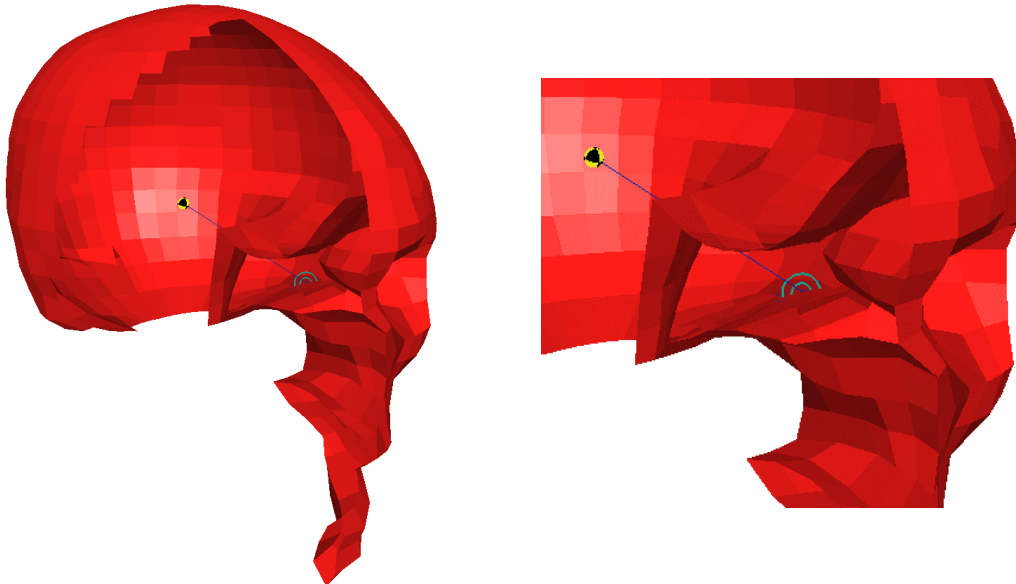
Figure 6-34 – Illustration of the definition of the CoM in HUMOS2 model

To get better results, the model (seated version) have implemented a four tri-axial accelerometers in a rigid structure (Figure 6-35), coupled to the skull us a helmet (this helmet was not used in the impact simulations). These accelerometers are connected in a 3-2-2-2 configuration, giving the sixty accelerations components, but imply some rigid connections between the skull and the helmet. This rigid connections gives a range of constrains in the skull that compromises the free deformation of the skull, relevant in direct impact situations, but full validated in the car occupant posture (sled tests).
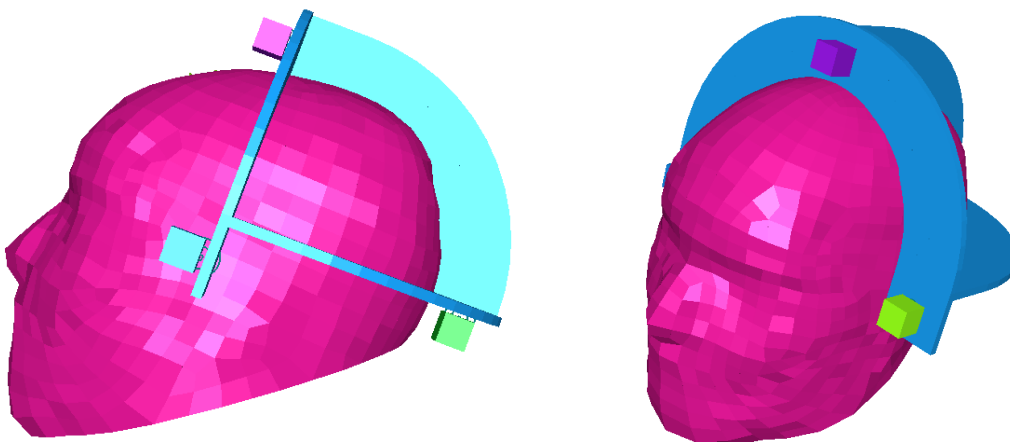
Figure 6-35 – Illustration of the helmet structure with four accelerometers in HUMOS2 model

These two ways to get the CoM acceleration of the head in HUMOS2 proves to be inaccurate in average and heavy direct impact situations, mainly in a spread load range as used in the impacts simulations.

6.4.2.2.1 Acceleration

Is different to measure the acceleration in the CoM of one body in own reference axis or in the referent axis of other body. The relation of the velocity and acceleration [4] is given by the system of equations (1):

$$\begin{cases} \mathbf{v}^A = \mathbf{v}^B + \boldsymbol{\omega} \times \mathbf{r} + \mathbf{v}^{rel} \\ \mathbf{a}^a = \mathbf{a}^B + \dot{\boldsymbol{\omega}} \times \mathbf{r} + \boldsymbol{\omega}\left(\boldsymbol{\omega} \times \mathbf{r}\right) + 2\boldsymbol{\omega} \times \mathbf{v}^{rel} + \mathbf{a}^{rel} \end{cases} \tag{6-3}$$

When the rotational component of the movement can be neglected (lower angular velocity), and if the point is part of the same body and the behavior is similar to a rigid body, we can assume that:

$$\begin{cases} \mathbf{v}^A = \mathbf{v}^B \\ \mathbf{a}^a = \mathbf{a}^B \end{cases} \tag{6-4}$$

Since the part of the head that is more closed to a rigid body is the skull (same assumption used in the original CoM methodology), but still with a not neglected deformation, we assume that one array of accelerometers distributed in several areas of the skull can give a good approximation of the real acceleration of the CoM. This assumption comes from the type of contact analyzed in the validation process, impact movement in the direction of the perpendicular axis with the contact plane, with rebound very close to the same axis, very low levels of head rotation, and reduced skull deformation.

In this process, a total of 98 accelerometers have been defined in the skull, as illustrated in the Figure 6-36 and distributed according with the Table 6-7.

The average value and error for each time step is defined by equations (6-5) and (6-6).

$$\overline{a}^t = \frac{1}{n} \cdot \sum_{i=1}^{n} a_i^t \tag{6-5}$$

$$\sigma\left(a^t\right) = \sqrt{\frac{1}{n-1} \cdot \sum_{i=1}^{n} \left(\overline{a}^t - a^t\right)^2} \tag{6-6}$$

One automatic decision criteria was used to refuse not normal values, using the statistic toll:

$$a_i^t \in \left[\overline{a}^t - 2 \cdot \sigma\left(a^t\right); \overline{a}^t + 2 \cdot \sigma\left(a^t\right)\right] \tag{6-7}$$

meaning that if a_i^t not belong to the interval, is refused. This toll filters all the points that have a probability less than a given probability to feet onto the interval.
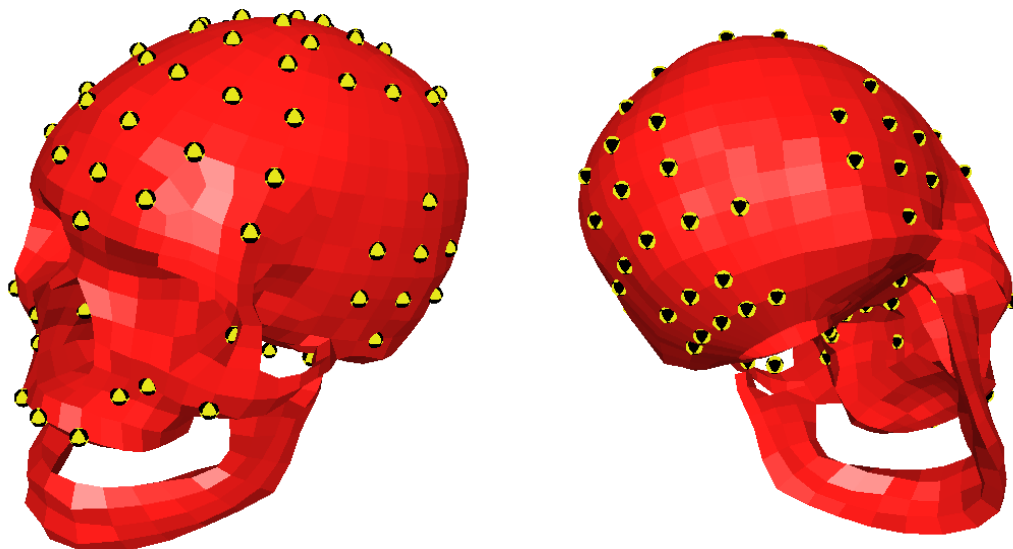
Figure 6-36 – Position of the accelerometers in the skull.

Table 6-7 – Distribution by region of the accelerometers defined on the skull.

Skull region	Number of accelerometers
Frontal	15
"Inferior"	14
Maxilla	17
Occipital	15
Parietal	21
Temporal left	8
Temporal right	8

With this change, the new simulations results have been computed for the new acceleration curve and new HIC's have been computed for the average curve. The average curve with the error curve gives one corridor to compare the results of Hybrid III and the results from the MBM implemented. The negative values of the lower border have been set as zero, since a negative value for the resultant acceleration don't have any physic meaning.

6.4.2.3 Results for the various models

The same impact configurations have been implemented in the head and neck MBM, and the simulations performed. The resultant head acceleration for each test was analyzed. The Figure 6-37 until Figure 6-44 shows for several impact configurations, the acceleration value for the HUMOS2 and Hybrid III.
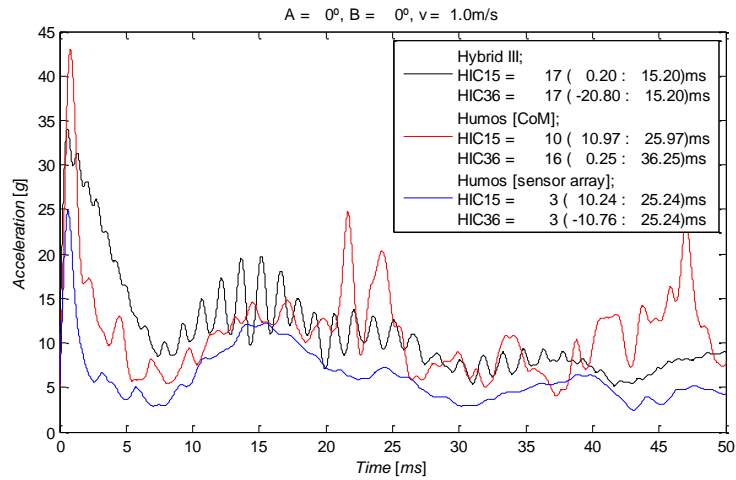
Figure 6-37 – Accelerations of the CoM in the head of the Hybrid III and HUMOS2 (CoM and equivalent CoM) for orientation 0-0, v=1.
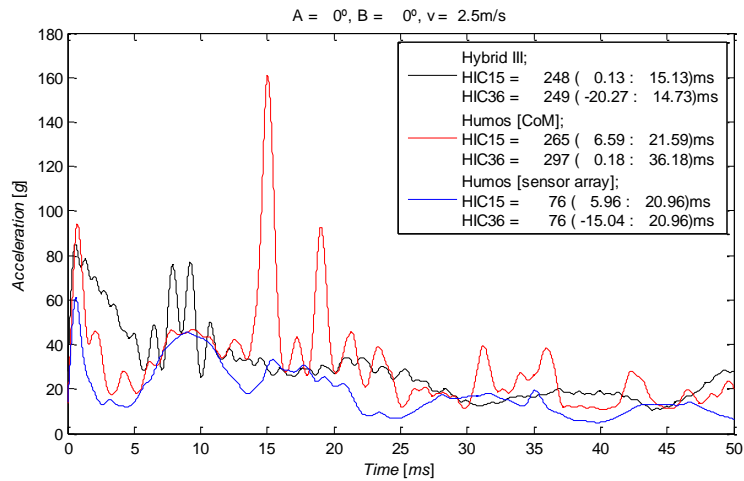
Figure 6-38 – Accelerations of the CoM in the head of the Hybrid III and HUMOS2 (CoM and equivalent CoM) for orientation 0-0, v=2.5.
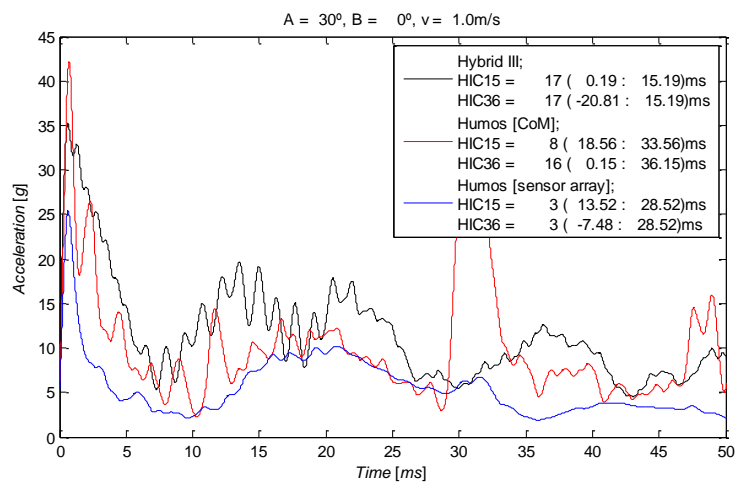
Figure 6-39 – Accelerations of the CoM in the head of the Hybrid III and HUMOS2 (CoM and equivalent CoM) for orientation 30-0, v=1.
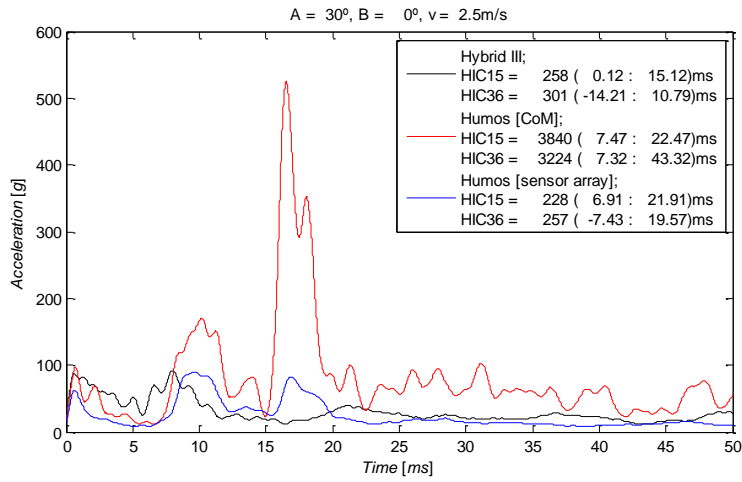
Figure 6-40 – Accelerations of the CoM in the head of the Hybrid III and HUMOS2 (CoM and equivalent CoM) for orientation 30-0, v=2.5.
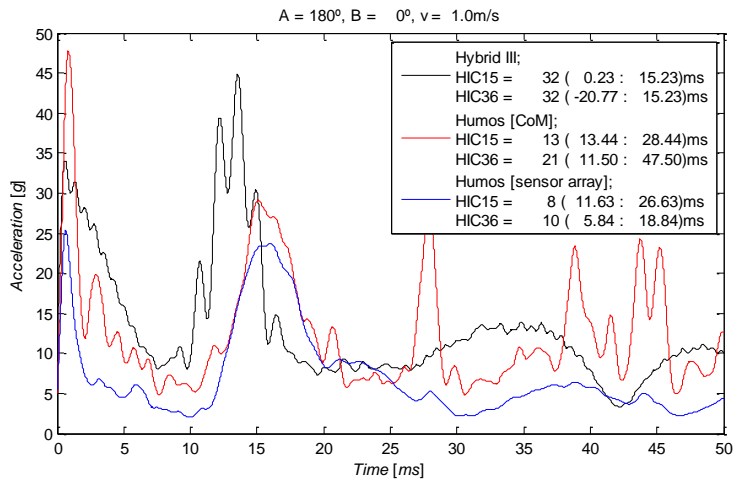
Figure 6-41 – Accelerations of the CoM in the head of the Hybrid III and HUMOS2 (CoM and equivalent CoM) for orientation 180-0, v=1.
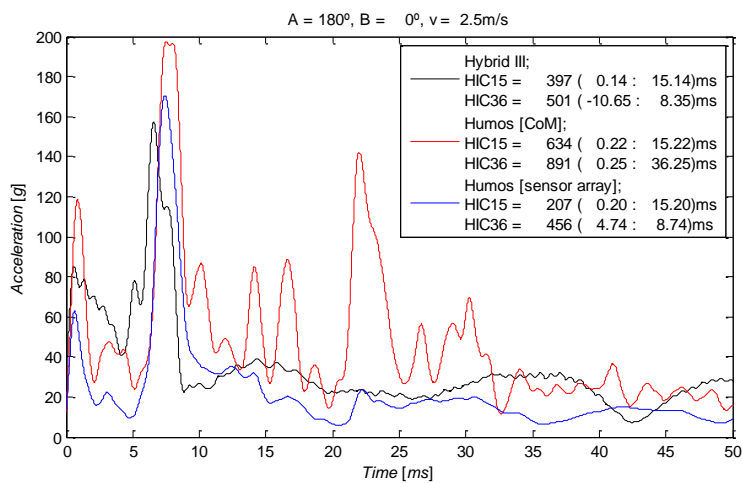
Figure 6-42 – Accelerations of the CoM in the head of the Hybrid III and HUMOS2 (CoM and equivalent CoM) for orientation 180-0, v=2.5.
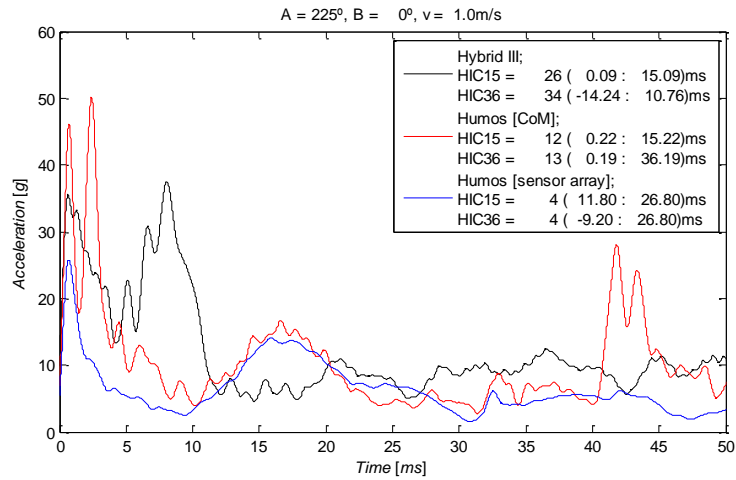
Figure 6-43 – Accelerations of the CoM in the head of the Hybrid III and HUMOS2 (CoM and equivalent CoM) for orientation 225-0, v=1.
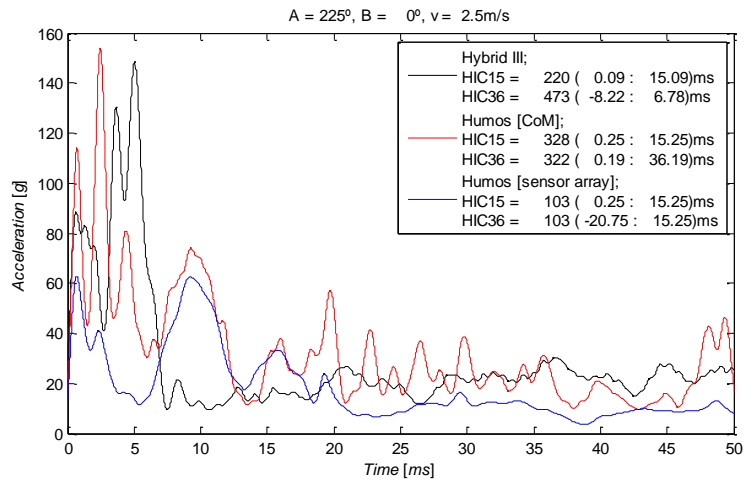
Figure 6-44 – Accelerations of the CoM in the head of the Hybrid III and HUMOS2 (CoM and equivalent CoM) for orientation 225-0, v=2.5.

The Figure 6-45 illustrates one case of the several, all similar relatively to convergence, it clear that the brain movement inside of the skull gives to the model ate least one more degree of freedom. For a short time interval reference, catching just the very first peek, in all cases, a better correlation is got, but that implies a greater divergence in results, mainly in displacement after impact.
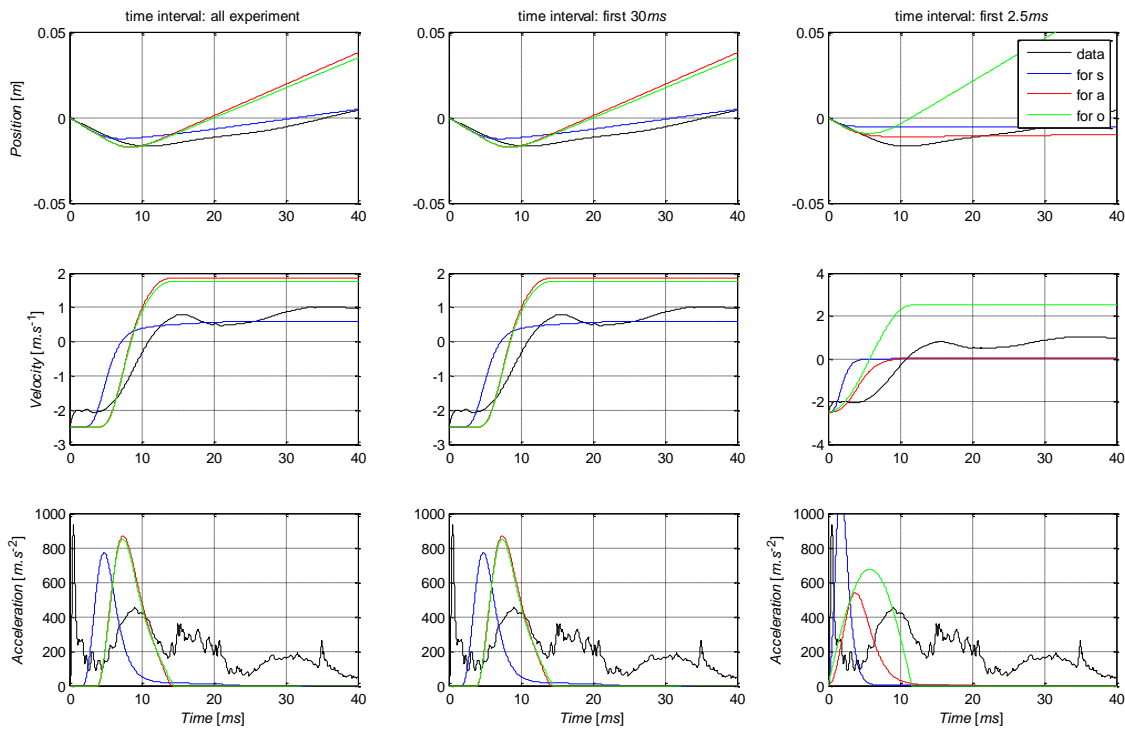
Figure 6-45 – Displacement, velocity and acceleration for the head equivalent CoM, and for the optimization 1D model (3 criteria's), for different time interval references (3) for A=180º, B=0º, and v=2.5m/s

From the two direction type of convergence we get that a simple 1 body for the head is not enough for an accurate head behaviour after impact. A model with a simple brain modelled as one body coupled with a linear spring and damper don't get any satisfactory convergence, since the find optimum was high dependent of the starting point. A more complex brain in head model is desired, as also a coupled face to react under frontal impacts in a more biofidelic way.

Another find was that when comparing the behavior of the tested head models, the behavior was with a good fit with the literature in the range of the validation protocol (velocity and direction). In all the simulations was found a different grade of divergence when the speed of contact have been increased or direction of impact. Such behavior can be see for the maximum measured acceleration (Figure 6-46) and HIC (Figure 6-47). Exception was a test with the head model used for pedestrian crash test.
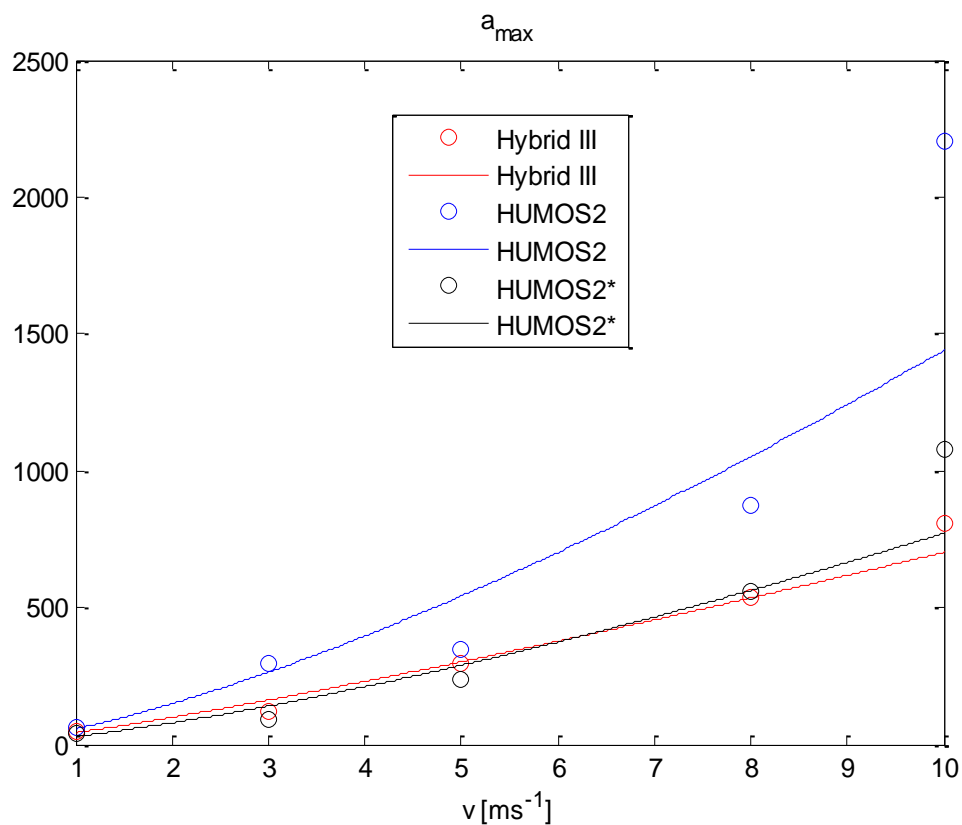
Figure 6-46 – Evolution for maximum acceleration for the compared head models
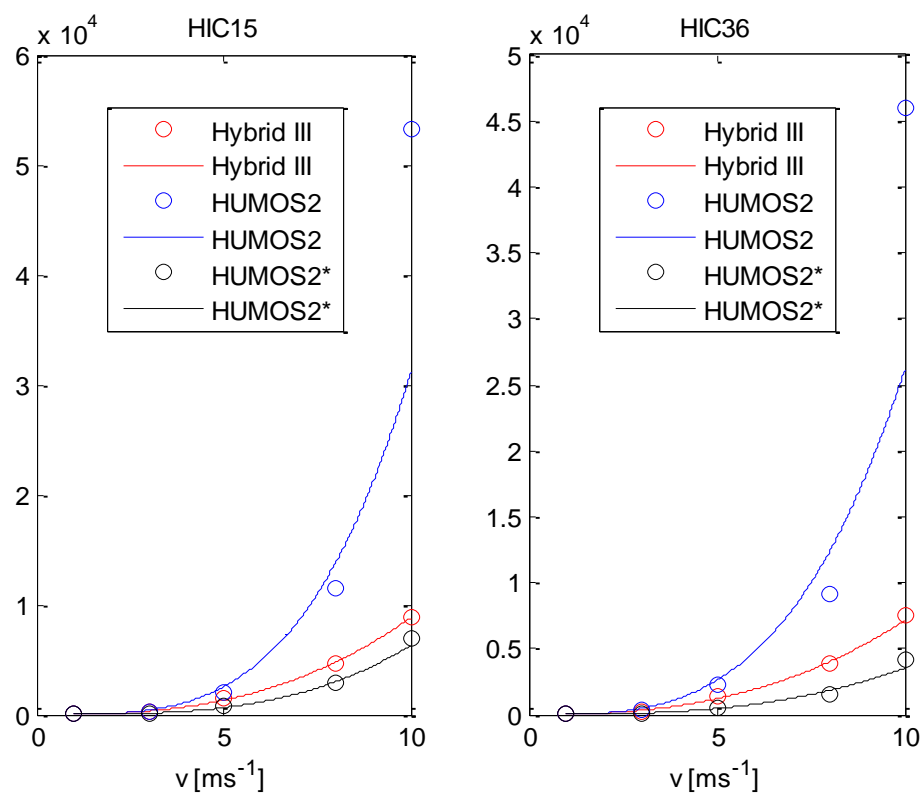
Figure 6-47 – Evolution for both HIC values for the compared head models

The full results for the head impact for the speed of 2.5 and 7.5 m/s is presented in the Figure 6-48 until the Figure 6-51 for the maximum acceleration, and HIC15 values.
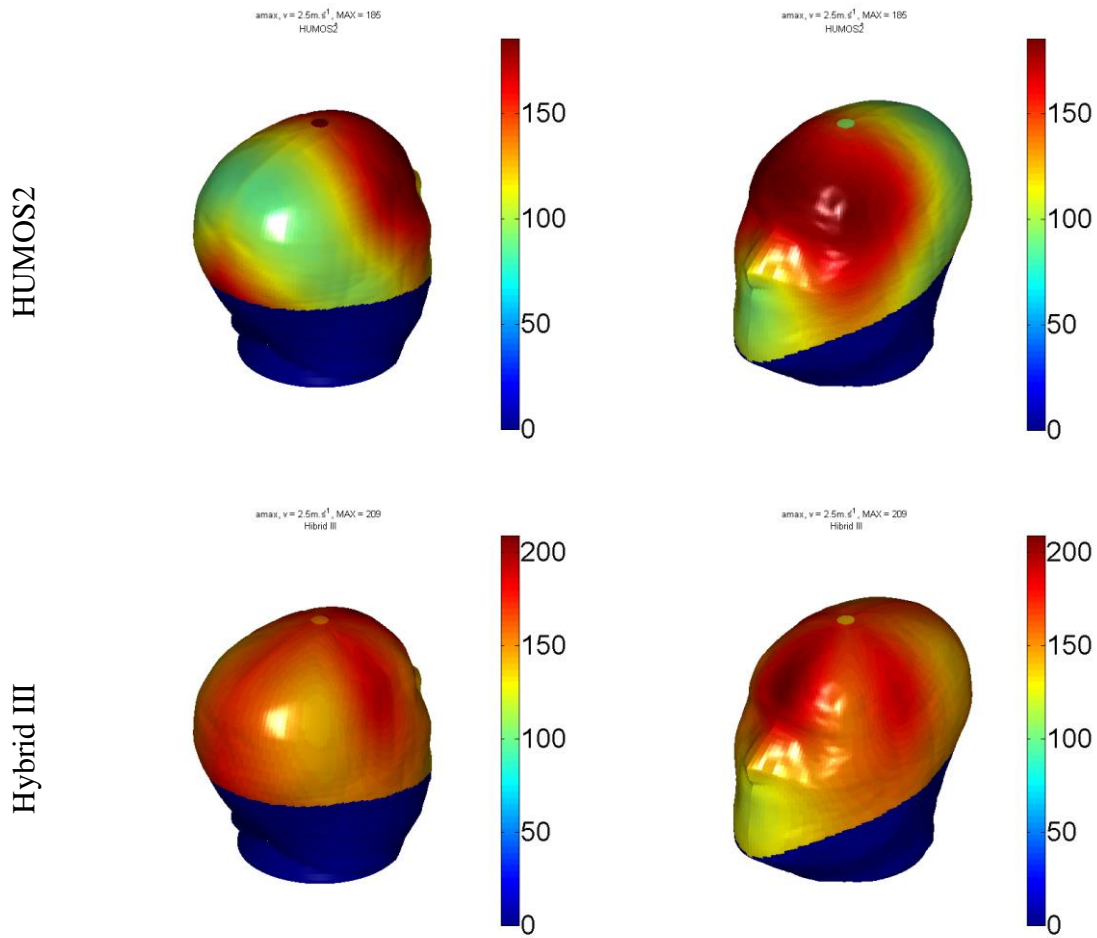
Figure 6-48 – Maximum acceleration gradient according with the load direction in both head FEM head's, for an impact speed of 2.5m/s.
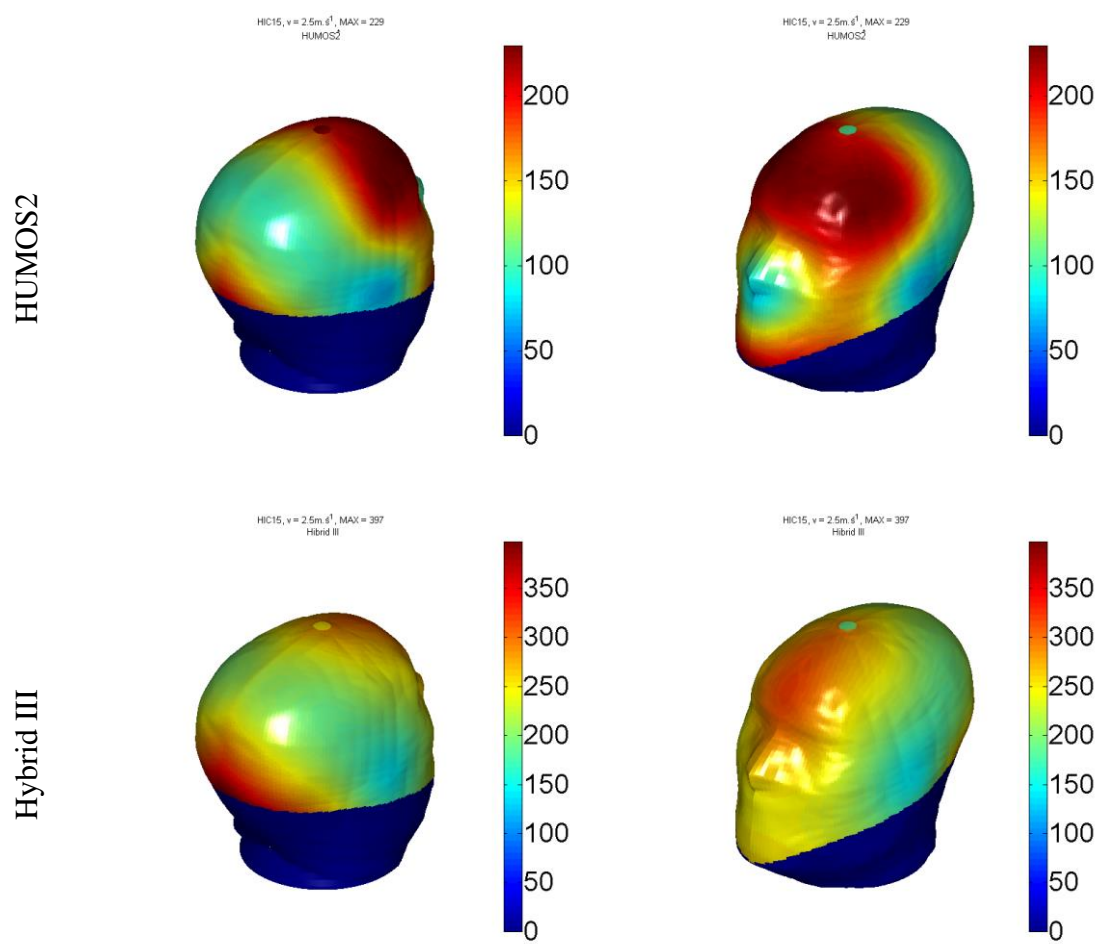
Figure 6-49 – HIC15 gradient according with the load direction in both head FEM head's, for an impact speed of 2.5m/s.
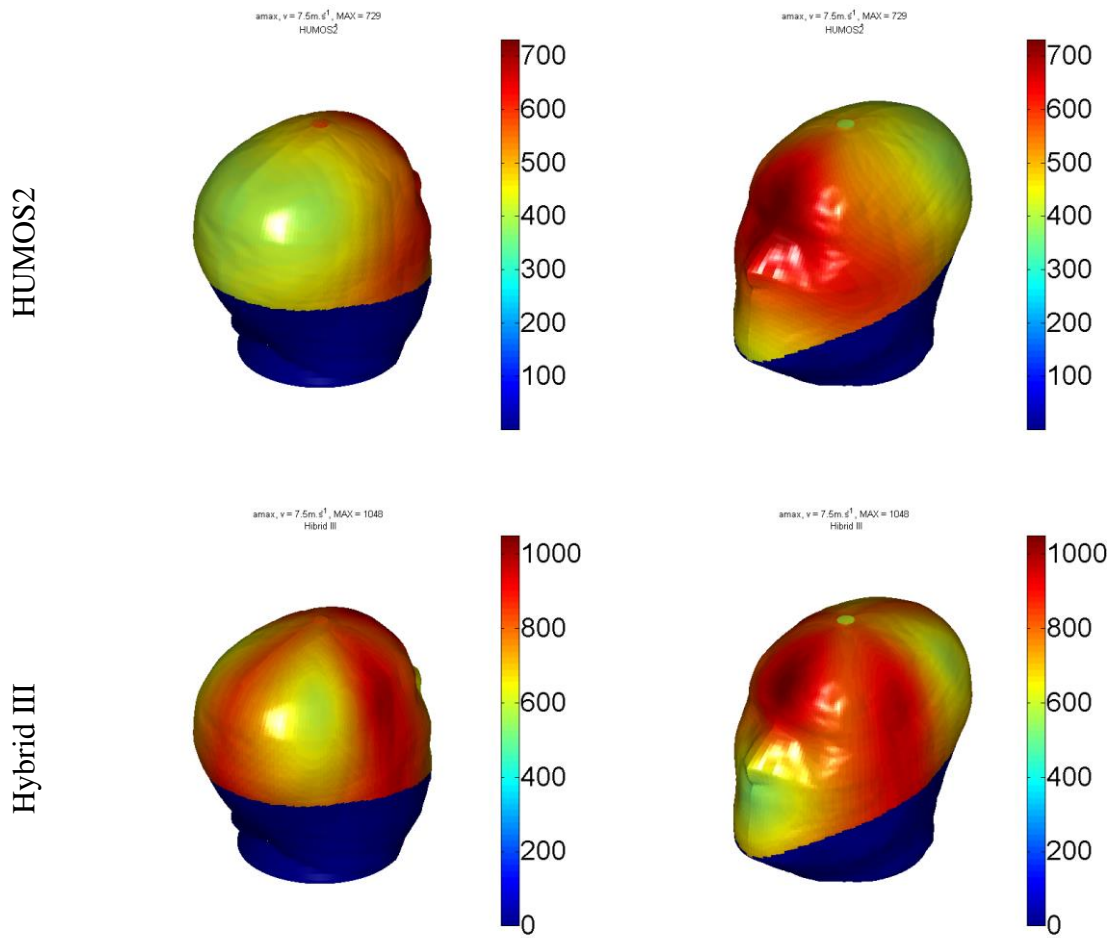
Figure 6-50 – Maximum acceleration gradient according with the load direction in both head FEM head's, for an impact speed of 7.5m/s.
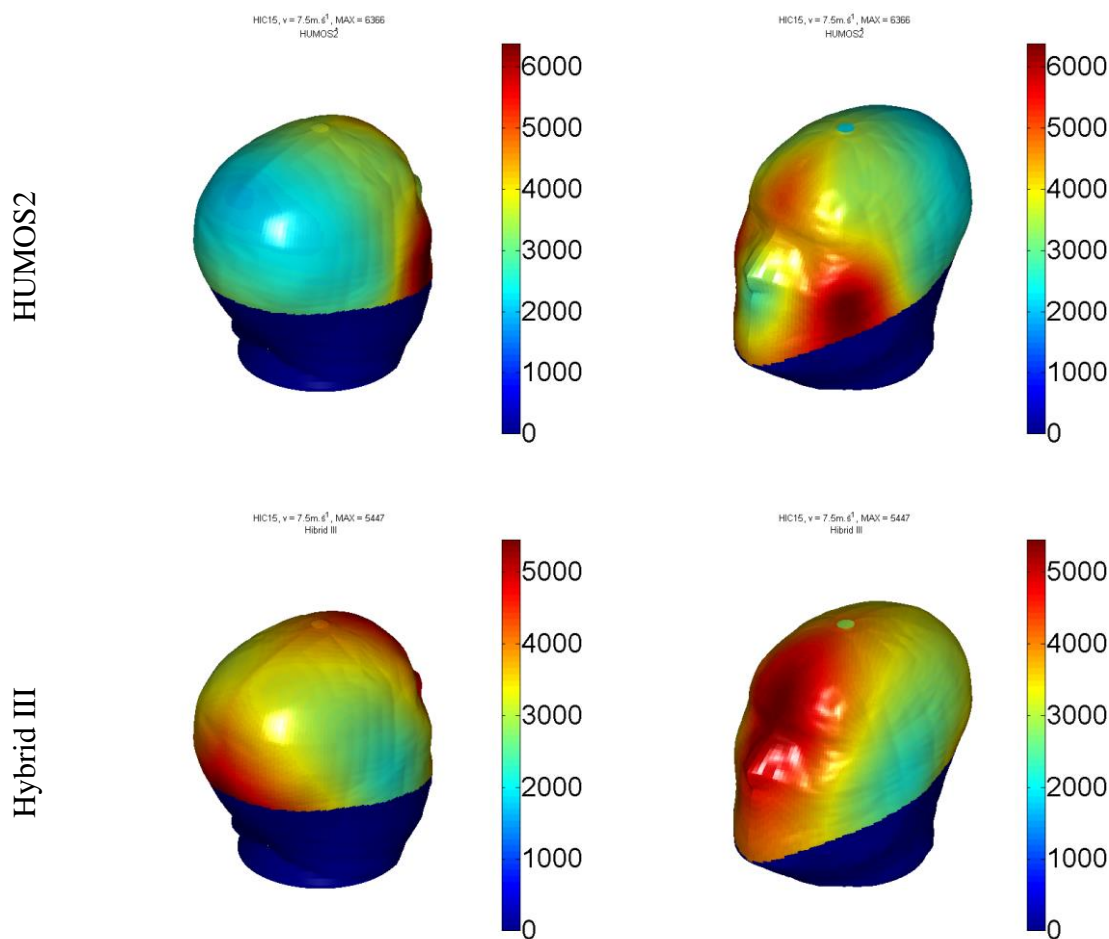
Figure 6-51 – HIC15 gradient according with the load direction in both head FEM head's, for an impact speed of 7.5m/s.

In all cases, can be seen a distinctive difference between both models when impacting in several directions and speeds.

6.5   Models accessories: Helmet and PTW

For the HBM, a set of other parts that not his body segments are needed, like the helmet, PTW, road and road furniture.

6.5.1   The Helmet

In a PTW accident, one of the factors that influence the body trajectory and even the type of injury is the range of movement in each joint on the body. Some protective equipment's have some of their work in joint reduction, like some boots (high reduction of the ankle movements) or in some neck collars (reduction of the movements in the neck area).

The data for the reduction or constraint in movement for protective equipment is completely unknown. One exception in such movement reduction is in the protective equipment that shows a clear movement constrain. In the helmet scenario, such reductions are clear from the interference between the helmet and the human body parts (e.g. the helmet impacts the shoulders sooner than the head for the same movement).

The added mass and respective inertia is other factor either, as a different rebound in impact.

The helmet is coupled to the head by a bracket joint. The contact parameters between the helmet and other surfaces have included the interface helmet-neck.

It's known that the relative movement between the helmet and the head is not totally neglected, like the movement of the brain is not neglected either. From the multi-directional impact directions found in PTW accidents and different ways that the helmet can move relatively to the head means a complex coupling model.

6.5.2   PTW model

The human model has been coupled to a PTW model. The base frame has been developed according to the first version of LMS PTW model (no suspension, with tire models).

6.5.2.1   PTW frame and tires

The implementation of the PTW frame and tires was done according to the model used by LMS in the MYMOSA consortium (Figure 6-52). This model includes a tire model for both wheels, characterization of the several components (swing arm, frame, and front fork). The PTW suspension was set rigid (no front or rear suspension). The mass of the driver are included in the frame. The external geometry was coupled to this frame.
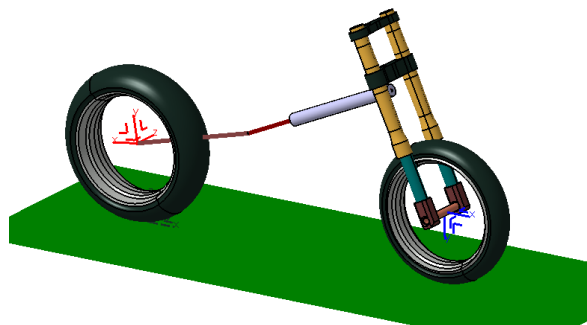
Figure 6-52 – PTW model with frame and tires

The PTW model was benchmarked in typical simulations using several parameters for the start, always in open-loop, to understand the behavior of the PTW in several scenarios. One of this behaviors can be observed in the Figure 6-53.
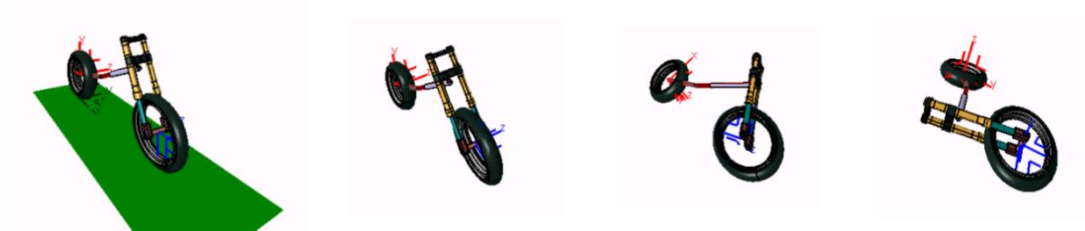
Figure 6-53 – Simulation of the PTW in open-loop

6.5.2.2   PTW geometry

The PTW body has been taken from Honda CBR 1000 3ds free model (artist-3d.com, Figure 6-54.a), translated to the stl format, simplified, converted to the iges format, prepared for contacts and coupled to the frame.

The PTW system has been then integrated with the human model defining new sets of contacts between the dummy, PTW and road. The dummy has been moved to a driving configuration, where it is easy to see the head locking ahead, as looking for the skyline, as expectable in a driving position (Figure 6-54.b).

Similar approach has been used for elements in the model as urban furniture and vehicles that have any direct role in the accident simulated.

Figure 6-54 – a) Original PTW model (artist-3d.com); b) Human model in Virtual.Lab with helmet, in a PTW and road scenario.

7

Results and discussion: Injury assessment and accident reconstitution

The body segments involved in any particular load observed in the accident simulation can be analysed in more detail. The standard criteria's as HIC, 3ms, max(g), ThAC and others can be obtained from a deformable not linear model. Furthermore, rib fractures and other injuries related to the deformable model can be evaluated.

The body segment from the dummy and the impacted objected are replaced in FEM for their equivalent FEM models, with the conditions obtained from the MBM simulation.

The mathematical parameters can be complemented with injury analysis from the result from the simulation, like broken bones, high deformed bodies, and energy or stress levels in organs. Critical aspects can be observed. The imposed deformations imposed to the aorta, heart, spleen and liver are possible to analyse. It's possible to evaluate the levels of energy found in the brain, or the relative displacement found between vertebras.

The association between the mathematical criteria's and the observation of the "injured" model gives a better assess to the trauma mechanisms, helping diagnosing the trigger effects and possible remedies to reduce/avoid such consequences.

7.1   Case 1: Pedestrian impact

The scenario of the pedestrian hit by a van is already partial described in the previous chapter. The current section will so focus in the injury assessment using FEM tools. The detail analysis will be in to body areas: head and trunk (thorax plus abdomen plus pelvis).

For injury assessment, HUMOS2 in RADIOSS is used, as already explained. The body in study is set with the initial conditions from the MB simulation in the time zero relatively to the body segment impact.

The critical parts concerning injuries are the head-windscreen contact and the trunk-bonnet contact.

For the effect, a windscreen and a bonnet FEM models was converted from LS-DYNA to RADIOSS, both validated and used in this simulations, with boundary conditions that mimic the respective parts in a vehicle. The conversion and validation of this parts and a full vehicle front (Figure 7-1) as part of the practical training received in ALTAIR facilities in Paris.
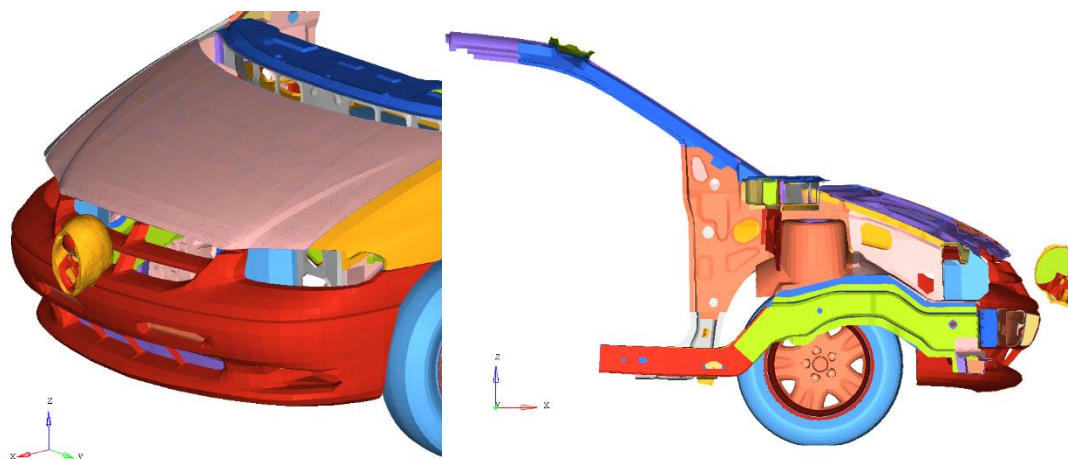
Figure 7-1 – Vehicle front converted to RADIOSS with a head to impact simulation

7.1.1   Injury assessment

The high HIC value in this accident indicates a high risk of death, or severe permanent damage. Such evidences of heavy trauma can be simulated, when the head from the HUMOS2 is impacted to one windscreen model with the same impact conditions found in the accident simulation (so called hybrid approach – full time multi-body simulation is followed by short time FE analysis). The Figure 7-2 shows a head section view, where the brain displacement is clear, and the destruction of the mandible and fracture in the maxilla is clear also. The Figure 7-3 shows the skull in its initial and final deformation status.

t=0ms   t=3ms

t=6ms   t=9ms
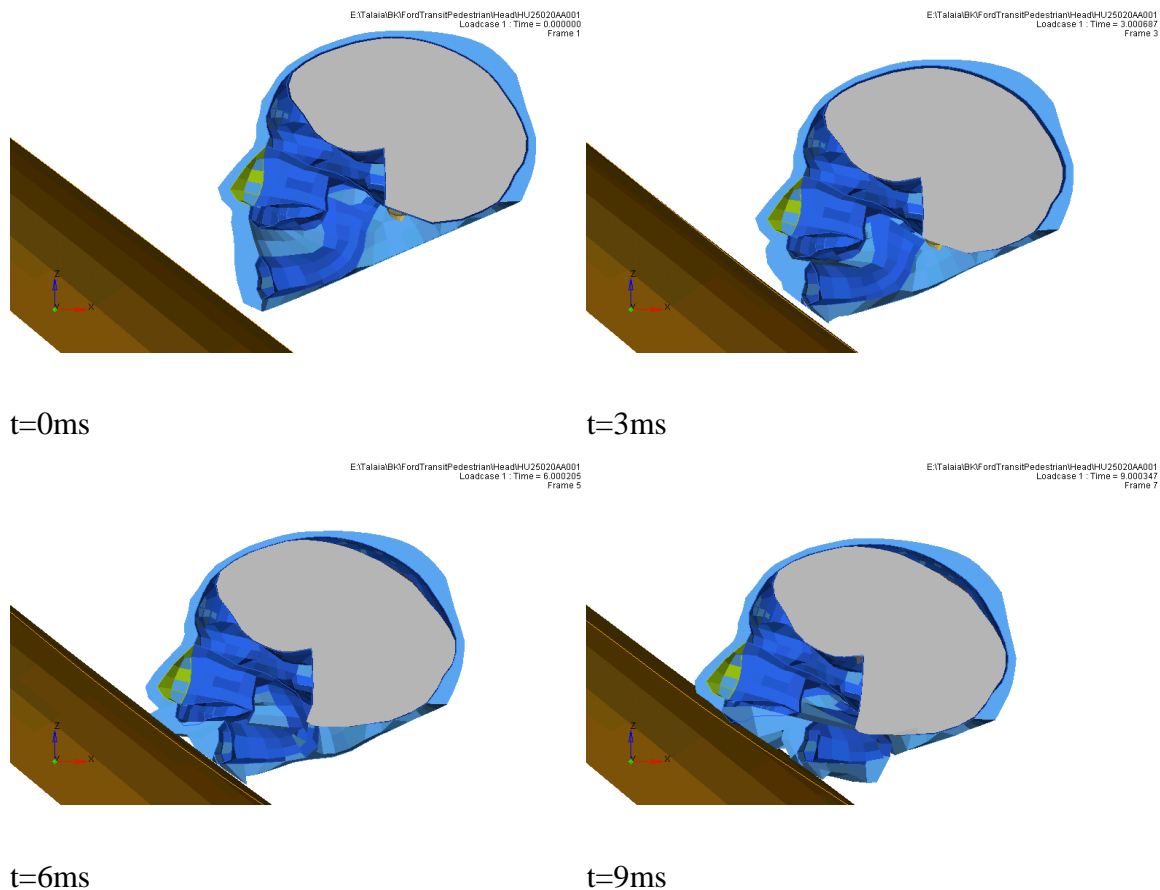
Figure 7-2 – Section of the head impacting the windscreen.

The deformation of the skull, the respective deformation in the brain and his relative displacement inside the skull, are in line with the high HIC values computed in the previous chapter for this scenario. Also the partial fracture of the maxilla and the mandible fracture can also points a face trauma in class LeFort II. All this in the head can not only trigger no recoverable damage into brain, also in case of breath fault, the mechanical ventilation can be compromise without intubation, meaning advanced medical stabilization in site.

Like the high value of HIC, the value of ThAC points out a high risk of trauma in a real human. The impact of the trunk with the bonnet simulated by these parts in RADIOSS points out also high levels of deformation, displacements and broken bones.

The neck, thorax, abdomen and pelvis from HUMOS2 have been configured to impact in a bonnet model in the same configuration and conditions as observed from the multi-body accident simulation.

a)

b)
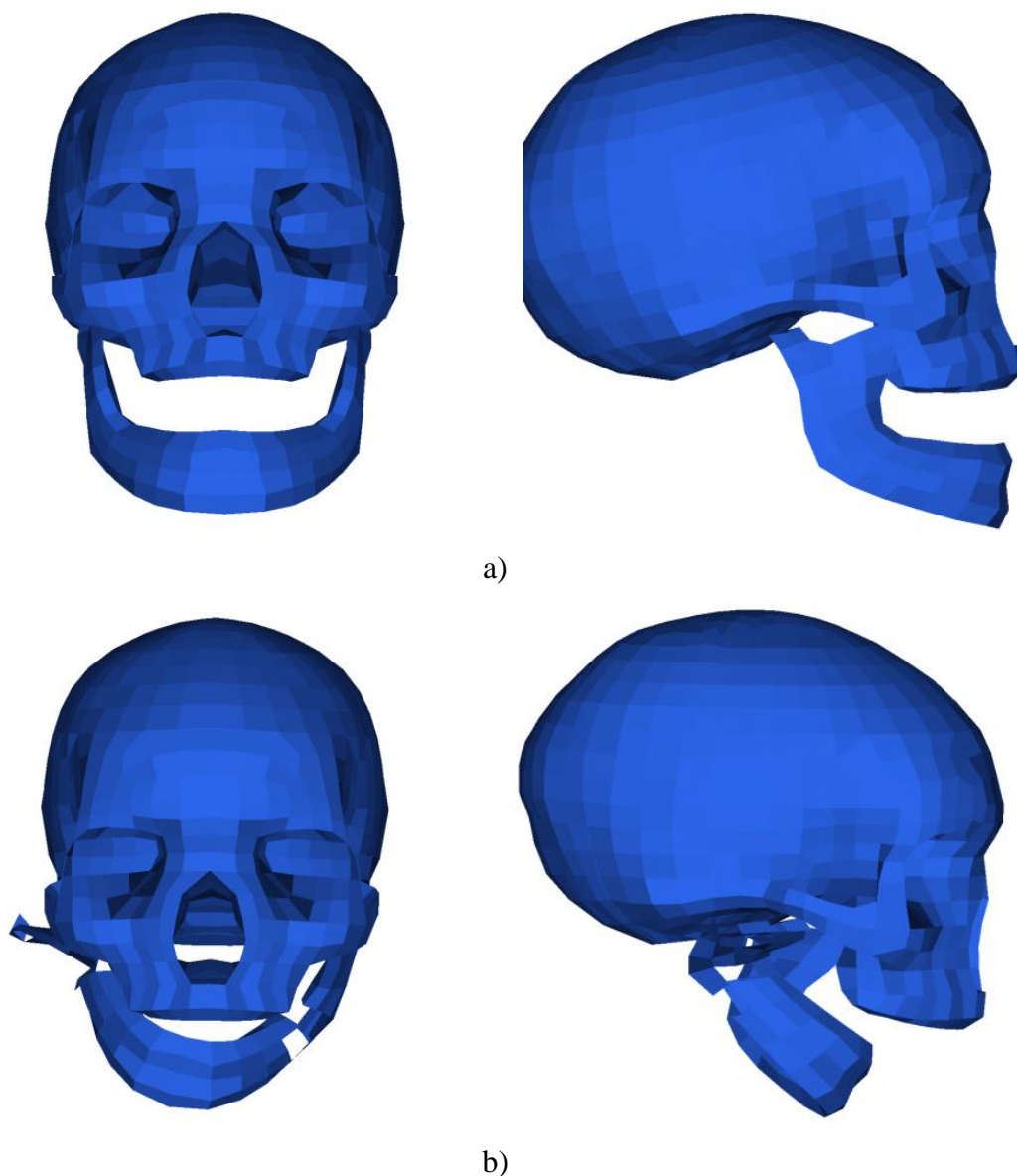
Figure 7-3 – Head impacting the windscreen: skull damage a) before impact; b) after 80ms of impact

A global view of the trunk section points out a high level of compression in the internal organs and viscera as shown in Figure 7-4. Such compression can be better observed in the Figure 7-5, Figure 7-6 and Figure 7-7 showing the deformations of the major critical organs: heart with aorta, liver, and spleen respectively. The imposed deformation of the bonnet can be seen in the Figure 7-4. The deformation in the internal organs can give clues about the probability of trauma in such organ, but no sure about if such trauma will occur.

0ms

15ms

30ms
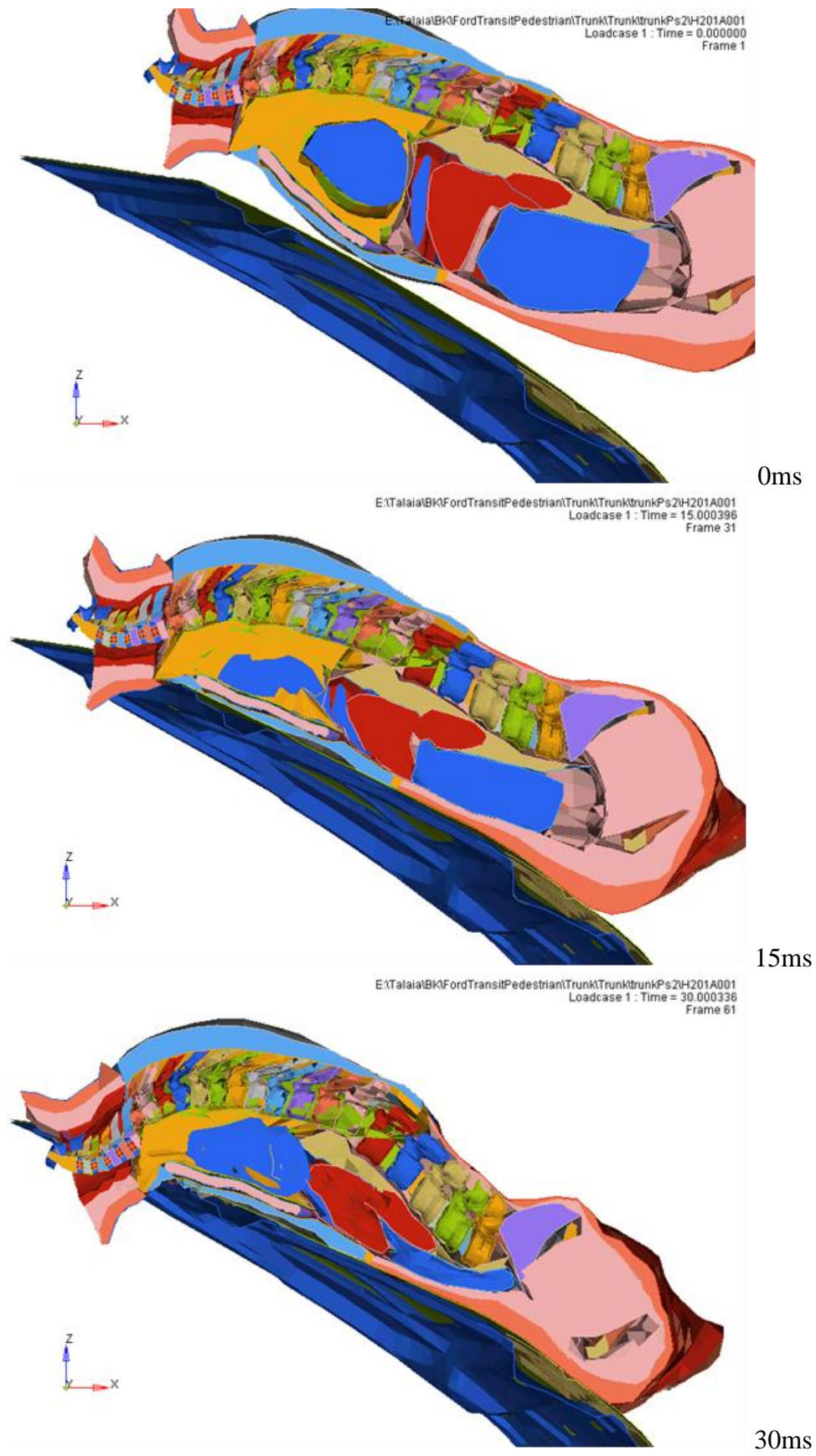
Figure 7-4 – Trunk impacting the bonnet

0ms   15ms   30ms
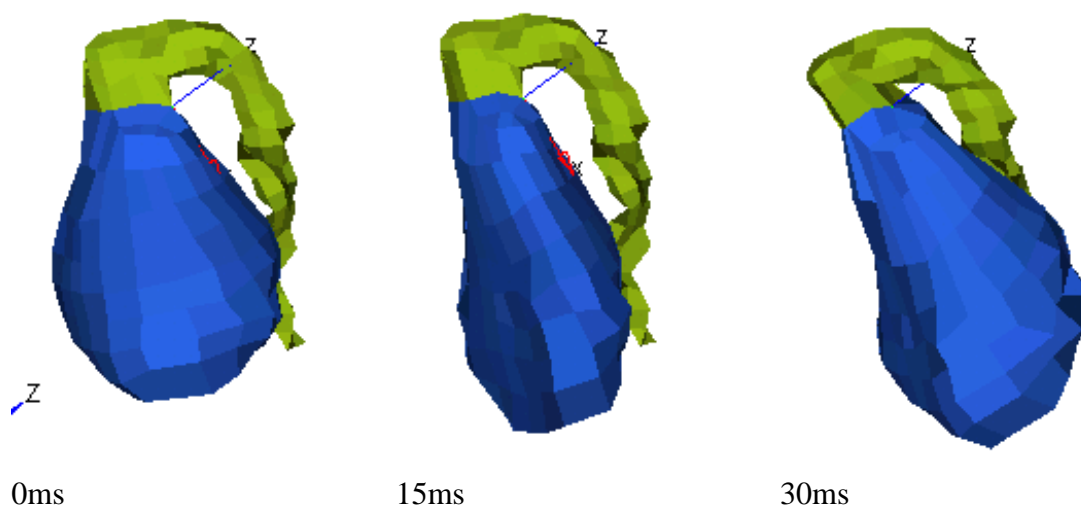
Figure 7-5 – Heart and aorta deformations

0ms   15ms   30ms
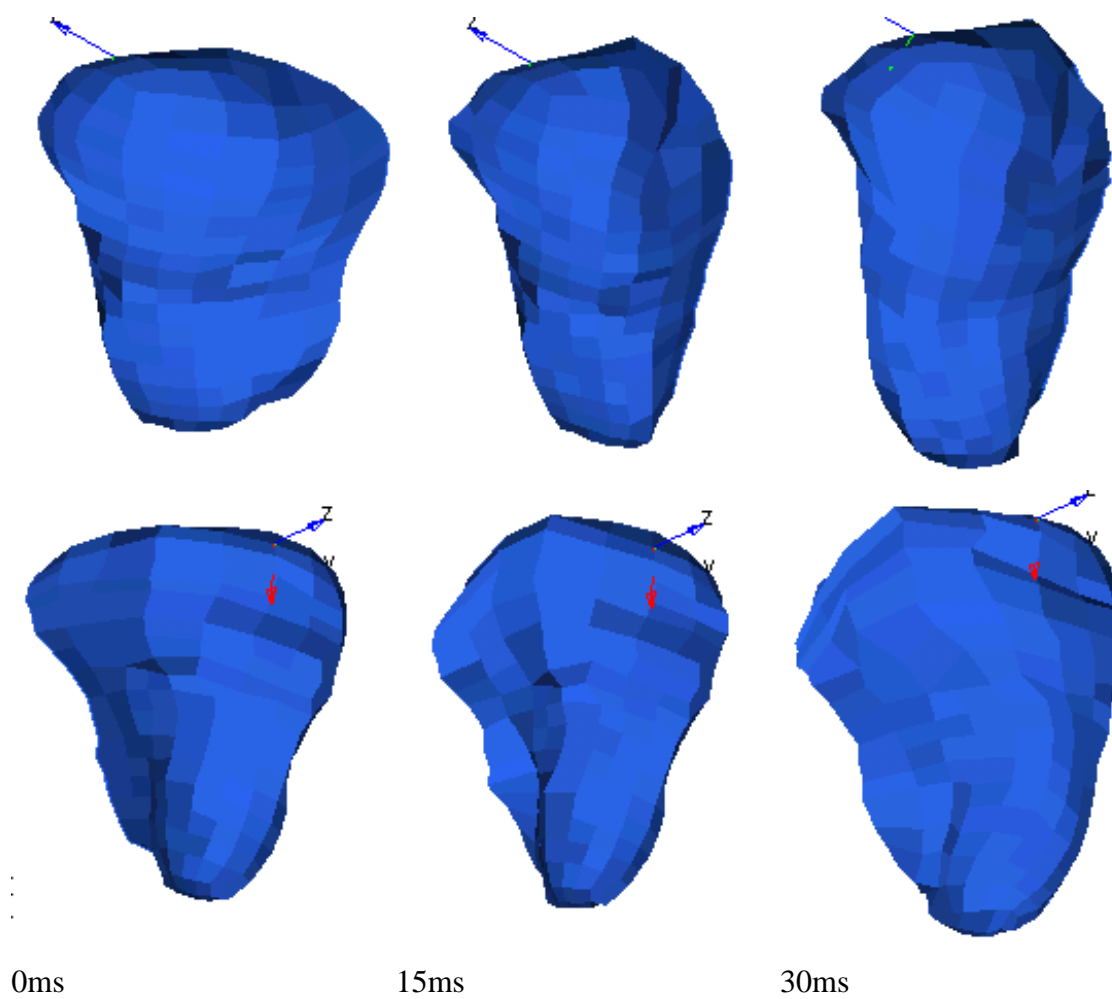
Figure 7-6 – Liver deformation (2 aspects view)

0ms   15ms   30ms
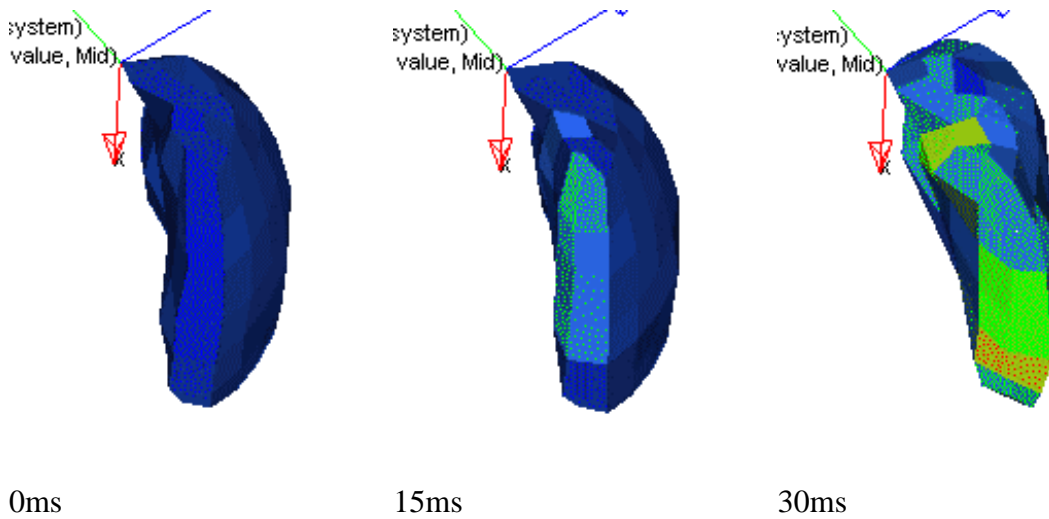
Figure 7-7 – Spleen deformation

The heart compression can indicates a probability of heart arrhythmia occurs, with fatal consequences, like the high displacement of the aorta associated to the section reduction can gives a probability of aorta rupture if in such moment the blood pressure reaches his peak value in aorta.

The high compression of the liver and spleen can cause trauma in such organ, but no direct correlation to the true level of damage.

The damage in the rib cage is better defined, since the literature already has well documented proprieties of the bone. The Figure 7-8 presents the rib cage after impact and the Figure 7-9 presents the rib cage deformed in maximum chest penetration. The number of broken ribs (more than 4 broken ribs each side) and the associated fracture of the sternum can cause ventilation complications for the lack of the rib cage stability. The broken bones are seen as eroded elements (gapes found in the bone continuity).

a)   b)
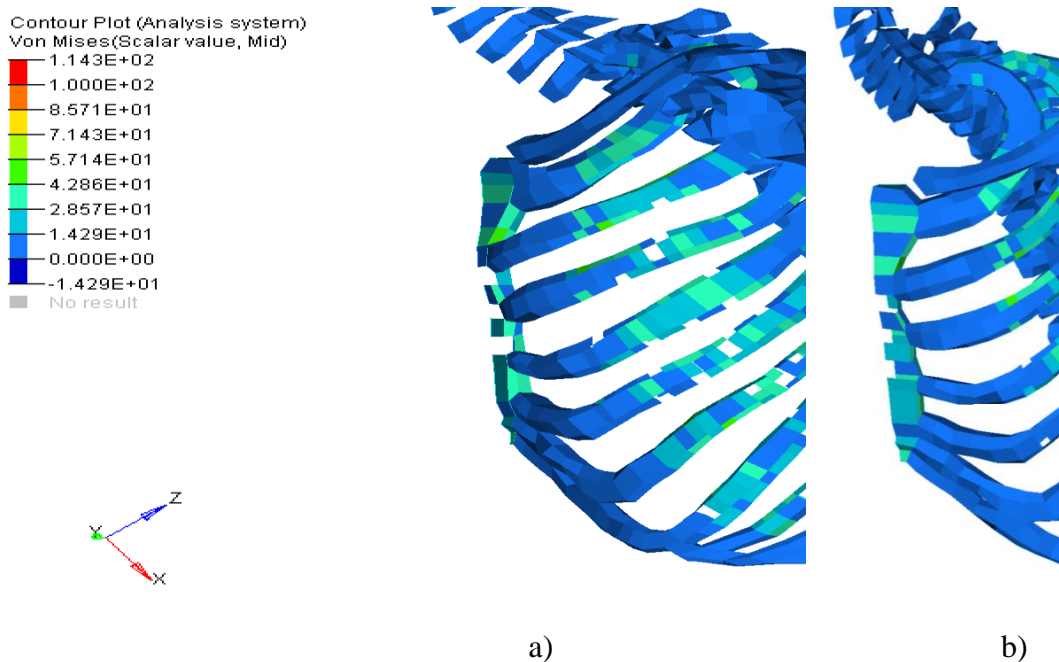
Figure 7-8 – Left section of the rib cage after impact, gradient of von Mises stress for the: a) lateral view; b) frontal-lateral view
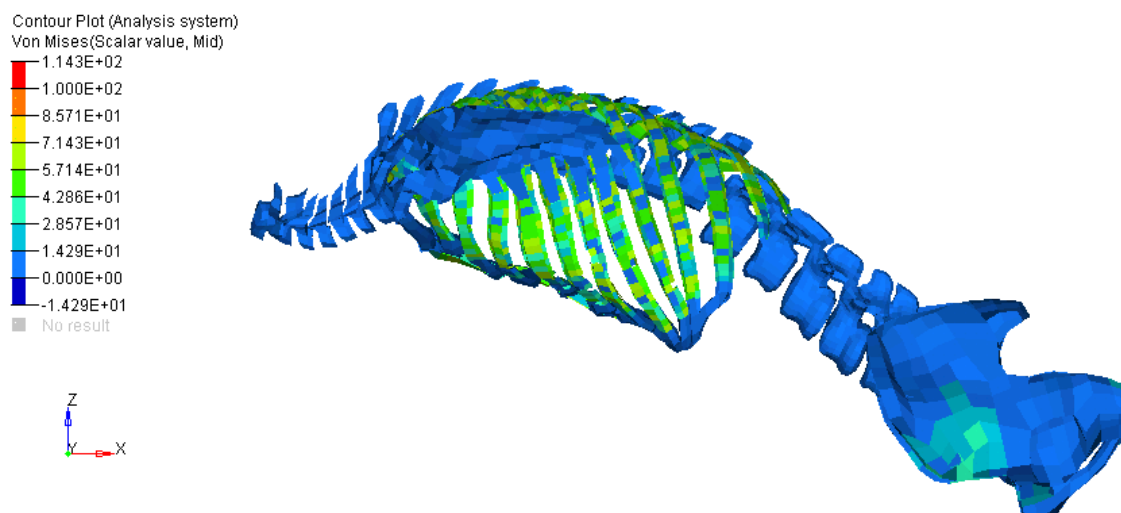
Figure 7-9 – Rib cage in deformation in maximum chest penetration

The number of broken ribs (more than 4 broken ribs each side) and the associated fracture of the sternum can cause ventilation complications for the lack of the rib cage stability.

The high displacement between the last thorax vertebra and the first lumbar vertebra can trigger paraplegia and mal function of some organs. The paraplegia can be triggered too by the high rotation of the sacral bones in relation to the last lumbar vertebra. The high loads imposed to the lumbar section of the spine come mainly from inertial load from the viscera with the lack of rigid support as found in thorax by the rib cage or pelvis by the pelvic bones, causing high shear stress in the lumbar extremities. Such shear stress turns in the miss alignment (see Figure 7-9) along the spine, as can be seen in the axis interruption in the transition between thorax and lumbar vertebras. Same effect from the shear stress gives the high rotation of the pelvic bone, indicating an over-extension in the last lumbar vertebra and the sacral bone.

7.2   Case 2: PTW impact with the van

The modelling approach done in the previous section for the pedestrian accident can be done in the same way to any person involved in any accident, so called vulnerable road user: pedestrian, cyclist and motorcyclist.

For the PTW rider, the work started from the analogue configuration of the pedestrian: a frontal impact. In opposition of the pedestrian crash, now with the PTW a variety of sub-scenarios have been taking in attention, where the variable is the pair of velocities of the colliding vehicles.

The HBM already used and validated in the pedestrian accident simulation have ben configured on a PTW driving position, with all new equivalent contacts defined including the PTW body (Figure 7-10). The van was driven in velocity with a fix deceleration of 0.8g in all cases. The contact between the front tire and the opposite vehicle in opposition of the tire model used with the floor, was a CAD contact to performance increase.
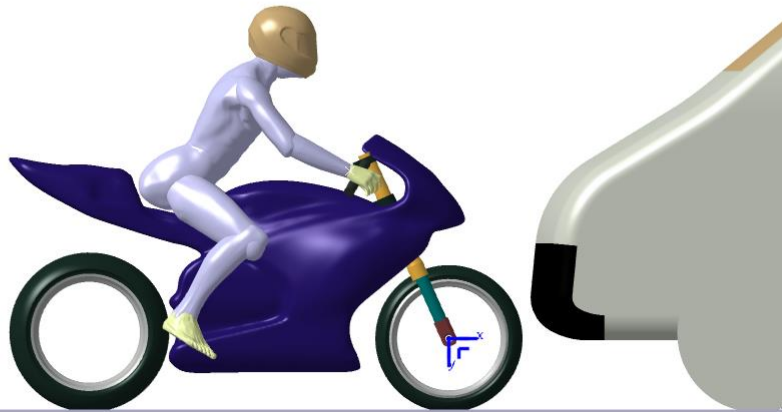
Figure 7-10 – Initial configuration for frontal impact between PTW and Van

The variation of speed in the Van was driven, neglecting the possible rebound of this vehicle against the PTW opposition. The suspension was also neglected. This two approximations are acceptable from the difference of mass between the van and the pair PTW plus rider.

In the Figure 7-11 (double page) is illustrated the configuration for the several pairs of velocities for the time 50ms and 100ms after first impact. The Table 7-1 shoes the respective HIC and max(g) values for the main impact and the secondary impact.
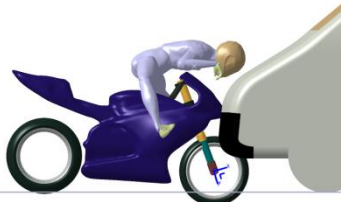
Table 7-1 – HIC15* and max(*g*)** values for the several initial velocities for the main and secondary impact

Velocity (*kph*)	Main Impact (with vehicle)		Secondary impact (with floor)	
PTW-van	HIC15	max(*g*)	HIC15	max(*g*)
48-0	1068	148	14	29
70-0	2339	339	40	82
70-50	9512	786	987	370
30-50	3397	410	484	478
30-30	1491	272	361	175
50-30	3076	430	509	341
70-30	6998	605	410	453
30-70	6967	637	4327	673
50-70	9362	803	174	71

* HIC threshold: green lower than 750, yellow until 1000, and red for greater values.
** max(*g*) threshold: green lower than 250, yellow until 350, and red for greater values.

	t = 50ms	t = 100ms
Van = 0kph PTW = 48kph		
Van = 0kph PTW = 70kph		
Van = 50kph PTW = 70kph		
Van = 50kph PTW = 30kph		
Van = 30kph PTW = 30kph		

	t = 50ms	t = 100ms
Van = 30kph PTW = 50kph		
Van = 30kph PTW = 70kph		
Van = 70kph PTW = 30kph		
Van = 70kph PTW = 50kph		
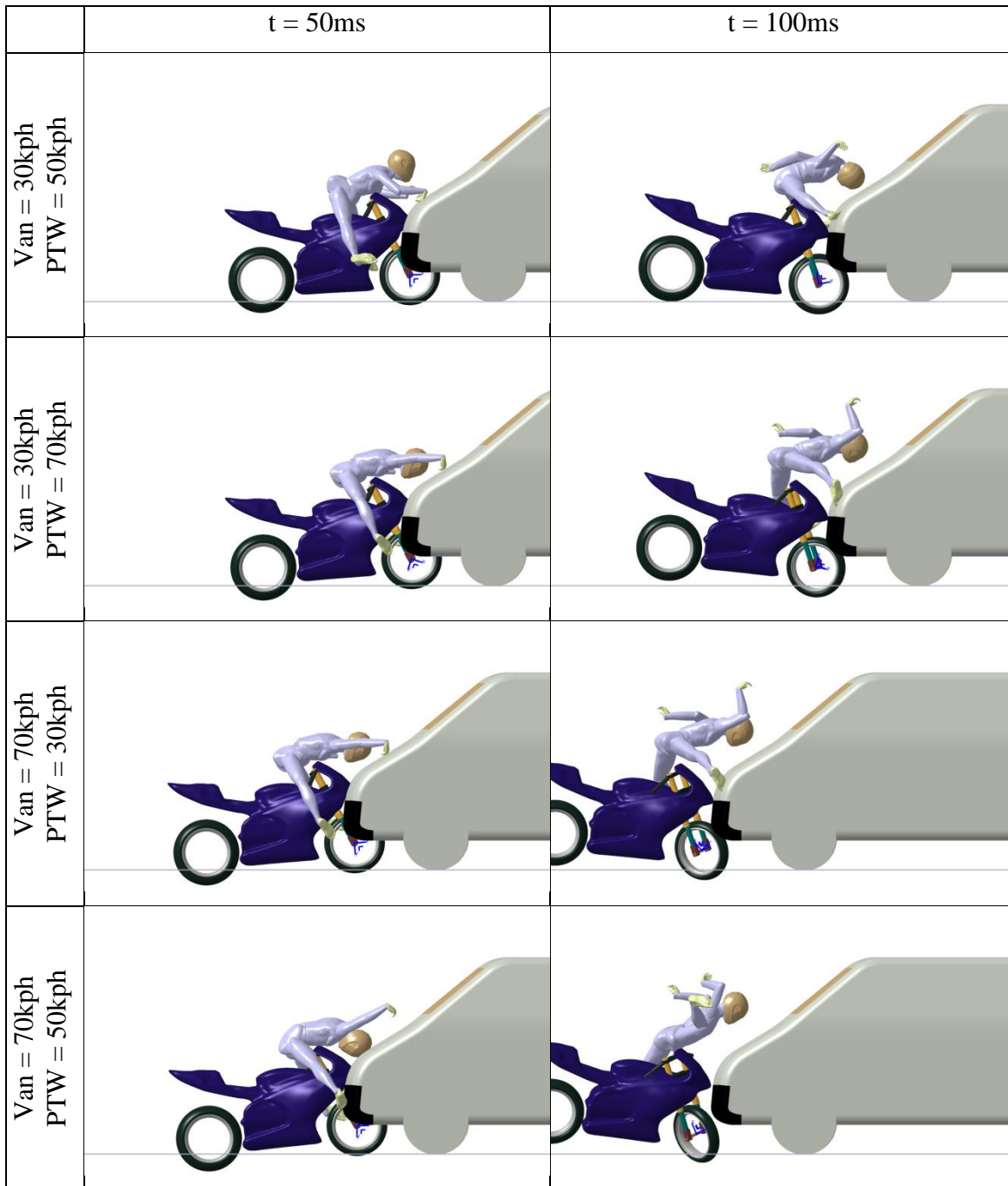
Figure 7-11 – Position for frontal impact between PTW and van for the different impact velocities for time 50ms and 100ms

The first aspect anyone detects is the energy difference between these two types of vehicles. The difference of velocities and energy will have a major role in the driver trajectory, but the differences between HIC values when we switch the vehicles velocities gives similar values, only being noticed a bigger head acceleration peak when the van impacts quickly.

We can observe that such impact configuration can initiate permanent damage in the brain for a speed pair of 30kph with 30kph with HIC15 equal to 1491. The lower HIC15 equal to 361 for the road impact foresees no major damage comparing to the previous one. We should maintain the assumption that the helmet remains in its position, and the first impact

have not reduced the ability of the helmet to absorb the second impact energy. The HIC value for the second impact is very sensitive concerning the way that the body "lands" in the ground. If the head impacts firstly the floor than e.g. the shoulders, the head will have a bigger deceleration peak. The fact that the head comes later in contact with the floor can be good in the moment, but it is not a mandatory condition for a better recover since the appearance of other minor traumas can cause short to middle term clinical complications. A lower HIC value in the head can come from high energy dissipation in the neck, something that can be fatal to the driver.

Comparing the HIC value for the pedestrian and the PTW driver, it is easy to see the importance of the helmet. Notice that in case of the helmet release after the first impact, the HIC value of the secondary impact will be much greater that can cause major injuries.

The data that provide the values presented in the Table 7-1 are plotted in the Figure 7-12 for the time interval that contains the primary crash (impact between the PTW and the vehicle, during the time from 0ms until 150ms), and Figure 7-13 for the time interval that contains the secondary crash (impact between the driver and the floor, after flying trajectory, time from 1s).
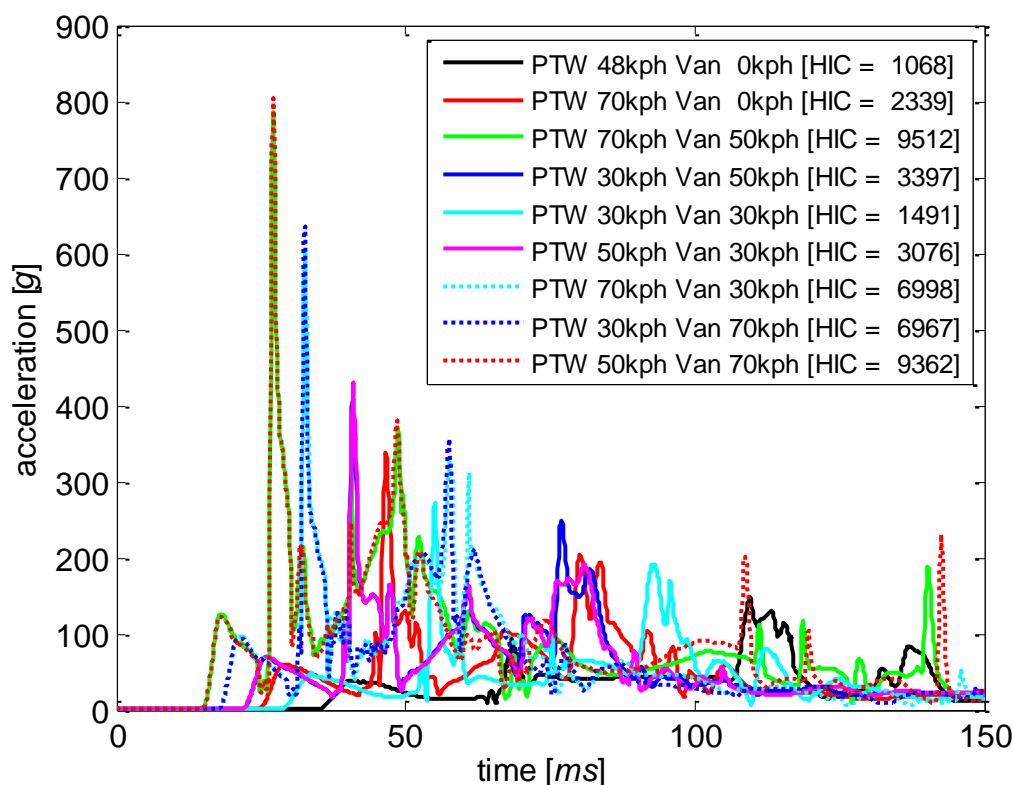
Figure 7-12 – Acceleration along the time for the first head impact (with vehicle) and respective HIC

In the Figure 7-12, it is recognized the same acceleration pattern for the impact velocities between the PTW and the van for [in kph]: 50-70 with 70-50, 30-70 with 70-30 and 30-50 with 50-30. This pattern is confirmed by their similar HIC values: 9362 with 9512, 6967 with 6998, and 3397 with 3076 respectively. The difference comes when the van is the fastest vehicle, the max(g) is slightly higher.

In the interval from 50ms until 100ms is notorious that each case starts to follow one independent trend, and the flying period starts in this interval. The flying time comes from the body projection after impacting the vehicle front. The rebound path will give different

accelerations in the various body parts, meaning that the head are subjected to different accelerations.

The Figure 7-13 shows also 2 cases (between all the other cases) when the head with helmet is jumping in the floor in similar way: PTW in 70kph and van in 50kph, and then PTW in 30kph and van in 70kph. The observed fast rebound will cause a high HIC value, but less high values for the HIC15 are present after and/or before the time interval for the computed HIC15, since these parameter only considers a time frame less or equal to 15ms. If the acceleration peaks are in a time frame bigger than 15ms, only the worst scenario (bigger HIC) are presented, but the others values of HIC for the other peaks can be in the same order of magnitude. These loads after the high values observed in the impact with the windscreen can amplify the trauma caused there.
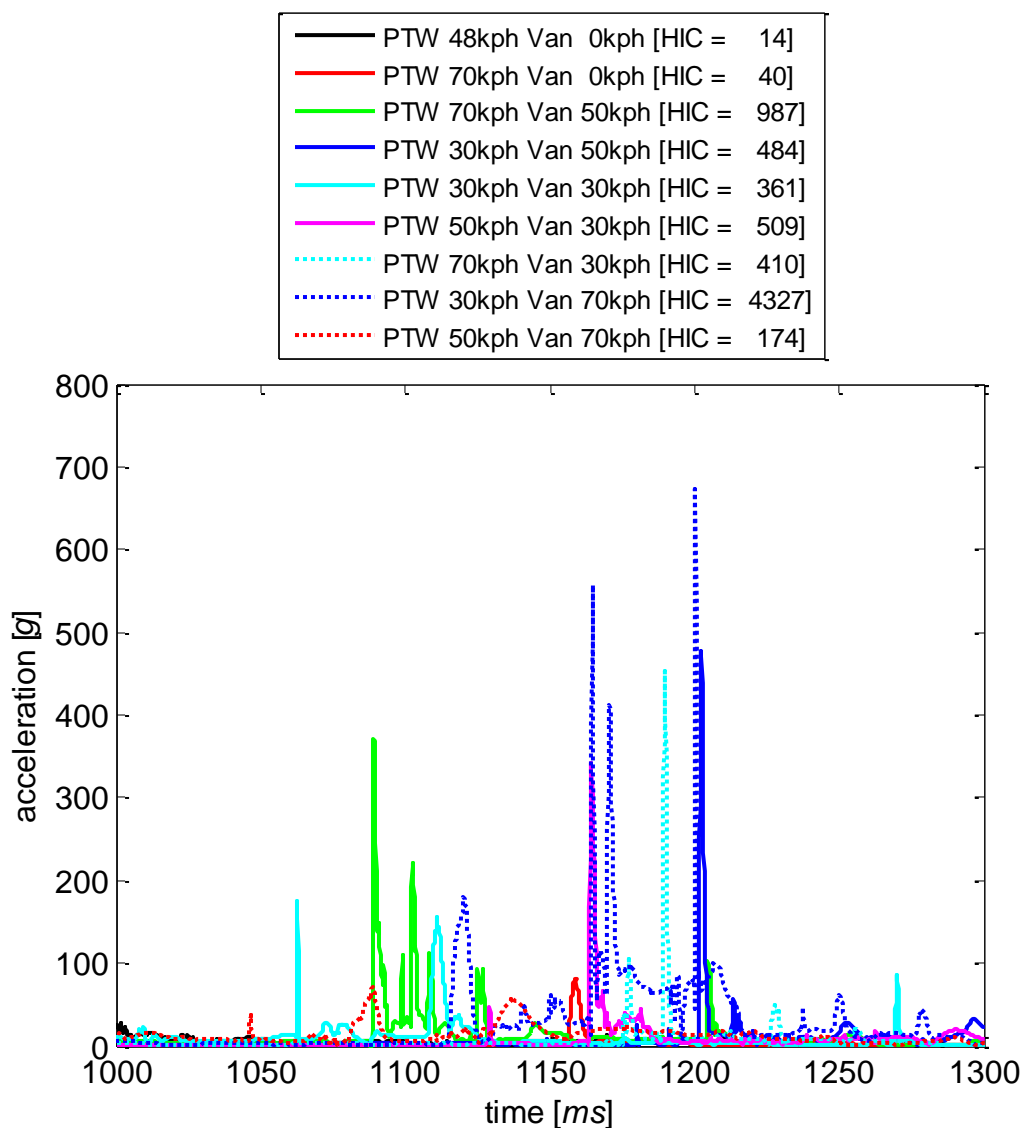
Figure 7-13 – Acceleration along the time for secondary impact

7.3   Case 3: PTW impact – Van or State

A frontal crash between a PTW and another vehicle as not the Van is simulated to benchmark the models in accident scenario. The scenario chosen is one frontal impact (Figure 7-14), both vehicles with an impact speeding of 30*kph*, with the other braking with a deceleration of 0.8*g*. The other vehicle is firstly a Van, and then, replaced by one estate. The different frontal geometry will have a direct impact in the consequences during the accident.
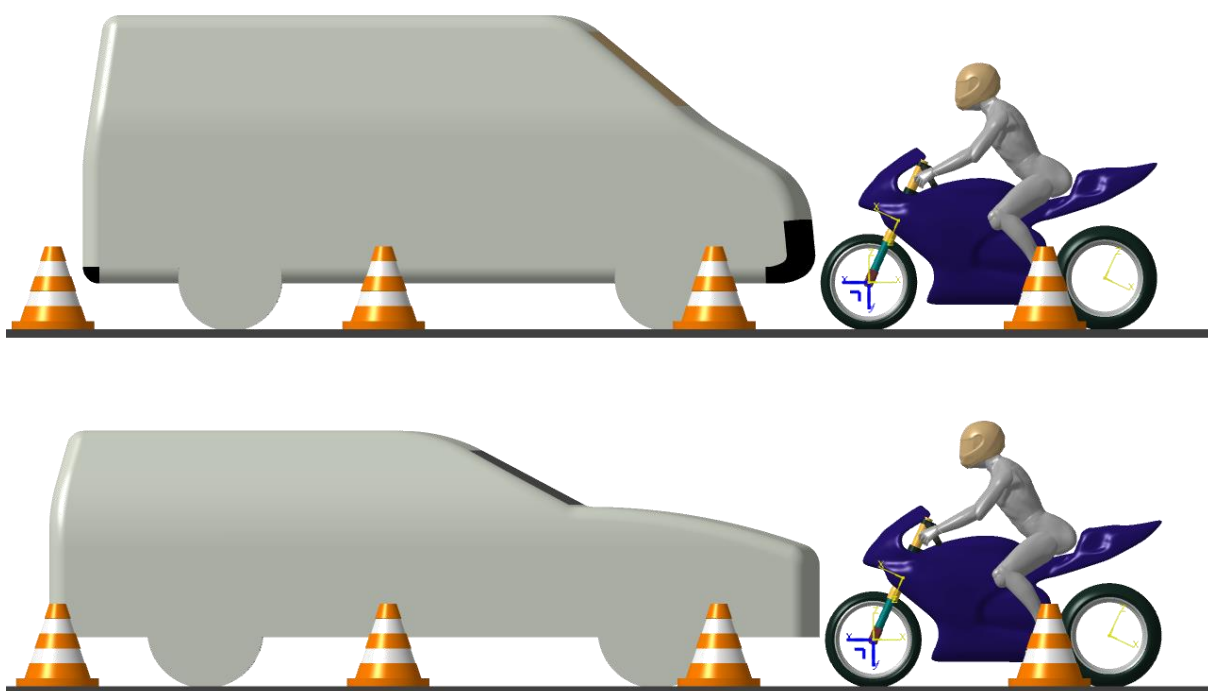
Figure 7-14 – pre-crash configuration for frontal impact other vehicle with a PTW

It is clear that the different frontal vehicle designs will be translated in different results (Figure 7-15). It is clear that the more aggressive van front will man a direct rebound of the PTW driver to the front, in opposition of what happens in the state situation. Such difference can have a heavy impact in the consequences concerning what happens when the PTW driver gets to the floor or to an obstacle in the road (Table 7-2)

Table 7-2 – HIC15 values

	van	sate
HIC 1st impact	5831	6800
HIC floor impact	6007	293
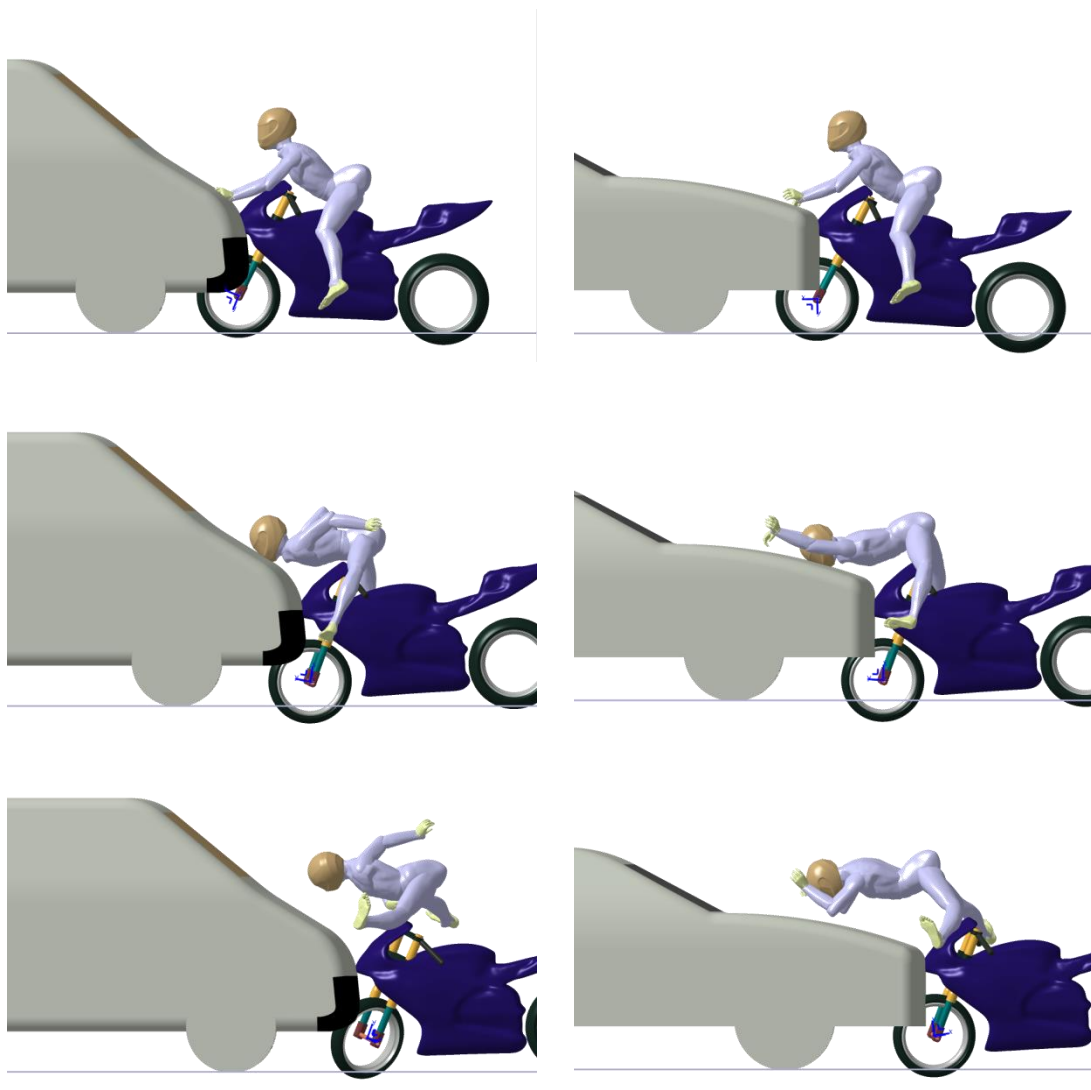
Figure 7-15 – Crash frames for 50, 100 and 150ms for the impact between PTW and other vehicle (van in right, state in left)

7.3.1   Injury assessment

After the MB simulation, the injury assessment using HUMOS2 was performed with focus to the head. A FEM of a helmet validated in LS-DYNA was converted and re-validated in RADIOSS (work done by the partner ALTAIR France, in the scope of the project MYMOSA) was used. Also parts of the vehicle front was used.

Another propose in this compilation was the addition of other sub-scenario: with or without helmet (same initial conditions to the Head in the FEM).

A third sub-scenario was also included, a not centered impact between the PTW and the van. This is a real scenario, documented by a report (confidential). In this a van similar to ours catches a PTW in the opposite direction, with speeds similar to ours also. The driver impacts in same region that seen in our model, but since not centered, the helmet impacts the base of the A pillar, being projected diagonally to near terrain close to the road. The driver was found without helmet, but proved that the helmet was in use in the first impacts. Was not found a reasonable explanation how the helmet gets out from the head between the van and floor impact (one possible explanation will be presented).

The two simulated scenarios gives an impact between the helmet and the vehicle bonnet. Being the helmet load in a direction that is not favorable to it, the bonnet itself is already a structure that is being optimized to reduce injuries in pedestrians (an unprotect head). Such bonnet optimization have implied a reduction of stiffness, a major distance of the anchorage points, greater gaps between the bonnet and structural components (high rigidity). Such optimization can also reduce the negativity as the cross fire (base of the wind shield and wipers support. The pillar A (windshield laterals), pillar B (middle pillar between front and rear door, or pillar C (or complex, structure of one or several rear pillars). So pillar by their nature shown aggressively in terms of stiffness in the impacted person point of view.

Taking in account the metal elasticity and plasticity, when occurs contact between the head and the bonnet (with or without helmet), is notorious the von Mises stress in the several scenarios. The Figure 7-16 and the Figure 7-18 shows respectively the von Mises stress field for all 6 scenarios: with and without helmet in a state, in a van and in the van A pillar. The Table 7-3 points the Maximum equivalent von Mises stress in MPa seen in the vehicle impacted component.

Table 7-3 – Maximum equivalent von Mises stress (MPa) in the vehicle

	State	Van	A Pillar, Van
With helmet	741	548	941
Without helmet	674	728	1087

The Figure 7-18 the cross section of the head and neck with or without helmet when impacting the vehicle. It's visible in the several images on the figure that the brain have a reasonable amount of displacement and deformation. The high level of deformation of the helmet shows that it as a safety equipment is doing for what it was designed. The helmet also rotates in relation to the head in both situations of impact with the van. Such rotation associated to the seen deformation, gives a gap to the escape of the helmet (the shim strap is in all models FEM with helmet)

The Figure 7-19 summarizes the equivalent von Mises stress in the cranium. Is notorious the reduction of magnitude that the use of helmet can produce. Notice that for the A pillar scenario, the helmet avoids the considerable skull fracture observed in the without helmet scenario. From the report photos of the comparable accident, the face appears relatively intact, pointing that if fracture have happened, was not the severity observed in the case without helmet, pointing that the driver was using helmet in such instant (corroborated by a deformation and reciprocal marks in the helmet and in the vehicle A pillar). The fact of the driver was dead after paramedics intervention in loco, only give us the global severity of the accident, can be the dead triggered by the high brain displacement in the first impact, head impact on the secondary impact (as shown in the MB simulation) or others as neck or trunk complications.
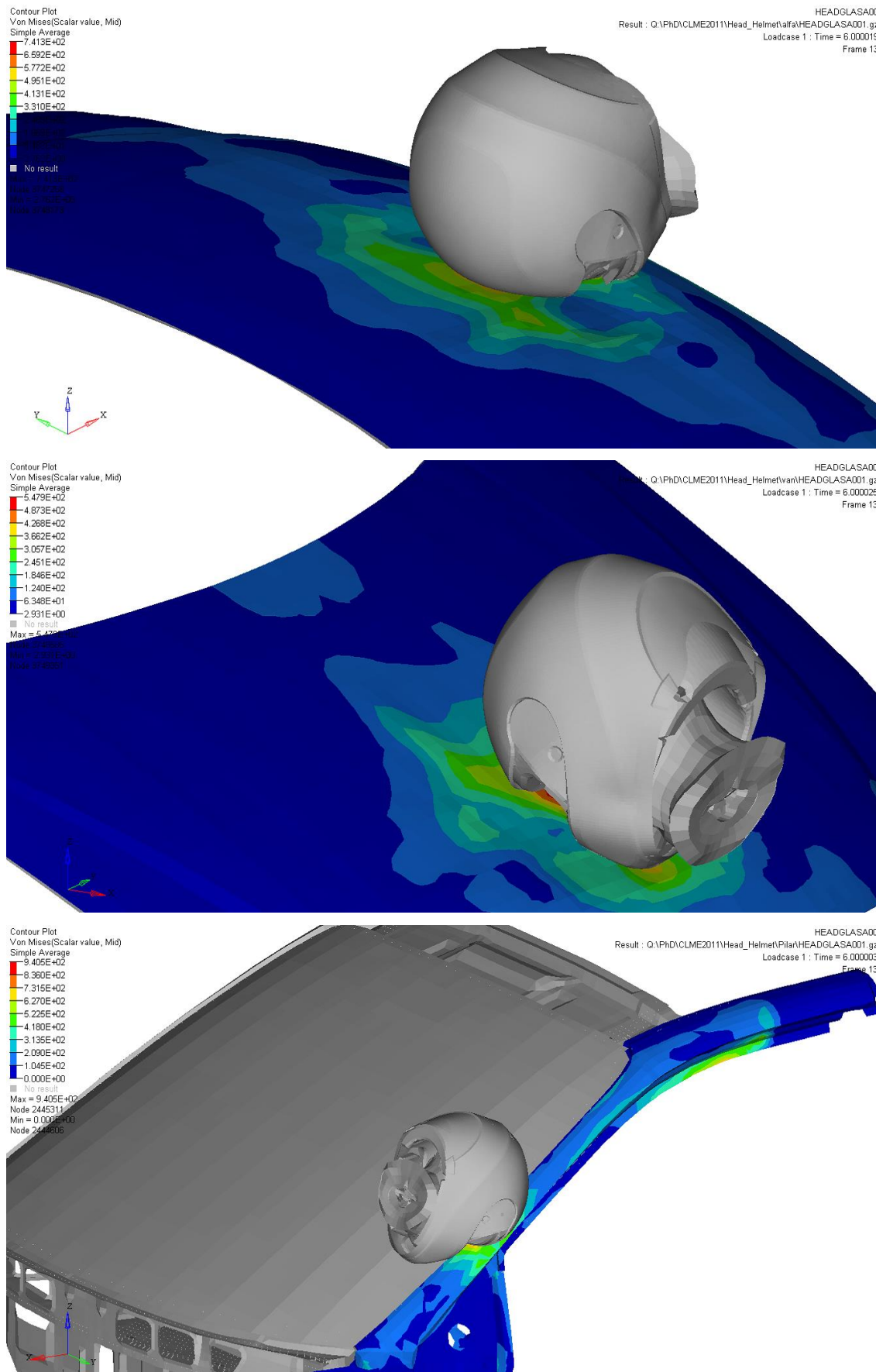
Figure 7-16 – Stress field where the helmet impacts: State, Van and the A pillar (all in peek value)
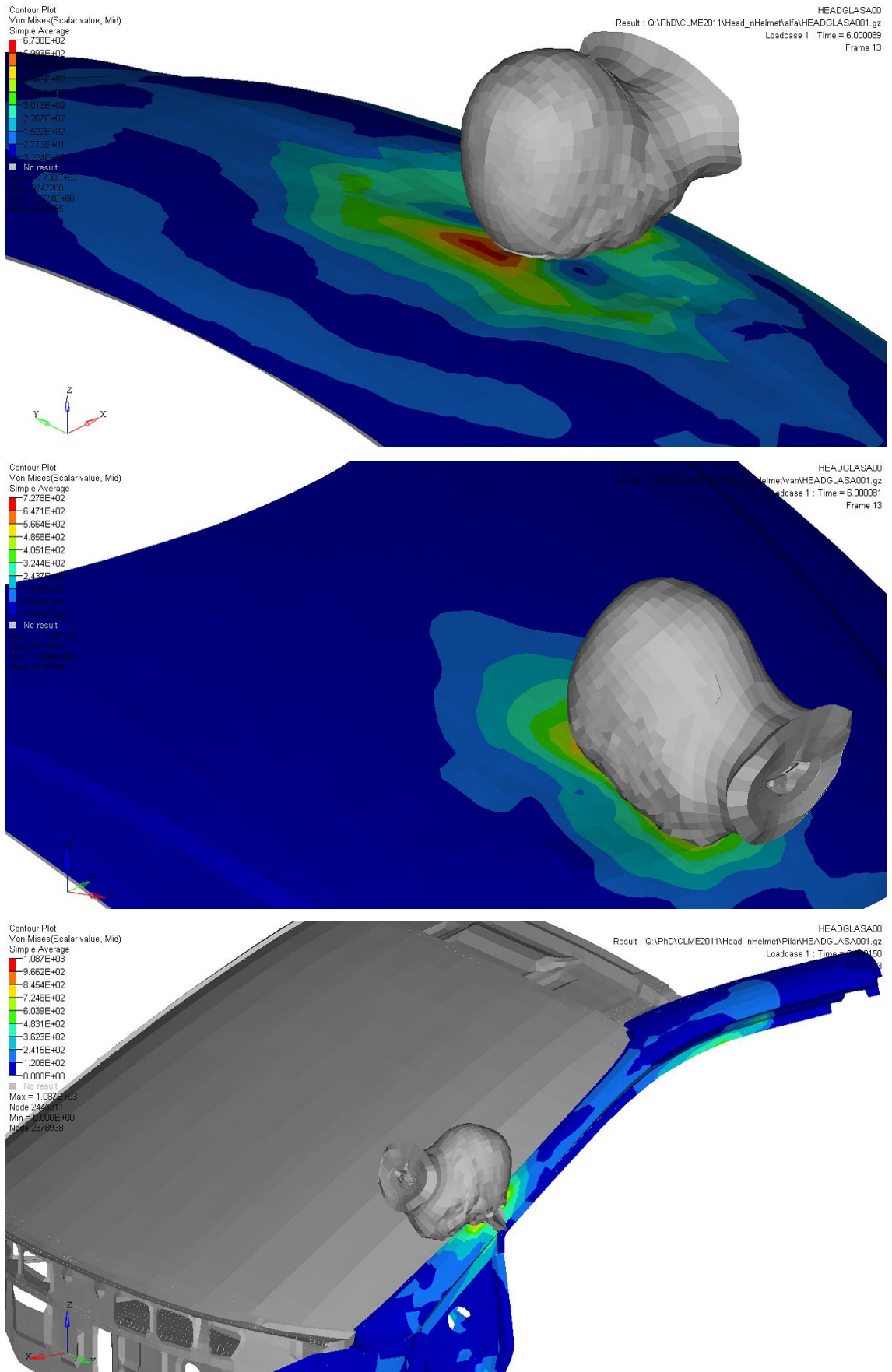
Figure 7-17 – Stress field where the head impacts: State, Van and the A pillar (all in peek value)

	With helmet	Without helmet
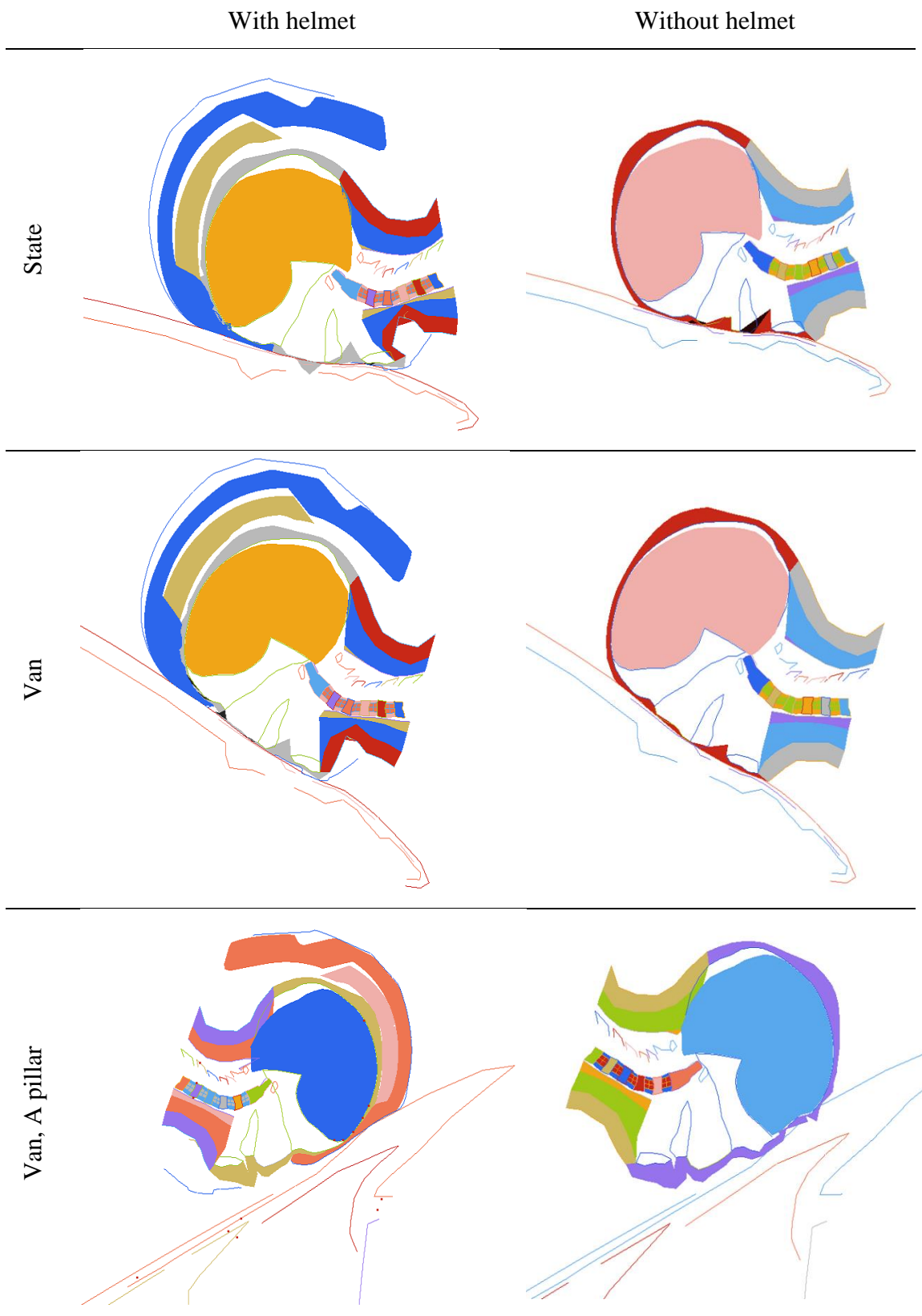
Figure 7-18 –Section of the head and neck with or without helmet for the several impact scenarios

With helmet   Without helmet

6.0ms – 39MP   4.5ms – 37MPa

7.0ms – 20MPa   7.5ms – 52MPa

5.5ms – 45MPa   7.5ms – 74MPa
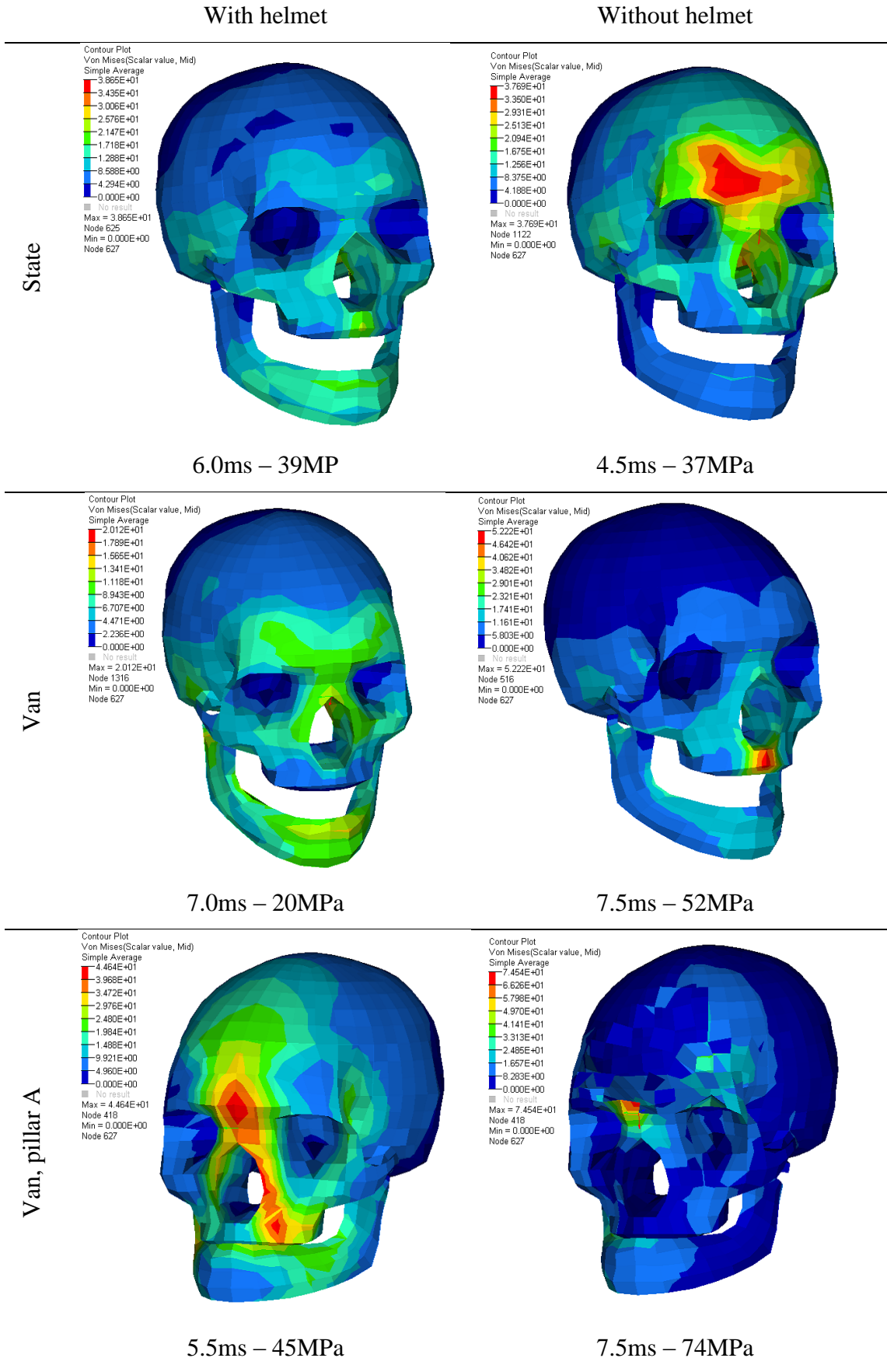
Figure 7-19 – Section of the head and neck with or without helmet for the several impact scenarios

8
Conclusions

The needs to understand the behaviour of the human body in the position of a driver in a PTW is motivated by the investigation of some problems concerning accidents and by searching solutions for the safety improvement.

It was proposed as guidelines the following points:

- Getting formation in the fields of multibody dynamics, anatomy and physiology, trauma, and accidentology applied to motorcyclists;
- Implement in a commercial software one multibody human dummy model for crash simulation,;
- Compute injury criteria's from the multibody human model;
- Analyze the effect of the impact in the human body in the physiology point of view by means of finite element analysis.
- Create a protocol to fast simulate a full crash scenario, with detail analysis in critical body parts.

Can be concluded that all this points have been fulfilled.

A high spread analysis of the motivation, how humans are modelled in similar conditions, the mathematical background and the anatomy, physiology and trauma have given a broad copter view of the disciplines involved in the full understand of the dynamics in a crash involving a PTW and his rider. This holistic approach have resulted in a great investment in training in all this spread range of areas. In fact, areas as human behaviour and theory colour have appeared as having also relevance in the crash occurrence or possible avoidance.

It's proposed a new approach to study and analyse the crash involving motorcyclists. It's proposed also the addition of the local after analysis of impact using more detailed FEM to see not only the injury indicators computed, but also see what will happens in the tissue level. And is proposed also the full path with a low computing cost, so can be easily applicable in terrain with a laptop or desk computer and reduce waiting time

The presented work proposes the multi-body model that is able to analyse the motion of a rider and a PTW in a crash situation. Such capability associated to the detailed injury assessment by means of FEM analysis gives a new proposal to better understand the consequences of the PTW drivers' exposition in crash scenarios.

The approach adopted to develop the motorcyclist human model suffered some limitations from some compromises assumed along the development of the project MYMOSA where this work was integrated. One of major conclusions is that a fresh approach is need to analyse any vulnerable road user, not matter if pedestrian, cyclist or motorcyclist. In fact, the proposed model and approach is more than a motorcyclist biomedical model, can be easily adopted as a more embracing vulnerable road user biomedical model. The limitations can be seen as a plus as the model is easier to integrate and be used in a software that is standard in the industry, implying low learning curves. Also fulfil the needs of integration inside the project work.

The added degrees of freedom in the MBM have means that we don't want to follow a "copy" or adaptation of a dummy like the hybrid III, but in opposition, start from sketch and rethink the all approach of the analysis of the accident simulation for vulnerable road users. This approach given some advantages, but points the need of future work to better modelling the articulations and to implement activation also.

It was shown for example that the classic single body multilayer head use is not satisfactory after the occurrence of the first direct impact. The work points the need of a

more elaborate head model, but still conceptual simple to be easily transposed to a real dummy head.

The crash analysis adopting a pipeline philosophy have proved also a more realistic way to see the consequences of the impacts. Some CAE platforms already provide full co-simulation support allowing FEM and MB coupling, and that will be soon an easily reality with the constant increase of computational power. But the pure MB analysis followed by detailed FEM analysis in critical parts and time-frames gives a faster and easy way to correlate directly the numeric injury indicators with the possible causes in the person. It will be from great interest if in future work this methodology can be applied to real accidents, but with the possibility to compare results with the legal medicine also. This approach means also that with graphical interface, a technician with minimum training and portable computer resources an easily full simulate a scenario and his assumptions variations in the terrain in a short period of time.

The presented crash scenarios have pointed some relevant points in the motorcyclist point of view: vehicle aggressiveness and protection equipment. A vehicle with a front more vertical is much more aggressive in a crash episode, not so much in some cases in the first impact, but also in the way that the person is projected meaning a much more violent second impact. The softness of the vehicles having pedestrians in mind can also save cyclists and motorcyclists. The helmet as safety equipment have a crucial part in the injury risk, but some aspects in this equipment are in need of further improvement also.

As future work, a more complex shoulder joint should be developed. The models can be also be provided of some type of activation, but this topic is still dependent of full parallel processing capability in the adopted software. As plus for the software, the model is already semi-parametric, and can easily be fully integrated and fully parametric with the aid of an advanced programmer.

The FEM analysis adopted proved to be a power tool to better understand the trauma mechanisms, but improvement should be considered also. Some international consortiums are investing in this topic, some of them integrating the UWB. New more biofidelic models will help to get better understand of the trauma mechanisms in regions that the current models have limitations (e.g. neck).

The output of this work in line to others done in the scope of MYMOSA should be for all the involved team a start point to improve safety and understand of the motorcyclists in particular and all road users inclusive.

To summarize our main goals for a motorcyclist biomechanical model, we have: the model to develop in this work as main function should be able to handle the freedom seen in a crash where a motorcyclist is present … should have also the ability to handle impacts in any arbitrary direction; the use of a multibody human model to see what happens during the all crash … and access to one full FEM human body… sections to see what will occurs in the human body when impact occurs; and how one impact triggers damage in the body tissues should be a must to better understand the involved mechanisms. As final remark, we achieved a methodology that can gives a good understand of the accident mechanisms of a motorcyclist, and also the other two fragile road users: cyclists and pedestrians. The multibody model react and behaves in a qualitative way as found in real accident reports. The parameters given are used to define the conditions to a more detailed FEM model, given detailed information and understand of what or where the body is more solicited. Concerning the possibility to access then protective equipment, can also and was shown how advantageous is it.

A1 Appendix 1 – Software implementation

The described multi-body model was implemented within the MATLAB code (version 2007a). The numerical simulations were performed using the integration function `ode113` with a maximal time step of 2 ms, a relative error of 10^{-4} and an absolute error of 10^{-6}.

The code can be structured by three parts: data preparation, simulation and visualization.

A1.1 Data preparation

The key information in the data preparation is the proprieties of the system and how this information is inserted. We must have a minimum of 5 variables: `initialC`, `mass`, `K`, `B` and `jointD`.

`initialC`: the initial position of each body: Cartesians coordinates and rotation of the each centre of mass, in SI units. The parameters are inserted in a single row, body by body, giving a total of 30 parameters (3 parameters for each body by 10 bodies).

`mass`: the mass properties of all bodies. It contains the mass properties of each body (mass and inertial moment), body by body, in a total of 20 parameters (1 mass and 1 inertial moment for each of 10 bodies).

`K`: the stiffness vector of the spring-damper in each joint (8 parameters). In the future versions, it will be updated to a structure variable of size 8, allowing non-linear stiffness.

`B`: the damping vector of the spring-damper in each joint (8 parameters). In the future versions, it will be updated to a structure variable of size 8, allowing non-linear damping.

`jointD`: the structure variable with all the local coordinates of the joints. The structure of the variable follows the next example (data according with Table A1-5):

```
% Joint distances - Rear suspension
jointD.l_02_01 = -0.314; % Back suspension - Rear whell
jointD.l_02_05 =  0.400; % Rear suspension - Body

% Joint distances - Suspension
jointD.l_04_03 =  0.150; % Suspension - Front wheel
jointD.l_04_05 = -0.400; % Suspension - Body

% Joint distances - Body
jointD.l_05_02_x = -0.00337; % Body - Rear suspension
jointD.l_05_02_y = -0.19297; % Body - Rear suspension
jointD.l_05_04_x =  0.61054; % Main Body - Fork
jointD.l_05_04_y =  0.22222; % Main Body - Fork
jointD.l_05_04_x0=  0;
jointD.l_05_04_y0=  0;
jointD.l_05_06_x = -0.13590; % Body - Trunk
jointD.l_05_06_y =  0.32254; % Body - Trunk
jointD.l_05_07_x = 0.49731; % Body - Lower Arm
jointD.l_05_07_y = 0.53330; % Body - Lower Arm

% Joint distances - Trunk
jointD.l_06_05 =  0.229; % Trunk - Main Body
jointD.l_06_09 = -0.293; % Trunk - Neck
jointD.l_06_08_x = -0.23719; % Trunk - Upper arm
jointD.l_06_08_y =  0.07061; % Trunk - Upper arm

% Joint distances - Lower Arm
jointD.l_07_05 =  0.171; % Lower Arm - Body
jointD.l_07_08 = -0.105; % Lower Arm - Upper Arm

% Joint distances - Upper arm
jointD.l_08_07 =  0.167; % Upper arm - Lower Arm
jointD.l_08_06 = -0.099; % Upper arm - Trunk

% Joint distances - Neck
jointD.l_09_06 =  0.046; % Neck - Trunk
jointD.l_09_10 = -0.073; % Neck - Head

% Joint distances - Head
jointD.l_10_09 = 0.063; % Head - Neck
```

The order of all the bodies is introduced according with the Table A1-1.

Table A1-1– List of bodies and respective number

Body	Body number
Rear wheel	1
Rear suspension	2
Front wheel	3
Suspension (Fork)	4
Frame	5
Trunk	6
Lower arm	7
Upper arm	8
Neck	9
Head	10

The list of the joints follows the Table A1-2.

Table A1-2– List of joints

Body number	Body	Joint
1	Rear wheel	Rear wheel – Rear suspension
2	Rear suspension	Rear suspension – Rear wheel
		Rear suspension – Frame
3	Front wheel	Front wheel – Suspension
4	Suspension	Suspension – Front wheel
		Suspension – Frame
5	Frame	Frame – Rear suspension
		Frame – Suspension
		Frame – Trunk
		Frame – Lower arm
6	Trunk	Trunk – Frame
		Trunk – Upper arm
		Trunk – Neck
7	Lower arm	Lower arm – Frame
		Lower arm – Upper arm
8	Upper arm	Upper arm – Lower arm
		Upper arm – Trunk
9	Neck	Neck – Trunk
		Neck – Head
10	Head	Head – Neck

A1.1.1 Variable `initialC`

These variables have all the coordinates of all bodies. To describe one body in planar space, 3 parameters are needed: 2 for the centre position and 1 for the rotation.

To describe n bodies, we will get a total of $3 \times n$ parameters. The parameters are introduced using the expression

$$initialC = \begin{bmatrix} R_x^1 & R_y^1 & \theta^1 & R_x^2 & R_y^2 & \theta^2 & \cdots & R_x^n & R_y^n & \theta^n \end{bmatrix}. \qquad \text{(A1-1)}$$

A1.1.2 Optional initial variables

The previous variables are needed to run the simulation, but the user can change some of the simulation parameters too. The most obvious are the time simulation (the default time is $1s$), or the sampling time (the default value as a frequency of $25Hz$). Other parameters are concerning integration parameters: maximum time step, relative and absolute tolerance.

The list of optional variables is: `T_total`, `frameT`, `maxStep`, `relTol`, and `absTol`.

`T_total`: the total simulated time, in seconds.

`frameT`: the sampling time, in seconds.

`maxStep`: the maximum time step, in seconds, for the integration (default value is $5 \times 10^{-3} s$).

`relTol`: relative tolerance, without dimensions, for the integration (default value is 10^{-4}).

`absTol`: absolute tolerance, without dimensions, for the integration (default value is 10^{-6}).

The variables `maxStep`, `relTol`, and `absTol` must be set together, since when the user prescribe one, must describe too the others two for the simulation function.

A1.2 Simulation

After the user collects all the data needed for the simulation, everything must be set to start the simulation. The key function is the `PTW2D`:

```
function [T,Y] = ...
    PTW2D (initialC, mass, K, B, jointD, T_total, frameT, maxStep, ...
    relTol, absTol)
```

that allows introducing the defined parameters and getting the time, positions and velocities of the bodies for the simulation. The input parameters are already explained in the section "data preparation", the output parameters are:

`T`: the time vector, starting in 0 and ending in `T_total`, with an increment of `frameT`.

`Y`: the matrix with positions and velocities of all the bodies, with a dimension $n \times 60$, where n is the length of the vector `T`, and 60 is the positions and accelerations. They can be read, having the same rule of the vector `initialC`: firstly the positions, grouped by body, followed by the velocities grouped by bodies too.

A1.2.1 The function **PTW2D**

This function handles all the simulation. The first task is a number of verifications, like number of input and output variables, and creating the default values not introduced by the user. Further, correction of parameters concerning the initial conditions and the mass characteristics is proceeded: added initial velocity zero and created the mass matrix.

Then, a resume table on the command window about the simulation parameters followed by a message indicating the start of the simulation (integration process) is printed:

```
+------------------------+---------+--------------+
|       VARIABLES        |  UNITS  |    VALUE     |
+------------------------+---------+--------------+
| Time simulated         |    s    |      1       |
| Sample frequency       |   Hz    |     25.0     |
| Maximum Step           |   ms    |     5.000    |
| Relative Tolerance     |    -    |  1.000E-004  |
| Absolute Tolerance     |    -    |  1.000E-006  |
+------------------------+---------+--------------+

 Starting the simulation ...
```

Previous to the simulation, a wait bar (Figure A 1) is created and the user can evaluate the integration progress, and the time is start counting to know the CPU time.
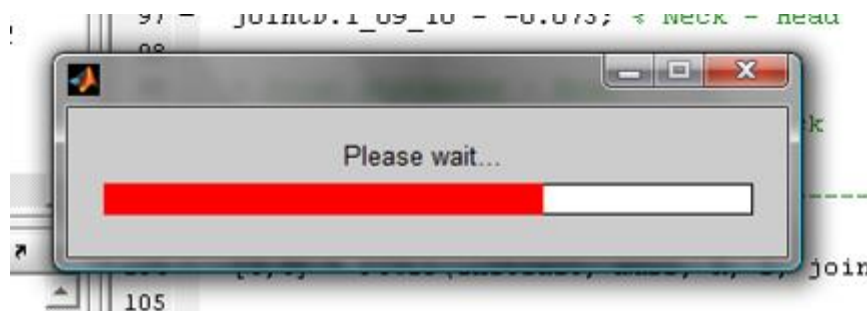
Figure A 1 – Wait bar during the compiling process

The integration function is called currently using the function `ode113` with the input function `PTWsys`:

```
% Start integrating
[T, Y] = ode113( @PTWsys, 0:frameT:T_total, initialC, options, ...
    initialC(3:3:s_var), mass, K, B, jointD, s_var, h, T_total);
```

where the variable `options` is defined by:

```
% Setting integration options
options = ...
    odeset('MaxStep',maxStep, 'RelTol', relTol, 'AbsTol', absTol);
```

After the integration part, the wait bar is closed and it is printed a message that indicates the used time:

```
    ... elapsed time 6.8762 s
```

A1.2.2 The function `PTWsys`

This is the function inside the integration function.

```
function dAll = ...
    PTWsys (t, All, iC, mass, K, B, jointD, s_var, h, T_total)
```

For the several inputs we have:

`t`: current integration time.

`All`: the variable to integrate.

`iC`: initial directions of the bodies.

`mass`: the mass properties of all bodies. It contains the mass properties of each body (mass and inertial moment), body by body, in a total of 20 parameters (1 mass and 1 inertial moment for each of 10 bodies).

`K`: the stiffness vector of the spring-damper in each joint (8 parameters). In the future versions, it will be updated to a structure variable of size 8, allowing nom linear stiffness.

`B`: the damping vector of the spring-damper in each joint (8 parameters). In the future versions, it will be updated to a structure variable of size 8, allowing nom linear damping.

`jointD`: the structure variable with all the local coordinates of the joints. The structure of the variable follows the next example (data according with Table A1-5):

`s_var`: matrix size (from mass matrix).

`h`: wait bar variable.

`T_total`: total simulated time.

One of the limitations of the integration function is that it can handle only with the first order differential equations. To cross over that limitation, is usual to use the following approach:

$$\begin{aligned} v &= \dot{x} \\ a &= \dot{v} \end{aligned} \qquad (A1\text{-}2)$$

From equation (A1-2), we get

$$\begin{aligned} \mathbf{All} &= \begin{bmatrix} \mathbf{x} & \mathbf{v} \end{bmatrix} \\ d\mathbf{ALL} &= \begin{bmatrix} \dot{\mathbf{x}} & \dot{\mathbf{v}} \end{bmatrix} \end{aligned} \qquad (A1\text{-}3)$$

These steps are done in the beginning and in the end of the function respectively. In the beginning of the function, the wait bar and used constants are actualized.

The code follows the mathematical approach. It starts by computing the Jacobean matrix, `Cq`, then the derivative of the Jacobean multiplied by the velocity, `Cqq`, and then the constrains matrix `C`. After that, the applied forces, `Qe`, are computed (including the external excitations). It computes the matrix generated from constrains and then, the Baumgarte's stabilization, `Qd`, is applied.

The last part is the computation of the output variables:

```
%% Matrix manipulation
Mi = mass^-1;
CqT = Cq';
Hll = (Cq*Mi*CqT)^-1;
Hql = -Mi*CqT*Hll;
lam = Hql'*Qe + Hll*Qd;
dV = Mi*Qe+Mi*CqT*lam;
dPos = V;
```

A1.3 Visualization

The third part of the code is the visualization of the results. The key variable is the `Y`.

To better understand the variable, the data follows the scheme:

$$\left(R_x^i, R_y^i, \theta^i\right) = \mathbf{Y}\left(i \cdot 3 - 2 : i\right)$$
$$\left(\dot{R}_x^i, \dot{R}_y^i, \dot{\theta}^i\right) = \mathbf{Y}\left(n + i \cdot 3 - 2 : n + i\right)$$

(A1-4)

where n is the number of bodies by 3.

A1.3.1 The function `PTWplot`

A function that generates a full animation of the simulation

```
function ptwAnimation = PTWplot (T, Y, jointD, initialC)
```

was implemented where the variables are described in previous sections.

The function generates a collection of ellipses to illustrate each body with the exception of the PTW frame that is a collection of the pre-defined points.

Then each time step (from the sampling data) generates a static figure of the PTW and the rider. The consequence of images gives a sense of animation helped by background vertical bars. In the animation, the current time and the kinematic data of the rear wheel (position, velocity and acceleration) are presented.

The collection of images is stored and can be accessed using the output `ptwAnimation`. This information can be used e.g. to create films of the simulation.

A1.4 Benchmarking

To evaluate the implemented code, the data described in the introduction part was used, according with the literature.

The initial positions and rotations of the centres of mass and inertial properties of the bodies are summarized in Table A1-3 and Table A1-4. The joint position relative to the local axis system is summarized in Table A1-5.

For visualization purposes, the user can see a list of various plots, and the animation of an entire simulation, displaying the PTW and the rider moving along the time.

Table A1-3 – Initial position and rotation of the various centers of mass

	Body number	$\overline{x}_P^i$	$\overline{y}_p^i$	θ^i
	-	$[m]$	$[m]$	$[°]$
Rear wheel	1	0.306	0.306	0.
Rear suspension	2	0.61523	0.36053	-0.1745
Front Wheel	3	1.82512	0.290	0
Fork	4	1.77382	0.43095	1.2217
Frame	5	1.01252	0.62296	0.
Trunk	6	0.91638	1.17101	1.7453
Lower arm	7	1.34786	1.21108	0.3263
Upper arm	8	1.10947	1.33741	0.5882
Neck	9	0.97523	1.50486	1.7453
Head	10	0.99887	1.63880	1.7453

Table A1-4 – Mass and inertial moment of all bodies

	Body number	m^i	J^i
	-	$[kg]$	$\left[\times 10^{-4} \; m\right]$
Rear wheel	1	15.50	5214.20
Rear suspension	2	10.00	2459.20
Front Wheel	3	20.00	7490.88
Fork	4	4.00	22.40
Frame	5	152.362	43361.57
Trunk	6	37.542	1011.218
Lower arm	7	4.044	61.850
Upper arm	8	3.538	24.206
Neck	9	0.965	24.206
Head	10	4.137	22.1552

Table A1-5 – Joint location according with the local axis reference

joint	$\overline{l}_x^{i,j}$	$l_y^{i,j}$
-	$[m]$	$[m]$
02-01	-0.314	0
02-05	0.400	0
04-03	0.150	0
04-05	-0.400	0
05-02	0.00337	0.19297
05-04	0.61054	0.22222
05-06	-0.13590	0.32254
05-07	0.49731	0.53330
06-05	0.22900	0
06-08	-0.23719	0.07061
06-09	-0.293	0
07-05	0.171	0
07-08	-0.105	0
08-06	-0.099	0
08-07	0.167	0
09-06	0.046	0
09-10	-0.073	0
10-09	0.063	0

A1.4.1 Numerical example

Several simulations were performed to see the behaviour of the model in several scenarios. In order to illustrate the capabilities following simulation were proposed: the first 3 seconds to observe the stabilization process (equilibrium) without any horizontal motion, then acceleration by 4 seconds followed by 3 seconds of stabilization, and 3 seconds of deceleration (80% front wheel and 20% rear wheel) and the following time to stabilize.

The system dynamic response for 20 seconds of simulation for the PTW frame, the trunk and the head is illustrated in Figure A 2 until Figure A 7 respectively. The initial and final position of the model is illustrated in Figure A 8. Horizontal direction is denoted by *xx* and vertical direction by *yy*.
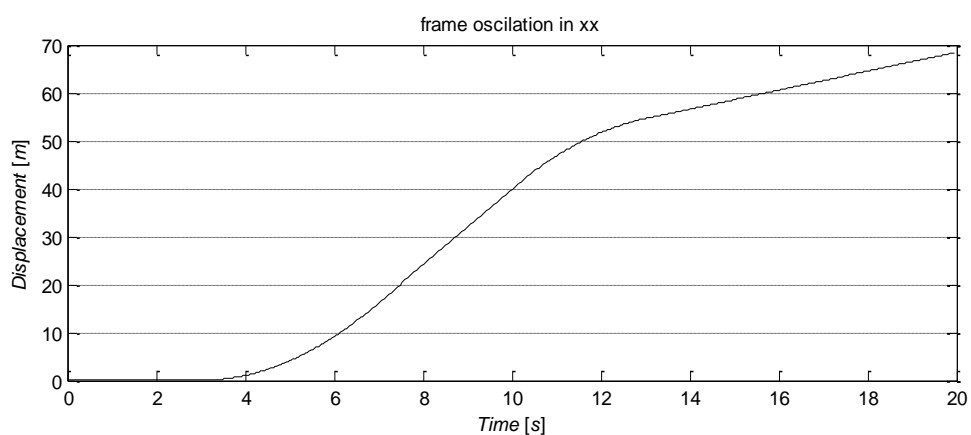
Figure A 2 – Frame oscillation in *xx* direction
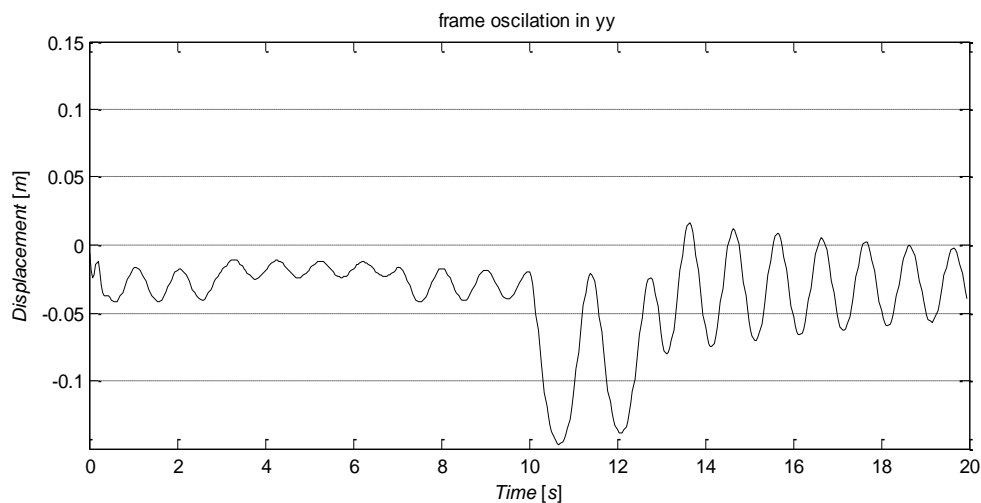
Figure A 3 – Frame oscillation in *yy* direction
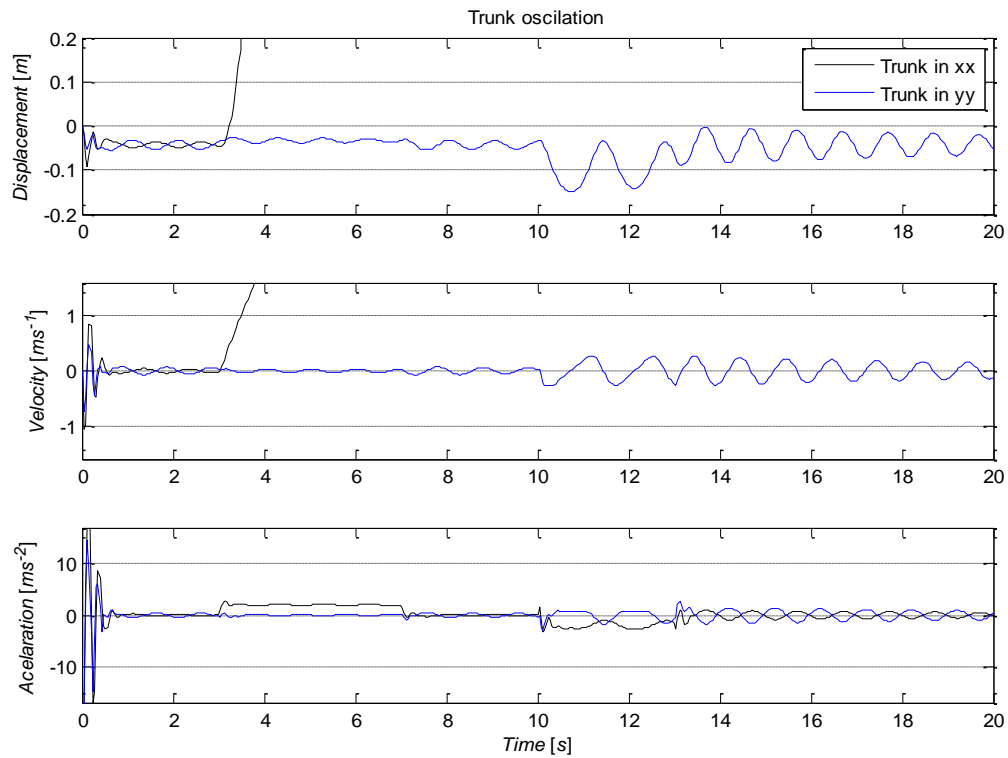
Figure A 4 – Trunk oscillation (translational)
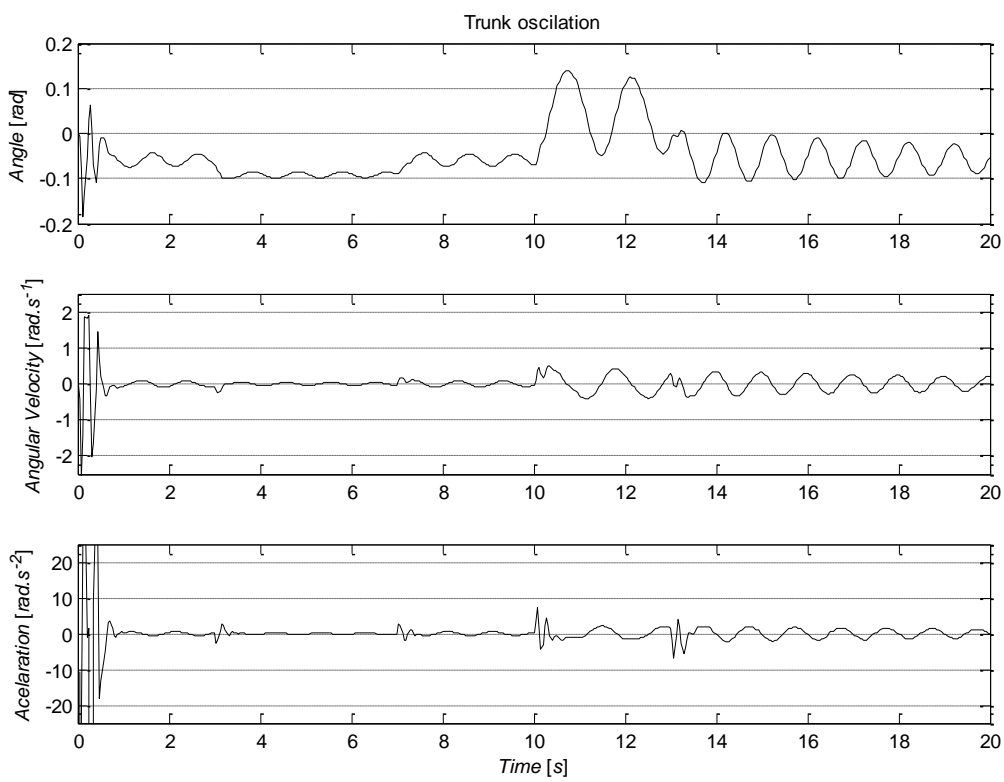
Figure A 5 – Trunk oscillation (rotational)
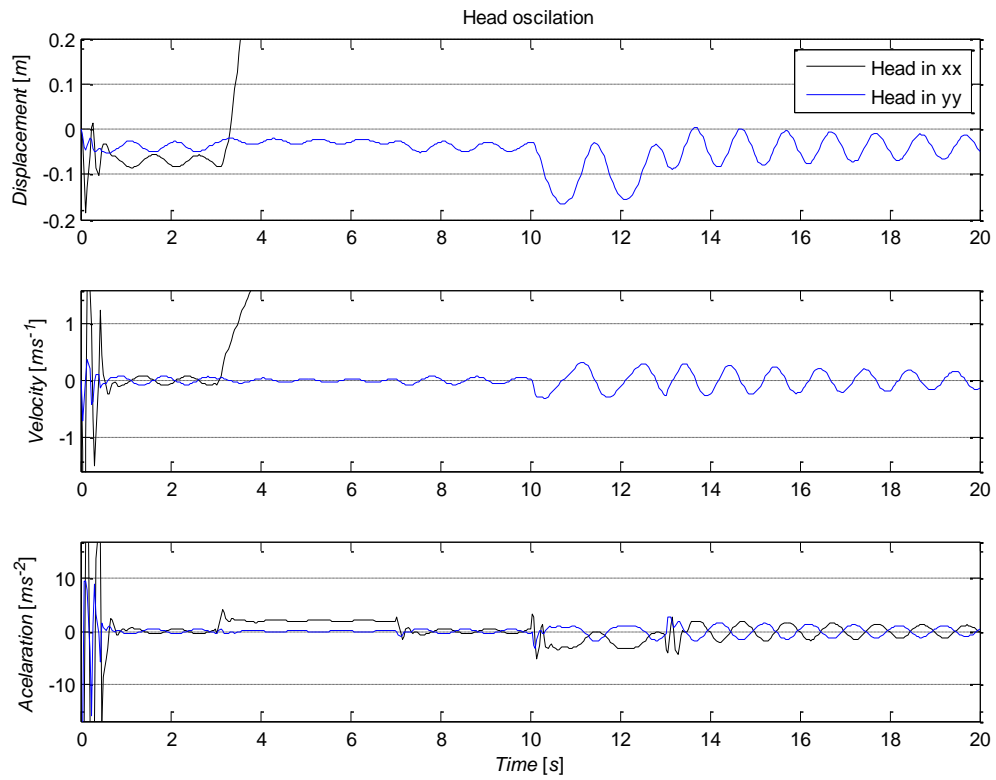
Figure A 6 – Head oscillation (translational)
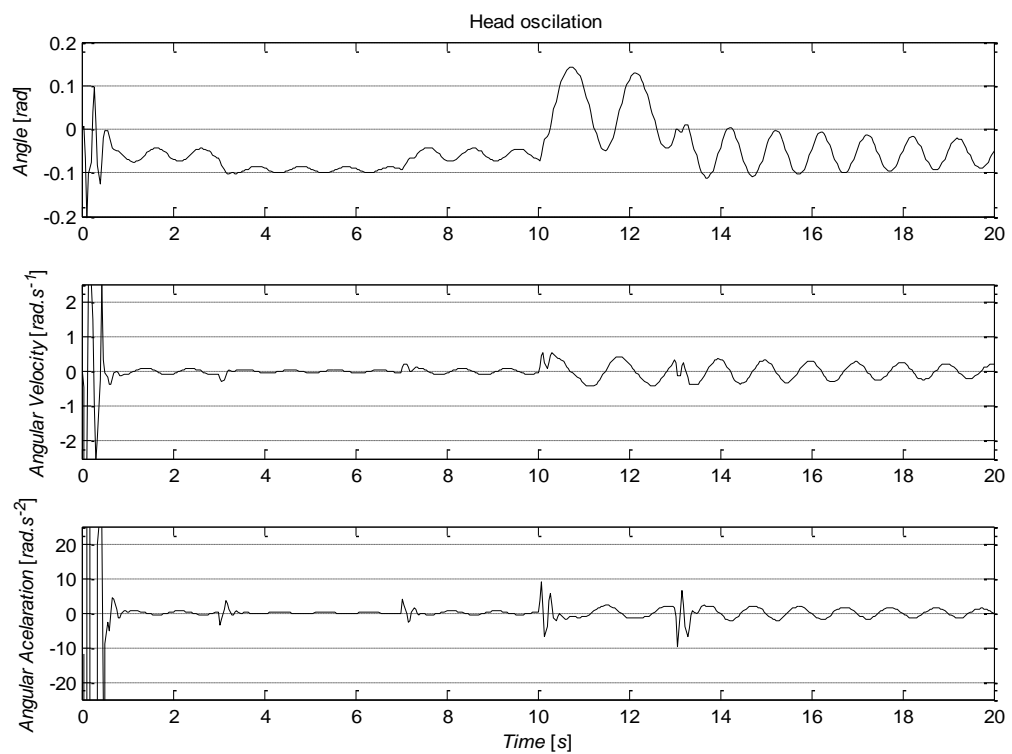
Figure A 7 – Head oscillation (rotational)
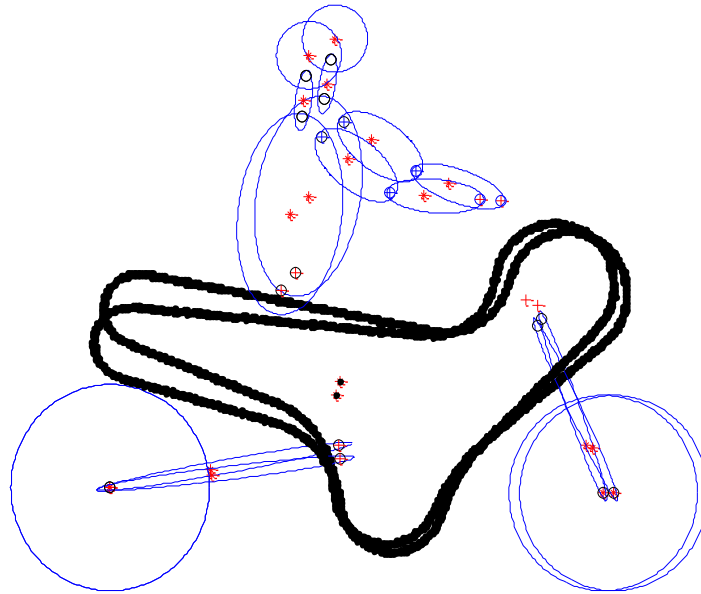
Figure A 8 – Initial and final position of the model

The simulation shows that for typical acceleration and deceleration values in the PTW, the vibrations are relatively low. We can get in this stage the response of the system to several external excitations, which allow a better understanding of the system dynamics. These simulations might be improved with more complex joint definitions and compared with experimental data taken in volunteers in laboratory (pre-defined acceleration and brake manoeuvres) and in real traffic environment.

The short movements of the head and the neck are obtained by the linearity of the used spring/damper and high stiffness in this anatomical position. The real values are for a relaxed articulation lower for this range of movements. The active joints have stiffness too, but with a time delay by the answer time of the human body (reflex time). The used values were compromises between a passive model and a more realistic behaviour. In this stage the value of damping was arbitrary by the lack of information in the literature for this parameter.

A2 Appendix 2 – Close-loop control

A close loop control scheme was considered to our model, and several benchmark have been performed.

A2.1 Control

In all HBM the joints we have as basic joint a revolution. So, to each spherical joint, we need in as minimum: two dummy bodies, three revolute joint, five sensors, three equations to get the angles (of each plan), three torsion springs (spring and damper, that can be constant or according with a table or equation), three outputs and three inputs (for control propose, were the outputs will be angle and the inputs torques). To test these requirements, the joints between the head and neck, and neck and thorax have been changed (Figure A 9).
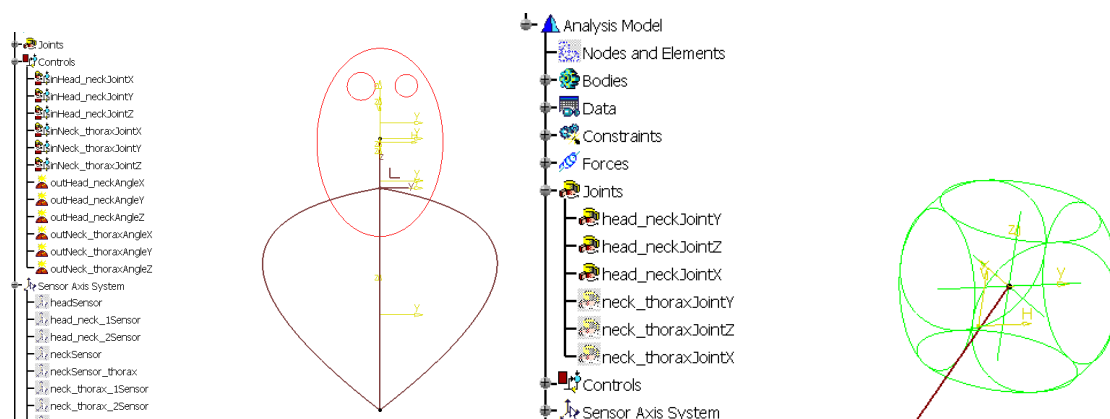
Figure A 9 – Basic Head-Neck-Thorax model and the three revolute joints in the head-neck joint Frame

To help to understand each joint, three drivers by joint was added, to allow the user to activate/deactivate them (one solution to restrain degrees of freedom).

The next step was star to integrate the model with the Simulink and control the movements of the joints. It was set to work with the fixed thorax and control the position of the neck and the head. We have started to control each DOF (Degree of Freedom) of the system, and in the end, all the six DOFs (Figure A 10 and Figure A 11).
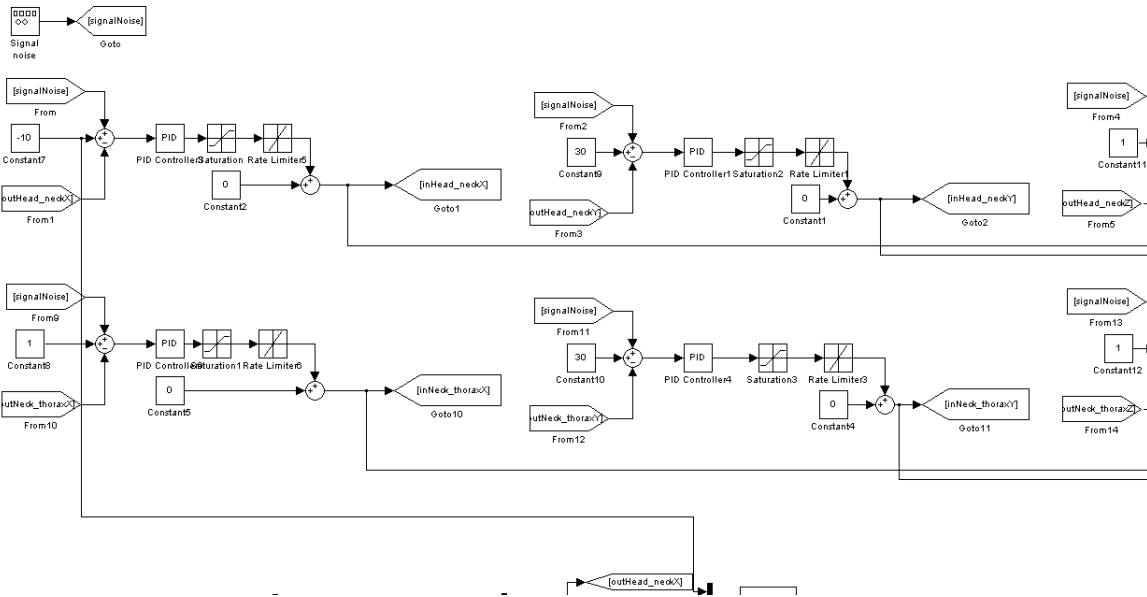
Figure A 10 – Control of head-neck-thorax (part of the Simulink diagram)
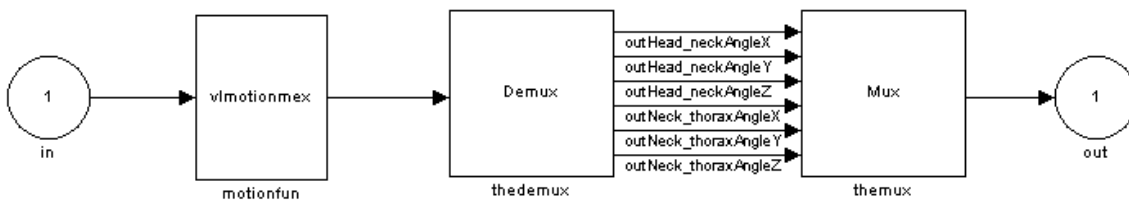
Figure A 11 – Detail of the box obtained from Virtual.Lab

To get a more realistic behavior, it's implemented limits for the slew rate and maximum torque (arbitrary values). It's observed that the model is very sensitive for this parameters like to the stiffness and damping values, particularly in terms of behavior.

The use of PID control seems to be not so good for this type of control, since the model is not linear, and a good set of parameters for one position are not suitable for other. Some results are shown in Figure A 12 and Figure A 13.
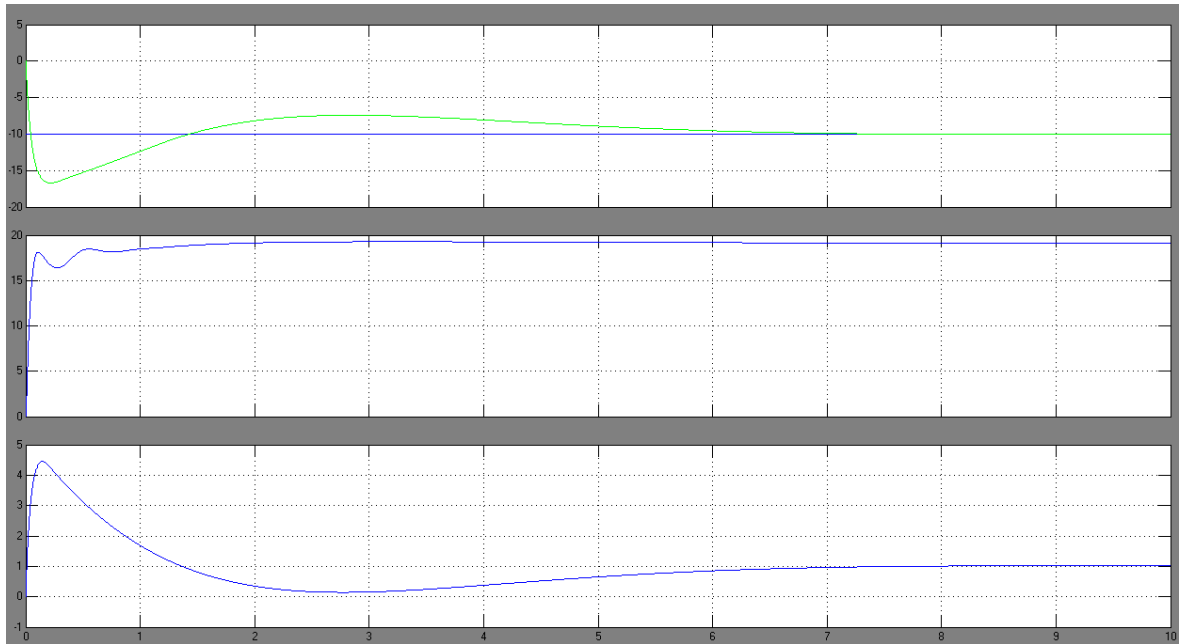
Figure A 12 – Variation of the angles in the head-neck joint along the time
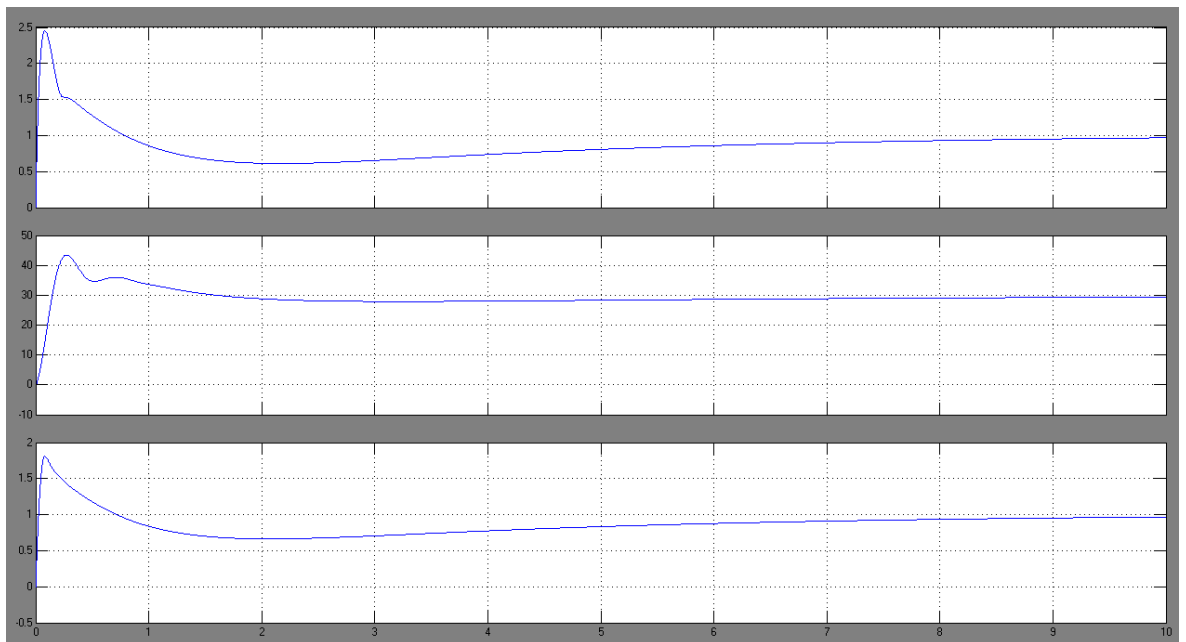
Figure A 13 – Variation of the angles in the neck-thorax joint along the time

A2.2 Remarks

The control was abandon after a new try using data for a close-loop table from MADYMO active model (data taken in cooperation with the MYMOSA partner TNO).

One of the major limitation was the high cost in CPU time added to the model without control (10 to 100 times or more slow).

The possibility to use parallel processing in Virtual.Lab is only supported in X32 platforms, but the HBM needs an X64 platform since needs at least a solo minimum memory of 5GB. This limitation points this approach to be revisited in future works.

A3 Appendix 3 – Publications

A list of publications produced under the scope of the presented thesis.

A3.1 Session organizer

Session organizer, chairman and moderator: "MYMOSA: The pros and cons of motorcycles", 2010, in ESOF2010 – EuroScience Open Forum 2010, Torino, Italy, July 2-7 (cited on Science: ScienceNow; cited on SciDevNet)

A3.2 International conferences

Talaia, P., Hynčík, L., Hajžman, M., 2011, "Trauma em motociclistas: influência da velocidade de impacto no acidente" (motorcyclists trauma: speed influence in the crash impact), cibem10 – X Congresso Ibero-Americano em Engenharia Mecânica, September 4-7, Porto, Portugal (abstract book pp. 384, article pp. 2985-91)

Talaia, P., Toma, M., Hynčík, L., Hajžman, M., Njilie, F., 2011, "Trauma em motociclistas: importância do capacete na redução de risco de trauma" (motorcyclists trauma: helmet importance in the reduction of risk of trauma), clmne2011 – 6º Congresso Luso-Moçambicano de Engenharia, August 29 – September 2, Maputo, Mozambique (abstract book pp. 825-6, article 273703R – 12 pages)

Talaia, P., Hynčík, L., Hajžman, M., 2011, "Trauma em motociclistas: influência da diferença de velocidade em acidentes envolvendo motociclos" (motorcyclists trauma: importance of the difference of speed on crash's involving PTW's), clmne2011 – 6º Congresso Luso-Moçambicano de Engenharia, August 29 – September 2, Maputo, Mozambique (abstract book pp. 827-8, article 273704R – 9 pages)

Talaia, P., Hynčík, L., Hajžman, M., 2011, "A Multipurpose Multi-body Human Model for Accident Reconstruction with Emphasis to PTW and Injury Assessment", CMNE2011 – Congress on Numerical Methods in Engineering, June 14-7, Coimbra, Portugal

Talaia, P., Hynčík, L., Hajžman, M., Parente, M., Fernandes, A., Natal, R., 2011, "Injury assessment using multibody and finite element human models under PTW accidents", EuroMech511 – EuroMech Colloquium 511: Biomechanics of human motion. New frontiers of Multibody Techniques for clinical applications, March 9-12, Ponta Delgada, Azores, Portugal, article 60 (12 pages)

Talaia, P., Hynčík, L., Hajžman, M., 2010, "A Multipurpose Multi-body Human Model for Accident Reconstruction with Emphasis to PTW and Injury Assessment", 6th World Congress of Biomechanics, August 1-6, Singapure, Singapure pp. 296-7

Talaia, P., Toma, M., Hajžman, M., Hynčík, L. Njilie, F., 2009, "A pedestrian model for accident simulation from the crash until full stop", ISB2009, XXII Congress of the International Society of Biomechanics, 298, Cape Town, South Africa, 5-9 July

Talaia, P., Moreno, D., Hajžman, M., Hynčík, L., 2008, "A 3D model of a human for powered two-wheeler vehicles", ISMA 2008 – International Conference on Noise & Vibration Engineering 2008, pp. 2229-2238, Leuven, Belgian, 15-17 September

Moreno, D., Talaia, P., De Cupyer, J., 2008, "A virtual motorcycle rider for closed-loop simulation of motorcycles", ISMA 2008 – International Conference on Noise & Vibration Engineering 2008, pp. 2207-2217, Leuven, Belgian, 15-17 September

Talaia, P., Brenna, C., Gkoumplia, E., Moreno, D., 2008, "Human model for power-two-wheel vehicles: one 2D and 3D model analysis", 8th International Symposium on Computer Methods in Biomechanics and Biomedical Engineering, CMBBE 2008, accepted, Porto, Portugal, 27 February – 1 Mars

A3.3 National conferences

Talaia, P., Hajžman, M., 2008, "The 2D model of a rider and a powered two-wheel vehicle", IM 2008 – Engineering Mechanics 2008, 12-15 May, Svratka, Czech Republic, pp. 1014-1024

A3.4 Reports

Giner, D., Kang, J., Toso, M., Ciubotaru, L., Manka, M., Donders, S., Talaia, P., Hajžman, M., Hynčík, L., Toma, M., Njilie, A. F., 2010, Integration into a vehicle/rider model for full-scale simulations, Deliverable nº 1.3, for the Marie Curie Actions project, RTN action MRTN-CT-2006-035965 "MYMOSA", of the European Community within the 6th Framework Program

Giner, D., Kang, J., Toso, M., Ciubotaru, L., Manka, M., Donders, S., Talaia, P., Hajžman, M., Hynčík, L., Toma, M., Njilie, A. F., 2010, Investigation of accident scenarios and validation of the vehicle/rider model, Deliverable nº 1.4, for the Marie Curie Actions project, RTN action MRTN-CT-2006-035965 "MYMOSA", of the European Community within the 6th Framework Program

Manka, M., Giner, D., Kang, J., Talaia, P., Hajžman, M., Hynčík, L., Toma, M., Njilie, F., 2009, Detailing of the underlying critical aspects, Deliverable nº 1.2, for the Marie Curie Actions project, RTN action MRTN-CT-2006-035965 "MYMOSA", of the European Community within the 6th Framework Program

Giner, D., Kang, J., Talaia, P., Hajžman, M., Hynčík, L., Evangeli, G., 2008, Development of overall methodology for accident simulations, Deliverable nº 1.1, for the Marie Curie Actions project, RTN action MRTN-CT-2006-035965 "MYMOSA", of the European Community within the 6th Framework Program

Giner, D., Kang, J., Talaia, P., Hajžman, M., Hynčík, L., Evangeli, G., 2008, Development of overall methodology for accident simulations, Deliverable nº 1.1, for the Marie Curie Actions project, RTN action MRTN-CT-2006-035965 "MYMOSA", of the European Community within the 6th Framework Program

A4 Appendix 3 – Training

A list stages, courses and formations under the scope of the thesis work.

A4.1 Stages

Stage of two months in ALTAIR France, in Paris, France, supervised by Eng. Franck Njiliet, PhD. And co-supervised by Ing. Milan Toma, PhD, in the work plan of Ph.D. thesis, supported by Marie Curie Actions project, RTN action MRTN-CT-2006-035965 "MYMOSA", of the European Community within the 6th Framework Program, 2009

Stage of one week in DEKRA, in Magdeburg, Germany, supervised by Eng. Thomas Mertens, in the work plan of Ph.D. thesis, supported by Marie Curie Actions project, RTN action MRTN-CT-2006-035965 "MYMOSA", of the European Community within the 6th Framework Program, 2009

Stage of two weeks in TNO, in Eindhoven, Netherlands, supervised by Eng. Lex van Rooij, in the work plan of Ph.D. thesis, supported by Marie Curie Actions project, RTN action MRTN-CT-2006-035965 "MYMOSA", of the European Community within the 6th Framework Program, 2008

Stage of one month in LMS International N.V., CAD division, in Leuven, Belgian, supervised by Eng. Joris De Cuyper, in the work plan of Ph.D. thesis, supported by Marie Curie Actions project, RTN action MRTN-CT-2006-035965 "MYMOSA", of the European Community within the 6th Framework Program, 2007

A4.2 Professional formation

Course on Optimization, organized by Noesis Solutions and LMS International (in UWB facilities), Pilsen. Czech Republic, 2009

Course on Stochastic mechanics, organized by University of West Bohemia, Pilsen. Czech Republic, 2009

MYMOSA training course on "PTW design", organized by UNIFI, with the CMEF, Ducati (facilities, laboratory and museum) and Piaggio (technical aspects, laboratories, facilities and museum), Prato – Bologna – Pontedera, Italy, 2008

DEKRA Training Course on Accident Research & Reconstruction, DEKRA Automobil GmbH, Germany, 2008

Training in LMS Virtual.Lab Motion, LMS International N.V., Belgian, 2007

Technical Writing Two Hour Workshop, Graduate School of Engineering and Physics Sciences, Imperial College London, United Kingdom, 2007

Intellectual Property in the Research Context, Graduate School of Engineering and Physics Sciences, Imperial College London, United Kingdom, 2007

Presentation Skills, Graduate School of Engineering and Physics Sciences, Imperial College London, United Kingdom, 2007

Project Management for Researches, Graduate School of Engineering and Physics Sciences, Imperial College London, United Kingdom, 2007

Training Course on Powered Biomechanics, TNO – The Netherlands Organization for Applied Scientific Research, Netherlands, 2007

International Summer Language School – Czech language course, 92h, University of West Bohemia, Czech Republic, 2007

References

1.   *MYMOSA: Towards Integrated Safety for Powered 2-Wheelers*.   [cited 2010; www.mymosa.eu].

2.   Giner, D., et al., *Development of overall methodology for accident simulations*, in *for the Marie Curie Actions project, RTN action MRTN-CT-2006-035965 "MYMOSA", of the European Community within the 6th Framework Program*. 2008.

3.   Manka, M., et al., *Detailing of the underlying critical aspects*, in *for the Marie Curie Actions project, RTN action MRTN-CT-2006-035965 "MYMOSA", of the European Community within the 6th Framework Program* 2009.

4.   Giner, D., et al., *Integration into a vehicle/rider model for full-scale simulations*, in *for the Marie Curie Actions project, RTN action MRTN-CT-2006-035965 "MYMOSA", of the European Community within the 6th Framework Program*. 2010.

5.   Tostmann, S. *Powered two-wheelers and Road Safety: taking stock -looking ahead*. in *Safety ACEM Conference*. 2006. Brussels.

6.   European Union Road Federation and International Road Federation, *"Intelligent Roads" - What can the Road community expect from GALILEO?* 2006.

7.   Anonymous. Internet.

8.   Compagne, J. *Improving motorcycling safety: A Shared Responsibility*. in *Safety ACEM Conference*. 2006. Brussels.

9.   Portal, R.J.F. and *Modelos de corpos múltiplos para a reconstituição de acidentes rodoviários*, in *Instituto Superior de Técnico*. 2006, Univ. Téc. de Lisboa

10.   Pou, C. *Barcelona motorbike mobility framework. Masterplan and road safety*. in *3rd ACEM Anuual Conference - "Improving Motorcycling Safety: A Shared Responsibility"*. 2006.

11.   *Wild Hogs – The Official Movie Site*. 2007   [cited 2007; wildhogs.movies.go.com].

12.   *Motorcycle Tours Germany – Nurburgring Mosel Rhine motorcycling holidays*. 2007 [cited 2007; http://www.wheeltrax.com/index.htm].

13.   Baker, S.P., et al., *The Injury Score: a Method for Describing Patients With Multiple Injuries and Evaluating Emergency Care.* The Journal of Trauma, 1974. **14**(3): p. 187-196.

14.   Petrucelli, E., J.D. States, and L.N. Hames, *The Abbreviated Injury Scale: Evolution, Usage and Future Adaptability.* Accid. Anal. & Prev., 1981. **13**: p. 29-45.

15.   *Anthropometry and Biomechanics*, in *Man-Systems Integration Standards*, NASA, Editor. 1995.

16.   *Human Performance Capabilities*, in *Man-Systems Integration Standards*, NASA, Editor. 1995.

17.   Schmitt, K.-U., P.F. Niederer, and F. Walz, *Trauma Biomechanics: Introduction to Accidental Injury*. 2004, Berlin: Springer-Verlag.

18.   Dempster, W.T., *Space Requirements of the seated operator: Geometrical, kinematic, and Mechanical aspects of the body with special reference to the limbs*. 1955, Michigan: Carpenter Litho & Prtg. Co., Springfield.

19.   DEKRA, *PTW with airbag crash test*. DEKRA.
20.   Hyde, J. *How Cadavers Made Your Car Safer*. Wired, 2010.
21.   BBC News *How the dead have helped the living*. 1998.
22.   King, A.I., et al., *Humanitarian Benefits of Cadaver Research on Injury Prevention.* The Journal of Trauma, 1995. **38**(4): p. 564-569.
23.   Wikipedia, *Sierra Sam*, Sam4.jpg, Editor. 2004.
24.   Science Museum / Science & Society, *Crash test dummy, 1970-1990*.
25.   Ford Motor Company, *Crash Test Dummies Then and Now*. 2011, Ford Motor Company.
26.   national museum of american history, *Hybrid II and Hybrid III crash test dummies*. 2010, National Museum of American History Smithsonian Institution.
27.   Humanetics, *CG dummies*. Humanetics.
28.   Nahum, A.M. and J.W. Melvin, *Accidental Injury: Biomechanics and Prevention*. 2nd ed. 2002, New York: Springer Science.
29.   Robert A. Denton, Inc. and Denton ATD, Inc., *History of Anthropomorphic Test Devices*.
30.   Wikipedia, *Hybrid III - Crash test dummy family*.
31.   the-automover. *Crash Test Dummies*. Available from: http://www.the-automover.com/dummy.htm.
32.   www.zcars.com.au. *Honda: POLAR III Revolutionary Pedestrian Dummy*. 2008; Available from: http://www.zcars.com.au/honda-polar-iii-pedestrian-dummy/.
33.   *alaska 4 - Modelling and Simulation of Mechatronic Systems*. Institute of Mechatronics of the Chemnitz University of Technology [cited 2007; http://www.tu-chemnitz.de/ifm/english/eindex.htm].
34.   *Universal Mechanism: road and railway vehicle dynamics, applied dynamics, general kinematics, inverse kinematics*. [cited 2007; http://umlab.ru/].
35.   *Cosmos*. [cited 2007; http://www.cosmosm.com/].
36.   *SolidWorks*. [cited 2007; http://www.solidworks.com/].
37.   *Dynamic Designer*. [cited 2007; http://www.design-simulation.com/DDM/index.php].
38.   *Autodesk Inventor*. Autodesk [cited 2007; http://www.autodesk.com/inventor].
39.   *Adams*. [cited 2007; http://www.mscsoftware.com/products/adams.cfm].
40.   *Virtual Prototype Simulation*. LMS Engineering Innovation [cited 2007; http://www.lmsintl.com/virtuallab].
41.   *TASS: Delivering transport safety solutions*. [cited 2007; http://www.madymo.com/cms/index.php].
42.   *Crash & Occupant Safety — ESI Group*. [cited 2007; http://www.esi-group.com/SimulationSoftware/crash.html].
43.   *Altair HyperWorks*. [cited 2007; http://www.altair.com/software/hw.htm].
44.   *The MathWorks - MATLAB and Simulink for Technical Computing*. [cited 2007; http://www.mathworks.com/].
45.   *DynaFlex - MapleConnect Third Party Products - Maplesoft*. [cited 2007; http://www.maplesoft.com/products/thirdparty/dynaflexpro/].
46.   *Modelica and the Modelica Association — Modelica Portal*. 2007]; http://www.modelica.org/].
47.   *SIMM by MusculoGraphics, Inc.* [cited 2007; http://www.musculographics.com/].
48.   *Catia V5*. [cited 2007; http://www.3ds.com/products-solutions/plm-solutions/catia/overview/].
49.   *Biomechanics Research Group*. [cited 2007; http://www.lifemodeler.com/].

50.   Iwamoto, M., et al., *Development of a finite element model of the total human model for safety (THUMS) and application to injury reconstruction*, in *2002 International IRCOBI Conference*. 2002. p. 31-42.

51.   Arnaux, P., K. Kayvantash, and L. Thollon, *The RADIOSS Human Model for Safety (HUMOS) – Validation of the Radioss HUMOS model; Definition of a model evaluation procedure – Model Version 14D*.

52.   Haug, E., et al., *Human Models for Crash and Impact Simulation*, in *Handbook of Numerical Analysis*, N. Ayache, Editor. 2004, Elsevier. p. 231-452.

53.   Imaizumi, H., T. Fujioka, and M. Omae, *Rider model by use of multibody dynamics analysis.* JSAE, 1996. **17**: p. 65-77.

54.   Robbins, D.H., *Anthropometric specifications for mid-sized male dummy – Volume 2*. 1983, University of Michigan: Michigan.

55.   Sharp, R.S., S. Evangelou, and D.J.N. Limebeer, *Advances in the Modelling of Motorcycle Dynamics.* Multibody System Dynamics, 2004. **12**: p. 251-283.

56.   Shabana, A.A., *Computational dynamics*. 2001: John Wiley & Sons, Inc.

57.   Fernandes, J.P.F., *Dynamic analysis of mechanical systems with imperfect kinematic joints*, in *Escola de Engenharia*. 2004, Universidade do Minho.

58.   Hajžman, M. and P. Polach, *Application of stabilization techniques in the dynamic analysis of multibody systems.* Applied and Computational Mechanics, 2007. **2**(1): p. 479-488.

59.   Bianco, S., *BMW C1 FF 200*. 2006: en.wikipedia.org.

60.   *Highway bars, Crash bars, engine guard bars*. 2008: www.motorcycleforums.net.

61.   Schwartsmann, C., O. Lech, and M. Telöken, *Fraturas: princípios e prática*. 2003.

62.   *Gray's Anatomy - The Anatomical Basis of Clinical Practice, Thirty-Ninth Edition*. 2005: Elsevier.

63.   Richardson, M.L. *Approaches To Differential Diagnosis In Musculoskeletal Imaging*. 2001 [cited 2007; http://www.rad.washington.edu/mskbook/facialfx.html].

64.   Silova, M., *Human motion analysis using multibody dynamics and optimization tools*, in *Instituto Superior Técnico*. 2003, Unniversidade Técnica de Lisboa: Lisboa.

65.   Euro NCAP, *European new car assessment programme (Euro NCAP) - Pedestrian testing protocol*. 2009, Euro NCAP.

66.   US Air Force, *Col. (Dr.) John Paul Stapp - heavy deceleration* 1950, Air Force Outreach: Air Force Outreach Photos

67.   US Air Force, *Col. (Dr.) John Paul Stapp*. 1950, Air Force Outreach: Air Force Outreach Photos

68.   Kovanda, J., et al., *Models of driver and passengers for application in road transport, road vehicles computer model in suitable environment, road vehicles non-protected passenger (driver), pedestrian impact*. 2005, Report for MPO Project FT-TA/024.

69.   Arbeitskreis Messdatanverarbeitung Fahrzeugscherheit, *Crash analysis criteria description - version 1.6.2*. 2005.

70.   Euro NCAP, *Euro NCAP Assessment Protocol – PP* 2009.

71.   Euro NCAP, *Pedestrian Test Protocol*. 2012.